Physicochemical characterization of DNA-based bionanocomposites using nonafibrous clay minerals : biological applications

Fidel Antonio Castro Smirnov

UNIVERSITE PARIS-SUD

ÉCOLE DOCTORALE : *Gènes, Génomes, Cellules.*
Laboratoire de Recombinaison / Réparation et cancer (REC),
CNRS *UMR8200 Stabilité génétique et oncogenèse,*
Institute Gustave Roussy.

Discipline : Molecular biophysics, life sciences and health.

THÈSE DE DOCTORAT

soutenue le 15/10/2014

par

Fidel Antonio CASTRO SMIRNOV

Physicochemical characterization of DNA-based bionanocomposites using nanofibrous clay minerals. Biological applications.

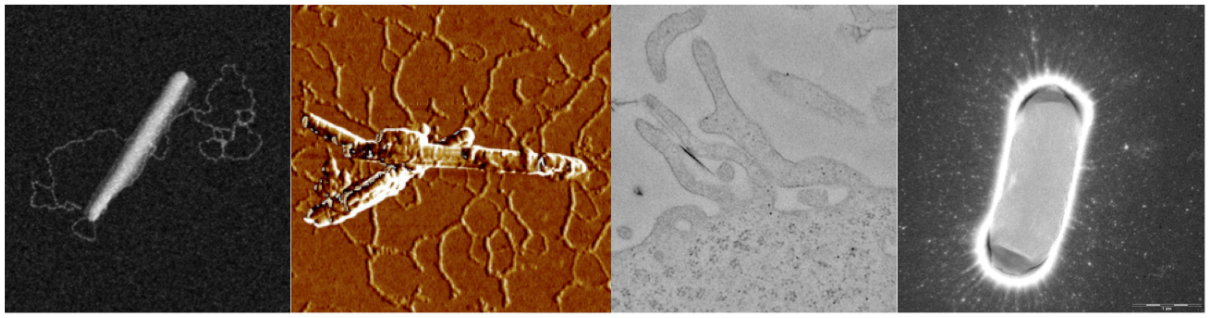

Directeur de thèse :	Bernard LOPEZ	Directeur de Recherche CNRS (IGR)
Co-directeur de thèse :	Oscar RODRIGUEZ HOYOS	Professeur à INSTEC (Cuba)

<u>Composition du jury</u> :

Président du jury :	Claude FORANO	Professeur, Directeur adjoint de l'ICCF
Rapporteurs :	Claude FORANO	Professeur, Directeur adjoint de l'ICCF
	Cedric BOISSIERE	Chargé de Recherche HDR, CNRS, Collège de France
Examinateurs :	Eduardo RUIZ-HITZKY	Professeur de Recherche, ICMM, CSIC (Espagne)
	Eric LE CAM	Directeur de Recherche CNRS (IGR)
	Pilar ARANDA	Senior Researcher, ICMM, CSIC (Espagne)

Con inmenso cariño:

A mi abuelo Fidel. Sus enseñanzas y su ejemplo son acicate e inspiración, ante la responsabilidad y el compromiso que entrañan para mí, llevar con dignidad y modestia su misma sangre y su mismo nombre.

A mi padre Fidel, mi paradigma intelectual y humano. Por su guía permanente y ejemplar en los caminos de la ciencia y de la vida.

A mi tío Raúl y a la memoria de mi tía Vilma. Por su afecto y apoyo de siempre, por su entrañable sentido de la familia.

Y a mi abuela Mirta. Por ofrecerme su amor y su dulzura, por su extraordinaria historia personal, plena de grandeza, lealtad y modestia.

Acknowledgements.

First of all I would like to thank Professor Claude Forano, Directeur Adjoint of the Institute of Chemistry of Clermont-Ferrand (ICCF), and Dr. Cedric Boissière, Chargé de Recherche CNRS in the Laboratory of Chemistry of Condensed Matter (UMR 7574) of the College de France, for accepting to evaluate my research work; and to all the members of the Jury: Professor Eduardo Ruiz-Hitzky, Professor Oscar Rodriguez, Dr. Bernard Lopez, Dr. Erick Le Cam, and Dr. Pilar Aranda.

I would like to express my deep and sincere gratitude to my supervisor, Dr. Bernard S. Lopez, for hosting me in the research group he leads, the Laboratory of Reparation, Recombination and Cancer (REC), belonging to the CNRS UMR 8200 at the Institute Gustave Roussy (IGR). Many thanks to him for the confidence he deposited on me taking the adventure of being the guide in this multidisciplinary research topic, for his patience and good mood during the hard process of learning so much about life sciences under his supervision. Similarly I wish to express my sincere thanks to my tutor, Dr. Olivier Piétrement, for his enthusiasm, enormous patience, valuable advices, and for his important support throughout never-ending experiments for the present Thesis.

A word of appreciation to Dr. Patricia Kannouche, head of the Unit of Genetic Stability and Oncogenesis (CNRS UMR 8200), for accepting me in the Unit she leads. I also want to thank Dr. Said Aoufouchi, Dr. Filippo Rosselli, Dr. Murat Saparbaev, Dr. Corinne Dupuy, Dr. Alain Sarasin, Professor Jean Feunteun, all from CNRS 8200, to Professor Karim Benihoud from the Group of Cancer-Targeting Viral Vectors, and to Dr. Eric Le Cam, head of the Laboratory of Maintenance des Génomes, Microscopies Moléculaires, CNRS UMR 8126, for fruitful discussions and important remarks. I owe my gratitude to Dr. Jeanne Ayache for trusting me and make a big time-consuming experiment with TEM on cells, which become to an important result for this Thesis. Thanks to Catherine Pioche-Durieu and Sonia Baconnais for fruitful discussion on cellular imaging; Alexandra Joubert for DNA preparation; as well as to Sophie Salomé for confocal microscopy and time lapse video microscopy assistance and to

Philippe Rameau (PFIC-IGR) for his help in FACS experiments. I am indebted to my fellow labmates, namely Dr. Josée Guirouilh-Barbat, Dr. Nicolas Siaud, Indiana Magdalou, Elodie Dardillac, Dr. Sandrine Ragu, Dr. Tangui Le Guen, A-Yeong So, Ahmed Mogharbi and Camille Gelot. Same gratitude to Françoise Royer, Christelle Bouchot and Ghislaine Zmudz for their permanent help.

The present PhD project started at the Group of Nanostructured Hybrid, Bio-hybrid and Porous Materials at the ICMM-CSIC, under the supervision of Professor Eduardo Ruiz-Hitzky, former Head of the Department of New Architectures in Materials Chemistry, Materials Science Institute of Madrid. I would like to express my warm and sincere thanks to him, who had the original idea of the research that leaded to the present Dissertation. All I have learnt from him was determinant in my scientific training. Thanks to him again for his knowledge and for his friendship. I would also like to thank Dr. Margarita Darder for her encouraging guidance at the beginning of the project, for her initial training in the synthesis of hybrid materials and for her help in the first experiments to synthesize the Sep/DNA bionanocomposite. I am deeply grateful to Dr. Pilar Aranda for her friendship, dedication, continuous help, and for her detailed and constructive revision of the manuscript. I would like also to thank other people from the ICMM-CSIC that during my stage there, and later, helped me in diverse aspects of my research: Dr. Francisco M. Fernandes, Dr. Bernd Wicklein, Dr. Ana C.S. Alcântara, Andrés Valera, Alfredo Jacas, Dr. Amalia Ruiz, Dr. M^{a} del Puerto Morales and Pedro A. Rodriguez.

I would like to acknowledge the funding from the University Paris Sud 11 (UPS), from the French Embassy in Cuba and from the CICYT, Spain (project MAT2012-31759). Many thanks to the Director of the Doctoral School at UPS Professor Pierre Capy, to the Ambassador Jean Mendelson, Bernard Grau, Aurelie Nogues, Olivier Tanes and Fabrice Mercorelli. I would also like to thank the Embassy of Cuba in France, especially to the Ambassador Orlando Requeijo Gual, José Antonio García, and to the staff of Cubana de Aviación, especially to Daysí Suarez, Ramón Martínez and Ana Margarita Godoy.

It is a big pleasure to thank my sincere friends who are "my family in France". They are Serge Ussorio (and his sons Greg and Jeremy); Francisco Galindo Velez and Fabiola Agudelo; Tania Martínez; Gilbert Brownston and his wife Maigualida, Dr. Salim Lamrani; Manuel Rodriguez, his son Guillaume and his wife Tania; Françoise Xavier Diaz; Carmen Guerrero; and Julio Garrido with his family.

I would like to show my special gratitude to my best friends in Cuba; it would be a very big list, but I would like to mention here my good friends Professor Oscar Rodriguez Hoyos, Professor Fernando Guzmán Martínez, Professor Sergio Luis Reyes, MSc. Joel Queipo Ruiz and MSc. Yorexis González. My sincere gratitude also to my colleagues at the Higher Institute of Technologies and Applied Sciences (InSTEC) and at the University of Informatics Sciences (UCI), especially to the Rectors Dr. Bárbara Garea and Dr. Miriam Nicado, respectively.

All my deepest affection to my family. To my grandfather Fidel (my beloved giant who with his ideas and his example encourages generations); to my uncle Raúl (for his continuous support and for his endearing sense of family); to my beloved heroines: my grandma Mirta and to the memory of my aunt Vilma; to my father Fidel Angel (my intellectual and human paradigm, for his continued and exemplary guidance in the ways of science and life to a child who has always wanted to be like him), to my mother Natalia (my first discovery and who gave birth to three scientists), to my aunts Meky and Mirta; to my younger brother José Raúl, to my sister Mirta (the most beautiful and smart sister I could ever had), her husband Rafael, and my amazing and marvellous nephews Fidel José, Gonzalo and Rafael.

Finally, a very well deserved word of thanks to Claudia, my lovely life companion. Her love, intelligence, character, sweetness, courage, and enthusiasm (and why not, her extraordinaire skills in the kitchen :) are a big treasure that obliges me, always and wherever I go (even under the sea with her), to be a better person every day.

To all I have appointed, and those who unforgivably I have not remembered, go my thanks and sincere gratitude.

Abstract

Among the various clay minerals, sepiolite, which is a natural fibrous silicate, is a potential promising nanocarrier for the non-viral transfer of bio-molecules. Indeed, sepiolite has been shown to interact with biological molecules such as lipids, polysaccharides and proteins. Here, we show that sepiolite efficiently binds different types of DNA molecules (genomic, plasmid, single strand and double strand oligonucleotides), introducing the first detailed study on the interaction mechanisms between sepiolite and DNA, as well as the physicochemical characterization of the resulting DNA-sepiolite bionanocomposites. The interaction mechanisms are suggested to be electrostatic interactions, van der Waals forces, cation bridges, and hydrogen bonding. Spectroscopy analysis showed that the binding of DNA to sepiolite was increased by polycations with valence dependent efficiency, and the DNA previously adsorbed could be recovered with an efficiency that could be modulated using a chelating agent (EDTA), preserving the DNA structure and biological activity. Fourier-transform infrared spectroscopy identified the external silanol groups as the main sites of interaction with the DNA. It was proved that it is possible to use sepiolite for extracting DNA from bacteria, for DNA purification and for purification from bacterial contamination. By combining fluorescence microscopy, transmission electron microscopy (TEM), time-lapse video microscopy and flow cytometry analysis (FACS), we show that sepiolite can be spontaneously internalized into mammalian cells through both endocytic and non-endocytic pathways. As a proof of concept, we show that sepiolite is able to stably transfer plasmid DNA into bacteria and mammalian cells. It was also proved that with the incubation of bacteria with the Sep/DNA bionanocomposite initially prepared in the presence of a low concentration of divalent cation, and using sonicated sepiolite (sSep), it is possible to increase the bacterial transformation efficiency from 20 to 30-fold compared to previously reported methods which are based in the “Yoshida effect”. Additionally, we show that the efficiency of sepiolite-mediated gene transfer can be optimized: the use of sSep and the exposure to the endosome disrupter chloroquine 100-fold and 2-fold stimulated DNA transfection efficiency, respectively. These results open the way to the use of sepiolite-based bionanocomposites as a novel class of hybrid nanocarriers for both potential gene therapy and the development of novel biological models of interest for academic and applied sciences.

Résumé

Le transfert d'ADN dans les organismes biologiques représentant un enjeu majeur, à la base de stratégies pour la thérapie génique et/ou le développement de nouveaux modèles biologiques d'intérêt, à la fois pour la recherche fondamentale et appliquée, en médecine, biotechnologique et agronomique. Le développement de nouveaux nano-vecteurs utilisant des bio-nanocomposés, permet le développement de stratégies non-virales pour le transfert de gènes ; elles représentent des approches prometteuses pour le traitement de maladies génétiques, de pathologies cardiovasculaires, du SIDA, de la maladie d'Alzheimer, de différents types de sclérose et du cancer.

Les minéraux argileux (silicates naturels d'aluminium ou de magnésium) constituent un des plus abondants groupes de solides inorganiques interagissant avec la biosphère. En particulier, ils ont été proposés pour être impliqués dans la synthèse pré-biotique de biomolécules à l'origine de la vie. Grâce à leurs propriétés fonctionnelles, les matériaux «bio-nanohybrides» résultant de la combinaison de biopolymères avec des minéraux de l'argile pourraient représenter une approche attractive pour des applications biomédicales tels que le développement de biocapteurs, des matrices de régénération de tissus, de vectorisation de drogues, de vaccination et de pansements.

La détermination de la nature des interactions des biomolécules adsorbées sur les argiles minérales revêt donc une importance majeure pour la connaissance de phénomènes fondamentaux aussi bien que pour des

applications technologiques allant de la compréhension de l'origine de la vie et des écosystèmes du sol, jusqu'à l'ingénierie du génome. Dans le travail présenté ici, nous nous focalisons sur la synthèse et la caractérisation physico-chimique d'un nouveau bio-nanocomposite, dans lequel l'ADN est assemblé à des nanofibres de l'argile connue comme sépiolite. En effet, la biocompatibilité associée à la taille nanométrique de la sépiolite confère aux nanoparticules dérivée de cette argile naturelle, des propriétés prometteuses pour son utilisation dans la vectorisation de drogues, et pourrait permettre de disposer de nouvelles stratégies de vectorisation de molécules biologiques telles que l'ADN.

La sépiolite est un silicate de magnésium naturel de formule théorique par unité cellulaire : $Si_{12}O_{30}Mg_8(OH,F)_4(H_2O)_4,8H_2O$. La structure de la sépiolite montre une alternance de blocs et de tunnels dans la longueur des fibres. Les blocs sont constitués de deux couches tétraédriques de silice entourant une couche centrale d'oxyde-hydroxyde de magnésium. La discontinuité des feuillets de silice autorise la présence de groupements silanol (Si-OH) aux extrémités des canaux que sont les tunnels ouverts à la surface externe des particules de sépiolite. Les canaux et les tunnels contiennent deux types de molécules d'eau : a) les molécules d'eau coordonnée, fixées aux ions Mg^{2+} localisés à la bordure des feuillets octaédriques, et b) l'eau zéolithique, qui est associée aux mêmes ions par des ponts hydrogènes. Un des avantages des argiles fibreuses, comparé aux argiles plus « conventionnelles » basées sur des silicates lamellaires (smectites et vermiculites) est la grande densité de groupes silanol à la surface, 2 SI-OH groupes/nm^2, ce qui permet la formation de ponts hydrogènes, en plus des interactions de van der Waals à l'interface polymère-silicate. De plus, la sépiolite présente des capacités d'échange de cations (<20

mEq/100g) provenant de substitutions isomorphes partielles du magnésium par l'aluminium et d'autres métaux trivalents, dans les feuillets octaédriques. La surface chargée négativement pourrait donc permettre aussi des interactions ioniques lors de l'assemblage de la sépiolite avec des cations inorganiques, ainsi qu'avec des molécules chargées positivement. La nature de la surface de sépiolite, montrant des surfaces étendues chargées négativement, associée à sa morphologie fibreuse, font de la sépiolite une plateforme potentielle de co-distribution de différentes sortes de molécules actives. En effet, la sépiolite a été montrée être capable d'interagir avec des polysaccharides, des lipides, des protéines et des virus, donnant naissance à une grande diversité de bionanocomposites. On peut souligner que la taille des nanofibres de la sépiolite sélectionnée dans ce travail, la rend compatible pour une internalisation dans les cellules de mammifères. De plus, la sépiolite possède une fluorescence naturelle stable. En tirant avantage de cette fluorescence naturelle, il devrait donc être possible de sélectionner les cellules contenant de la sépiolite par les techniques conventionnelles de tri-cellulaire. Enfin, la sépiolite est un silicate naturel et abondant qui est considéré comme non toxique et non carcinogénique par l'agence internationale de recherche sur le cancer (dépendant de l'OMS) et les réglementations européennes. Les tests *in vitro* et *in vivo*, ainsi que les études épidémiologiques, ont confirmé qu'au moins la sépiolite du bassin du Tage en Espagne, ne présentait aucun risque pour la santé.

Dans ce travail nous montrons que la sépiolite fixe efficacement l'ADN, nous présentons une étude détaillée des mécanismes d'interaction entre la sépiolite et l'ADN, ainsi qu'une caractérisation physico-chimique du

bionanocomposite ADN-sépiolite résultant. Nous montrons également que la sépiolite peut être spontanément internalisée par dans les cellules. De plus, nous présentons des preuves de concept montrant que ce système est capable de transférer de l'ADN de façon stable dans les cellules de mammifères et que l'efficacité du transfert de gène par la sépiolite peut être optimisée. En conséquence, la sépiolite pourrait constituer une plateforme prometteuse pour la vectorisation de différentes molécules biologiques, dans les cellules de mammifère.

La sépiolite utilisée dans ce travail est une forme commercialisée provenant des dépôts de Vallecas-Vicalvaro près de Madrid. Une première analyse en microscopie électronique à transmission (TEM) nous a permit d'établir la distribution de tailles de nos échantillons. La largeur moyenne des fibres était de 15 nm et environ 80% des fibres étaient de longueur comprise entre 200 et 400 nm (le maximum étant 800 nm). Par conséquent, la petite taille (associée à la faible toxicité décrite) des fibres de sépiolite, la rend potentiellement adéquate pour un accès intracellulaire dans les cellules de mammifères.

En tirant parti de la fluorescence naturelle de la sépiolite (dans le vert excitation à 488 nm et émission entre 498 et 530 nm ; dans le rouge, excitation à 532 nm et émission entre 542 et 685 nm) nous pouvons suivre son incorporation spontanée dans les cellules de hamster V79. L'analyse a été effectuée par microscopie confocale et confirmé en vidéo-microscopie. Cette analyse montre l'incorporation (mais aussi la décorporation) spontanée de la sépiolite. La cytométrie de flux (FACS) nous a permit d'établir une cinétique

d'incorporation : 45% et 55% des cellules étaient fluorescentes après respectivement 6 heures et 24 heures de contact avec la sépiolite.

Une analyse par TEM a confirmé l'internalisation de la sépiolite dans les cellules de mammifère et a révélé que les fibres de sépiolite cytoplasmiques étaient entourées de membranes endosomiques, suggérant une entrée par endocytose. Plus particulièrement, des structures classiques d'endocytose et de macropinocytose ont été observées à la jonction membrane/sépiolite. On peut aussi noter que quelques fibres de sépiolite n'étaient pas entourées de membranes endosomiques, suggérant une voie alternative à l'endocytose pour l'internalisation de la sépiolite.

L'implication de la macropinocytose et d'autres mécanismes d'endocytose a été confirmée par une analyse par FACS, en présence d'inhibiteurs : la chloroquine, qui bloque l'endocytose dépendante des clathrines, et l'amiloride qui inhibe la macropinocytose. Alors que la chloroquine ne réduit que de 20% l'internalisation de la sépiolite dans les cellules, l'amiloride la fait chuter de 50%, montrant que le mécanisme principal est la macropinocytose, de façon cohérente avec les observations en TEM.

Dans le but d'utiliser la sépiolite comme vecteur d'ADN, nous avons alors montré que l'ADN pouvait réellement se fixer sur la sépiolite. De façon intéressante, nous avons montré que les cations polyvalents stimulaient l'efficacité de fixation de l'ADN à la sépiolite. L'analyse en spectrométrie UV a montré en effet l'adsorption de l'ADN sur la sépiolite. De façon intéressant la présence de cations polyvalents (Mg^{2+}, Ca^{2+}, spermidine, spermine) stimulent fortement l'adsorption de l'ADN de façon directement corrélée à la valence des

cations. La vitesse d'adsorption semble très rapide car la plupart des molécules d'ADN sont instantanément adsorbées. Ce résultat suggère une prédominance des interactions électrostatiques entre la sépiolite et l'ADN avec les liaisons hydrogènes des groupements silanol localisés à la surface externe du silicate.

Pour les modifications de charge de surface, en présence des cations multivalents et de l'ADN, le potentiel zêta a été déterminé par une analyse électro-cinétique. De plus, une analyse par spectrométrie infrarouge par transformée de Fourrier (FITR) a montré que l'interaction de l'ADN avec la sépiolite se faisait par les groupements silanol externes mais pas avec les groupements hydroxyl des feuillets octaédriques de la sépiolite.

L'analyse par TEM et microscopie en force atomique (AFM) a confirmé que les fibres de sépiolite étaient recouvertes d'ADN, à leur surface externe. En cohérence avec l'analyse FITR, certaines molécules d'ADN montrent une fixation à l'extrémité des fibres et peuvent lier deux fibres différentes.

Nous avons alors comparé l'efficacité d'adsorption de différents conformations d'ADN: ADN linéaire duplexe (en moyenne 300 bp) contenant des séquences complexes (ADN de sperme de saumon), plasmides circulaires (5,7 kb), ADN linéaire duplex (dsDNA, 15 bp), ADN simple brin (ssDNA, 15 nt). A faible concentration (inférieur à 300 $ng.\mu l^{-1}$), le comportement de toutes ces formes d'ADN était similaire. A plus haute concentration le ssDNA a montré une adsorption deux fois moins efficace.

Nous avons alors posé la question de la possibilité de désorption de l'ADN de la sépiolite. L'EDTA est un agent de chélation des ions métalliques tels que, entre autres, les ions Mg^{2+}, Ca^{2+}, Fe^{3+}. En déplaçant et séquestrant les

polycations nécessaires à la fixation de l'ADN sur la sépiolite, il pourrait permettre de récupérer l'ADN fixé. De façon intéressante, nous avons obtenu la désorption de l'ADN du bionanocomposite en incubant celui-ci avec de l'EDTA. En utilisant un ADN plasmidique, nous avons pu estimer la qualité de l'ADN récupéré après fixation à la sépiolite. La répartition des différentes isoformes d'ADN (super-enroulé, cercle ouvert, linéaire) ne s'est pas trouvé modifié par la fixation sur la sépiolite. Ceci montre que la sépiolite n'altère pas la qualité de l'ADN et que cette méthode peut être envisagée comme une nouvelle méthode de purification d'ADN.

Dans le but de tester la capacité du bionanocomposé à transférer de l'ADN dans les cellules de mammifères, un composé à été synthétisé (Sep/DNA) avec le plasmide pCMV qui code pour un gène conférant aux cellules la résistance à la G418. L'interaction du composé Sep/DNA avec les cellules a été vérifiée. Le composé Sep/DNA montre un retard d'internalisation comparé à la sépiolite seule, vraisemblablement due à la modification du potentiel zêta en présence d'ADN. Cependant, les fréquences d'internalisation deviennent similaires après 6 heures de contact avec les cellules. L'efficacité de transfert d'ADN dans les cellules a été alors mesurée en sélectionnant les colonies cellulaires résistantes à la G418, après exposition des cellules au Sep/DNA. Après 10 jours de sélection en présence de G418, la présence de colonies résistantes démontre la capacité de la sépiolite à transférer de façon stable un ADN exogène dans les cellules de mammifère. L'efficacité de transfection a alors été comparée en présence des différents cations. La présence de $CaCl_2$ stimule légèrement la fréquence de transfection comparé à la spermidine et à la spermine, vraisemblablement en raison de la trop forte

affinité de l'ADN pour la sépiolite, dans ces conditions. Enfin, il faut noter que la sépiolite est capable de transférer de l'ADN dans différents types cellulaires de mammifères tels que les V79 (cellule de hamster) ou les U2OS (cellules humaines d'ostéosarcome).

La sépiolite a la propriété de s'agréger spontanément ce qui peut constituer une limitation pour une dissémination homogène. Dans le but de désagréger la sépiolite, nous l'avons appliqué des ultrasons (sSep). Des bionanocomposites ont été synthétisés avec le plasmide et la sépiolite soniquée (sSep/DNA). De façon spectaculaire, la sonication de la sépiolite stimule deux ordres de grandeur l'efficacité de transfection dans les cellules humaines. En effet, le nombre de colonies transfectantes (résistante à la G418) est passé de 3 à 350 (par μg d'ADN) avec la sSep en comparaison de la sépiolite. La sonication de la sépiolite permet donc une stimulation de plus de 100 fois de l'efficacité de transfection.

La transfection dans les cellules de mammifères implique plusieurs étapes : l'interaction externe avec les cellules, l'internalisation et le re-largage de l'ADN dans la cellule. La chloroquine est une base faible peut pénétrer rapidement à travers la membrane plasmique et s'accumuler dans des vésicules acides en augmentant leur pH. En empêchant l'acidification des endosomes, elle inhibe les enzymes d'hydrolyse telles que les protéases et les nucléases capables de dégrader les protéines et les ADN. De plus, la chloroquine provoque un gonflement conduisant à la rupture des membranes des vésicules endosomiques, en augmentant la pression osmotique dans les compartiments acides. En raison de ces propriétés, la chloroquine a été montrée comme capable de stimuler l'efficacité de transfert de l'ADN. En

revanche la chloroquine peut affecter l'efficacité d'internalisation en bloquant les voies liées à la grande clathrine. Donc l'exposition à la chloroquine peut avoir deux conséquences opposées sur l'efficacité de transfection qui doit donc résulter de la balance entre ces deux phénomènes opposés. Cependant nous avions montré précédemment que l'endocytose clathrine-dépendante n'était utilisée que marginalement avec la sépiolite. Nous avons donc mesuré l'efficacité de transfection par sSep/DNA en présence d'amiloride ou de chloroquine. Alors que l'amiloride ne produit pas un effet significatif, le traitement à la chloroquine a stimulé la fréquence de transfection d'un facteur 2 dans les cellules humaines. Ces données montrent que, dans les cellules humaines et avec le sSEP/DNA, la chloroquine promeut l'échappement des endosomes plus efficacement que l'inhibition de l'internalisation.

Au vu de nos résultats, nous avons aussi testé la possibilité de stimuler de transformation d'un plasmide dans les bactéries. Nous avons dans un premier temps visualisé l'interaction de la sépiolite avec les bactéries, par TEM. Dans nos analyses nous montrons des contacts entre la sépiolite et les membranes bactériennes. Dans la majorité des cas, ces contacts sont localisés à l'extérieur des bactéries mais dans certains cas, les fibres de sépiolite transpercent la bactérie.

A partir de ces données nous avons posé l'hypothèse que nous pourrions augmenter l'efficacité de transfection basé sur l'effet Yoshida. L'hypothèse en vigueur de l'effet Yoshida est que les forces de friction au moment de l'étalement bactéries au râteau sur le milieu agar favoriserait la pénétration de l'ADN. Dans cette méthode l'ADN n'était pas pré-assemblé à la sépiolite et celle-ci n'était pas soniquée. Nos résultats suggéraient qu'il était

possible d'augmenter l'efficacité de transformation bactérienne. En effet, nous avons montré que le pré-assemblage de l'ADN sur la sépiolite et la pré-incubation du complexe Sep/DNA avec les bactéries, avant l'étalement sur les boites, stimule de plus de 10 fois l'efficacité de transformation des bactéries.

Nous avons alors analysé l'impact des différents cations sur l'efficacité de transformation. Nos résultats montrent que l'efficacité de transformation est inversement corrélée avec la valence des cations, ce qui pourrait provenir d'une plus forte interaction entre l'ADN et la sépiolite. Enfin, nos résultats montrent que l'utilisation de sépiolite soniquée (sSep) stimule encore de plus de 2 fois l'efficacité de transformation bactérienne. Au total, en comparaison avec les méthodes précédentes, les modifications que nous avons apporté (provenant des connaissances de récoltées dans l'étude présente) ont augmenté l'efficacité de transformation bactérienne de 20 à 30 fois.

Compte tenu du fait que nous avons déterminé les conditions de désorption de l'ADN de la sépiolite, nous avons testé la possibilité d'extraire de l'ADN plasmidique des bactéries. Une culture de bactéries contenant un plasmide a été réalisée; après lyse des bactéries le surnageant a été incubé avec de la sépiolite en présence de magnésium ; enfin l'ADN a été élué par une solution d'EDTA. Nous avons ainsi pu récupérer de l'ADN plasmidique (environ 80 μg pour 20 ml de culture bactérienne saturée). De plus l'indice de pureté (A_{260}/A_{280}) était de 1,7, indiquant un bon niveau de pureté de l'ADN plasmidique. L 'analyse, par électrophorèse et TEM, des différentes isoformes a montré une grande majorité des formes super-enroulées ce qui est indicateur d'un ADN plasmidique de bonne qualité. Enfin, l'ADN extrait peut être digéré

par une enzyme de restriction montrant ainsi qu'il est qualité propre à être utilisé pour des expériences de biologie moléculaires.

En conclusion, nous avons réussi à synthétiser un nouveau bionanocomposite, en assemblant de l'ADN sur de la sépiolite et nous avons caractérisé ce complexe par différentes méthodes complémentaires. Nous avons aussi montré que la sépiolite était capable de transférer stablement de l'ADN dans les cellules de mammifères et dans les bactéries, et nous avons développé des stratégies permettant de stimuler fortement l'efficacité de transfert. Grâce à ses caractéristiques la sépiolite représente un nano-vecteur prometteur. En effet, en plus des propriétés décrites et caractérisées ici, la sépiolite possède deux caractéristiques supplémentaires : premièrement, grâce à sa fluorescence naturelle, il doit être possible de trier les cellules contenant le complexe Sep/DNA par cytométrie de flux ; deuxièmement comme la sépiolite est capable aussi de fixer des protéines, elle pourrait donc permettre de co-transférer des enzymes et de l'ADN, ce qui peut représenter un développement futur intéressant notamment pour de nouvelle stratégies de thérapie génique.

Grâce à son faible coût, la simplicité et la facilité des méthodes de synthèse décrites dans ce travail, les capacités de transfert de gène, les possibilités d'augmenter l'efficacité de transfert et les développements futurs prometteurs, la sépiolite représente donc une méthode attractive de transfert de gène dans les cellules de mammifères.

Abbreviations

AIDS acquired immunodeficiency syndrome

AFM atomic force microscopy

Al-OH Aluminol groups

AEC anion-exchange capacity

ATP Adenosine triphosphate

BDMA Benzyldimethylamine

bp – base pairs

CEC cation-exchange capacity

CME clathrin-mediated endocytosis

CNTs Carbon nanotubes

CvME caveola-mediated endocytosis

DEAE Diethylaminoethyl

DMEM Dulbecco's modified Eagle's medium

DNA Deoxyribonucleic acid

dsDNA double-stranded deoxyribonucleic acid

EDTA Ethylenediaminetetraacetic acid ($C_{10}H_{16}N_2O_8$)

EGFP enhanced green fluorescent protein

EMSA electrophoretic mobility shift assay

FACS fluorescence activated cell sorting

FBS fetal bovine serum

FE-SEM field emission-scanning electron microscopy

FTIR Fourier transform infrared

GFP green fluorescent protein

GTP guanosine triphosphate

HDTMA hexadecyltrimethylammonium

HEPES 4-2-hydroxyethyl-1-piperazineethanesulfonic acid

HR homologous recombination

IARC International Agency of Research on Cancer

IR Infrared

LDH layered double hydroxide

LDHs layered double hydroxides

LB Luria-Bertani (medium for the growth of bacteria).

MEM modified Eagle's medium

Mg-OH hydroxyl groups

OD600 Optical density at 600 nm

PMED particle-mediated epidermal delivery

PEI polyethyleneimine

PGEs pencil graphite electrodes

PVA Polyvinyl alcohol

RNA Ribonucleic acid

Si-OH Silanol Groups

Sep Sepiolite

Sep/DNA sepiolite/DNA

ssDNA single-stranded deoxyribonucleic acid

sSep sonicated sepiolite

SWCNTs single-walled carbon nanotubes

siRNA small interfering RNA

SMGT sperm-mediated gene transfer

SPE solid phase extraction

Tris tris(hydroxymethyl)methylamine

UV ultra-violet

Contents.

RESULTS AND DISCUSSION

Structure of Chapter 1

1. **General Introduction.**

   1.1 Gene therapy and DNA transfection.

   1.1.1 Transfection methods.

   1.1.2 Nanocarriers for DNA transfection.

   1.1.3 Nanocarriers based on clay minerals for DNA transfection.

   1.1.4 Comparison of transfection methods.

   1.1.5 Cellular internalization and intracellular fate of the nanocarriers.

   1.2 Clay minerals.

   1.2.1 Kaolin group (kaolinite and halloysite).

   1.2.2 Smectites.

   1.2.3 Micro and nano-fibrous clay minerals: sepiolite and palygorskite.

   1.2.4 Layered double hydroxides (LDH).

   1.3 Bionanocomposites: new tool and strategies for biomedical applications.

   1.4 Interaction of clay minerals with DNA: applications and their role with evolution of life.

   1.5 Interactions between sepiolite and DNA. The Yoshida effect and bacterial transformation.

   1.6 Objectives of the Dissertation.

1. General introduction.

Transfer of DNA into biological organisms is a pivotal issue to design novel promising strategies for gene therapy and/or the development of new biological models of interest for both academic and applied medical, biological/biotechnological, and agronomic research. Remarkably, the development of novel nanocarriers, using bionanocomposites, for non-viral gene transfer constitutes a hopeful approach for treatment of genetic disorders, cardiovascular diseases, AIDS, Alzheimer, multiple sclerosis and cancer.[1–5]

Clay minerals (natural silicates of aluminium and/or magnesium) represents one of the most abundant groups of inorganic solids in interaction with the biosfere.[6] They have been implicated in the prebiotic synthesis of biomolecules at origins of life.[7] Because of their functional properties, bionanohybrids materials resulting from the combination of biopolymers with nanoparticles, as for instance clay minerals[8–12], represent seductive prospects for biomedical applications[13,14] such as biosensors, scaffolds for tissue engineering, effective drug-delivery nanovehicles, vaccination, and wound dressings. [15–22]

Therefore, the determination of the nature of the interactions of biomolecules adsorbed on clay minerals is of crucial importance for biological fundamental knowledge as well as for applications spanning from the understanding of the origin of life, soil ecosystem, to genome-engineering.[23] Here, we focused on the synthesis and physicochemical characterization of new DNA-based bionanocomposites, in which nucleic acids are assembled to sepiolite nanofibrous clay. Indeed, its biocompatibility and nanoscale dimensions of sepiolite provide to this nanoparticulated natural silicate of very

promising properties for their application as drug delivery systems, and might also providing new strategies for vectorization of biological molecules such as DNA.

Sepiolite is a natural hydrated magnesium silicate [24,25] of theoretical unit cell formula $Si_{12}O_{30}Mg_8(OH,F)_4(H_2O)_4,8H_2O$ [26,27]. The structure of sepiolite shows an alternation of blocks and tunnels that grow up in the fiber direction. The blocks are constituted by two layers of tetrahedral silica sandwiching a central magnesium oxide-hydroxide layer. The discontinuity of the silica sheets gives rise to the presence of silanol groups (Si-OH) at the edges of the channels, which are the tunnels opened to the external surface of the sepiolite particles [28]. Tunnels and channels are filled with two types of water molecules:

- coordinated water molecules, which are bonded to the Mg^{2+} ions located at the edges of octahedral sheets, and
- zeolitic water, which is associated to the former ions through hydrogen bonding.

One of the advantages of fibrous clays compared to “conventional” clays based on layered silicates (*i.e.* smectites and vermiculites) is the high density of surface silanol groups, *ca.* 2 Si–OH groups/nm^2, which allows hydrogen bonding in addition to van der Waals interactions at the silicate interface interacting with diverse organic species[24]. Moreover, this silicate shows a cation-exchange capacity (<20 mEq/100 g) resulting from partial isomorphous substitutions of magnesium by aluminium and other trivalent metals in the octahedral sheet belonging to the structure of sepiolite. So, the negatively charged surface could assure also ionic interactions in the assembly of sepiolite with inorganic cations, as well as molecular positively charged species. The

nature of sepiolite surface showing large specific surface area, negatively electrical charge together its fibrous morphology make sepiolite as a platform for co-delivery of different kinds of bioactive species. Indeed, sepiolite has been shown to interacts with polysaccharides[29,30], lipids[15], proteins [31–33] and virus[34] giving rise to a great diversity of bionanocomposites[14]. It must be remarked that the length of nanofibers corresponding to the sepiolite selected in this work make it suitable for cellular intake, and interestingly have a natural and perfectly stable intrinsic fluorescence. Therefore, taking advantage of this natural fluorescence, it should be possible to select cells containing sepiolite by conventional cell sorting techniques. Finally, sepiolite is a natural and abundant silicate which is considered non-hazardous and non-carcinogenic by the International Agency of Research on Cancer (IARC) and the European guidelines.

Toxicity of sepiolite clay mineral is controversial as it is apparently related to fiber length and crystallinity, which are determined by the geological origin of the silicate[35]. Consistently, *in vitro* and *in vivo* tests, as well as epidemiological studies, have also confirmed that at least sepiolite from Taxus Basin deposits in Spain does not constitute a health risk[36].

In this context, the Nanostructured Hybrid, Biohybrid and Porous Materials Group belonging to the Materials Science Institute of Madrid (ICMM-CSIC) has pioneered the innovative development of biohybrid materials based on layered and fibrous clay minerals combined with biopolymers[8,15–17,29,31,32,34,37–39,39–42] such as polysaccharides (chitosan, alginate, pectin, carrageenans...), proteins (gelatin, zein), lipids (phosphatidylcholine), and more recently DNA[41] in collaboration with the group of Reparation, Recombination and Cancer

belonging to the Institute Gustave Roussy (IGR). Indeed, after preliminary results obtained at the ICMM-CSIC, the project in which Sepiolite/DNA (Sep/DNA) bionanocomposite would be synthesized, characterized and studied for possible biomedical applications will be then carried out at IGR, the results being integrated in the present PhD dissertation.

In order to show the fundamentals and to update the basic concepts related with the multidisciplinary aspects of this Thesis, it will be necessary to introduce some basic concepts on different topics related with life and material science. Therefore, the present chapter (Chapter 1) will introduce and discuss the gene therapy and DNA transfection, clay minerals, bionanocomposites, the interaction between clay minerals and DNA, particularly between sepiolite and DNA, and finally, some aspects about bacterial transformation. In turn, Chapter 2 deals with the used methods for synthesis, characterization and protocols developed in this Dissertation.

The results with the main salient features of this investigation are presented and discussed in the following four chapters: Chapter 3 starts with a characterization of sepiolite fibers with atomic force microscopy (AFM) and transmission electron microscopy (TEM). By combining fluorescent microscopy, TEM, time-lapse video microscopy and flow cytometry analysis (FACS), the interactions of sepiolite fibers and mammalian cells were studied, including dose response of sepiolite dispersion in cancerous cells, the capacity of internalization and mechanisms of cellular entry. A detailed physicochemical characterization (using spectrophotometer, AFM, TEM, FTIR and zeta potential) of sepiolite-DNA interactions will be showed in Chapter 4. UV-vis spectroscopy will be used to prove that sepiolite efficiently binds different kinds of DNA

(genomic, plasmid, single strand and double strand oligonucleotides) with a controlled efficiency, and that it will be also possible to have a controlled desorption of previously adsorbed DNA onto sepiolite.

Biological applications of Sep/DNA bionanocomposite are detailed in the following two chapters. In Chapter 5 the study of the internalization of Sep/DNA in mammalian cells is presented, in which will be also proved that the bionanocomposite is actually able for stably transfer plasmid, with a transfection efficiency that can be optimized, being this the main result of the Thesis. In addition, some other biological application of the sep/DNA bionanocomposite in bacteria, such as the improvement of bacterial transformation, and also DNA extraction from bacteria using sepiolite, are introduced in Chapter 6.

1.1. Gene therapy and DNA transfection

The application of the methods and principles of physics to the study of biological systems supposed an outstanding revolution for modern science. A paradigmatic case of this was the identification of deoxyribonucleic acid (DNA). Thus, in 1869 the Swiss physician Friedrich Miescher was the first one to achieve the isolation of what he called “nuclein”[43]. However, more than a century later, there are still a lot of open questions around the physical properties of DNA, for instance: How does DNA respond to force and negative torque? How does confinement of DNA in cellular nuclei affect the structure and dynamics of DNA?[44]

The most remarkable success related to DNA description occurred in 1953, when the physicist Francis Harry Compton Crick, together with the biologist

James Dewey Watson, proposed in the journal Nature the double-helix model of DNA structure accepted until today[45].

Beside DNA, there is another type of nucleic acids: the ribonucleic acid (RNA). Both, the DNA and the RNA are polymeric chains in which the repeating units (known as nucleotides) are joined by covalent bonding between the sugar of one nucleotide and the phosphate group of the next one, and form into a long polymer or strand of DNA. The result is an alternating sugar-phosphate backbone. The DNA molecule comprises two helical chains each coiled round the same axis.

In the DNA molecule, a single strand is irregular and if it consists of N monomers, there can be 4^N different combinations of bases, so the molecule carries 2^{2N} bits of information. The sequence of the complementary strand is entirely determined by the template strand, and therefore double stranded DNA does not carry more information than single stranded, even though it uses twice the amount of material. In spite of this, almost all organisms encode their genetic information on double-stranded DNA[44]. Usually the DNA and RNA are referred as polynucleotides, and when we talk about small polymers, with only a few nucleotides, we referred them as oligonucleotides.

The phosphate group is a strong acid, and this is the reason that the DNA and RNA are referred to as nucleic acids. Each monomer in the DNA or RNA provides a negative charge at physiological pH. The sugar chain is the backbone of the molecule. Each monomer is associated with a nitrogenous base. There are two kinds of bases called purines and pyrimidines. DNA has

two purines, adenine (A) and guanine (G) and two pyrimidines, thymine (T) and cytosine (C). RNA has the same except that uracil (U) replaces thymine.

The fundamental role of nucleic acids is the storage and transmission of genetic information, since they are present in any life form. Each organism carries in each of their cells at least one copy of all its genetic information, required by it, and this is termed "genome". Genome size varies greatly between organisms. For example the genome of a virus may be only a few thousands of base pairs (bp), while the human genome contains about $2x10^9$ bp of DNA distributed in 23 chromosomes. The genome of the bacteria E. Coli has a size approximately of $4.7x10^6$ bp.

Taking into account the key role of DNA molecule in the functioning of living organisms and also that, as a nucleic acid, is one the three chief molecules together with proteins and carbohydrates in living organisms, DNA applications vary from medical applications (*e.g.* DNA vaccines), forensics and advanced technology, to anthropology, basic sciences and DNA nanotechnology. Among most important opportunities in DNA nanotechnology is the fabrication of nanomachines with useful functions[44], such as programmable DNA based motors that move on linear tracks[46], DNA nanorobots that kill cancer cells[47] and DNA nanohybrids for a next-generation of data storage devices[48,49].

In the last two decades, potential therapeutic bio-macromolecules like nucleic acids, including plasmids and small interfering RNA (siRNA), have been widely explored for treatment or prevention of various human diseases[50], like cancer[51–57], genetic disorders[58–60] and cardiovascular diseases[61–63]. In terms of

delivery, therapeutic nucleic acids must be transported to the nucleus before producing their biological effects.

Plasmids are small circular DNA molecules that are naturally maintained in bacteria. To describe non-viral DNA transfer in bacteria and non-animal eukaryotic cells (like yeast and plant cells) is used the term “transformation” (or bacterial transformation). Such a mechanism is thought to have been involved in gene transfers during evolution and particularly in transfers among unrelated organisms such as plants and bacteria[64].

The process of deliberately introducing foreign nucleic acids or even proteins such as antibodies into the nucleus of mammalian cells using a non-viral method is called “transfection” (from a blend of “trans”- and “infection” terms). Transfection has origins as far back as the 1950s[65]. Transfectants are cells that have incorporated the foreign DNA. If foreign DNA is integrated in their genome, cells are called stable transfectant; and if DNA does not integrate in the genome but genes are expressed for a limited time such as three-four days, then cells are called transient transfectants.

Gene therapy, in essence, is defined as the insertion, removal, or manipulation of one or multiple genes inside a cell to cure a specific disease[66]. It has long been regarded a promising treatment for many diseases, including inherited through a genetic disorder (such as hemophilia, human severe combined immunodeficiency, cystic fibrosis, etc) or acquired (such as AIDS or cancer)[67]. Gene therapy has three components[68]:

1. Identification of the gene that is mutated in the disease and obtaining a healthy copy of that gene.
2. The carrier or delivery vehicle called vectors to deliver the healthy gene to a patient's cells, and
3. Additional DNA elements or proteins that turn on the healthy gene in the right cells and at the right levels.

Figure 1.1 shows the percentage of indications addressed in gene therapy from 1996 clinical trials reported this year (2014).

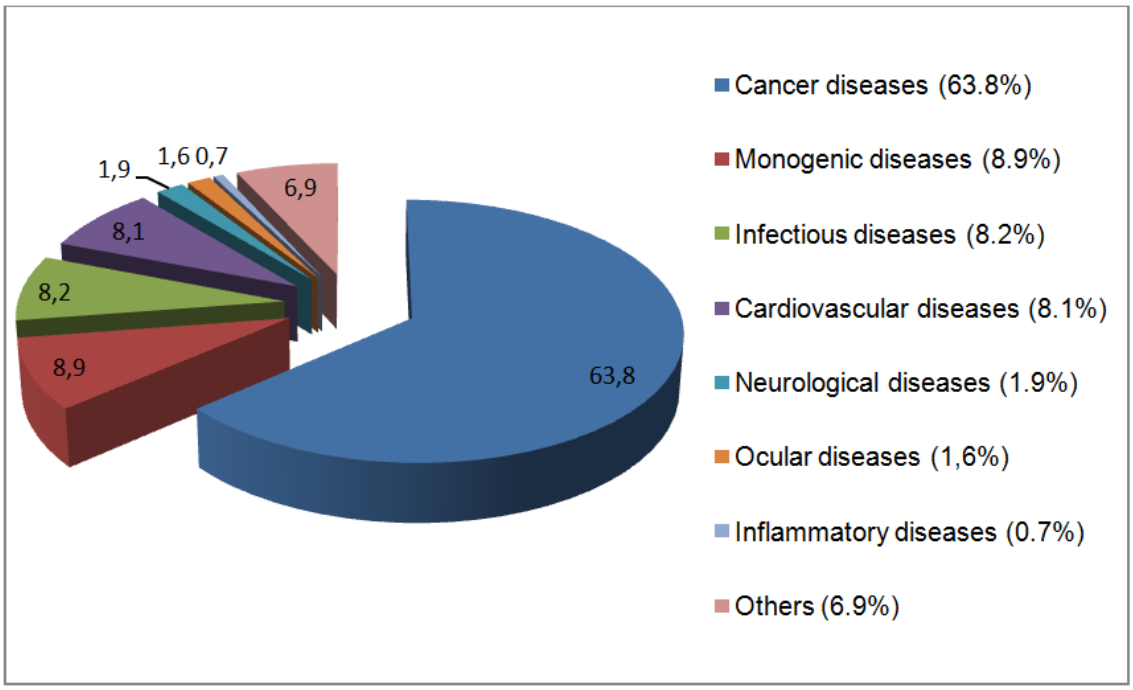

Figure 1.1 Indications addressed by gene therapy clinical trials (adapted from the Journal of Gene Medicine, © 2014 John Wiley and Sons Ltd in http://www.wiley.co.uk/genmed/clinical, update June 2014).

1.1.1. Transfection methods.

There is a broad range of different transfection methods, which were summarized in figure 1.2. Starting from viral vectors to non-viral delivery

systems, where two groups were identified: chemical and physical methods. Common transfection instrument-based methods include electroporation, biolistic technology, micro/nanoinjection and laserfection/optoinjection. Since chemical delivery typically relies on the use of electrostatic interactions between cationic compounds and the negatively charged backbone of nucleic acids, transfection reagents are commonly composed of cationic liposomes and cationic polymers, that form electrostatic complexes with the nucleic acids, being in this way two typical classes of non-viral chemical vectors methods[69]. They also include calcium phosphate precipitation for DNA transfection[70]. The use of nano-sized carriers or nanocarriers was included in the group of physical methods. This is the case of inorganic nanoparticles, magnetic nanoparticles for magnet-mediated transfection or magnetofection, and the recent use of clay minerals and layered double hydroxides (LDHs, also called anionic clays) to prepare DNA-based bionanocomposites suitable for DNA transfection.

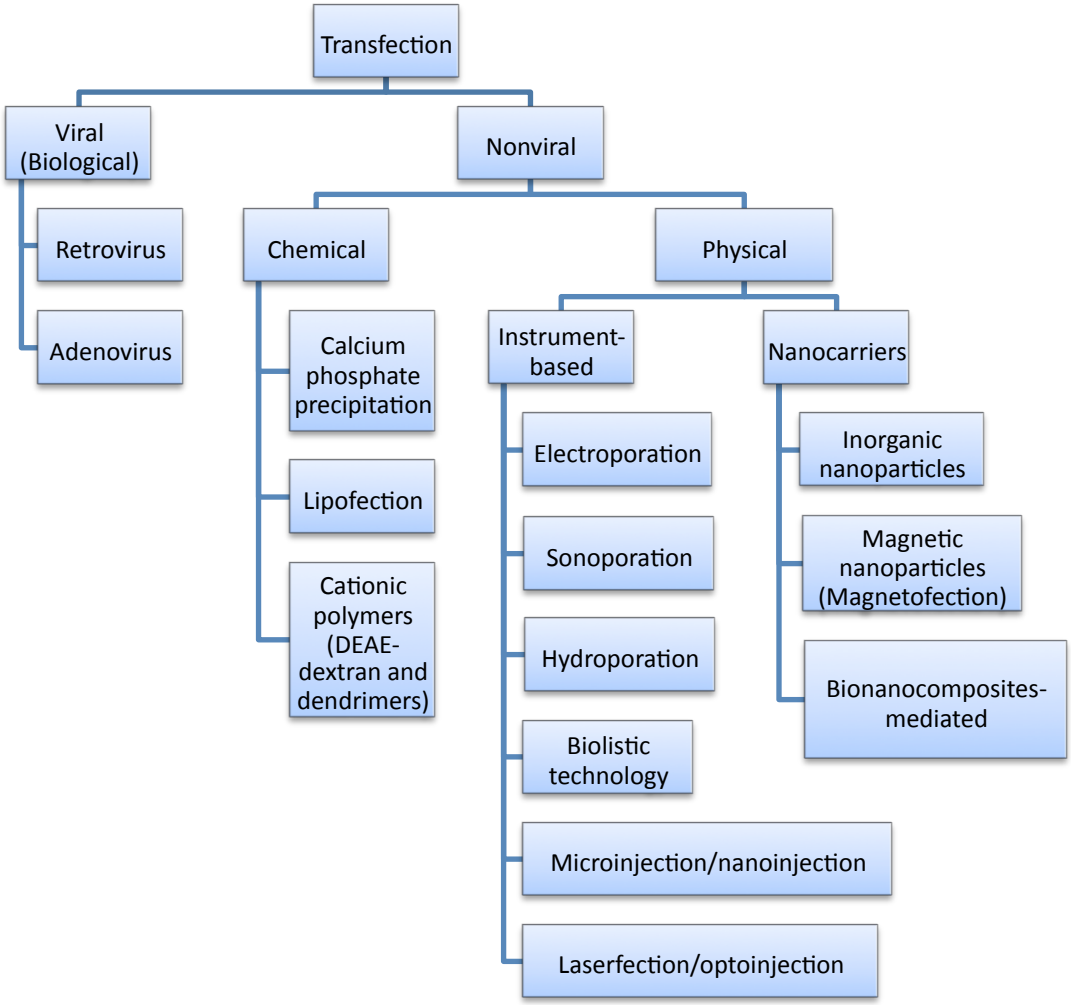

Figure 1.2 Classification of different transfection methods.

Gene delivery using physical principles has attracted increasing attention. These methods usually employ a physical force to overcome the membrane barrier of the cells and facilitate intracellular gene transfer. The simplicity is one of the characteristics of these methods[67]. The genetic material is introduced into cells without formulating in any particulate or viral system.

Electroporation is a physical transfection method[71], which exposes a cell to a high-intensity electric field that temporarily destabilizes the membrane. During this time the membrane is highly permeable to exogenous molecules present in

the surrounding media. DNA then moves into the cell through these holes, and when the field is turned off, the pores in the membrane reseal, enclosing the DNA inside.

Hydroporation, also called hydrodynamic gene delivery method, is the most commonly physical method used for gene delivery to hepatocytes in rodents[72]. Similar to the mechanism of electroporation where membrane pores are generated by ion movement in an electric field, the hydrodynamics-based procedure generates membrane pores by a highly pressured solution in the liver[72]. Intra-hepatic gene delivery is achieved by a rapid injection of a large volume of DNA solution via the tail vein in rodents, that results in a transient enlargement of fenestrae, generation of a transient membrane defect on the plasma membrane and gene transfer to hepatocytes[73]. This method has been frequently employed in gene therapy research. In order to apply this simple method of gene administration to the clinic, efforts have been made to reduce the injection volume and avoid tissue damage[67].

Sonoporation utilizes ultrasound to temporally permeabilize the cell membrane to allow cellular uptake of DNA. This method has been applied in the brain, cornea, kidney, peritoneal cavity, muscle, and heart, among others. Low-intensity ultrasound in combination with microbubbles has recently acquired much attention as a safe method of gene delivery[74]. The use of microbubbles as gene vectors is based on the hypothesis that destruction of DNA-loaded microbubbles by a focused ultrasound beam during their microvascular transit through the target area will result in localized transduction upon disruption of the microbubble shell while sparing nontargeted areas. The therapeutic effect of

ultrasound-targeted microbubble destruction is relative to the size, stability, and targeting function of microbubbles[67].

Biolistic transformation[75] is the delivery of nucleic acids into cells via high velocity nucleic acid–coated metal microparticles (tungsten or gold), more commonly referred to as a gene gun. This method can also deliver DNA *in vivo* for gene therapy, as for example in particle-mediated epidermal delivery (PMED)[76], shown to induce protective levels of antibody and T-cell responses in animals and humans against a wide variety of diseases, including influenza. Biolistic transformation could be also called ballistic DNA injection, particle bombardment or micro-projectile gene transfer[67]. The accelerating force for DNA-containing particles can be high-voltage electronic discharge, spark discharge or helium pressure discharge. One advantage of this method is that it allows delivering of precise DNA doses. However, genes express transiently, and considerable cell damage occurs at the centre of the discharge site[67]. This method has been used in vaccination against the influenza virus[76] and in gene therapy for treatment of ovarian cancer[77].

Microinjection is the direct injection of naked DNA. The DNA is directly injected through a needle-carrying syringe into tissues. Several tissues have been transfected by this method: muscle, skin, liver, cardiac muscle, and solid tumors[73]. DNA vaccination is the major application of this gene delivery system[78]. The efficiency of needle injection of DNA is low; moreover, transfection is limited to the needle surroundings. Interestingly, some recent reports indicates a new low-invasive gene delivery method with the use of nanoneedle technology for DNA delivery using atomic force microscopy (AFM)[79], which could be called nanoinjection. The nanoneedle is 200 nm in

diameter, 6 μm in length, is operated using an AFM system and could be inserted into the nucleus directly without causing significant cell damage[80]. With nanoinjection a highly efficient gene delivery of over 70% was achieved in human cells, which compared very favorably with other major nonviral gene delivery methods (lipofection approximately 50%, microinjection approximately 10%)[81].

In the laserfection/optoinjection[82–84], the procedure uses laser light to transiently permeabilize a large number of cells in a very short time. Various substances can be efficiently optoinjected, including ions, small molecules, dextrans, siRNA, plasmids, proteins, and semiconductor nanocrystals, into numerous cell types.

The use of cationic lipids as transfecting agents of DNA has received an increasing attention in the last two decades[85]. Cationic liposomes include lipid-mediated gene delivery, which is also referred to as lipofection, or liposome-based gene transfection. It uses lipids to cause a cell to absorb exogenous DNA. Transfer of genetic material into the cell takes place via liposomes, which are vesicles that can merge with the cell membrane since they are both made of a phospholipid bilayer.

Cationic polymers include polyethyleneimine (PEI) and dendrimers. Dendrimers have attracted intense interest since their emanating research in the 1980s and are extensively studied as efficient DNA delivery vectors in gene transfer applications[86], due to their unique features based on the well-defined and multivalent structures[87].Cationic polymers differ from cationic lipids in that they do not contain a hydrophobic moiety and are completely soluble in water. Given their polymeric nature, cationic polymers can be synthesized in different

lengths, with different geometry (linear versus branched). The most striking difference between cationic lipids and cationic polymers is the ability of the cationic polymers to more efficiently condense DNA. There are three general types of cationic polymers used in transfection: Linear (histone, spermine, and polylysine), branched and spherical.

Calcium phosphate is the oldest and most inexpensive non-viral chemical procedure for DNA transfection. The protocol involves mixing DNA with calcium chloride, adding this in a controlled manner to a buffered saline/phosphate solution, and allowing the mixture to incubate at room temperature. This step generates a precipitate that is dispersed onto the cultured cells. Cells via endocytosis or phagocytosis take up the precipitate. Additional modifications to the calcium phosphate method that can achieve higher efficiencies include glycerol shock[88] and/or chloroquine treatment[89].

1.1.2. Nanocarriers for DNA transfection.

Searching for efficient and safe transport nanocarriers to delivery biomolecules and drugs into cells has been challenging and exciting area of research[90]. Increasing efforts in research and development worldwide have been devoted to various inorganic materials as novel non-viral nanocarriers in the last decade[91–93]. Many inorganic materials, such as gold, carbon nanotubes, inorganic nanoparticles, silicon oxide, iron oxide and LDH, have been studied for this purpose[90].

Although recent studies indicate that carbon nanotubes (CNTs) exhibit high toxicity[94–96] and could be carcinogenic[97], it was reported that CNTs also provide another promising vector system for the target delivery of drugs,

proteins and genes because of their good biocompatibility, low cytotoxicity, unique physicochemical properties in chemistry, electrics, optics and mechanics[90]. More importantly, CNTs offer some interesting advantages over spherical nanoparticles for biomedical and biological applications. For instance, their large inner volume allows the loading of small biomolecules while their outer surface can be chemically modified to render themselves various novel features that can be used to load proteins and genes for effective drug delivery[98–100].

Inorganic nanoparticles generally possess versatile properties suitable for cellular delivery, including wide availability, rich functionality, good biocompatibility, potential capability of targeted delivery (*e.g.* selectively destroying cancer cells but sparing normal tissues) and controlled release of carried drugs[90]. They can be easily prepared and surface-functionalized. They exhibit good storage stability, are not subject to microbial attack[74], show low toxicity and promise for controlled delivery properties, thus presenting a new alternative to viral carriers and cationic carriers. However, it is noted that the cellular transfer efficiency with existing inorganic nanoparticles is relatively low[90].

Silica-coated nanoparticles are biocompatible structures that have been used for various biological applications including gene therapy due to its biocompatibility[101]. Mesoporous silica nanoparticles have shown gene transfection efficiency “in vitro” in glial cells[102]. Gold nanoparticles have been lately investigated for gene therapy. For instance, gold nanorods have been proposed to deliver nucleic acids to tumours[74]. The near-infrared light can penetrate deeply into tissues; therefore, the surface of the gold could be

modified with double-stranded DNA for controlled release[103]. After irradiation with near-infrared light, single stranded DNA is released due to thermal denaturation induced by a photothermal effect[67].

One interesting kind of nanocarrier, which increases transfection efficiency, are certain magnetic nanoparticles. The magnet-mediated transfection or magnetofection uses magnetic force acting on gene vectors that are associated with magnetic particles[104,105]. Then, application of magnetic force drives the nucleic acid–particle complexes toward and into the target cells, where the cargo is released.

1.1.3. Nanocarriers based on clay minerals for DNA transfection.

The potential to employ clay-based nanohybrids (bionanocomposites), for non-viral gene delivery is also being explored in recent years. The protective effect of clay nanoparticles has been convincingly demonstrated by the ability of clays to mediate the transfection of gastro-intestinal cells following oral delivery of DNA clay-complexes[106].

Gene delivery with montmorillonite indicated protection against DNA degradation within both the acidic environment of the stomach and the nuclease-rich intestinal environment[107], and successfully delivered the DNA into cells of the small intestine. Another approach employed montmorillonite modified with alkylammonium cations to which is assembled DNA to achieve transfection of dermal fibroblasts, albeit at a low efficiency[2]. Authors propose that the presence of the hexadecyltrimethylammonium (HDTMA) cations intercalated into the interlayer of montmorillonite is able to act as a layer expander that facilitates DNA accommodation, however not experimental proof

of this intercalation is afforded. Anyway, DNA remains adsorbed on the organoclay and it was successfully transfected into the nucleus of human dermal fibroblast and expressed enhanced green fluorescent protein (EGFP) gene with green fluorescence emission[2].

An hybrid material using the layered silicate rectorite was developed as novel non-viral vector, which combines the advantages of both biopolymer and clay in a gene delivery system[108]. Rectorite was employed to enhance the utility of chitosan as a gene delivery vector. Incorporation of rectorite significantly improved the complexation of DNA compared with chitosan alone and enhanced the transfection efficiency to achieve 90% transfection after 5 days in vitro. Robust GFP expression in the gastrointestinal tract following oral delivery again indicated the protective effect of the clay on the plasmid[108].

Gene transfer using clay minerals was already reported in the production of transgenic animals. The sperm-mediated gene transfer (SMGT) is based on the intrinsic ability of sperm cells to bind and internalize exogenous DNA molecules and to transfer them into the oocyte at fertilization[109]. Recently, halloysite clay nanotubes were used as a transfection reagent to improve transgene transmission[110], proving that nano-SMGT is able to transmit exogenous DNA molecules to bovine embryos. In this research, four transfection systems were used: naked DNA (without carrier), lipofection, chemical (with a polymer), and halloysite clay nanotubes. According to their results, nanotransfectants were more effective than other common transfection methods for SMGT[110–114].

Biocompatible nanoparticles, like inorganic LDHs, possessing negligible toxicity, high anionic exchange capacity, and pH dependent solubility, have attracted increasing attention as nano-carriers for drugs and bio-active

molecules[1,111–114]. A number of experiments have been reported involving the intercalation (loading) of nucleotides, oligonucleotides and genes into the LDH interlayer[1,114,115], the cytotoxicity of LDH materials to the cells[115,116], the cellular uptake of LDH nanoparticles[1,116,117], and the in vitro gene transfection tests in different cell lines[1,116] as well as target delivery by conjugating the antibody protein[116]. These investigations indicate that the use of LDH nanomaterial as delivery vectors can improve the cellular uptake of biomolecules[118], and could be used as an effective gene delivery system[119]. Thus, for instance, it has been reported that by using LDH nanoparticles as vectors, the transfer of ATP into HL-60 cells can be speeded up by 25, 12 and 4 times as compared with the ATP solution delivery after incubation for 2, 4 and 24 h, respectively, at 37 ◦C and pH = 7.4[118].

It was also reported the LDHs as DNA delivery vector in order to enhance anti-melanoma immune response[120]. Here, over 60% tumour-free and inhibition of melanoma growth was observed in mice that treated with DNA/LDH complexes, whereas no tumour-free mice were found in the control group. After treatment with DNA/LDH complexes, it was observed a significant delay in tumour growth and potent prolongation of mean survival time (from 35 to 50 days). These results suggested that the LDHs mediated cellular transportation could significantly enhance the therapeutic efficacy of DNA immunization, as well as protective immunity against tumour[119].

1.1.4. Comparison of transfection methods.

A comparison of viral and non-viral transfection methods, with advantages and disadvantages, are shown in table 1.1. Chemical methods for non-viral

transfection are also compared in table 1.2 and physical methods in table 1.3 - 1.4. Information about some methods were summarized, adapted and complemented from http://www.bio-rad.com, and https://www.mirusbio.com.

Transfection method	Advantages	Disadvantages
Viral vectors	High efficiency; Simplicity of infection; Sophisticated endosomal releasing mechanisms[121].	Limited clinical application because strong immunogenicity and potential fatal adverse effects[122–125]; Possible oncogenic effects; Labor intensive; P2 containment required for most viruses; Institutional regulation and review boards required; Viral transfer of regulatory genes or oncogenes is inherently dangerous and should be carefully monitored; Host range specificity may not be adequate; Many viruses are lytic; Need for packaging cell lines.
Non-viral nanocarrier	Relatively low toxicity and immune response; biocompatibility and controllability.	Generally poor efficiency[126].

Table 1.1 Comparison between viral and non-viral transfection methods.

Transfection method	Advantages	Disadvantages
Lipid-mediated gene delivery	Deliver nucleic acids to cells in a culture dish with high efficiency; Easy to use, minimal steps required; adaptable to high-throughput systems; Using a highly active lipid will reduce the cost of lipid and nucleic acid, and achieve effective results.	Not applicable to all cell types
Cationic polymers	Inexpensive, easy to perform and quick, can be applied to a wide range of cell types.	In high concentrations can be toxic to cells; Transfection efficiencies will vary with cell type; Can be used only for transient transfection; Typically produces less than 10% delivery in primary cells.
Calcium phosphate	Inexpensive, high efficiency (cell type dependent), can be applied to a wide range of cell types, can be used for transient and stable transfection.	Ineffective for hard-to-transfect cells;Very sensitive to changes in pH, often lacks reproducibility, and requires large quantities of DNA.

Table 1.2 Comparison between chemical transfection methods.

Transfection method	Advantages	Disadvantages
Electroporation	Easy to perform, High efficiency in a wide range of cell types	High cell mortality
Hydroporation	Simple, convenient, and efficient method for intracellular delivery in vivo in hepatic cells[72].	Other tissues have not been fully explored. Hydrodynamic impact at cellular level is not homogenous. High injection volume and tissue damage.
Sonoporation	Non-invasive and site-specific. Could make it possible to destroy tumour cells after systemic delivery, while leave non-targeted organs unaffected[74].	Gene delivery efficiency seems to be dependent on the intensity of the pulses, frequency and duration[73].
Laserfection/ Optoinjection	Very efficient; works with many cell types; fewer cell manipulations needed.	Requires the cells to be attached; expensive laser-based equipment needed.
Biolistic particle delivery	Simple, rapid, versatile technique; Cell type independent; Uses small amounts of DNA; Delivers single or multiple genes; No carrier DNA needed; Can deliver large DNA fragments; No extraneous genes or proteins delivered; Requires little manipulation of cells; High reproducibility; allows delivering of precise DNA doses.	Generally lower efficiency compared to electroporation or viral- or lipid-mediated transfection; Limited bacterial transfection data; Preparation of microparticles; Instrument cost; Genes express transiently and considerable damage occurs at the centre of the discharge site.
Microinjection	Can be used for many animals.	Laborious (one cell at a time); Technically demanding and costly.

Table 1.3 Comparison between instrument-based transfection methods.

Transfection method	Advantages	Disadvantages
Inorganic nanoparticles mediated transfection. (Silica coated, gold)	Wide availability, rich functionality, good biocompatibility, potential capability of targeted delivery (*e.g.* selectively destroying cancer cells but sparing normal tissues) and controlled release of carried drugs[90]. They can be easily prepared and surface-functionalized, exhibit good storage stability, are not subject to microbial attack[74], show low toxicity and promise for controlled delivery properties.	Relatively low cellular transfer efficiency.
Magnet-Mediated Transfection	Rapid; Increased transfection efficiency by the directed transport, especially for low amounts of nucleic acids; High transfection rates for adherent mammalian cell lines and primary cell cultures (suspension cells and cells from other organisms also successfully transfected but need to be immobilized); Mild treatment of cells; Can also be performed in the presence of serum.	Relatively new method; Requires adherent cells; suspension cells need to be immobilized.
CNT´s mediated transfection	Large inner volume which allows the loading of small biomolecules; the outer surface can be chemically modified to render themselves various novel features that can be used to load proteins and genes.	High toxicity; could be carcinogenic.
Clay minerals – based nanocarriers for transfection .	Rich array of possible interactions between clay and DNA and other biomolecules with potential interest for the synthesis of new bionanocomposites for transfection; protective effect of clay nanoparticles against DNA degradation; negligible toxicity. The incorporation of certain clays could significantly improve the complexation of DNA.	Low transfection efficiency; variable clay dose response in different cell lines; more work is needed to elucidate the mechanisms for the potential in vitro cytotoxicity of certain clay formulations, cellular uptake and the controversial importance of the effect of particle size and surface area in cytotoxicity.

Table 1.4 Comparison of different nanocarriers for non viral gene therapy.

1.1.5. Cellular internalization and intracellular fate of the nanocarriers.

The success of any gene transfer procedure strictly depends upon the efficiency of nucleic acid internalization by the target cells. As a matter of fact, making gene transfer more safe and efficient remains the most relevant challenge to the clinical success of gene therapy[127].

The plasma membrane lipid bilayer, which is apolar and hydrophobic, constitutes an impermeable barrier to large and charged macromolecules such as DNA and RNA, since, at physiological pH, phosphates in the nucleic acid backbone are deprotonated and thus negatively charged. Nucleic acids are also unstable in physiological conditions and generally unable to cross the cell membrane. Therefore, the entry of these polyanions into the cells needs to be facilitated, usually by exploiting the same cellular mechanisms that normally allow macromolecule internalization. Alternatively, nucleic acids can be loaded vectored into the cells within biological particles that are naturally capable of crossing biological membranes, such as viruses[127].

Nanocarriers are promising tools for biology, because they provide a unique opportunity to overcome cellular barriers to improve the delivery of therapeutic nucleic acids and proteins[128]. These barriers include susceptibility of DNA to be degradated by endogenous nucleases in serum or blood, incapability of DNA to cross plasma membrane unassisted because their negative charges and hydrophilic behaviour. Then, an effective nucleic acid delivery nanocarrier must be able to perform several functions to achieve successful transfection:

- Have a good biocompatibility and low cytotoxicity.

- Be available or readily synthesised with adequate particle size.
- Bind nucleic acids.
- Protect nucleic acids from enzymatic degradation.
- Have an optimum zeta potential and surface functionalization to promote cellular uptake.
- Have physicochemical stability during the whole delivery process.
- Promote endosomal escape and release nucleic acids into the cytoplasm.
- Promote nuclear entry.

As the increasing of the delivery efficiency of nanocarriers remains an important challenge for the clinical development of non-viral vectors[129], it is crucial to study one of the most important steps for non-viral gene delivery: the cellular process (including cellular uptake, transport, endosomal escape and nuclear localization).

Between all intracellular events, the cellular uptake mechanism is the most essential to the nanocarrier efficiency and intracellular fate. Different cellular uptake pathways have different intracellular fates[69]. Some researchers have shown that cellular uptake could affect other cellular processes and, consequently, transfection efficiency[130,131]. Understanding cellular uptake mechanisms, the intracellular fate of the nanocarrier, and their effects on transfection efficiency is crucial to engineering successful reagents or vectors for non-viral gene transfection[132].

After the vectors attach to the cell membrane, there are various mechanisms of nanocarrier cell internalization that are dramatically influenced by its physicochemical properties (size, surface charge properties and shape) and the nature of the target cells[130]. The cellular uptake is divided in endocytic pathways and non-endocytic pathways, which are summarized in figure 1.3. Endocytic groups involves phagocytosis and non-phagocytosis pathways which encompasses macropinocytosis, clathrin- and caveola-mediated endocytosis[133] (CME and CvME respectively).

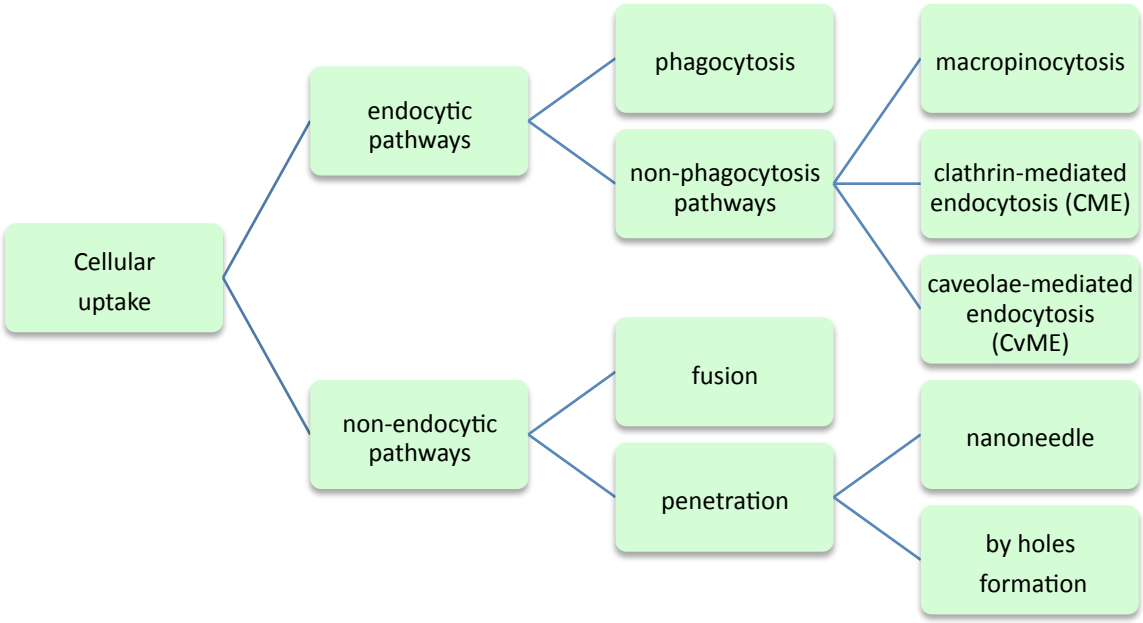

Figure 1.3 Different mechanisms for cellular uptake.

As it is possible to observe in figure 1.4, different endocytosis pathways yield different intracellular fates for vectors, which could potentially explain why the same vector differs in its transfection efficiency in various cell modes. After their entry into the cells, vectors must escape from the endosome or avoid the endo-lysosomal (endosomal and lysosomal) pathway through certain

endocytosis pathways[69]. After escaping the endosome and then entering the cytoplasm, vectors must release DNA or siRNA and finally perform their function in the cytoplasm[134]. In addition, DNA has to be transported into the nucleus.

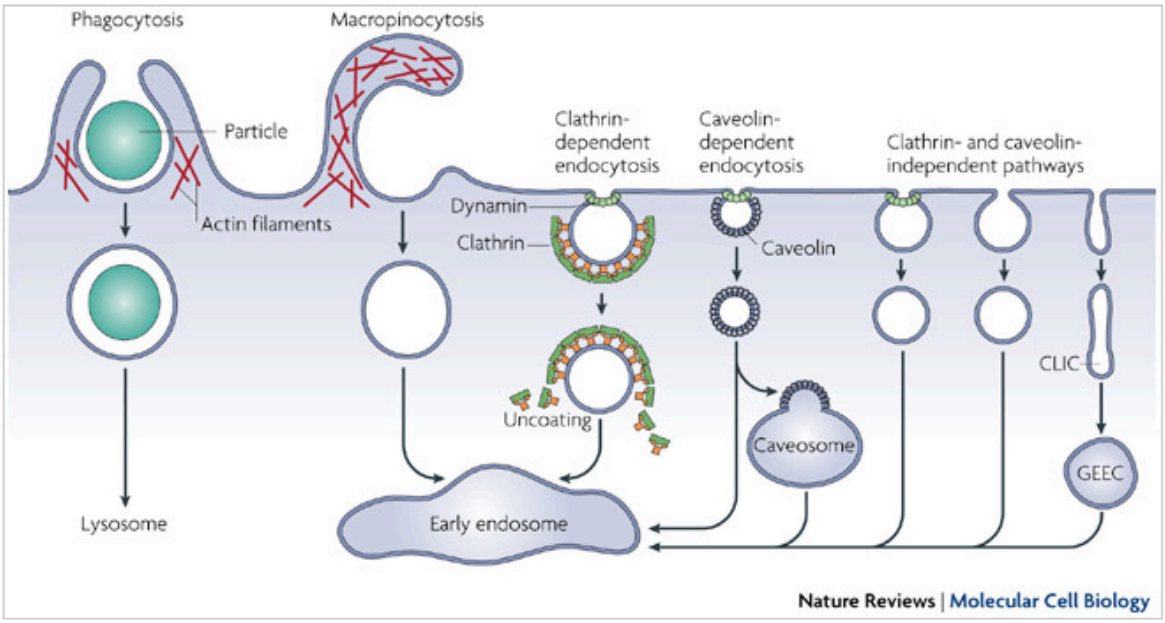

Figure 1.4 Schematic representation of different endocytic pathways, from reference[119].

As it is also possible to observe in figure 1.4, after endocytosis the exogenous particles are immediately transported into the endocytic vesicles. Initially, the delivery vectors are trapped in the early endosomes where the pH drops from neutral to around pH 6. Early endosomes may fuse with sorting endosomes in which the internalized content can be recycled back to the membrane and transported out of the cell by exocytosis[50]. Nucleic acids that fail to be released from these acidic vesicles will ultimately be degraded[136,137].

Like some kind of cellular protection, exogenous particles, including delivery systems and nanocarriers are more often trafficked to late endosomes

which are rapidly acidified to pH 5–6. Subsequently, the late endosomes fuse with lysosomes concomitant with a further reduction to acidic pH (approximately pH 4.5) and degradation by proteases and other degradative enzymes.

Therefore, the pH reduction and the enzymatic degradation process in endosomes/lysosomes is an efficiency-limiting step for successful nucleic acid delivery[134]. Ideal vectors should release their contents from these acidic compartments at an early stage to prevent the fate of lysosomal destruction.

The transfection efficiency of nucleic acid delivery systems is correlated not only to the level of cellular uptake but also with their ability to escape from endosomal compartments[138]. The cellular endosome is a major barrier to efficient gene transfer, and therefore an endosome escape mechanism is a necessary feature of nonviral complexes. Some nucleic acid delivery systems successfully attain high cellular uptake, but fail to achieve good transfection, partly due to their deficiency of endosomolytic property[139].

Phagocytosis is a special type of endocytic pathway which plays a critical physiological role in the defence of the organism against nonself elements, infectious agents (most bacteria and some viruses) as well as exogenous inert particles including drug delivery nanoparticles[133]. It primarily exists in professional phagocytes such as macrophages, monocytes neutrophils, and dendritic cells[140]. Phagocytic pathway is mediated by cup-like membrane extensions that are usually larger than 1 μm to internalize large particles such as bacteria or dead cells. Understanding of the mechanism of phagocytosis is very helpful to the non-viral gene therapy of macrophage-dominated immune diseases such as rheumatoid arthritis. In addition, a phagocytosis-like

mechanism was proposed for the uptake of large lipoplexes and polyplexes that are larger than can be taken up by the classic CME pathway[141].

Compared with phagocytosis, other nonphagocytic pathways such as CME, caveolae-mediated endocytosis (CvME), and macropinocytosis occur in almost all kinds of cell types[142]. CME is the best-characterized type of endocytosis, which occurs constitutively in all mammalian cells, and fulfils crucial physiological roles, including nutrient uptake and intracellular communication. For most cell types, CME serves as the main mechanism of internalization for macromolecules and plasma membrane constituents[133].

This pathway is receptor-dependent, clathrin-mediated, and GTPase dynamin-required[143]. In this pathway, a series of downstream events are activated after the recognition of ligands by receptors on the cell surface. Clathrins assemble in the polyhedral lattice right on the cytosolic surface of the cell membrane, which helps to deform the membrane into a coated pit with a size about 100–150 nm[144]. This process is energy dependant mediated by GTPase dynamin. As the clathrin lattice formation continues, the pit becomes deeply invaginated until the vesicle fission occurs. In the next step of the CME pathway, the endocytosed vesicles internalized from the plasma membrane are integrated into late endosomes and finally transported to lysosomes[69].

Other pathways have been recently described, such as CvME, considered the major one. Caveolae are characteristic flask-shaped membrane invaginations, having a size generally reported in the lower end of the 50–100 nm range[145–148] typically 50–80 nm. They are lined by caveolin, a dimeric protein, and enriched with cholesterol and sphingolipids. Caveolae may

constitute 10–20% of the cell membrane which is an expression of its abundance in endothelial cells[149]. CvMEs receive increasing attention for drug delivery applications using nanocarriers[133].

Macropinocytosis is another type of clathrin-independent endocytosis pathway[150], that non-specifically takes up a large amount of fluid-phase contents through the mode called fluid-phase endocytosis[151]. It occurs in many cells, including macrophages[145]. Macropinocytosis occurs via the formation of actin-driven membrane protrusions, which is similar to phagocytosis. However, in this case, the protrusions do not zipper up the ligand-coated particle; instead, they collapse onto and fuse with the plasma membrane[133]. The macropinosomes have no apparent coat structures and are heterogenous in size, but are generally considered larger than 0.2 μm in diameter[150,152]. This endocytic pathway does not seem to display any selectivity, but is involved, among others, in the uptake of nanocarriers[133].

The endocytosis inhibitors for the study of intracellular fates of complexes are also very important[69] in order to distinguish between different pathways, and more importantly, for increasing the DNA delivery efficiency since they could be able to promote endosomal escape. For example, to distinguish the phagocytic and macropinocytic pathways with CME and CvME pathways, the commonly used inhibitors and methods for phagocytic and macropinocytic pathways are: inhibitors of sodium-proton exchange “amiloride and its derivatives”, F-actindepolymerizing drugs “cytochalasin D and latrunculins”, inhibitors of phosphoinositide metabolism “wortmannin and LY290042”, and protein kinase C activator “phorbol esters”. Within these inhibitors, amiloride and its derivatives may be considered as the first choice for their fewest side effects[69]. Other

inhibitors like monensin and bafilomycin A can inhibit the acidification of endosomes, thus preventing their maturation and fusion into lysosomes[153].

Chloroquine is a weak base that can rapidly penetrate the plasma membrane, accumulate in acidic vesicles and increase the pH of the acidic compartment[154,155]. Preventing endosome acidification subsequently inhibits hydrolytic enzymes such as proteases and nucleases[156]. In addition, Chloroquine also causes the swelling and rupture of endosomal vesicle by increasing the osmotic pressure inside the acidic compartment[137]. Since it can neutralize acidic compartment and induce rupture of endocytic vesicles, adding chloroquine has been shown to improve nucleic acid transfer[157].

Last but not least, the cell-dependence of inhibitors should be noted when experiments are carried out.

To date, two non-endocytic pathways were reported. First one is the most studied and characterized related to the formation of holes in the cell membrane, called “penetration”[158,159]. In this case, the vector could have the ability to be taken up without endocytic events[160], and can directly penetrate cell membranes in a receptor-, and energy-independent way. An analogous case of penetration was also reported for direct translocation of CNTs through the plasma membrane[161], which has been termed by some as the “nanoneedle” mechanism[100,162–165]. It was also reported that cells exhibited different uptake pathways (both energy-dependent and independent mechanisms) for CNTs with different dimensions in terms of diameter and length[166,167] depending on nanotube length, degree of aggregation (and aggregate dimensions) and

surface coat, which could be critical parameters that can switch uptake mechanisms from one to another[166].

The second non-endocytic pathway is called “fusion”, which is special for lipoplexes, as it can cause a direct release of DNA to the cytoplasm before entering the endocytic pathways. However, more and more evidences suggest that fusion with the cell membrane contributes minimally to the overall uptake of lipoplexes, while the CME plays an important role in the uptake of lipoplexes[168]. There have been few studies on non-endocytic pathways, and more efforts are needed to have a comprehensive understanding of these pathways for the improvement of non-viral gene delivery.

There are many factors that are involved in the selection of uptake pathways of non-viral gene complexes. These factors include particle size, particle surface charge, particle shape, cell type, and even culture condition. Because the complexes of different nanocarriers as vectors for DNA or siRNA are usually a group of heterogeneous particles with diverse sizes, surface charges, and shapes, several uptake pathways may be involved in the internalization of one kind of complexes into a single cell type[69]. Particle size is a very important factor for the pathway selection of complexes. Macropinocytosis is also very important for the uptake of large particles of polyplexes (>500 nm)[132]. Complexes with sizes smaller than 500 nm are mainly taken up by CME and CvME[131].

The charge density of a complex is also an important factor for its uptake. The cell membrane consists of a bilayer of lipid and anionic membrane proteins. These anionic proteins are very helpful to the uptake of cationic complexes. However, once the net positive charge falls to neutral, the uptake efficiency will

be inhibited a lot. This is because the neutral charge density will weaken the interaction between complexes and membrane proteins, and it will also increase the aggregation of complexes, which will make them large and hard to be internalized[69].

Consequently, driving forces for transfection such as electrostatic, hydrophobic and hydrophilic (polar) forces, are determined by surface functionalization, in order to load/carry biomolecules onto nanocarriers. In a similar way, functionalization can also alter the adhesive interactions with cell membranes, especially the electrostatic interaction. It was already reported that electrostatic interaction is the primary force to drive nanocarriers to approach the cell surface while hydrophobic and hydrophilic interactions help recognise the specific domains of cell surface[90]. The zeta potential is the critical parameter that indicates the strength of electrostatic interaction, which could vary from 6 to 50 mV. A higher zeta potential provides a stronger driving force, leading to a fast approaching and quick adhering onto the surface of a cell. On the other hand, a lower zeta potential causes a slow approaching to the cells and thus nanocarriers may flow away from the targeted cells during the circulation. There may be an optimum zeta potential for the nanoparticle-biomolecule delivery to a specific cell under a certain condition[90].

For cellular delivery it is also very important to have the right balance between chemical stability and biodegradability. Excepting anionic clays *i.e.* LDHs (section 1.2.3), most of nanocarriers like inorganic nanoparticles are chemically stable, constituting an excellent feature so that their physicochemical properties can be kept unchanged during the whole delivery process. However, the chemical stability also keeps nanoparticles from being biodegraded in

plasma and cytoplasm of a human body. As a result, these nanoparticles will be either accumulated in cells, circulated in plasma or metabolised away. Most nanoparticles are believed to accumulate in the cells once they are endocytosed. This is because it would be difficult for such big nanoparticles to be exocytosed. In this case, the nanoparticles inside the cells act as an inducer of a time-bomb for the cell when more nanoparticles are endocytosed[90].

The influence of particle shape on endocytosis has been only recently investigated. The predominance of certain factors like the nature, size and the surface charge of the nanodevices; multiple endocytic pathways that can also be involved simultaneously (CME, CvME, macropinocytosis), could lead to differences between preferred optimal shape. For example, in some cases, it was found that spherical nanoparticles had a higher and faster rate of endocytosis compared to rods or disks, as demonstrated using different nanoparticles[169,170]. On the contrary, other studies suggested preferential uptake of rod-shaped[171] or cylindrical[172] particles. Thus, no general tendency can be determined yet. The influence of particle shape on the intracellular trafficking also deserves more insight[133].

We will now introduce the clay minerals as a novel physicochemical strategy for vectorization of biological molecules.

1.2. Clay minerals.

In Earth, the so-called clay minerals represents one of the most abundant groups of inorganic solids in interaction with the Biosphere[6] . They are silicates of aluminum and/or magnesium structured in tetrahedral and octahedral

environments arranged as sheets that share oxygen atoms. Clay minerals have been implicated in the prebiotic synthesis of biomolecules and the origins of life. They are considered very interesting materials due to their wide variety, abundance in nature, low cost, low toxicity and environmental friendliness. They also present high reactivity and modification capacities, giving them a large number of applications ranging from more conventional (in ceramics and paper fabrication) to the newest (rheological agents, selective adsorbents and diverse advanced materials)[173]. The long history of the use of clay minerals in the context of human health and disease is largely attributable to its rich physical-chemistry behaviour[8,14], as well as their ability to interact with many compounds including those from biological origin, forming nanostructured hybrids materials[13].

Clay minerals showing two types of morphology have been used for the preparation of bio-nanohybrid material:

- Layered silicate structures (phyllosilicates) that crystallize into micro- and nanometer-sized particles, a typical example is montmorillonite, which is an aluminosilicate belonging to the smectite minerals group that shows cation-exchange and expandability properties. In general, the plate-like particles of phyllosilicates are made up of a finite number of either 1:1- or 2:1-type layers. The small particle size combined with the permanent structural charge of certain clays, notably those in the smectite class such as montmorillonite, beidellite, saponite, and hectorite, results in significant surface reactivity which has profound implications in marine and terrestrial ecosystems, and

provides the basis for a wide range of industrial, environmental, and agricultural applications[13,174].

- Fibrous silicates (non-planar), includes sepiolite and palygorskite clay minerals. Sepiolite is an hydrated magnesium silicate whose main characteristics are determined by its textural behavior and surface reactivity[24,25]. The structure and morphology of palygorskite are strongly related to those of sepiolite, although it shows higher aluminium content and narrower structural tunnels[25]. Interestingly, both fibrous silicates act similarly assembling biopolymers via hydrogen bonding through the silanol groups located at the external edges of the fibers[14,31].

1.2.1 Kaolin group (kaolinite and halloysite).

One of the relevant groups of clay minerals is the 1:1 phyllosilicates group in which are included kaolinite and halloysite. Elemental layeres of kaolinite are built-up by one tetrahedral silica sheet and one octahedral alumina sheet, the units of which stack to a greater degree than other clays[173]. The layers of kaolinite are held together by hydrogen bonding supplemented with dipole-dipole and van der Waals interactions. The result is that kaolinite tends not to undergo interlayer expansion in water, though swelling can be induced in contact with certain compounds such as those able to form hydrogen bonds, supplemented by dipole–dipole and van der Waals interactions, with the inter-layer surface. Most kaolinites carry a small amount of negative charge coming from isomorphic substitutions in the layer, which is comparable to, but much more smaller than montmorillonite[175].

Of greater importance than the probable presence of negatively charged sites at the (siloxane) basal surface, is the variable charge that develops at the edge surface of kaolinite particles as the pH of the ambient solution is varied. This pH-dependent charge largely arises from the protonation (under acid conditions) and deprotonation (under alkaline conditions) of "under-coordinated" aluminol groups exposed at particle edges[176].

Halloysite is also a 1:1 aluminosilicate clay mineral with the empirical formula $Al_2Si_2O_5(OH)_4$. Halloysite naturally can occur as small cylinders, which average 30 nm in diameter with lengths between 0.5 and 10 micrometres. Compared with other tubule clay as imogolite, have smaller diameter and much lower loading capacity for macromolecules[177]. Two common forms are found[178]:

- Hydrated (the clay exhibits a 1 nm spacing of the layers).
- Dehydrated (meta-halloysite, the spacing is 0.7 nm)

This clay mineral has also special relevance as container for delivery of diverse species including drugs and other bioactive species (self-healing, anticorrosion, antimicrobial agents, proteins, DNA, drugs, etc.) of interest in biomedical applications[177]. Due to the tubular microstructure and the biocompatibility of halloysite nanotubes, halloysite-polymer nanocomposites have demonstrated good drug encapsulation and sustained release abilities, gaining them extensive use as tissue engineering scaffolds and drug carriers[179].

1.2.3 Smectites.

Smectites are the most important clay minerals group in terms of the clay–polymer interaction.[176]. In smectites, the unit structure consists of layered

sheets each constituted by two tetrahedral silica sheets sandwiching an octahedral sheet formed from a metal cation such as Al^{3+} or Mg^{2+} (Figure 1.5a).

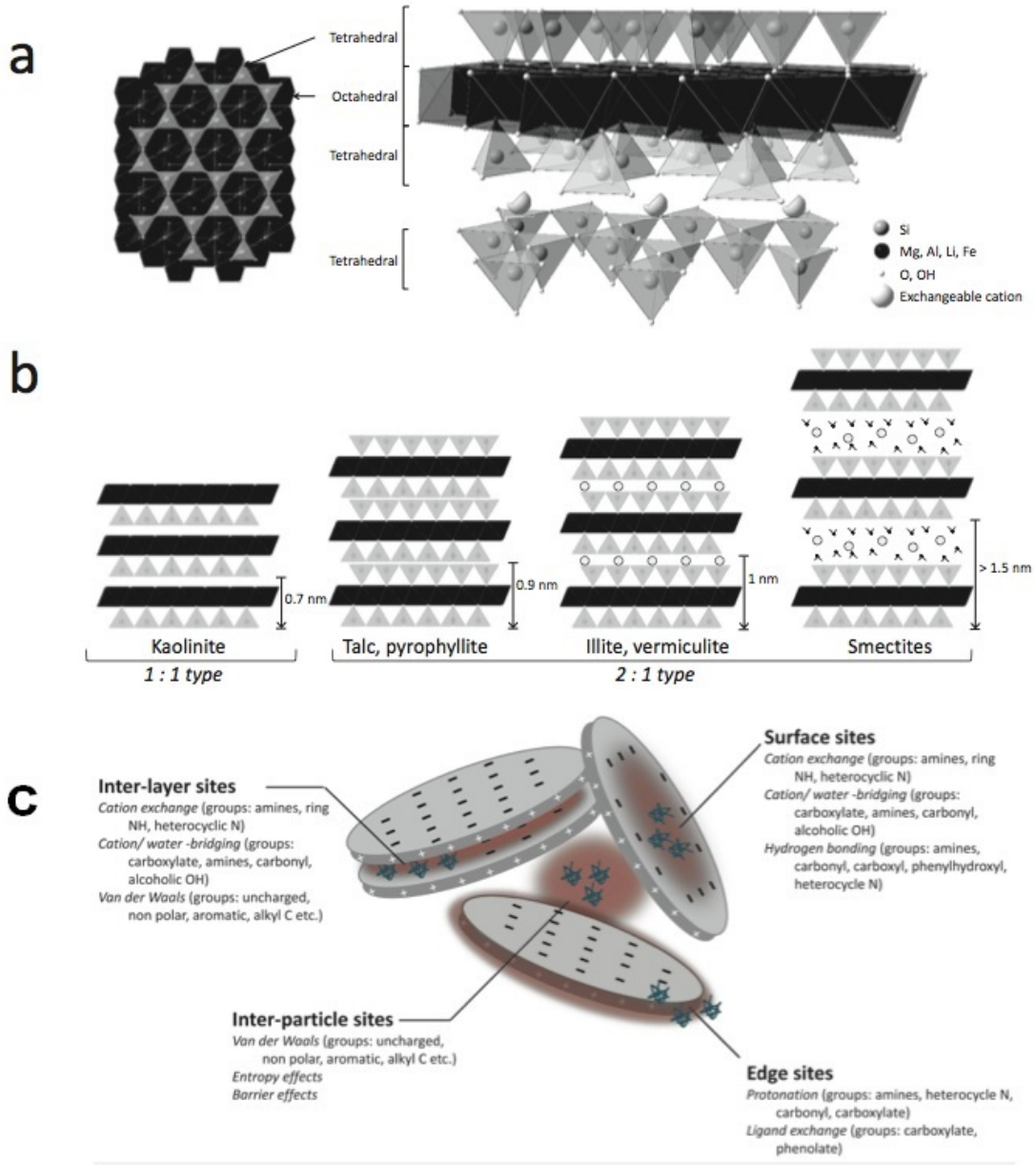

Figure 1.5 A) Schematic representation of the structure of smectite crystals. B) Examples of different crystal structures of clay minerals showing the nature of their individuals layers. C) Potential interactions sites in smectite particle (surfaces, inter-layer pores and inter-particle spaces) for association with organic molecules involving diverse type of mechanisms (adapted from Dawson and Oreffo 2013).

The smectite sheets are therefore isostructural with talc or pyrophyllite, but whereas the 2:1 sheets of talc are electrostatically neutral, the layers of the smectites possess a net negative charge due to random isomorphic cation substitutions in the octahedral and tetrahedral sheets compensated by hydrated interlayer cations[173]. The magnitude of the negative layer charge in smectites is an average over the whole particle. The layer charge heterogeneity has implications for the synthesis of polymer– montmorillonite nanocomposites. Further, the (negative) basal charge of smectites is independent of suspension pH since it arises from isomorphous substitution within the structure. Morevoer, the necessity for compensating the charge with cations located in the interlayer region drives to interesting cation-exchange properties in these phyllosilicates. The weaker charge in smectites compared to illite and vermiculite allow easier accessibility of species to the interlayer region of smectites (Figure 1.5b)[175].

As well as the structurally generated negative surface charge, broken bonds at the crystal edges with unsatisfied valences yield localized positive charges (or negative charges at high pH), which play an important role in the colloidal properties of clay particle suspensions. The propensity for swelling and delamination of the charged smectite particles, gives rise to a rich selection of potential interactions between organic molecules and the clay particle surfaces, inter-layer pores and inter-particle spaces involving a range of mechanisms including cation exchange, hydrophobic interactions, hydrogen bonding, cation bridging, anion exchange and proton transfer depending on ambient pH, and the size and electrostatic properties of the interacting molecule (Figure 1.5c)[175,180].

Smectites have been applied to successfully treat the symptoms of gastritis caused by non-steroidal anti-inflammatory drugs[6]. Derives from their ability to absorb excess water and their aid in heces compaction, smectite is also used in the treatment of symptomatic diarrhea. The high adsorptive capacity of the silica gel that results in the acidic medium is thought to further aid anti-diarrheic action. As topical agents clay minerals (principally kaolinite, talc, and smectites) confer benefit by adhering to the skin, forming a protective film[106].

1.2.3 Micro and nano-fibrous clay minerals: sepiolite and palygorskite

Fibrous clays minerals family members are sepiolite and palygorskite, also known as attapulgite, both of them with a crystalline structure related to 2:1 phyllosilicates but where the disruption of the layers results to the presence of channels along the fiber lengths (Figure 1.7). Sepiolite is a natural hydrated magnesium silicate [24,25] of theoretical unit cell formula $Si_{12}O_{30}Mg_8(OH,F)_4(H_2O)_4,8H_2O$ [26,27]. Sepiolite shows an alternation of blocks and tunnels that grow up in the fiber direction. The blocks are constituted by two layers of tetrahedral silica sandwiching a central magnesium oxide-hydroxide layer. The discontinuity of the silica sheets gives rise to the presence of silanol groups (Si-OH) at the edges of the channels, which are the tunnels opened to the external surface of the sepiolite particles [28]. Substitution of aluminum by magnesium in the octahedral layers yield a moderately high permanent surface charge which imparts a high adsorptive capacity[176], given the channelled fibrous structure. Tunnels are filled with both the coordinated water molecules, which are bonded to the Mg^{2+} ions located at the edges of octahedral sheets, and the

zeolitic water, which is associated to the former by hydrogen bonding. One of the advantages of fibrous clays compared to layered silicates (smectites and vermiculites) is the very high density of silanol groups, ca. 2 Si–OH groups/nm^2, which allows hydrogen bonding in addition to van der Waals interactions at the polymer- silicate interface [24,25], togheter with other interactions as shown in figure 1.6.

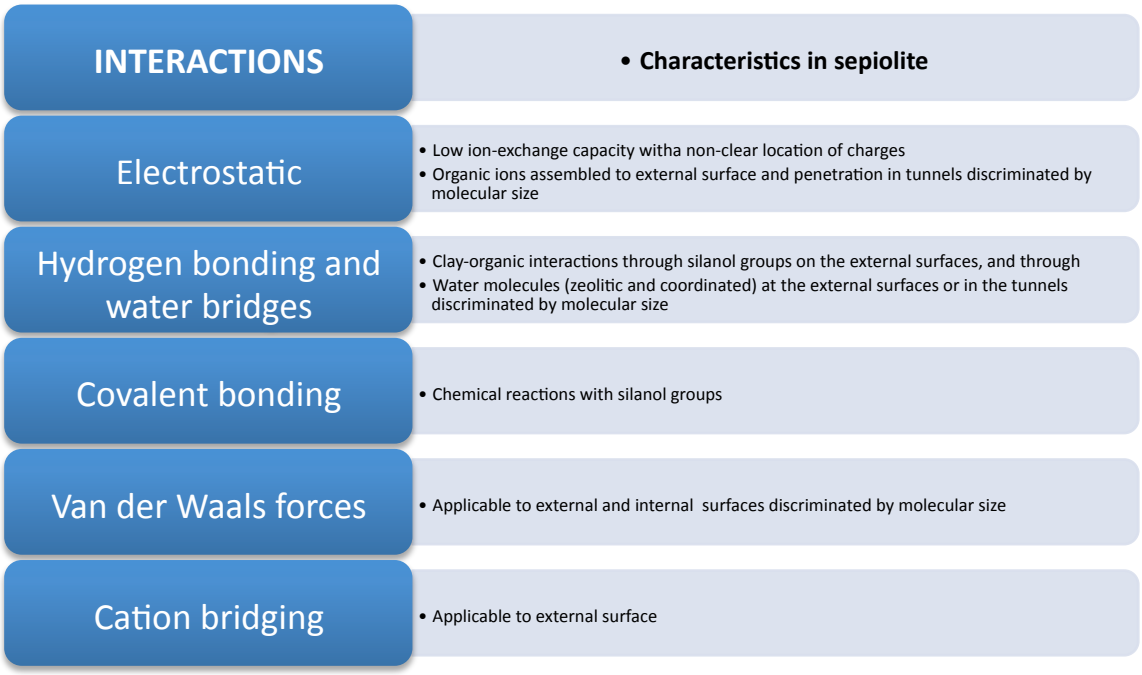

Figure 1.6 Different mechanisms of sepiolite – organic interactions. Adapted from Ref. [25].

Palygorskite shows an alike morphology than sepiolite but contains a higher content in aluminum replacing magnesium in the octahedral layers. Dimensions of the cross-section of sepiolite tunnels are 1.06 × 0.37 nm^2 whereas in palygorskite are 0.64 × 0.37 nm^2 , allowing the access of only small-size molecules such as water and methanol[24].

Two types of water molecules are located inside the tunnels and the channels of both sepiolite and palygorskite silicates: coordinated water molecules, bonded to Mg^{2+} at the edge of octahedral sheets, and zeolitic water molecules, filling the intracrystalline cavities. The coordinated water is strongly bonded to the silicate making thermal treatments above 400 ^{o}C under dynamic vacuum necessary for its removal. Zeolitic water molecules are easily removed just by exposure to vacuum or by thermal treatment at about 100 ^{o}C. The loss of the coordinated water produces structural collapse of the structure (folding) and the fall down of the tunnels as revealed by XRD patterns and other techniques[28].

Toxicity of sepiolite and palygorskite is controversial as it is apparently related to fiber length and crystallinity, which are determined by the geological origin of the silicate[35]. Sepiolite shows typical fiber length of about 1-2 μm, although in certain cases (e.g. China, Finland) the fibers are much longer. Typical dimensions of the cross-section of a sepiolite fiber from Vallecas-Vicálvaro deposits (Spain) are 25 x 4 nm, which corresponds to about nine unit cells in width and only three in thickness[9]. *In vitro* and *in vivo* tests, as well as epidemiological studies, have also confirmed that at least sepiolite from Taxus Basin deposits in Spain does not constitute a health risk[36]. Studies carried out on humans exposed to sepiolite seem to bear out the fact that exposure to this mineral involves no risk[181–183].

The International Agency for Research on Cancer (IARC), which belongs to the World Health Organization reviewed the literature and studies, and concluded the following: “there is inadequate evidence in humans to determine the carcinogenicity of sepiolite. There is limited evidence in

experimental animals for the carcinogenicity of long sepiolite fibres (>5 mm). There is inadequate evidence in experimental animals for the carcinogenicity of short fibres (< 5 mm)" (IARC Monographs on the evaluation of Carcinogenic Risks to Humans, Vol.68 of 1997). IARC's overall evaluation concluded that 'sepiolite cannot be classified as carcinogenic to humans (Group 3)'[25].

Palygorskite crystals form planar or ball-like aggregates or bundles similar to those of sepiolite and fibrous aggregates less than 5 μm long, although they can exceptionally reach up to 100 μm in length[184]. The IARC classifies long palygorskite fibres (>5 μm) as Group 2B (possibly carcinogenic to humans) and short palygorskite fibres (<5 μm) as Group 3 (they cannot be classified as carcinogenic to humans) (IARC, 1997b)[184].

Sepiolite and palygorskite have a big versatility for assembling organic species to produce organic–inorganic hybrid materials, with a high impact in new applications. The assembly of organic species to sepiolite has a major interest in the introduction of functionality to enlarge the applications of the raw clay. Importantly the large surface conferred by its multi-layer fibrous structure and the great variety of sites for interaction with polar and ionic species (Figure 1.7), making sepiolite a good candidate for being a platform for co-delivery of different kinds of macro-molecules. Indeed, sepiolite has been shown to interacts with polysaccharides[29,185], virus[34], lipids[15] or proteins[31–33]. In many cases, such as gene therapy, the co-delivery of a RNA or a protein encoding for a nuclease cleaving the target endogenous sequence and the correction DNA, constitute promising strategies. More interestingly, sepiolite fibers present a nano-size dimension, which make them suitable for cellular intake, and have a

perfectly stable and natural intrinsic fluorescence. Taking advantage of this natural fluorescence, it is possible to follow the fate of sepiolite into cells, to select cells containing sepiolite and to achieve high contrast in electron microscopy, which facilitates their intracellular localization. This silicate is also biocompatible, abundant, and not expensive.

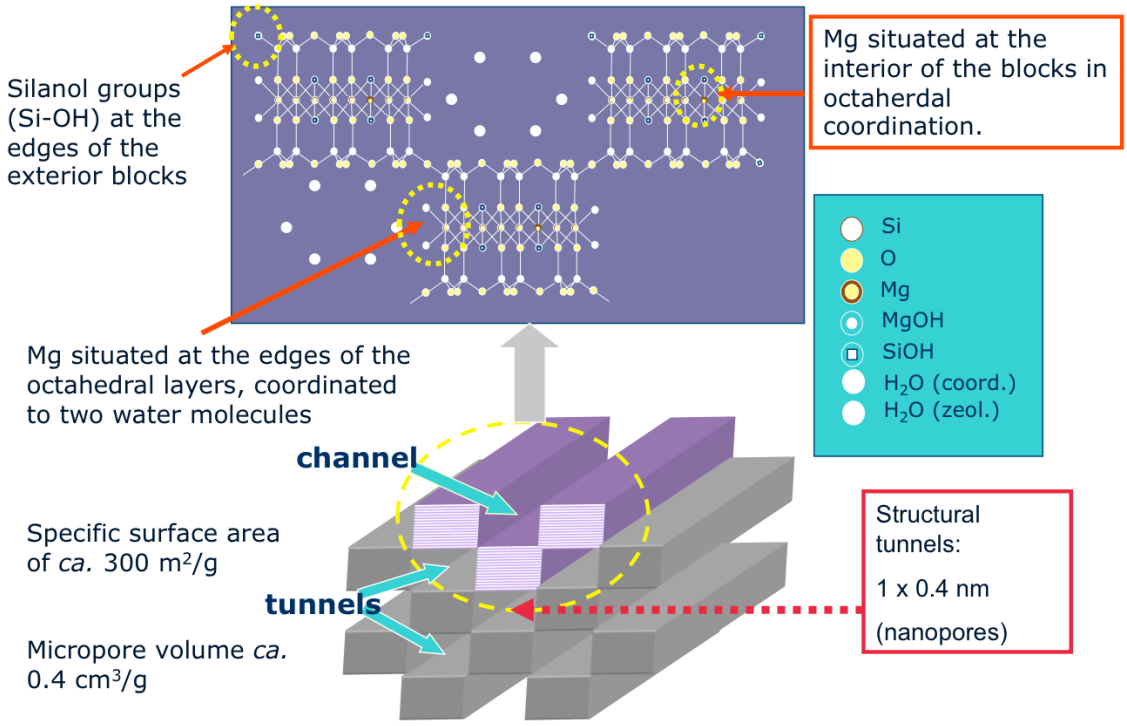

Figure 1.7 Schematic representation of sepiolite structure and textural features (based on Ref. [24]).

1.2.4 Layered double hydroxides (LDH).

Another interesting type of materials related to clays are layered double hydroxides (LDH), also known as hydrotalcite-like, hydrotalcite-type or anionic clays. They are a class of anionic exchanging layered solids that naturally exist but that can be readily synthesised in laboratory and also at industrial level. The term LDH is used to designate synthetic or natural layered hydroxides with two or more kinds of metallic cations in the main layers and hydrated interlayer domains containing anionic species[186,187]. LDH has a general chemical formula:

$M^{II}_nM^{III}(OH)_{2(n+1)}(A^{m-})_{1/m}\cdot xH_2O$, where n = 2 - 4, M^{II} represents a divalent metal cation (Mg, Zn, Ca, Co, Fe, Ni, Cu, etc.), M^{III} represents a trivalent metal cation (Al, Fe, Cr, Ga, etc.), and A^{m-} an anion (Cl^-,CO_3^{2-}, NO_3^-etc)[90]. A typical example is magnesium – aluminium LDH or hydrotalcite: $Mg_6Al_2(OH)_{16}CO_3\cdot 4H_2O$, which was the first member of its natural mineral family that was identified in Sweden in 1842.

The crystal structure of LDH is related to that of $Mg(OH)_2$ in which the partial isomorphous substitution of Mg^{2+} ions by Al^{3+} gives to the brucite-like layers a positive charge and the resulting negative charge deficiency is relatively delocalized with respect to the inter-lamellar plane. In hydrotalcite the positive charge is balanced by carbonate anions, which are located in the interlayer region between the two brucite-like layers (Figure 1.8). This gallery also contains water molecules, hydrogen bonded to layer OH and/or to the interlayer anions. The electrostatic interactions and hydrogen bonds between the layers and the contents of the gallery hold the layers together, forming the three-dimensional structure[187].

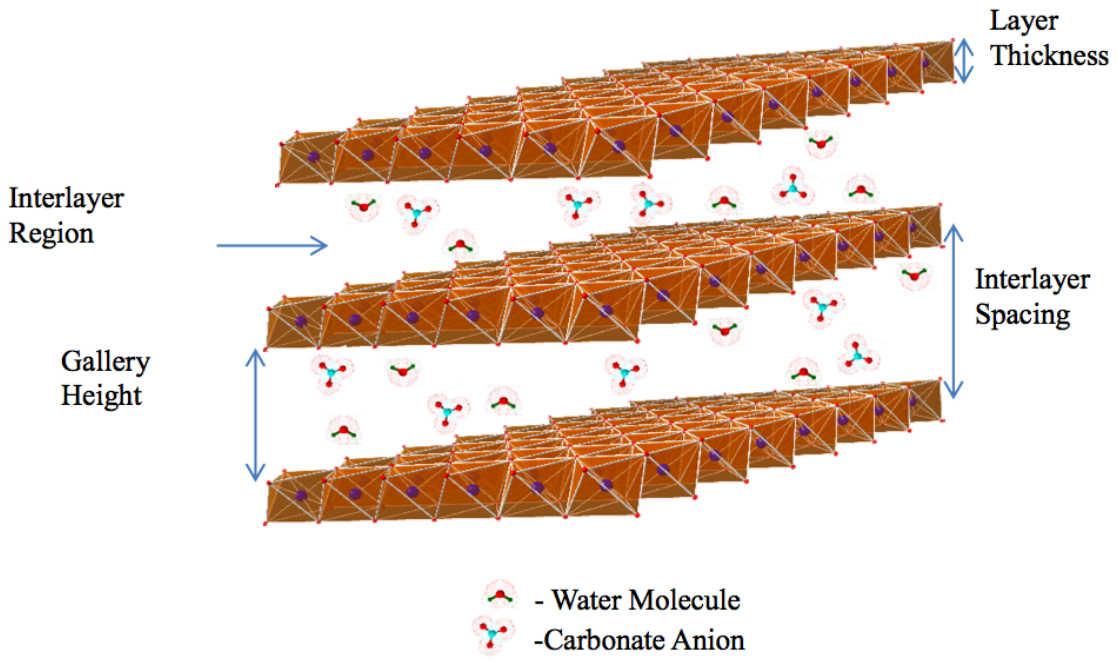

Figure 1.8. Schematic representation of the structure of magnesium – aluminium LDH (hydrotalcite).

More interestingly, not only can the layer cations of these materials be replaced among a wide range selection of cations, but also the anions located at the interlayer region can be exchange by diverse organic or inorganic, simple or complex anions, polyoxo species, anionic coordination compounds[188], polymers[189] and biopolymers[190]. Anions such as Cl^- and NO_3^- in the interlayer can be exchanged by biomolecules provided or anionic sites, such as amino acids and peptides[191], polysaccharides[190], nucleotide monophosphates and DNA chains etc.[114] Furthermore, a unique property, which makes them diverse from other cationic-layered materials, is that they are capable of recovering the double-layered structure after thermal decomposition under mild conditions[117]. This property results of interest in view to prepare biohybrids that require the intercalation of large molecules containing anionic sites[117].

LDH materials have found vast applications in the fields of catalysts, catalyst precursors, anion absorption and environmental remediation[192], finding also in recent years promising usages in biomedicine[90]. Properties such as high chemical versatility, anionic exchange capacity (AEC), and low cytotoxicity, are leading to a promising future in drug delivery and release, opening up wide possibilities for researches and development for its clinical application. Compared with old-fashioned drug delivery methods which are suffering from problems such as drug degradation, poor bioavailability, and low circulation stability, the LDHs, as a new drug carrier, is much simpler to synthesize in the laboratory, have a high drug transportation efficiency, high drug loading density, low toxicity to target cells or organs and excellent protection to loaded molecules from undesired enzymatic degradation[193]. Recently LDHs have been employed for clinical disease diagnosis, chemical industry and as a drug carrier responsible for delivering therapeutic and bioactive molecules such as peptides, anti-inflammatory drugs, and even small nucleic acids to mammalian cells *in vitro* or *in vivo* with the purpose of crossing the cell membrane into the cytoplasm[119].

1.3. Bionanocomposites: new tool and strategies for biomedical applications.

The development of functional hybrid materials, based on the bottom-up assembly at the nanometric scale of polymeric moieties with nano- and micro-metric sized inorganic solids, is widely known especially for clay-based materials[194]. The growing relevance of the resulting nano-architectures is due to

the possibility to obtain advanced nano-structured materials whose properties cover a wide range of applications, including electrical, electrochemical, optical, optoelectronic, magnetic, catalytic, selective molecular adsorption, ionic-molecular recognition or controlled release of bioactive species[195–200]. An outstanding example of these improvements is achieved by polymer-clay nanocomposites[201–203]. In fact, currently this class of hybrid materials receives increasing attention not only for applications related to improved mechanical properties but also due to its functional properties (*e.g.* thermal, barrier properties, electrical conductivity, etc.).

The term bionanocomposite – equivalent to nanobiocomposites employed by certain authors – is used to describe biohybrid materials in which the species of natural origin are biopolymers (polysaccharides, lipids, proteins, nucleic acids, etc.), assembled at the nanometer scale with inorganic solids of diverse structure and morphology. Some bionanocomposites often mimic the composition, structure, and behavior of natural hybrid materials present in different living organisms[204–208]. Many important advances using biomimetic approaches involve carbonates and phosphates, for instance to prepare artificial nacre, bone, and other bionanocomposites[208–215] but silica, silicates and polysiloxanes also offer a viable alternative for preparation of biohybrids since their chemistry is extremely versatile, allowing the formation of hierarchical superstructures, supramolecular materials and other multifunctional bioinspired systems[8,37,194,195,215–218]. Among those, bionanocomposites in which the inorganic component is a silicate belonging to the clay minerals family are probably the most relevant[9,14,40].

Advanced applications[8,9,198,200,219–221] show the benefit associated with the use of biological sources of polymers to generate the so-called green plastics or green nanocomposites, avoiding therefore the indiscriminate consumption of petroleum derivates and enhancing the biodegradability as opposed to the non- ecological conventional plastics[222]. Moreover, as indicated for biohybrids, in general bionanocomposites also lie on the borderline between the inorganic and the living world, being of extreme importance due to their non-toxic, biocompatible, and biodegradable behaviour in view to become good candidates for biomedical applications (biosensors, tissue engineering, artificial bone, drug-delivery nanovehicles, vaccination, wound dressing, gene therapy, etc.)[1–3,5,14,15,17,34,117,198,200,221,223–225].

The firstly reported clay-based bionanocomposites refer to the intercalation of chitosan in layered silicates[226]. At low concentrations of chitosan in slightly acid aqueous solutions the intercalation of the polymer progresses by a cation- exchange reaction until incorporation of a monolayer of the biopolymer in the interlayer region of montmorillonite. The use of high amounts of polysaccharide exceeding the cation-exchange capacity (CEC) may lead to the uptake of chitosan in a bilayer configuration, being the excess of intercalated biopolymer accompanied of counter-ions in order to compensate the excess of positively charged groups of chitosan chains. In this situation the initial CEC of the clay is reversed to an AEC in the resulting bio-nanocomposite. These AEC properties are of special interest for the development of active phases in electrochemical sensors for anions detection[39]. In the same way, it is possible to prepare bionanocomposites based on the assembly of chitosan to sepiolite[29]. The resulting materials show improved mechanical properties and also

functional properties related to their anionic exchange capacity, which could be of interest for electroanalytical applications. The basic assembly processes for the preparation of fibrous-clay-based bionanocomposites regard mostly adsorption favoured by interactions[12,15,29,33,42] of the biopolymers and other biomolecules with the silanol groups on the external clay surface.

Bionanocomposites based on the assembling of collagen and gelatin to different types of inorganic substrates are of special relevance in biomedicine[10]. In sepiolite-gelatin bionanocomposites the clay play a significant role as it can control the cristallinity of the gelatin matrix, having an important impact on the mechanical properties of the resulting bionanocomposites. At 20% mass fraction of sepiolite the elastic modulus of the bionanocomposite increased by a factor of 2.2 as a result of both the mechanical reinforcement of the silicate inside the polymer matrix, but also as a result of the crystallinity variation induced by the clay particles[33].This last group of bionanocomposites can be of interest for biomedical applications especially in tissue engineering related to the development of scaffolds for bone regeneration[10]. For tissue-engineering applications it is required that the bionanocomposites are provided of adequate macroporosity and good mechanical properties. The development of such types of fibrous clay-biopolymer nanocomposite materials exhibiting a hierarchical porosity, with micro and mesoporosity, together with macropores of tens and hundreds of micrometers requires their conformation as foams. Amongst the diverse foaming techniques the most common procedure in the case of bionanocomposites consists in the application of freeze-drying or supercritical drying processes to biopolymer-clay hydrogels[42]. In biomedical applications the resulting biohybrids can be of interest as carrier of pharmaceutical and

biological species[42,211]. Functional proteins and enzymes may also be introduced in the bionanocomposite foam by mixing them with the starting components prior to freeze-drying. In this last case, the biocompatibility of the foams helps to preserve the catalytic activity of entrapped enzymes allowing the development of bioreactors. A recent example of this application is a macroporous PVA foam in which the reinforcing agent is a phospholipid-modified sepiolite used as support of urease enzyme, which introduces the catalytic functionality in the system[227].

1.4 Interaction of clay minerals with DNA: applications and their role with evolution of life.

The knowledge of the interaction between nucleic acids and mineral surface has led to several applications and fundamental issues about evolution of life. Indeed, it has long been proposed that surface chemistry of clay minerals, could have played a crucial role in the prebiotic formation of molecules basic to life[228]. Moreover, mineral surfaces may also have been important for the prebiotic organization and protection of nucleic acids, which has bearing on the prebiotic origin of an RNA World[229,230]. In addition, the adsorption of DNA on mineral surfaces might favour horizontal gene transfer into living organisms, which may play a significant role in evolution of living species.

On the other hand, the interactions of DNA and clay minerals have been extensively investigated in research, clinical diagnosis and ecosystem security among other fields of applications.

It is worth to mention that such interactions between biomolecules (particularly the DNA) and clay minerals show a complex and specific picture depending of a number of factors, which includes some internal characteristics (physical and chemical properties of clay minerals, proteins and nucleic acids; the length of DNA molecule) as well as some properties of the environment in which the interactions come into play (mineralogy of the sorbent, the ionic strength and pH of the medium)[231]. For instance, in the presence of monovalent cations, DNA adsorbs onto sand by means of physical attraction forces (van der Waals), whereas in the presence of divalent cations electrostatic interactions prevail because polyvalent cations act as a bridge[232]. In the particular case of the adsorption of proteins and nucleic acids (DNA, RNA) on natural clay minerals of layer phyllosilicates such as montmorillonite, kaolinite and illite, the interaction mechanisms are suggested to be cation exchange, electrostatic interactions, hydrophobic/hydrophilic interactions, ligand exchange, cation bridge, water bridge, hydrogen bond and van der Waals forces. Ligand exchange is a reaction process, in which the phosphate groups at the two ends of the nucleic acid molecules are directly bound to the hydroxyl group on the surface of clay minerals. The multivalent cations such as Ca^{2+} and Mg^{2+} existing in the medium may be responsible for cation bridge process[233,234].

The strands of DNA possessed a strong negative charge due to the phosphate groups. for instance pH and ion strength of absorption solution[23]. For some DNA molecules, the adsorption occurs in interlamellar channels by cation bridges between the negative phosphate groups of DNA and the negatively charged tetrahedral silica layer on the clay surface via exchangeable cations as media[23]. Nevertheless, large biomolecules are usually adsorbed at the planar

surface and broken edges of clay minerals. The Al^{3+} groups at the broken edges coordinate with water molecule. This leads to acidic binding sites due to enhanced ionization of water molecule[23]. Consequently, negatively charged substances tend to be bound at the edges X-ray diffraction analysis showed that the basal spacing of montmorillonite and kaolinite were not altered after the adsorption of DNA from Bacillus subtilis, indicating that this DNA did not significantly intercalate the clays[235]. Scanning and transmission electron microscopy showed that the binding of DNA from Bacillus subtilis was primarily on the edges of montmorillonite and kaolinite[236].

With the increasing commercial applications of transgenic plants, it is also necessary to study the interactions mechanisms of nucleic acid molecules and recombinant proteins released from transgenic plants on clay surface in soils. The binding of these biomolecules by clay minerals will influence cultures of soil microorganisms and reduce their availability as a source of carbon and/or nitrogen for microbe[237,238]. Early reports regarding DNA adsorption onto clay minerals were related with the adhesion of nucleic acids from vegetal, animal or microbial cells, which are released into the soil at their death[239]. The understanding of mechanisms involved in DNA adsorption onto soil particles could provide information for improving soil DNA extraction yields. This would also be useful for monitoring the fate of free DNA in the soil, including its ability to be transferred to soil microbes via transformation[240]. Many species of bacteria normally inhabiting soil and sediment have been reported to develop a natural state of competence by taking up extracellular DNA[241,242].

A better understanding of the fundamental processes involved in reversible DNA adsorption to mineral surfaces (such as silica) under different

experimental conditions (conformation of DNA buffer composition, pH, ionic strength, electrolyte type and valence,) will help optimize methods for preparing nucleic acid samples[243]. The silica solid support is implemented either in the form of a filter membrane[244] or as silica-coated magnetic particles[245]. The DNA adsorption to silica has been attributed to electrostatic interactions, hydrogen bonding, and was also attributed to an increase in entropy, whereby ordered water molecules that solvate the DNA and surface are released during the adsorption process[246].

The neutralizing bridges between the phosphate groups of DNA and the negatively charged tetrahedral silica layer on the clay surface lead to the indirect adsorption and contribute to increasing DNA's stability and resisting DNA-degrading enzymes[247]. DNA does not significantly intercalate into the clay layers through ionic exchange reaction and probably is primarily absorbed on the edges of the clay minerals or on the planar surfaces by ligand exchange, electrostatic forces and hydrogen bonding, etc. Thus, it has been found that more than 50% of salmon sperm DNA was directly adsorbed on the positive charged edges of montmorillonite by electrostatic forces[248]. Only 21.9% of salmon sperm DNA molecules were adsorbed onto kaolinite by electrostatic forces and ligand exchange suggesting that other interaction forces such as hydrogen bonding and hydrophobic force also played more important roles in the adsorption of DNA onto the kaolinite[23].

Imogolite (a hydrous aluminosilicate nanofiber having outer surface of Al-OH groups) is one of the important clay minerals contained in volcanic ash soils[249]. A novel hybrid hydrogels were prepared from imogolite nanofibers and DNA by utilizing strong interaction between the Al-OH on imogolite surface and

phosphate groups of DNA[250]. DNA could be protected even under severe conditions by the hybridization with imogolite[250].

Recently, it was reported the protective effect of three kinds of clay minerals (rectorite, montmorillonite and sericite) against damage to adsorbed DNA induced by heavy ions like cadmium and mercury[251]. In this case there was also a strong evidence that the mechanisms for DNA adsorption on clay involve electrostatic forces, cation bridging and ligand exchange.

In this context, the adsorption of extracellular DNA and RNA molecules and proteins on the surface active particles of clay minerals have also received much attention[252,253]. It was found in the bibliography several reports regarding the protection of adsorbed DNA against enzymes and the ability of adsorbed DNA to transform bacteria. For example, it was reported that the transforming ability of chromosomal and plasmid DNA bound on montmorillonite persisted for 15 days in non-sterile soil under moist conditions[254]. Moreover, there is much evidence that extracellular DNA can persist for periods of time up to several months or years, and maintain its biological activities such as the ability to transform bacterial cells, to transmit the genetic information contained in their sequences and to interact with molecules in the soil environment[23]. Adsorption of DNA on soil components, particularly on clay minerals such as montmorillonite, illite, and kaolinite, is thought to be involved in protection of nucleic acids against nucleases, and could explain the high content of DNA in soils[64].

The level of protection of DNA by soil particles varied significantly with DNA configuration and the type of the adsorbent. Supercoiled plasmid DNA

associated with kaolinite was easily degraded by nucleases as compared with linear chromosomal DNA. DNA adsorbed on quartz was more resistant to degradation by DNase I than that adsorbed by minor mineral fractions of the sand in 20 mM $MgCl_2$. Illite provided a lower level of protection for DNA molecules than montmorillonite and kaolinite. However, the protection of DNA by soil particles to enzymatic degradation is not totally understood, as is also the influence of parameters such as mineral constituents, organic matter, and particle size of soil colloids[235].

In fact, very little is known and there are still a lot of open questions about the protection mechanism itself, and the influence of parameters such as clay type, the size of DNA or its conformation. For instance, does adsorption physically prevent DNA from being attacked by nucleases? Or is protection related to adsorption of enzymes on clay, which induces conformation alterations leading to a decrease in activity? Moreover, how is the remaining clay-adsorbed DNA available for bacterial transformation, and what are the consequences of a partial protection on the transformation efficiency? Finally, will partial degradation have the same effect on transformation frequencies when the processing of the transforming DNA in the bacterial cell occurs via homologous recombination or autonomous replication?[64]

Beside the protection against enzymatic attack, there are another important issue regarding the indispensable role of clay minerals in protecting the adsorbed DNA against ionizing radiations, which is strongly related to the conditions under life was created. Belongs to this topic the problem of the surviving of life buildings blocks in the presence of solar irradiation that at the primordial Earth was much more extreme than today. It is know that UV and X-

ray emissions fade as a star ages. In particular, $4.5x10^9$ years ago, X-ray radiation from the Sun was two orders of magnitude higher than today and, moreover, the Earth atmosphere was most probably unable to shield the solar radiation at these wavelengths. It is interesting to investigate the existence of survival conditions for biological molecules under harsh irradiation such as from a young Sun[255].

Indeed, it was demonstrated the protective effect of montmorillonite and kaolinite on adsorbed DNA against ionizing radiation[255]. The clay adsorbed DNA is not damaged by X-rays for energy doses up to $5.8x10^4$ erg. Clay minerals could have protected the building blocks of life on the primordial Earth when the solar X-ray emission was much stronger than today[255]. It was also checked experimentally the ability of the possibly widespread prebiotic, clay mineral montmorillonite to protect the catalytic RNA molecule from UV-induced damages[256]. When the effect of UV radiation on solutions of free and clay-adsorbed DNA has been investigated, it turns out that nucleic acid which is adsorbed on clay (montmorillonite/kaolinite) undergoes less radiation damage than free nucleic acid[257]. Sepiolite and smectites were also researched on their abilities to form complexes with organic compounds which absorb UV-radiation[258,259].

In synthesis, biomolecule–clay mineral complexes provide protection against strong radiation, photo-degradation and inactivation of the associated biomolecule[23]. Consequently, results obtained in different fields strengthen the hypothesis of a clay-surface-mediated origin of genetic material[228]. Complementing previous models of chemical evolution on mineral surfaces, in which selection was the consequence of the limited mobility of macromolecules

attached to the surface, it was also offered an alternative realization of prebiotic group-level selection: the physical encapsulation of local replicator communities into the pores of the mineral substrate[260]. They might have served as primitive vessels for amino acids, purines, and pyrimidines. They concentrated these bio-molecules on their surface and catalyzed the polymerization of biomolecules. In other words, clay minerals help synthesis and preservation of biopolymers which finally lead to the origin of life on the earth[261].

1.5 Interactions between sepiolite and DNA. The Yoshida effect and bacterial transformation.

To date, studies about interactions between DNA and sepiolite lead to two applications. The first one is related to the use of sepiolite to design a novel electrochemical DNA sensor and anticancer drug sensor based on sepiolite and single-walled carbon nanotubes (SWCNTs)-modified pencil graphite electrodes (PGEs)[262]. The second, which appear in some papers, is related to the use of sepiolite for bacterial transformation based on the so-called "Yoshida effect"[263–268].

In the first study it was reported the novel surface for the electrochemical detection of anticancer drug–DNA interactions based on Sep and SWCNTs-modified PGEs[262].

As mentioned above, the second application of the interaction between DNA and sepiolite is taken as advantage for bacterial transformation.

As it is already well known, the ability of introducing individual molecules of plasmid DNA into cells by transformation has been of central importance to

the recent rapid advancement of plasmid biology and to the development of DNA cloning methods[264]. Molecular genetic manipulation of bacteria requires the development of plasmid-mediated transformation systems leading to the introduction of exogenous plasmid DNA into bacterial cells. These transformation systems include techniques already introduced (see 1.1.1) such as:

- Chemical transformation. The most widely used transformation methods today are $CaCl_2$ treatment for E. coli and polyethylene glycol (PEG)-induced transformation of bacterial protoplasts.
- Electro-transformation or electroporation.
- Biolistic transformation. Tungsten particles and submicrometer particles produced with polyol gold particles were used in biolistic process for the transformation of prokaryotic cells.
- Sonic transformation.
- Tribos transformation or hydrogel exposure method, based on the Yoshida effect. Is a gene introduction method using sliding friction and nanosized acicular materials.

The last one was a conceptually novel transformation technique for the transfer of exogenous plasmid DNA into bacterial cells, based on novel phenomenon called the Yoshida effect (in honor of its discoverer). The Yoshida effect could be described as following: when a colloidal solution containing nano-sized acicular material and bacterial cells is stimulated by sliding friction at the interface between hydrogel and an interface-forming material, the frictional coefficient increases rapidly and the nano-sized acicular material and bacterial cells form a chestnut bur-shaped complex. This complex increases in size and

penetrates the bacterial cells, thereby forming a penetration-intermediate, due to the driving force derived from the sliding friction[263].

A hydrogel shear stress greater than or equal to 2.1 N is essential for the Yoshida effect to occur and has been observed with agarose, gellan gum, and κ-carrageenan. In addition, polymers such as polystyrene, polyethylene, acrylonitrile-butadiene rubber, and latex rubber, as well as silicate minerals such as quartz and jadeite, are all suitable interface-forming materials. With regard to nanosized acicular materials, the Yoshida effect has also been confirmed with multi-walled carbon nanotubes, maghemite (γ-Fe_2O_3), chrysotile, and sepiolite, having diameters of 10–50 nm[264].

In molecular biology, “competence” is the ability of a cell to take up extracellular DNA from its environment. It could be natural (a genetically specified ability of bacteria which is thought to occur under natural conditions as well as in the laboratory), and induced or artificial competence (which arises when cells in laboratory cultures are treated to make them transiently permeable to DNA). The great majority of bacterial species does not show a naturally occurring ability to take up DNA. This fact prompted an intense search for methods to induce competence by special treatment. The advantage of transforming bacterial cells based on the Yoshida effect is that competent cell preparation is not required.

Most of the published work referred to the use of chrysotile asbestos fibers[269–273], which had carcinogenic potential and biological activity[274], and the authors suggest the usage of a specific apparatus for optimized application of sliding friction forces[275], which could discourage possible users. Due to the

obvious health risks associated with chrysotile, the usefulness of sepiolite which has been mentioned by Yoshida and colleagues as an alternative source of nanofibers, was then confirmed later in a simple and rapid method of bacterial transformation[265]. Reported results for transformation efficiency of E. coli was in the range of 1×10^5 transformants per µg of plasmid in the case of 8.9 Kbp plasmid (pWH1266) and 2×10^6 in the case of 2.7 Kbp plasmid (pUC19), with the following protocol[265]:

- Autoclave a suspension of 0.01% sepiolite in deionized water supplemented with 5 mM HEPES and 200 mM KCl (sepiolite suspension).
- Centrifuge 500 µl of a bacterial culture (0.5–1 OD).
- Resuspend it in 100 µl sepiolite suspension.
- Add 50 ng of transforming DNA.
- Spread it on a 1–2% agar plate containing the appropriate selective agents. Spreading should be continued for approximately 30 s after liquid has soaked into the agar which is indicated by an increase in the frictional resistance.

The important point here is that there is no previous pre-assembly step of a bionanocomposite Sep/DNA.

In a following study, it was reported that many problems were confronted when this newest method was tried. Only a few transformants were obtained even when 100 ng of plasmid pET15b was used, and a successful result seemed difficult to repeat[266]. They increase the concentration of sepiolite to 0.1% and made the sepiolite suspension in LB instead of HEPES with KCl;

increased the time of streaking the plate to spread the transformed cells up to 100 s; and vortex the mixture (plasmid, sepiolite and cell in LB medium) vigorously in a microtube up to 10 min; to finnaly obtain 1.5 x 10^4 transformants per 100 µg of pET15b[266]. It was also reported the use of CNTs to obtain the same result compared to the use of sepiolite.

Interestingly, they reported other different results that we will discuss in Chapter 6. They are[266]:

- The transformation efficiency was reduced greatly, and even failed to produce transformants when ultrasonicated sepiolite was used, while the transformation efficiency was the highest when the sepiolite was untreated.
- These results suggested that the fibers alone hardly influenced the success of the plasmid transformation.
- Heterogeneous DNA still could enter the cell even without absorbing on the sepiolite fibers.
- The transformation might need the larger size of sepiolite to destroy the cell wall for the plasmids to enter the cell envelope through the temporary nanochannels formed in the cell membrane.
- Following the optimization described above, high-efficiency transformation could be reached and the results could be repeated well.
- They propose that the mechanism for the DNA transformation based on sepiolite might be explained as follows: "*the formation of nanochannels is driven by nanomaterials through the bouncing forces arising among the nanomaterials, bacteria and microtubes during the*

vortex mixing step. The heterogeneous DNA can simultaneously enter the cells via the nanopores, so that it can be maintained and expressed. To produce enough bouncing forces, the nanofibers should be fixed on the large particles of the nanomaterial aggregates. Otherwise, only nano-size fibers failed to produce transformants".

Later, another study also based on Yoshida effect and using sepiolite to transform Pseudomonas was reported[267]. They also optimized the protocol of Yoshida[271]. The variables taken into account were the number of cells to be transformed (ranging from 10^7 to 10^{10} cfu/ml), the concentration of sepiolite (from 20 to 500 µg/ml) suspended in NaCl 0.9%, the amount of plasmidic DNA (from 10 ng to 1 µg) and the spread time (from 30 s to 3 min)[267]. An important variation was the fact that they resuspend the bacterial pellet in 100 µl of the transforming solution consisting of sepiolite (100 µg/ml) suspended in NaCl 0.9% previously mixed with 100 ng of plasmidic DNA. The best result was close to 10^5 transformants per µg of plasmid DNA.

The same author reported in a further work that sepiolite (which is also currently used as a dietary coadjuvant in animal feed, as it increases animal growth parameters and improves meat and derived final product quality) promotes the direct horizontal transfer of antibiotic resistance plasmids between bacterial species[268]. The conditions needed for plasmid transfer (sepiolite and friction forces) occur in the digestive tracts of farm animals, which routinely receive sepiolite as a food additive. Furthermore, this effect may be aggravated by the use of antibiotics supplied as growth promoters[268].

Recently, another simple bacterial transformation method was reported, by simple spreading cells withusing magnesium- and calcium-aminoclays instead of asbestos, sepiolite or CNTs[276]. In this case, the transformation efficiency of E. coli XL1-Blue and S. mutans exhibited ~ 2×10^5 and ~ 6×10^3 transformants per μg of plasmid DNA using magnesium-aminoclay[276]. In contrast, transformation efficiency was higher in S. mutans than that in E. coli XL1-Blue for calcium-aminoclay[276].

1.6. Objectives of the Dissertation.

The focus of this research is the synthesis and characterization of DNA-based bionanocomposites in which nucleic acids (DNA) are assembled to the sepiolite (Sep) nanofibrous clay. The chief objective is to investigate the resulting Sep/DNA bionanocomposites as a nanoplatform for the potential use in non-viral transfer of bio-molecules both for gene therapy and for the development of novel biological models of interest in Academia and applied biotechnology.

The starting point is the characterization of commercial sepiolite fibers from Vallecas-Vicálvaro deposits close to Madrid, Spain, in order to verify its potential use for intracellular uptake into mammalian cells. As a special and necessary task we will perform dose response experiments of sepiolite nanofibers in mammalian cells intending to establish the optimal working concentration.

With the goal of determining the nature of the interactions of DNA assembled to sepiolite, the adsorption of different DNA conformations (genomic,

plasmid, single strand and double strand oligonucleotides) onto sepiolite will be investigated, as well as the desorption of DNA initially adsorbed. Furthermore, the possibility to modulate the adsorption and desorption efficiency of DNA on and from sepiolite will be explored, which could be useful in order to extract DNA from bacteria.

The interaction of both, sepiolite nanofibers and Sep/DNA bionanocomposites with mammalian cells will be analyzed, including their cellular internalization pathways and intracellular fate, with the aim of verifying whether sepiolite can actually be used as a platform for DNA delivery into mammalian cells.

Special attention will be given to the assessment of the ability of sepiolite for stable transfer of plasmid DNA into bacteria, mammalian and human cells. The transfection efficiency of the bionanocomposite Sep/DNA will be estimated, and the ways in which the efficiency of sepiolite-mediated gene transfer in bacteria and mammalian cells could be optimized will be explored.

Structure of Chapter 2

2.4.5. Atomic force microscopy (AFM).

2.4.6. Fluorescence microscopy.

2.4.7. Confocal microscopy.

2.4.8. Time lapse video microscopy.

2.4.9. Fluorescence-based flow cytometry: Fluorescence-activated cell sorting (FACS).

2.4.9.1. Time kinetic for sepiolite uptake in mammalian cells.

2.4.9.2. Time kinetic for Sep/DNA bionanocomposites uptake in mammalian cells.

2.4.9.3. Endocytosis inhibition.

2.5. Protocols.

2.5.1. Cell culture.

2.5.2. Cell transfection.

2. Materials and methods.

2.1. Starting Materials and reagents

2.1.1. Sepiolite

Pangel S9 consisting in a commercial sample of very high sepiolite content (>95%), provided with a cation exchange capacity (CEC) value close to 15 mequiv/100 g was received from TOLSA S.A. (Madrid, Spain).

The total specific surface area of this sepiolite was determined by N_2 adsorption-desorption isotherms and found to be 310 m^2/g from Brunauer-Emmett-Teller (BET) calculations, whereof the external specific surface area is 165 m^2/g.

A sepiolite suspension of 2 mg/ml was prepared in 10 mM TrisHCl buffer, pH=7.5, under a vigorous vortexing at maximum speed during a minimum of 10 min in order to properly disperse the clay.

Another stock solution of 2 mg/ml was prepared using a sonicated sepiolite (sSep) obtained after sonication of the sepiolite suspension, 3 times at 30% of amplitude for 10 s each time using a Vibra cell 75042 from Bioblock Scientific, and then autoclaved for intracellular experiments.

2.1.2. Deoxyribonucleic acid (DNA).

Different types of DNA molecules were used:

a) A commercial preparation of DNA, low molecular weight, from salmon sperm, was supplied by Sigma-Aldrich (31149-50G-F, lot# 0001393538). The

lyophilized DNA was dissolved in 10 mM TrisHCl, pH=7.5, to provide a 1.9 mg/ml stock solution.

b) circular DNA plasmid (5.7 kbp long, pCMV) was obtained by amplification of bacterial culture and purified using the commercial kit from Macherey-Nagel. DNA PUC19 plasmid was supplied by New England BioLabs at 1mg/ml (pUC19 Vector #N3041S, lot# 0361204).

c) single stranded DNA custom oligos 15nt long (ss-Oligo), were provided by Eurogentec (M13sense 5'-gtaaaacgacggcca-3' and M13 antisense 5'-tggccgtcgttttac-3'). The lyophilized solids were dissolved in MilliQ water to provide respective solutions of each single stranded DNA sense.

d) double stranded DNA oligos 15bp long (ds-oligo) were obtained by an annealing reaction in the presence of 10X NEBuffer provided by New England Biolabs and heating for 3min at 95^{o}C and then slow decrease of the temperature. Later on, the buffer was changed to 10 mM TrisHCl pH = 7.5 using the Micro Bio-Spin^{TM} chromatography columns and their corresponding protocol.

2.1.3. Other reactives and reagents.

Spermidine trihydrochloride (S2501-5G), Spermine tetrahydrochloride (118F-008215), Trizma (T6066-1KG) were purchased from Sigma.

2.2. Synthesis of DNA-based bionanocomposites using sepiolite.

2.2.1. Influence of cations in DNA adsorption onto sepiolite.

The adsorption of DNA molecules onto sepiolite was firstly studied carrying out experiments of adsorption in isothermal conditions at 25 ºC. A set of eight aliquots of 50 µl of sepiolite/DNA (Sep/DNA) mixtures were prepared containing in this order: 25 µl of the stock solution of the sepiolite suspension (2 mg/ml); 5 µl of 10 mM TrisHCl for the case of Sep/DNA alone, and 5 µl of 10 times concentrated solutions of 5 mM $MgCl_2$, or 5 mM $CaCl_2$, or 1 mM spermidine or 1 mM spermine for the respective case; and 20 µl of eight different concentration of salmon sperm DNA solution. The final sepiolite concentration was fixed to 1 mg/ml, and the final DNA concentration ranging from 70 to 800 ng. μl^{-1}. Then the Sep/DNA mixtures were stirred for 24 h at 25^{o}C at 700 rpm using a Thermomixer (Eppendorf) and then centrifuged for 5 min at 5000 rpm. Finally, the DNA concentration in the supernatants was measured using a Nanodrop ND1000 spectrophotometer (UV-vis spectroscopy). Experiments were carried out 3 times for each experiment.

2.2.2. Adsorption of different DNA molecules conformation.

Several adsorption isotherms were worked out using commercial salmon sperm DNA, plasmid (5.7 Kbp), 15 nt ss-oligos, and 15 bp ds-oligos. The reaction conditions was fixed to 10 mM TrisHCl, pH=7.5, 5 mM $MgCl_2$.

For each set of 3 experiments, a set of eight aliquots of 50 µl of Sep/DNA mixtures were prepared containing in this order 25 µl of the 2 mg/ml of the sepiolite suspension, 5 µl of 50 mM $MgCl_2$ and 20 µl of eight different

concentration of DNA solutions (between 100 and 1600 ng.μl^{-1}). All the Sep/DNA mixtures were stirred for 24 h at 25^{o}C and 700 rpm using a Thermomixer from Eppendorf. Finally the mixtures were centrifuged for 5 min at 5000 rpm, and the DNA concentration in supernatants was measured using Spectrophotometer Nanodrop ND1000 (UV-vis spectroscopy).

2.3. Desorption of DNA from Sep/DNA bionanocomposites.

2.3.1. Desorption of DNA using various EDTA concentrations.

Initially, 12 aliquots of 0.5 ml of Sep/DNA samples were prepared using salmon sperm DNA at 640 ng.μl^{-1} in a sepiolite dispersion (1 mg/ml) in 10 mM TrisHCl and 5 mM $MgCl_2$. Three samples were re-suspended in 0.1 ml solution of 10 mM TrisHCl, and the rest nine samples were re-suspended in 10 mM TrisHCl and EDTA at 5, 10 and 50 mM (three samples by each different EDTA concentration). After 15 min of incubation at room temperature, all samples were centrifuged at 5000 rpm for 5 min, and the supernatant was analyzed using Spectrophotometer Nanodrop ND1000 (UV-vis spectroscopy).

2.3.2. Desorption of DNA from bionanocomposites prepared in media containing different cations.

Twelve aliquots of 0.5 ml of Sep/DNA samples were prepared using salmon sperm DNA at 640 ng.μl^{-1} in sepiolite dispersion (1 mg/ml) in 10 mM TrisHCl. 3 were obtained with 10 mM $MgCl_2$, 3 with 10 mM $CaCl_2$, 3 with 1 mM spermidine and 6 with 1 mM spermine (three samples by each different polyvalent cation).

After 120 min of incubation at room temperature, all samples were centrifuged at 5000 rpm for 5 min, and the supernatant was analyzed using UV-vis spectroscopy. Then, after three subsequent steps of re-suspension of the Sep/DNA bionanocomposite (first one in 0.1 ml of 10 mM TrisHCl and the other 2 times the bionanocomposite was re-suspended in 0.1 ml of 10mM TrisHCl and 10 mM EDTA), the total amount of desorbed DNA was determined by UV-vis using Spectrophotometer Nanodrop ND1000.

2.3.3. Desorption of DNA from bionanocomposites prepared in media containing spermine.

After a previous adsorption of salmon sperm DNA in 0.5 ml of volume reaction containing 500 µg of sepiolite, the pellet was re-suspended firstly in 10mM TrisHCl in order to remove and analyze the DNA which was not strongly enough bounded to sepiolite, and then could be spontaneously desorbed by resuspension without chelation agent.

After, the pellet was resuspended for second time but in this case with 10 mM TrisHCl and 10 mM EDTA. A third resuspension was carried out also with 10 mM TrisEDTA in order to verify the amount of bond DNA after the first resuspension in presence of chelation agent. The solution was then centrifuged and the supernatant (with desorbed DNA) was analyzed using Spectrophotometer Nanodrop ND1000 (UV-vis spectrophotometer).

2.4. Characterization methods and instrumentation.

2.4.1. UV-vis spectroscopy.

Ultraviolet-visible spectroscopy (UV-vis) is an analytical technique, referred to adsorption spectroscopy in the ultraviolet – visible spectral region. In this work a NanoDrop 1000 Spectrophotometer from Thermoscientific was used to determine the concentration and purity of double and single – stranded DNA in aqueous solution.

Figure 2.1 NanoDrop 1000 Spectrophotometer.

For nucleic acid quantification, measurements are based on the modification of the Lambert-Beer law, to use an extinction coefficient with units of ng- cm/μl. Using this extinction coefficient gives a manipulated equation:

$$c = (A * e)/b$$

Where **c** is the nucleic acid concentration in ng/microliter, **A** is the absorbance in AU, **e** is the wavelength-dependent extinction coefficient in **ng-cm/microliter** and **b** is the path length in cm. The generally accepted extinction coefficients for nucleic acids are: Double-stranded DNA: 50 ng-cm/μl; Single-stranded DNA: 33 ng-cm/μl.

The purity of DNA is obtained by the "**260/280"** ratio **(**ratio of sample absorbances measured at 260 nm and 280 nm respectively). A ratio of ~1.8 is generally accepted as "pure" for DNA. If the ratio is appreciably lower it may indicate the presence of protein, phenol or other contaminants that absorb strongly at or near 280 nm. The **260/230** ratio is a secondary measure of nucleic acid purity, the values for "pure" nucleic acid being often higher than the respective 260/280 values. They are commonly in the range of 1.8 - 2.2. If the ratio is appreciably lower, this may indicate the presence of contaminants.

2.4.2. Fourier-Transform Infrared Spectroscopy (FTIR).

FTIR spectra were recorded with a Bruker IFS 66v/S FTIR spectrophotometer. Samples of 10 mg of pure sepiolite and Sep/DNA (powdered materials collected after centrifugation and drying at room temperature) were prepared as self-supporting films avoiding the use of additives such as KBr, and then placed in the sample holder and scanned from 4000 to 250 cm^{-1} with 2 cm^{-1} resolution. A set of samples studied by FTIR spectroscopy were prepared in 10 mM TrisHCl pH=7.5, sepiolite 1 mg/ml and in presence of 10 mM NaCl, 10 mM KCl, 10 mM $MgCl_2$, 10 mM $CaCl_2$, 1mM spermidine and 1 mM spermine. A second set of samples were prepared similarly but incorporating DNA (commercial salmon sperm DNA), with a mean final concentration 650 $ng.\mu l^{-1}$, then stirred overnight at 25°C and 700 rpm using a Thermomixer from Eppendorf. Finally the mixtures were centrifugated for 5 min at 5000 rpm, supernatants were removed and pellets were dried at room temperature.

2.4.3. Zeta potential measurements.

A set of 1 ml samples were prepared in 10 mM TrisHCl pH=7.5, sepiolite 1 mg/ml and in presence of 10 mM $MgCl_2$, 10 mM $CaCl_2$, 1mM spermidine and 1 mM spermine. A second set of samples were prepared similarly but incorporating DNA (commercial salmon sperm DNA), with a mean final concentration 710 ng.$\mu l^{-}1$. Zeta-potential measurements of 1 ml suspensions were performed on a Malvern ZetasizerNano ZS. Z-average values in intensity at pH 7 were used as mean hydrodynamic size (Dh), and the Z potential was measured in a 0.01 M KNO_3 solution. HNO_3 or KOH was added to the solution to alter the pH.

2.4.4. Transmission Electron Microscopy (TEM).

The transmission electron microscope uses an electron beam to bombard the specimen and produce a magnified image. It produces a projection of the entire surface of the sample including possible internal structures due to the interaction of the accelerated up electrons with the focused sample resulting in transmitted electrons passing through the thickness of the sample (the ones collected and analyzed with TEM).

The microscope Zeiss 912AB possesses a high voltage electron emitter (thermionic emission by Lanthanum Hexaboride crystal or wolfram filament). After the beam passes through the condenser lens aperture it reaches the sample and three types of transmitted electrons are generated: elastic, inelastic scattered electrons and un-scattered electrons (see figure 2.2A). Elastic scattering is predominant when the electrons encounter heavy elements (like U,

Pt, Os, W) present in the sample changing its trajectory but maintaining its kinetic energy.

In another way the inelastic scattering is predominating when the electrons encounter light elements (C, O, N, H) changing slightly its trajectory and losing kinetic energy. Depending on the type, structure and thickness of the sample, two different types of sample preparation (or staining) were performed otherwise it would be invisible in TEM. The biological samples are composed by light elements thus without staining the images present low z-contrast.

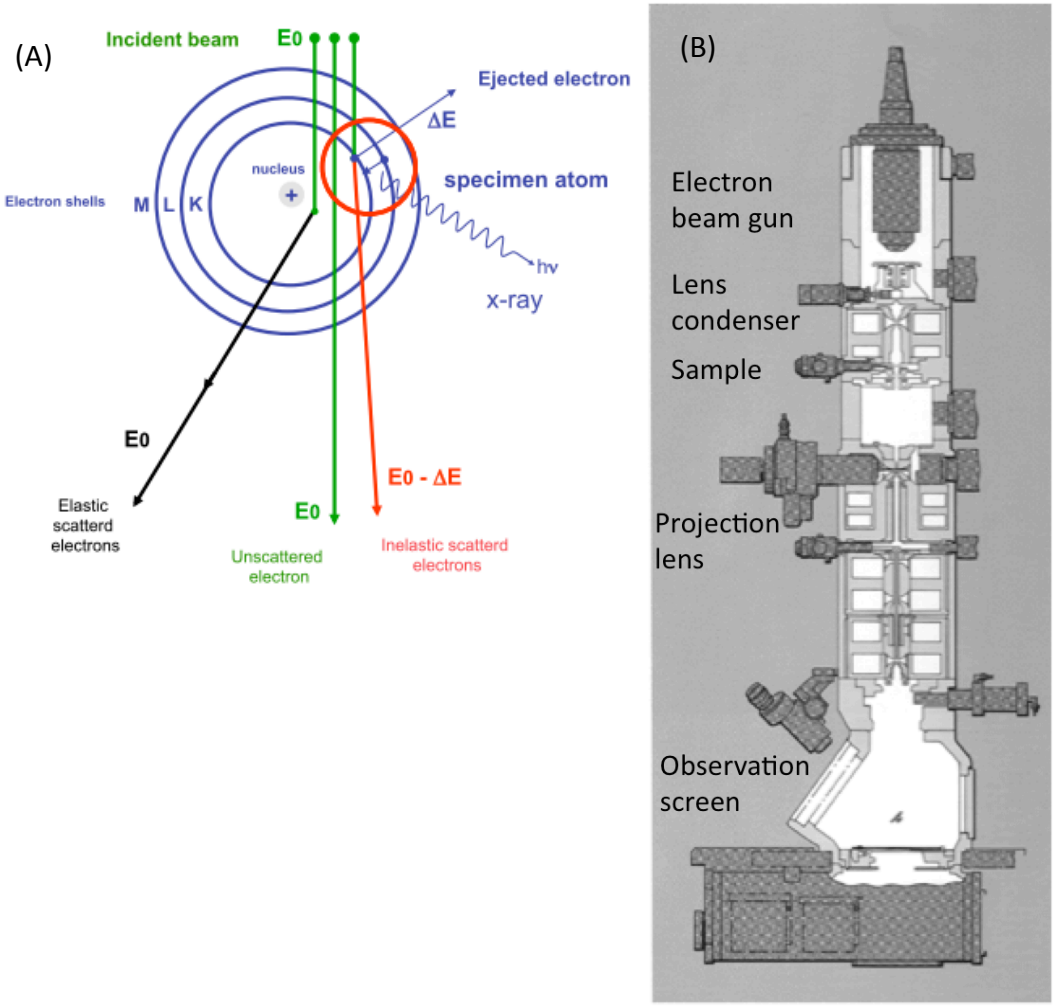

Figure 2.2 (A) Electron-matter interaction *and (B) Schematic representation of a TEM column.*

The sample preparation techniques depend on the sample and addressed questions. Most of TEM methods have been developed in connection with the study of viruses or proteins sizes at least 300 or greater than 400 kDa. These biological macromolecules are usually observed in bright field with a so-called negative staining method.

The TEM imaging of DNA or DNA-protein complexes is rare and has been made possible thanks to the development of specific methodologies using physicochemical properties of DNA. The negative charge of DNA required the use of a spreading agents like cytochrome c or positive ionization of carbon films. Dark field imaging mode is the mainly used observation technique. In the dark field mode the direct transmitted beam is excluded from the image formation process resulting in a dark background. For our analysis the high angle elastic scattered electrons (called scattering contrast) were mainly selected since was Off-axis Dark field mode was aimed to use.

The TEM grid for sample preparation is a thin metal layer in which a carbon film was deposited for the adsorption of particles. After the carbon deposition, the grids were functionalized with Pentylamine. This is done by the glow discharge using a homemade device developed in Eric Le Cam‘s group (special equipment not commercially available designed by Dubochet *et al.* in 1971). These molecules create a positively electrically charged surface allowing the DNA sample to spread out due to its negative charge.

Then, a 5 µL diluted drop of the sample is deposited in the grid during one minute. Then a drop of uranyl acetate at 2% is deposited in the top of the sample during one minute and carefully with a filter paper the sample is soaked up by capillarity. In this case the heavy metal selectively coats the sample

allowing an ultra-structure observation. This is due to a chemical reaction between the heavy metal and the constituents of the material (for instance uranyl ions and DNA phosphate groups) – see figure 2.2A.

2.4.4.1. Analysis of DNA, sepiolite and Sep/DNA bionanocomposites.

Samples were prepared from 5 µL of sepiolite or sep/DNA solution deposited for 1 min on a 600-mesh copper grid covered with a thin carbon film, activated by glow-discharge in the presence of pentylamine[277]. Grids were washed with aqueous uranyl acetate 2% (w/v), dried with ashless filter paper and observed in the dark-field mode with a tilted illumination, using a Zeiss 912AB transmission electron microscope. Images were recorded at magnifications of 50000×, 85000× and 140000× with a ProScan 1024 HSC digital camera and iTEM acquisition software (Olympus Soft Imaging Solution).

2.4.4.2. Analysis of sepiolite and Sep/DNA bionanocomposites in cells.

V-79 cells were prepared using 2,5% gluteraldehyde fixative solution in 0.1 M cacodylate buffer solution (pH =7.4) for 1 h and then rinsed in the same buffer solution (3 x 5 min). A post fixative step was performed with 1% OsO_4 in cacodylate buffer and then, the cells were water rinsed (3 x 10 min). Cells were dehydrated in ethanol solution (90% 2 x 10 min) and 100% (3 x 10 min). The substitution was made in epon/acetone solutions in the volume ratio of 1/3, 1/2 and 3/1 each of them for 1 h. At the last substitution step, a new bath of epon

was carried out for 1 h before the last one overnight. Cells were then encapsulated with new epon with Benzyldimethylamine (BDMA) harderner for polymerization at 60°C for 24 h.

Sample preparation of cell thin sections for TEM observation, was performed using a Leica Ultracut UCT ultra-microtome. The experimental conditions were: use of a 35° diamond knife, section thickness of 90 nm with 1.6 mm/s speed rate. Cell thin sections were deposited on carbon/collodion grids before staining with 2% uranyl acetate solution in water during 20 min and with lead citrate for 3 min.

In order to investigate the sepiolite uptake mechanisms in cells, TEM analysis were performed on four types of samples. They correspond to sepiolite incubation times in cell culture that allow catching the first steps from the internalization by the membrane surface to the inner part of cytoplasm and nucleus, *i.e.* : 0, 0.5 , 1 and 6 h. The sepiolite fibers-cell interaction was analyzed by TEM using a 80 KeV 902 Zeiss TEM microscope equipped with an electron energy filter in column. Bright-field TEM imaging mode was carried out using zero loss energy filtering.

2.4.5. Atomic Force Microscopy (AFM).

The Atomic Force Microscopy[278] (AFM) is a high-resolution imaging technique, that associates nanometric resolution and topographical characterization of single biological molecules in their physiological environment. The atomic force microscope belongs to the family of Scanning Probe Microscopy (SPM).[278]

The SPM family members are all based on the interaction between a sharp probe and a surface. The AFM uses a very sharp tip radius of 10 nm typical curvature passing over a surface (commonly named cantilever, see Figure 2.3).

The atomic force microscope provides a magnified image of surface topography by keeping constant the atomic force interaction between the tip and surface as the sample is moved in the X and Y directions. This sample movement is performed by a piezoelectric tube, which beside the XY motion also allows movement in the direction Z. The interaction is kept constant by a feedback system that accurately adjusts the value of the piezo Z, applying the appropriate voltage. The representation of these voltages becomes the topographic image of the sample.

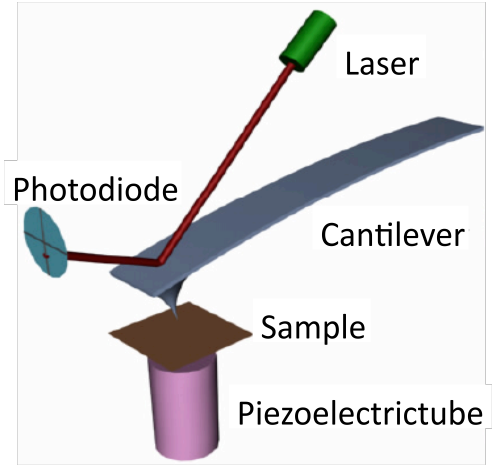

Figure 2.3. Schematic representation of the basic components of the mechanical part of the used AFM: the cantilever with the detection system, the sample and the piezoelectric tube to XYZ scanning.

One of the essential parts of the AFM is the probe or tip that interacts with the sample surface. Normally, these tips are constructed on silicon or

silicon nitride using micro-fabrication techniques, and are located at the end of a micro-lever of around 100 to 200 μm length and 20 to 40 μm wide. The force constant (K) and the resonance frequency (ϖ_{res}) constitute the essential characteristics of the cantilevers and vary between 0.015 N/m and 100 N/m and between 5 and 500 kHz, respectively.

The motion of the cantilever is usually detected using a laser beam, which is reflected, at the end of the cantilever, and then the reflected beam goes to a photodiode segmented into 4 sections. The cantilever deflection is measured by the resulting signal from the difference in intensity between the upper and lower quadrants, and this signal is proportional to the normal force. Similarly, the torsion of the cantilever is measured by the intensity difference between the lateral quadrants and is proportional to the named lateral force.

The essential components of the AFM are typical the cantilever, the detection system of the cantilever deflection, the sample, and the piezoelectric tube which performs the XVZ scanning. A schematic representation, which shows these elements, can be seen shown in Figure 2.3.

AFM imaging of sepiolite, DNA and Sep/DNA bionanocomposites was performed on a freshly cleaved mica surface treated with 50 μM spermidine for 1 min. [279]. Excess of spermidine solution was blotted with filter paper and 3-5 μL of 5 nM. The sample was deposited on the mica surface, incubated for 1-2 min, and rinsed with 25 μL of 0.2 % (w/v) uranyl acetate[280]. The surface was blotted and dried. Imaging was carried out in Tapping Mode, with a Multimode system (Bruker) operating with a Nanoscope V controller (Bruker) using silicon AC160TS cantilevers (Olympus) with resonance frequencies of ~300 kHz. All

images were collected at a scan frequency of 1 Hz and a resolution of 1024 × 1024 pixels. Images were analyzed with Nanoscope V software. A third-order polynomial function was used to remove the background.

2.4.6. Fluorescence Microscopy.

Cells were washed in PBS and fixed in 4% formaldehyde. Coverslips were mounted in mounting medium (Dako) supplemented with DAPI (Sigma). Images were acquired on an Axio Imager Z1 microscope using the Axio Vision software (Zeiss).

2.4.7. Confocal microscopy.

Images were acquired on a confocal Leica SpE with the objective 63x (ACS AP063.0x1.30 oil). The pictures were 1024 by 1024 pixels, taille pixel: 174.6 µm.

2.4.8. Time lapse video microscopy.

One day before the acquisition, 10^5 of V79 cells were plated in Lab-Tek Chambered #1.0 Borosilicate Cover Glass System 155380 (2 chambers), in modified Eagle's medium (MEM) containing 10% fetal bovine serum (FBS). Just before the acquisition, the cellular medium was changed with a new MEM with 10 ng.µl^{-1} sonicated sepiolite (sSep). Images were acquired every 6 min 30

sec within 18 hours 20 min on an Olympus Fluoview FV10i with the objective UPLSApo60x.

2.4.9. Fluorescence-based flow cytometry: Fluorescence-activated cell sorting (FACS).

2.4.9.1. Time kinetic for sepiolite uptake in mammalian cells.

100 μl of sepiolite dispersion was prepared as following: 45 μl of sepiolite at 2 mg/ml and 55 μl of 10 mM TrisHCl. 8.9 ml of cellular medium (MEM) was added and gently homogenized. Finally, 3 ml of sepiolite at 10 $ng.\mu l^{-1}$ in cellular medium was added in each set of 3 wells with 2 x 10^4 of V-79 cells in each well. Cells were collected after trypsinization and measured in FACS after 1, 4, 6 and 24 h of addition of sepiolite. Samples were analysed with a C6 flow cytometer using the C6 Flow software (BD Accuri). 10,000 cells were counted for each sample.

2.4.9.2. Time kinetic for Sep/DNA bionanocomposites uptake in mammalian cells.

100 μl of Sep/DNA dispersion was prepared as following: 45 μl of sepiolite at 2 mg/ml, 20 μl of 50 mM $CaCl_2$, 5 μl of 10 mM TrisHCl and 20 μl of PUC19 plasmid at 400 $ng.\mu l^{-1}$. Then 8.9 ml of cellular medium (MEM) was added and gently homogenized. Finally, 3 ml of sepiolite suspension at 10 $ng.\mu l^{-1}$ in cellular medium was added in each well with 2 x 10^4 of V-79 cells in each well. Cells were collected after treatment with trypsin and measured in FACS after 1, 4, 6, and 24 h of addition of Sep/DNA complex.

Samples were analysed with a C6 flow cytometer using the C6 Flow software (BD Accuri). 10,000 cells were counted for each sample.

2.4.9.3. Endocytosis inhibition.

V79 hamster cells and U20S human cancer cells were incubated with 1 ml of 100 µM amiloride at 37°C[20,281]. The treatment was performed 30 min before the addition of 10 ng.µl^{-1} sepiolite suspension to the cells. Amiloride HCl dihydrate (Catalog No. S2560) was provided by Selleck Chemicals (www.selleckchem.com), in a 10 mM / 1 ml stock solution. It was used for selective inhibition of macropinocytosis in mammalian cells.

For clathrin-dependent endocytosis inhibition, V79 hamster cells and U20S human cancer cells were incubated with 3 ml of 10 µM chloroquine at 37°C. The treatment was performed 30 min before the addition of 10 ng.µl-1 sepiolite suspension to the cells. Chloroquine diphosphate salt (C6628-25G lot # BCBK7067V), was supplied by Sigma Aldrich. A 100 mM stock solution was prepared by dissolving 200 mg chloroquine in 3.9 ml water by gentle vortex, and then sterilize filtering through a 0.22 µm filter.

Measurements were performed by FACS in CyFlow Space from Partec. 10,000 cells were counted for each sample.

2.5. Protocols.

2.5.1. Cell culture.

Chinese hamster cells were grown in dishes as monolayers in modified Eagle's medium (MEM) containing 10% fetal bovine serum (FBS). U2OS human osteosarcoma cells were grown in dishes as monolayers in Dulbecco's modified Eagle's medium (DMEM) from Life Technologies containing 10% (v/v) FBS. Cells were incubated at 37^{o}C with 5% CO_2 in air and 100% humidification. MEM, DMEM and FBS were purchased from Life TechnologiesTM.

2.5.2. Cell transfection

Sep/DNA bionanocomposite with 80 µg of sepiolite and 2 µg of bounded DNA was prepared in 70 µl solution in presence of $CaCl_2$ in this order: 40 µl of sepiolite at 2 mg/ml, 14 µl of 50 mM $CaCl_2$, 7.8 µl of 10 mM TrisHCl and 8.2 µl of pCMV plasmid encoding for the resistance gene to G418 at 490 ng.µl^{-1}. For the comparison of efficiencies of bionanocomposites prepared in presence of spermidine and spermine, the procedure was the same but using 14 µl of 1 mM spermidine and 14 µl of 1 mM spermine, respectively. After 2 h of incubation at 25^{o}C and stirred at 700 rpm in Thermomixer from Eppendorf, 5.83 ml of cellular medium (MEM) was added and gently homogenized. Finally, 6 ml of bionanocomposite suspended in cellular medium was added in two wells (3 ml in each well) with 2 x 10^{4} of V-79 cells in each well. After two days, cells were washed with PBS and new medium was added with antibiotic G418 at 600

ng.μl^{-1} in order to start the selection. After 10 days cells colonies were stained with Giemsa (25% in ethanol).

For human cells, sep/DNA bionanocomposite with 80 μg of sepiolite and 3 μg of bounded DNA was prepared in 70 μl solution in this order: 40 μl of sepiolite at 2 mg/ml, 14 μl of 50 mM $CaCl_2$ and 16 μl of pCMV plasmid at 490 ng.μl^{-1}. After 2 h of incubation at 25^{o}C and stirred at 700 rpm in Thermomixer from Eppendorf, 8.9 ml of cellular medium (DMEM) was added and gently homogenized. Finally, 9 ml of bionanocomposite suspended in cellular medium was added in three wells (3 ml in each well) with 1 x 10^4 of U2OS cells in each well. Experiment was done with both vortexed and sonicated sepiolite. After two days, cells were washed with PBS and new medium was added with antibiotic G418 at 800 ng.μl^{-1} in order to start the selection. After 10 days cells colonies were stained with Giemsa. Cell transfection was carried out in 6-well plates.

RESULTS AND DISCUSSION

Structure of Chapter 3

3. **Characterization of sepiolite fibers and its interactions with mammalian cells.**

   3.1. AFM and TEM characterization of sepiolite fibers.

   3.2. Sepiolite – mammalian cells interactions.

   3.3. Spontaneous internalization of sepiolite into cells.

3. Characterization of sepiolite fibers and its interactions with mammalian cells.

3.1. AFM and TEM characterization of sepiolite fibers.

A report on the use of atomic force microscopy (AFM) technique for the quantitative size evaluation of sepiolite fibers in three dimensions of a clay from Turkey was recently reported[282]. This AFM study revealed that the average fiber dimensions of the fibers of this Turkish clay were determined as 249 × 1127 × 29 nm (width × length × height)[282].

As it was already mentioned in section 1.2, the length of sepiolite fibers is determined by the geological origin of the silicate. Sepiolite fibers selected in this work were obtained from a commercial sepiolite from Vallecas-Vicálvaro deposits (close to Madrid, Spain) which is known to have relatively small fibers[1]. Thus, AFM has allowed to measure the fibers dimensions of the Spanish clay used in the present work, showing that they are smaller than Turkish ones (Figure 3.1). Indeed, it was possible to observe fibers smaller than 800 nm in form of aggregates. In order to carry out a more stringent analysis and in view to determine the fibers size distribution, we have also applied transmission electron microscopy (TEM). Measurements showed that the mean value for the fiber width was 15 nm, and around 80% of fibers were between 200 and 400 nm length, the maximal length being 800 nm (Figure 3.2). Therefore, the small size of sepiolite nanofibers from the clay from Madrid area make this silicate

[1] Data from TEM and FE-SEM images of sepiolite from the Taxus Basin (Pangel S9). E. Ruiz-Hitzky and P. Aranda, personal communication.

potentially suitable for intracellular uptake into mammalian cells, in addition to the low toxicity associated with the silicate composed of fibers of small size (at the nanometric scale).

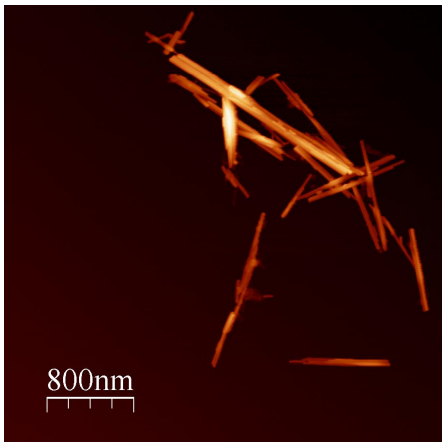

Figure 3.1 Atomic force microscopy (AFM) image of sepiolite fibers taken from dispersion of sepiolite at 1 mg/ml in water, stirred in Vortex for 5 min at maximum speed.

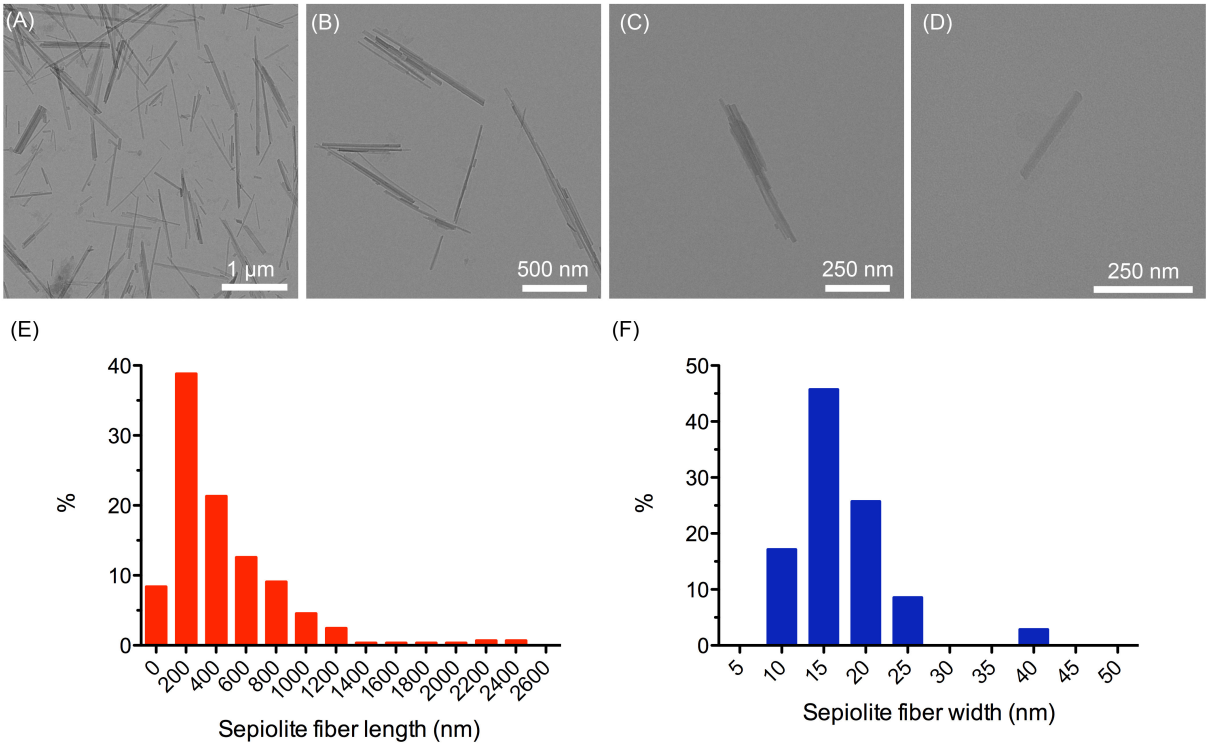

Figure 3.2. Analysis of the size distribution of sepiolite fibers. A-D: TEM images of sepiolite fibers (1 mg/ml sepiolite dispersion in 10 mM TrisHCl, pH=7.5) E: sepiolite fiber length distribution (nm), F: sepiolite fiber width distribution (nm).

3.2. Sepiolite – mammalian cells interactions.

In order to verify whether sepiolite can actually be used as a biomolecule platform delivery into mammalian cells, we then analyzed its interaction and behaviour with mammalian cells, focusing the study mainly in its capacity for being internalized into cells. We took advantage of spontaneous fluorescence of sepiolite (in green, excitation at 488 nm and emission in 498 nm – 530 nm; in red, excitation at 532 nm and emission in 542 nm – 685 nm) to monitor its spontaneous uptake into cells.

A time-kinetic of sepiolite uptake in V-79 cells was carried out monitored by fluorescence-activated cell sorting (FACS), which allows to monitor fluorescent cells upon contact with naturally fluorescent sepiolite (Figure 3.3). In this experiment we used different concentrations of sepiolite, *i.e.* 1, 5, 10, and 50 and 100 $ng.\mu l^{-1}$. 6 hours after the addition of sepiolite, around 10% of cells remained fluorescent at sepiolite concentration of 1 $ng.\mu l^{-1}$, and from 30 to 50% with sepiolite at concentrations of 5 and 10 $ng.\mu l^{-1}$, respectively (Figure 3.4). From the toxicity point of view, it is worth to mention that with the highest concentrations of sepiolite used in this experiment, *i.e.* 50 and 100 $ng.\mu l^{-1}$, the last viable data was obtained at 6 hours after addition of sepiolite. At sepiolite concentration of 100 $ng.\mu l^{-1}$ only 6.9% of cells were in the region corresponding to living cells, and after this time it was no possible to reach 10,000 counts of living cells with this two concentrations. A sepiolite concentration less than 50 $ng.\mu l^{-1}$ is not toxic for the cells, as they could be growing even with the presence of sepiolite several days before.

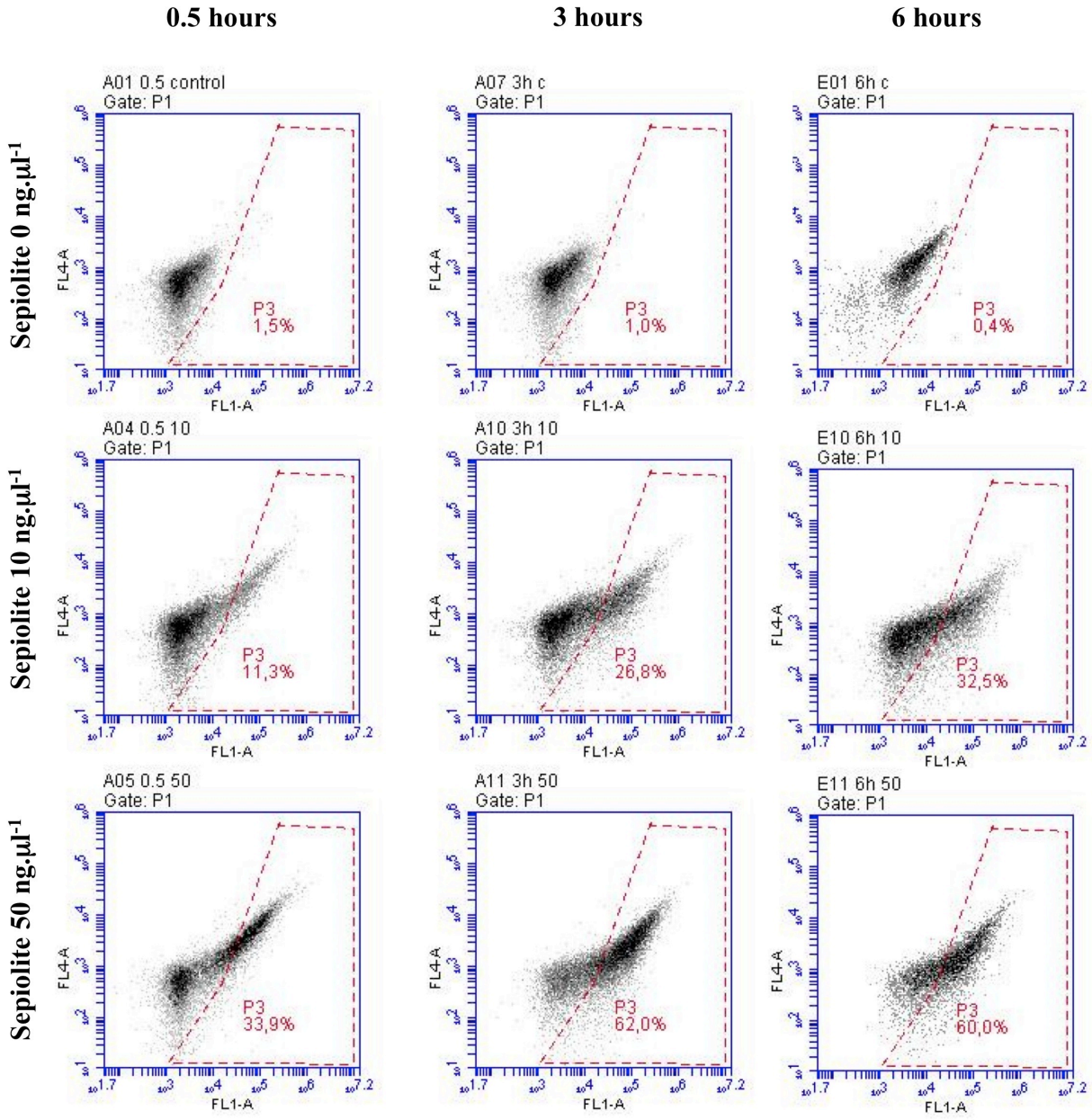

Figure 3.3 Dots-plots from fluorescence activated cells sorting (FACS) experiment, for data corresponding to 0.5, 3 and 6 hours after the addition of sepiolite into V79 cells at different concentrations (0 ng.µl^{-1}, 10 ng.µl^{-1}, and 50 ng.µl^{-1}). The zone P3 corresponds to green fluorescent cells (channel FL1A, 530 nm) due to the presence of sepiolite. 10,000 cells were counted in all experiments. The working concentration for sepiolite was fixed to 10 ng.µl^{-1} for experiments with mammalian cells.

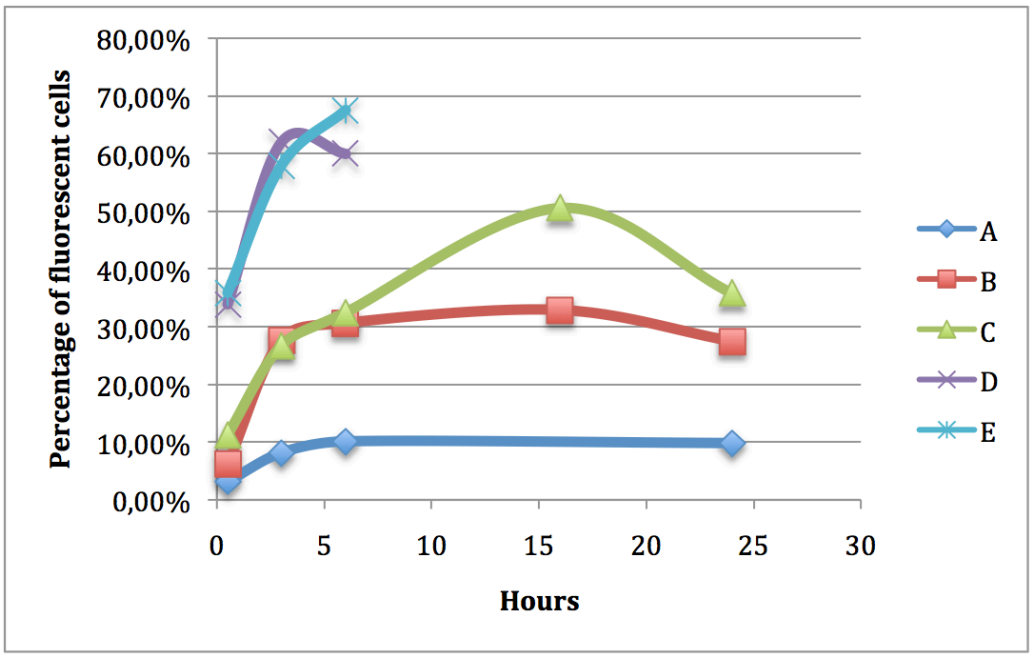

Figure 3.4 Results obtained with fluorescence activated cells sorting (FACS) for the time kinetics of sepiolite uptake in V79 cells for different sepiolite concentrations (one experiment). Sepiolite concentrations: A: 1 ng.μl^{-1}, B: 5 ng.μl^{-1}, C: 10 ng.μl^{-1}, D: 50 ng.μl^{-1}, E: 100 ng.μl^{-1}.

3.3. Spontaneous internalization of sepiolite into cells.

The data obtained with FACS show that sepiolite can indeed, interact with cells. However, to demonstrate the internalization, we performed different microscopy analysis. First laser confocal microscopy analysis detected sepiolite fibers inside the V79 cells at different concentrations (Figure 3.5 and 3.6). In figure 3.5 is possible to observe the big natural fluorescence of sepiolite fibers at different wavelength. Sepiolite is fluorescent in the green and red regions (in FACS experiment it was observed more fluorescence in green than in red), and not fluorescent in blue and infrared. Fluorescence becomes higher in aggregates of sepiolite fibers.

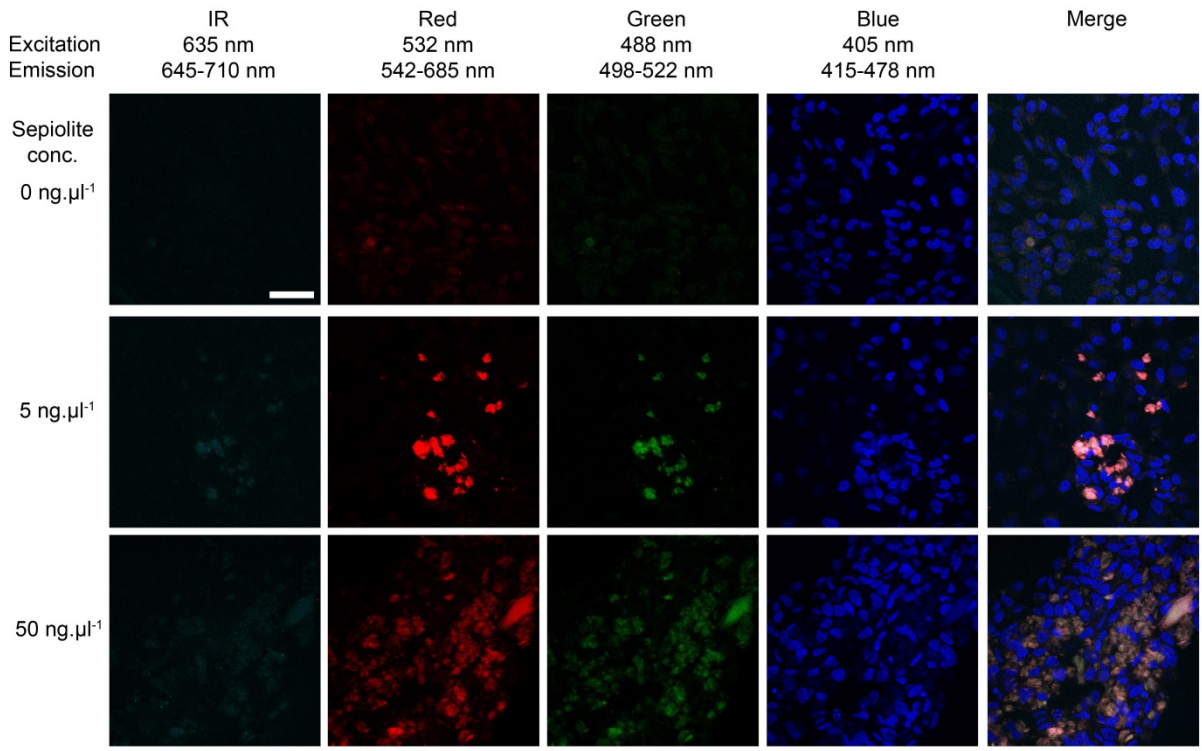

Figure 3.5 Laser confocal microscopy images of sepiolite fibers inside V79 cells. Concentration of sepiolite dispersion in MEM: 0, 5 and 50 ng.μl^{-1}. Channels: IR (infrared), red, green and blue, at given excitation and emission wavelengths. Sepiolite has a natural fluorescence in green and red, and is not fluorescent in blue and infrared. The blue fluorescence represents the Daco-Dapi staining of the cells nucleus. In merged images, we confirm that sepiolite fibers were uptaken by the cells. Wavelengths of excitation and fluorescence emission are indicated. The scale bar represents 25 μm.

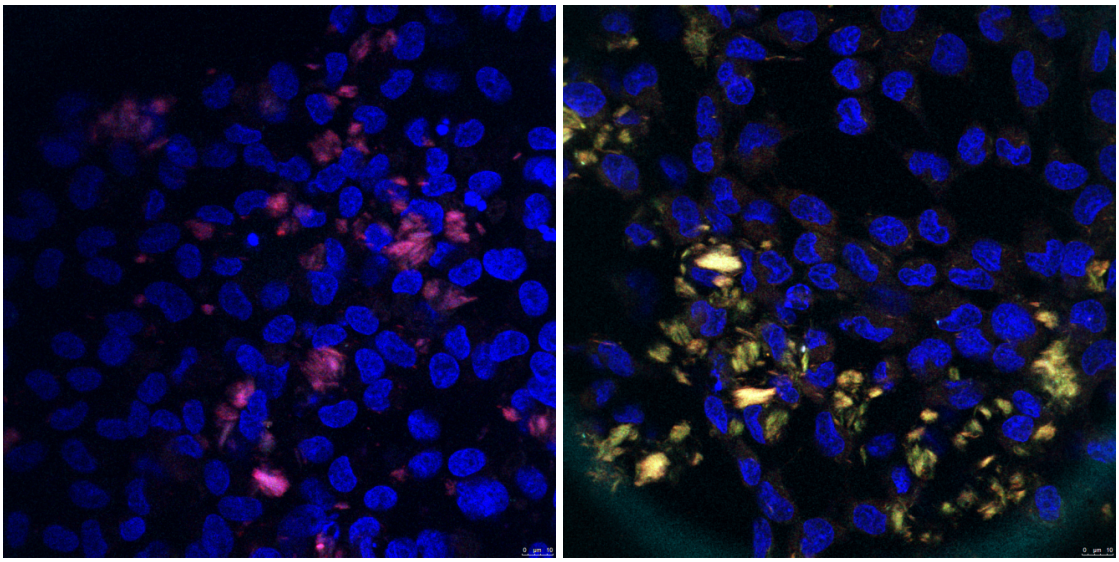

Figure 3.6. Laser confocal microscopy image of of sepiolite fibers inside V79 cells. Concentration of sepiolite dispersion in MEM: 10 ng.μl^{-1}(Left) and 50ng.μl^{-1} (Right).

Fluorescence microscopy was also used to observe different sepiolite fiber localization in V79 cells (Figure 3.7). In the majority of cases, sepiolite fibers were found in the cytoplasm and close to the nucleus.

After the analysis of FACS and fluorescence microscopy images, it was possible to select a working concentration for sepiolite dispersion in further experiments involving mammalian cells. It was shown that a concentration of 10 ng.μl^{-1}, at least 45% of cells becomes fluorescent after 6 hours of contact with sepiolite, and even one and two days after. According to the obtained results, the working condition for sepiolite-cells interaction experiments was fixed to 10 ng.μl^{-1}. Observation of cells by optical microscopy confirmed that cells are still growing in presence of sepiolite fibers, which is an indication of the low cytotoxicity of sepiolite from Madrid at that dose.

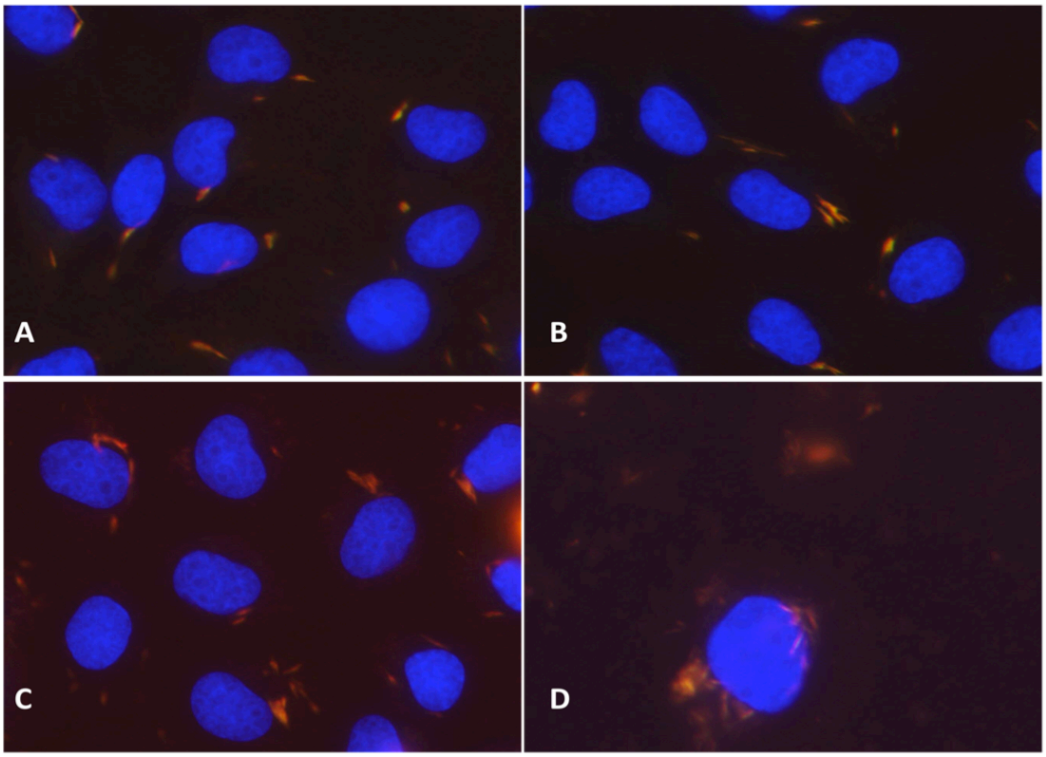

Figure 3.7. Fluorescence microscopy images of sepiolite fibers inside V79 cells. Concentration of sepiolite dispersion in MEM: A-B: 5 ng.μl^{-1}, C:10 ng.μl^{-1} and D: 50 ng.μl^{-1}.

Spontaneous uptake of sepiolite fibers into cells was then confirmed by time-lapse video microscopy. Of note, this analysis showed both the intake and the outtake of sepiolite. Interestingly, the transfer of sepiolite fibers from one cell to another into cells was also observed, which could constitute a promising strategy for further intracellular applications.

To detail the cell structure and mechanisms involved, and to increase resolution analysis of the interaction of sepiolite with cells, we performed an analysis by TEM. V-79 cell were incubated with sepiolite at 10 ng.μl^{-1} in cellular medium, and then prepared for TEM analysis. Interestingly, TEM observation distinguished different steps for sepiolite internalization from the membrane surface (Figure 3.9) to the inner part of the cytoplasm, as shown in Figure 3.8

showing a set of three different cells with their corresponding sepiolite fiber localization. Importantly, after 0.5 hours of contact, sepiolite fibers mainly localized at cell surface, while after 1 hour, sepiolite localized both at surface and cytoplasm. Finally, after 6 hours of contact, sepiolite localized in cytoplasm with some internalization states into the nucleus.

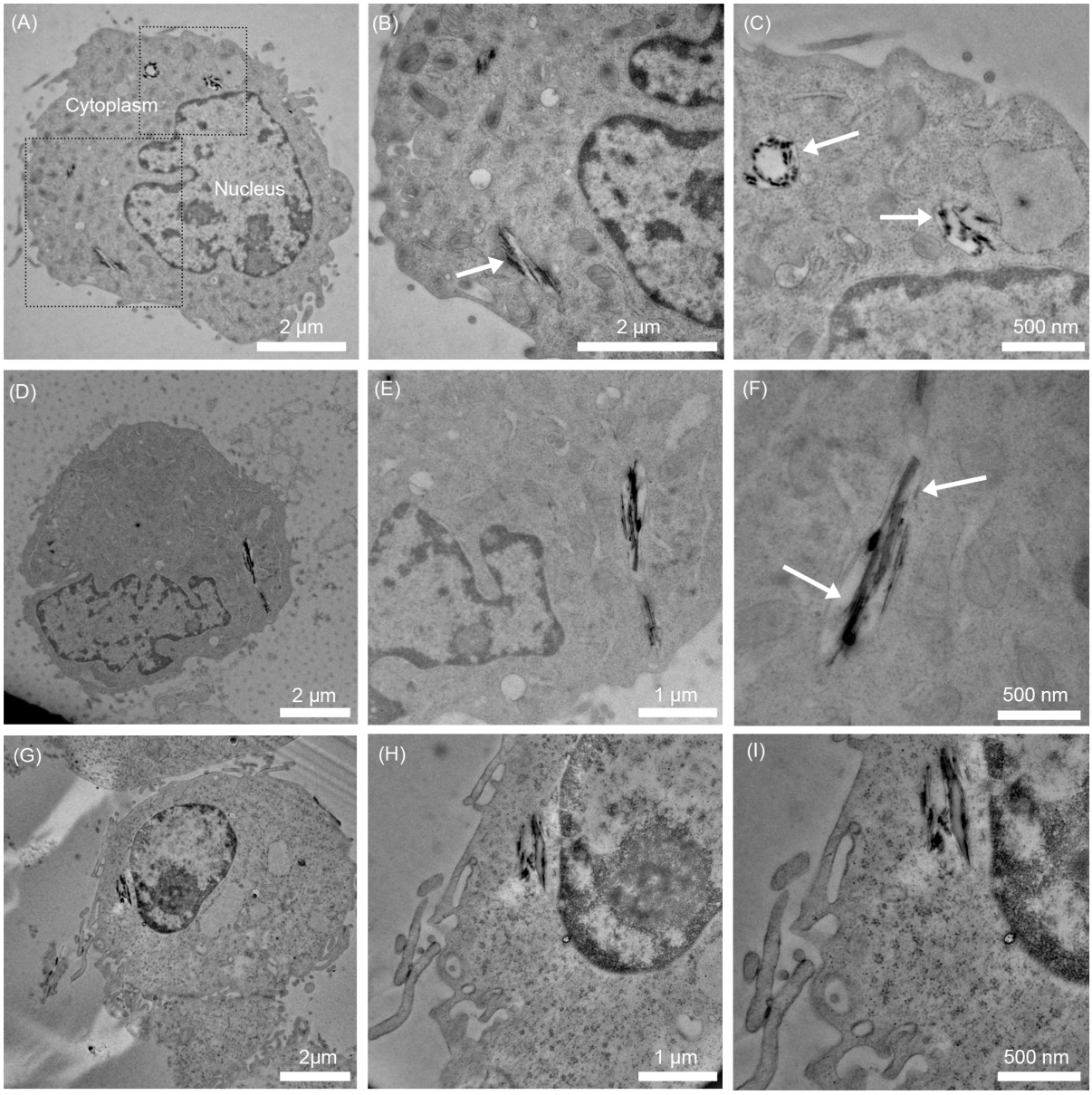

Figure 3.8. TEM images of a set of three different V79 cells (A, D and G) with zooming in respective internal sepiolite fiber localizations (10 ng.μl^{-1} sepiolite in 5.10^6 cells).

Remarkably, TEM analysis revealed that cytoplasmic sepiolites fibers were embedded into endosomes membrane (Figure 3.8C), suggesting the entry of the fibers by endocytosis, resulting from membrane invagination (Figure 3.9C), and consistently with observations done by time lapse video microscopy.

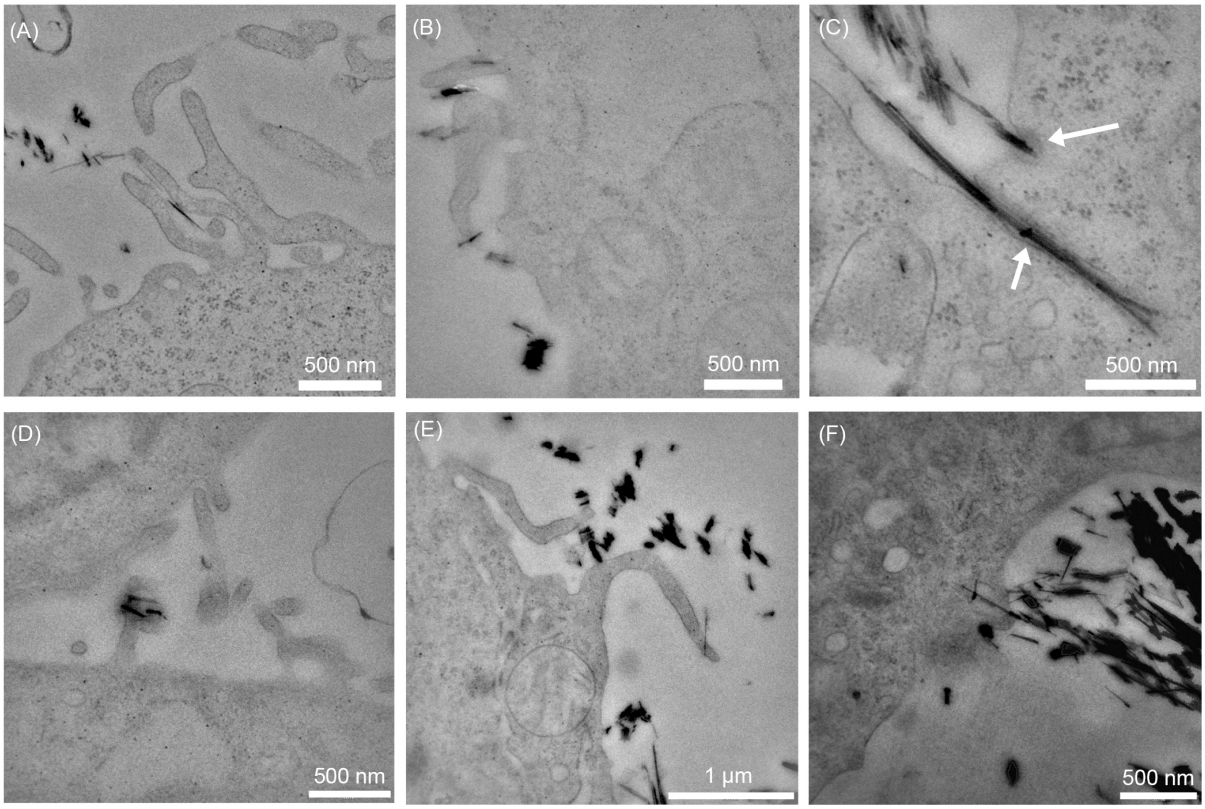

Figure 3.9 TEM images of V79 cells showing different cellular uptake mechanisms of sepiolite fibers.

More specifically, classical structures of endocytosis and macropinocytosis were observed at the junction cell membrane/sepiolite (Figures 3.9A-D). It should be noted that macropinocytosis occurs via the formation of actin-driven membrane protrusions called pseudopods[133], which are clearly visible here (Figures 3.9A-D). These structures fuse with the plasma

membrane, leading to internalized sepiolite cavities inside the cytoplasm, either surrounded by a membrane (white arrow in Figure 3.8C) or not (Figure 3.8B).

It should be also noted that some internalized sepiolite fibers were not embedded into membranes, suggesting a non-endocytic pathway for the sepiolite uptake. Direct sepiolite fiber insertion (Figure 3.9C) inside the cells could result from a combination of two factors. The first one is related to the particular physical-chemistry properties (*i.e.,* surface chemistry behaviour) of the sepiolite fibers, allowing them to adsorb lipids from the cellular membrane and then going inside the cells. Actually, phospholipds such as phosphatidylcholine show high affinity to bind the external surface of sepiolite fibers giving rise to biohybrid materials that mimics cellular membranes[16,17,283]. The second factor is related to the geometry of sepiolite fiber which, as occurs in other needle-like materials such as CNTs, allows a direct insertion bypassing the classic mechanisms[19]. This mechanism was also found in studies of internalization of functionalized CNTs, in which was observed a dependence with the fiber size and the surface charge in the internalization of CNTs in cells[18,19].

In order to confirm that macropinocytosis and other endocytosis mechanisms are involved in sepiolite internalization into the cells, we measured by FACS the percentage of fluorescent cells, upon incubation of them with sepiolite in the presence of endocytosis inhibitors: chloroquine, which blocks clathrin-dependent endocytosis[20], and amiloride, which inhibits macropinocytosis[281]. Thus, 10 μM of chloroquine reduced sepiolite internalization into V79 cells of 20%, while 100 μM amiloride caused the 50% of inhibition. These data pointed out that sepiolite internalisation into cells mainly

results from macropinocytosis, which is also consistent with the sequence observed in the pictures obtained by TEM (see Figure 3.9D).

Taken together all of these results it can be postulate that sepiolite nanofibers are spontaneously and efficiently internalized by the cells. Thus, since sepiolite can binds various biological molecules it can be concluded that this nanoparticulated silicate is a good candidate for uses as a nanocarrier, constituting a new form for vectorization of biological molecules like DNA.

Aiming at using sepiolite for DNA transfer, the next step was to prove that DNA actually binds to sepiolite, and to ascertain the nature of the physicochemical interactions in the resulting sepiolite/DNA bionanocomposite materials (Sep/DNA).

Structure of Chapter 4

4. **Synthesis and physicochemical characterization of sepiolite-DNA (Sep/DNA) bionanocomposites.**
   - **4.1. Previous results.**
   - **4.2. Synthesis of Sep/DNA bionanocomposites. DNA adsorption onto sepiolite.**
   - **4.3. Influence of cations with different valence on DNA adsorption onto sepiolite.**
   - **4.4. Adsorption efficiency of different DNA conformations.**
   - **4.5. DNA desorption from sepiolite.**
   - **4.6. Physicochemical characterization of Sep/DNA bionanocomposites.**

4. Synthesis and physicochemical characterization of sepiolite-DNA (Sep/DNA) bionanocomposites.

4.1. Previous results.

With the aim to use sepiolite as an intracellular nano-platform for DNA transfer, the next step in this work was to prove that DNA molecules actually bind to sepiolite, and to study the nature of the physicochemical interactions between both components in the sepiolite/DNA (Sep/DNA) bionanocomposite.

In fact, in previous assays which are not included in this PhD dissertation, it has been verified diverse aspects concerning the viability of the DNA binding to sepiolite[41]. Adsorption isotherms were worked out, at acidic pH (in presence of 50 mM HAc/NaAc, pH 4.8), determining the amount of adsorbed DNA from UV-vis and elemental chemical analysis data. According to those previous results, nucleic acids (low molecular weight DNA from salmon sperm) were spontaneously adsorbed on the external surface of microfibrous sepiolite through hydrogen-bonding interactions with the external silanol groups present on this silicate. Adsorption isotherm (Figure 4.1A) was of the L-type, indicating a high affinity of DNA to be adsorbed in this inorganic solid. This affinity provokes the agglomeration of DNA biopolymer on the fibrous clay particles, as shown field emission-scanning electron microscopy (FE-SEM) images (Figure 4.1B and 4.2C).

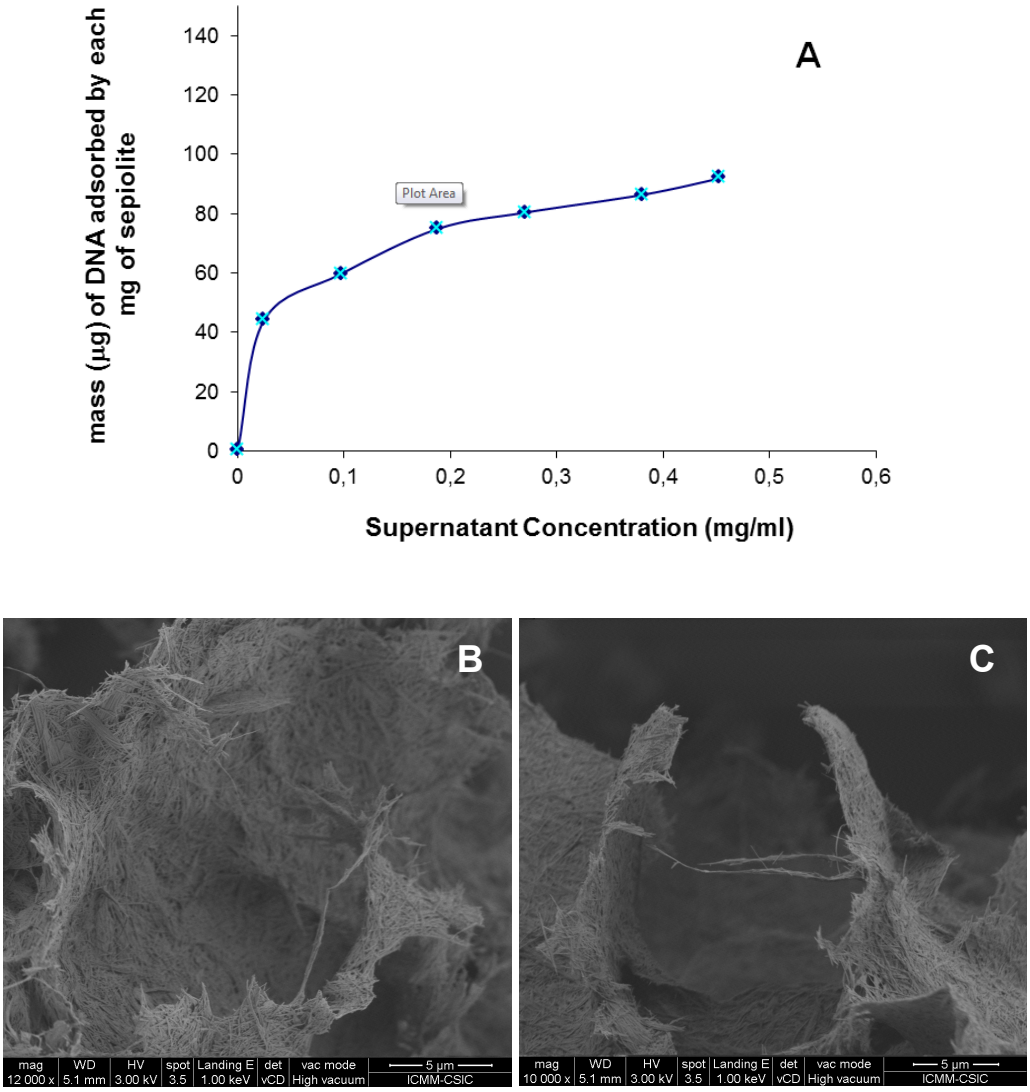

Figure 4.1 Results from a previous study carried out at the ICMM-CSIC[41] *on DNA adsorbed onto sepiolite. A) Adsorption isotherm of salmon sperm DNA (50mM HAc/NaAc pH=4.8) on sepiolite at 30°C (equilibrium at 24 hours under agitation. B), C) FE-SEM images of the Sep/DNA bionanocomposite prepared in this acidic medium condition.*

Based on those promising results, the present study intends to synthesize Sep/DNA bionanocomposites using a media close to neutral pH (ph 7.5), as such conditions appears to be more suitable for biological and biomedical applications.

4.2. Synthesis of Sep/DNA bionanocomposites. DNA adsorption onto sepiolite.

Adsorption isotherm experiments carried out at pH=7.5 also revealed an efficient adsorption of DNA onto sepiolite nanofibers (Figure 4.2A and 4.2B). At low initial concentration of DNA, up to 400 ng.μl^{-1}, the adsorption behaviour can be considered as a convex simple-component Langmuir isotherm. At higher DNA concentrations (>400 ng.μl^{-1}), the curves suggested a multi-layer adsorption and saturation. The saturation point was found for an initial DNA concentration of 630 ng.μl^{-1}, corresponding to the maximum of spontaneous DNA adsorption onto sepiolite (around 80 μg of DNA adsorbed per mg of sepiolite). At the highest concentrations of added DNA (>630 ng.μl^{-1}), the adsorption abruptly decreased. This shows that the adsorption process depends on both the initial DNA and sepiolite concentrations. For DNA initial concentration lower than 100 ng.μl^{-1}, more than 30% of DNA was adsorbed. This value dropped to 12% for initial DNA concentration ranging from 200 ng.μl^{-1} to 650 ng.μl^{-1}, and less than 10% for initial DNA concentrations higher than 650 ng.μl^{-1} (Figure 4.2B).

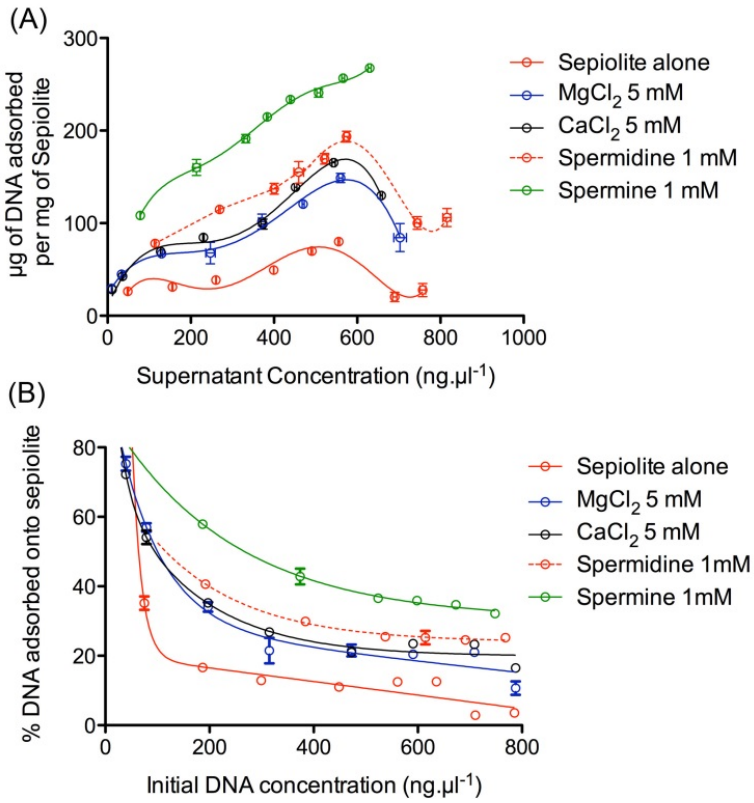

Figure 4.2 (A) Adsorption isotherm of DNA on sepiolite carried out in presence of various multivalent cations. Reaction conditions: 10 mM TrisHCl pH=7.5; sepiolite concentration fixed at 1mg/ml and the mass to 50 µg. Adsorption experiments at 25°C for 24 hours under agitation at 700 rpm in a Thermomixer from Eppendorf. (B) Same experimental data expressed in terms of initial DNA concentration vs. percentage of DNA adsorbed onto sepiolite.

Importantly, supplying polyvalent cations, such as Mg^{2+}, Ca^{2+}, spermidine (triamine with formula $C_7H_{19}N_3$) and spermine (tetraamine with formula $C_{10}H_{26}N_4$) to the suspension, strongly increased the adsorption of DNA onto sepiolite (Figure 4.2A and 4.2B). This observation suggests that the presence of any of those cations favours the adsorption process probably as a result of cation bridges interactions[284,285] together with electrostatic interactions between DNA and sepiolite surface. Indeed, divalent cations may interact with the Si-OH groups of the sepiolite surface and reduce electrostatic repulsion between the DNA and the sepiolite acting as bridges for bonding DNA molecules, as it has been reported for interactions of DNA with other type of silicate substrates[286].

Moreover, the binding of the cations may depress intramolecular electrostatic repulsion among DNA molecules subunits, leading to a higher diffusion coefficient of DNA due to its more compact conformation [286].

More specifically, divalent cations two-fold increased DNA adsorption (Figure 4.2A). In this case, the maximum of adsorption was found in samples prepared at 700 ng.μl^{-1} of initial DNA concentration, in the presence of $MgCl_2$ which leads to 160 μg of DNA adsorbed per mg of sepiolite. In the presence of $CaCl_2$, DNA slightly bound more efficiently to sepiolite, compared to $MgCl_2$. This could be attributed to the fact that Mg^{2+} forms weaker "outer-sphere" complexes with the phosphate backbone of plasmid DNA, and Ca^{2+} forms "inner-sphere" complexes with the phosphate backbone of plasmid DNA, which decreases the net negative charge and hence decreases the electrostatic repulsion between phosphates, resulting in a more compact structure of the plasmid molecule[286].

Adsorption of DNA leads, from solutions of higher concentration, (>750 ng.μl^{-1}) to an abrupt decrease of DNA adsorbed in sepiolite. This observation suggests that at such concentration DNA may be composed of large agglomerates instead of individual DNA molecules, and single sepiolite nanofibers would interact with agglomerates instead with single DNA molecules which results in a lower efficiency in DNA adsorption.

On the other hand, polyamine cations like spermidine (trivalent) and spermine (tetravalent) stimulated the adsorption more efficiently than divalent cations, as previously shown for mica surface[287]. In presence of spermidine, the adsorption curves remained with the same shape with a maximum in the adsorption that corresponds to the same initial DNA concentration than in experiments carried out in presence of divalent cations, but reaching around

200 μg of adsorbed DNA per mg of sepiolite. In this system it is possible to reach more than 100 μg of DNA adsorbed even when the initial DNA concentration is higher than 900 ng.μl^{-1} (Figure 4.2A).

In the presence of spermine, the adsorption was significantly more efficient, and no decrease of the DNA adsorption was found for DNA initial concentrations higher than 750 ng.μl^{-1}, in contrast to experiments carried out in the presence of divalent and trivalent cations. Conversely to the other systems the maximum in adsorption was found for an initial DNA concentration of around 900 ng.μl^{-1}, corresponding to 270 μg of DNA adsorbed per mg of sepiolite. These results may be explained by the ability of polyamines to condense DNA, which leads to a sharp increase of local DNA concentration close to sepiolite surface where these ions should be located.

From the isotherm curves it is clear that the presence of multivalent cations also increased the percentage of initial DNA adsorbed onto sepiolite, keeping constant the same initial DNA concentrations (Figure 4.2B). In the presence of divalent and trivalent cations, 20% to 30% of DNA is adsorbed at initial concentrations ranging from 300 ng.μl^{-1} to 700 ng.μl^{-1} and increased over 50% when the initial concentration is lower than 100 ng.μl^{-1}. In the presence of the tetravalent cation, 30% to 40% of DNA was adsorbed onto sepiolite, at initial concentrations higher than 400 ng.μl^{-1}; the percentage raising over 50% at initial concentrations below 300 ng.μl^{-1} (Figure 4.2B).

The overall adsorption process appears to be very rapid. Indeed, for 50 μg of sepiolite we observed only a slight increase of about 3% in the total amount of DNA adsorbed between few minutes and 24 hours after putting in contact the DNA with sepiolite in the presence of a divalent cation ($MgCl_2$)

(Table 4.1). This result indicates that most of DNA molecules are adsorbed instantaneously onto the sepiolite, pointing out to a predominance of electrostatic interactions between sepiolite and DNA, together with hydrogen bonding with silanol groups located at the external surface of the silicate.

Time (min)	0	30	60	90	120	180	1440
Percentage of adsorbed DNA with respect to the initial content in solution.	16.79%	16.99%	16.28%	17.59%	17.65%	19.07%	20.10%
μg of DNA adsorbed by 50 μg of sepiolite	5.63	5.70	5.46	5.90	5.91	6.39	6.74

Table 4.1 Time kinetics for DNA adsorption onto sepiolite (one experiment. Reaction conditions: 10 mM TrisHCl PH=7.5, 5 mM $MgCl_2$, initial concentrations: sepiolite 1 mg/ml, DNA 670 ng.μl^{-1}.

4.3. Influence of cations with different valence on DNA adsorption onto sepiolite.

In order to examine further the effect of the cation valence on DNA adsorption onto sepiolite, it was tested the effect of increasing concentration of the studied cations in the medium, while keeping constant DNA concentration (Figure 4.3). Importantly, the efficiency of DNA adsorption appeared to be directly correlated to the cation valence. Indeed, tetravalent cation (spermine)

was more efficient than the trivalent cation (spermidine) and both were much more efficient than divalent cations ($MgCl_2$ and $CaCl_2$). For example, DNA adsorption was as efficient with 1 mM spermidine (trivalent cation), than with 100 mM divalent cation ($MgCl_2$ and $CaCl_2$), and spermine (tetravalent cation) was even more efficient (Figure 4.3).

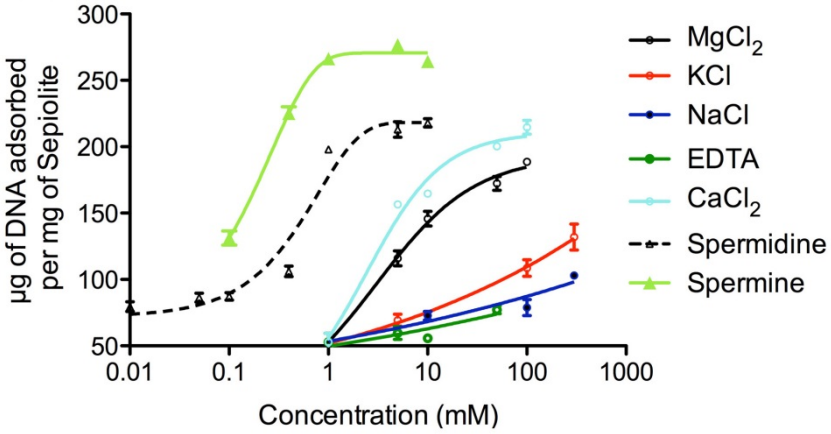

Figure 4.3 Effect of the presence of cations with different valence on DNA adsorption. Reaction conditions: 10 mM TrisHCl pH=7.5, salmon sperm DNA and sepiolite concentrations fixed at 615 ng.μl^{-1} and 1 mg/ml, respectively. 50 μg of sepiolite were used in each experiment. Adsorption took place at 25^{o}C for 24 hours under agitation at 700 rpm using a Thermomixer from Eppendorf.

Surprisingly, the presence of monovalent cations (e.g. NaCl and KCl) slightly favoured DNA adsorption (Figure 4.3), which is not the case in other type of clay minerals, for which monovalent cations cause the screening of electrostatic interactions on montmorillonite[286] or the decrease of the correlation force involved in DNA adsorption on mica[288]. At pH=7.5, both DNA and sepiolite surface are negatively charged, therefore the presence of monovalent cations could screen the interaction between silanol groups and negative charges on DNA phosphate backbone[289] and so decreases the DNA adsorption. However, as previously advanced[287], this charge screening effect could also reduce the

electrostatic energy barrier between DNA and sepiolite, and then DNA adsorption increases, allowing the DNA molecule to approach the negative surface close enough for adsorption by van der Waals forces.

Among the tested monovalent cations, KCl was slightly more efficient than NaCl. However, the use of 100 mM of KCl and 300 mM of NaCl leads to the same DNA adsorption efficiency than 5 mM of $MgCl_2$. In addition, monovalent cations are three orders of magnitude less efficient than the tetravalent cation. For example the amount of DNA adsorbed in presence of 0.1 mM spermine is almost the same as in the presence of 300 mM KCl (Figure 4.3). Surprisingly, with EDTA (ethylenediaminetetraacetic acid with formula $C_{10}H_{16}N_2O_8$) a poor but significant residual efficiency of DNA adsorption was still preserved (Figure 4.3).

The competition between monovalent and divalent cations was already studied in the case of DNA adsorption onto muscovite mica[287,288]. It is known that in this layered silicate there is a strong competition between these both types of ions, causing the monovalent cation a screening in the clay surface involving a decrease of the attraction force between DNA and mica. This attractive force results from the correlations interactions between counterions adsorbed on both mica and DNA surfaces. One of the major features of this correlation force is its dependence upon the valence of the counterions[288]. Indeed this force is attractive provided that the cations are divalent or of higher valence. The correlations of the monovalent cations do not contribute to the attraction force.

Surprisingly, we did not observe the same behaviour with sepiolite (Figure 4.3). However, the competition between counterions with different

valence still occurs (see Figure 4.4), but to a lesser degree. Indeed, for a constant $MgCl_2$ concentration, we observed a decrease of the amount of adsorbed DNA for increasing NaCl concentration (see Figure 4.4.A), which is a typical feature of Mg^{2+}/Na^{+} counterion competition. Nevertheless, the valence of the counterion is not the only parameter involved in DNA adsorption since we observed a clear difference between NaCl and KCl. As it was shown previously in fig 4.3, KCl is more efficient that NaCl among the tested monovalent cations for DNA adsorption. Moreover, at high $MgCl_2$ concentration, the DNA adsorption remains almost the same even when the KCl concentration rises to 300 mM (Fig. 4.4B). This result suggests a strong interaction between KCl and sepiolite surface.

The weak competition between counterions for DNA adsorption onto sepiolite could lead to a higher stability of the Sep/DNA bionanocomposite when it would be in presence of different salts with different valences, as for example in the interior of cells. This property confers ability for intracellular applications of Sep/DNA.

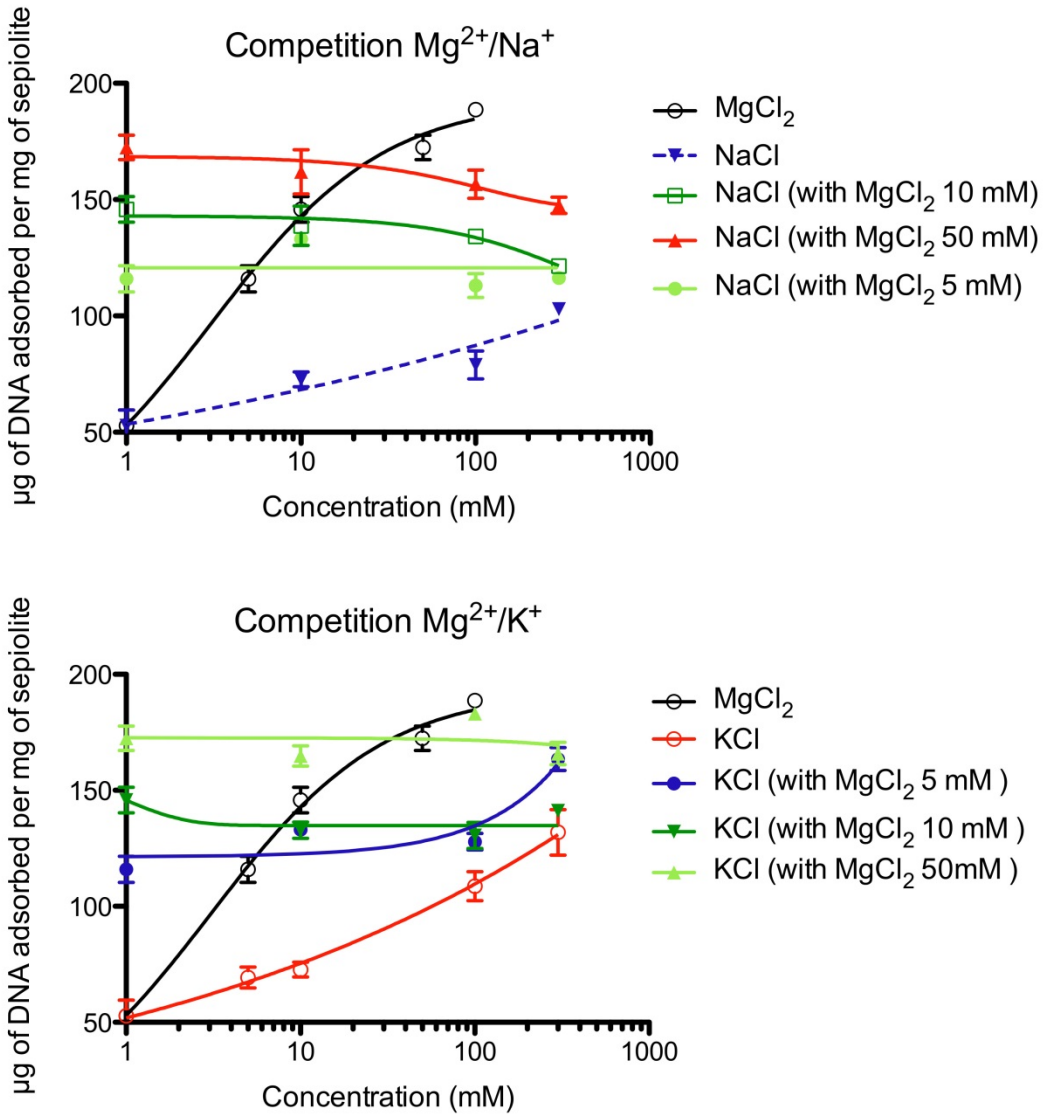

Figure 4.4 Competition between monovalent and divalent cations in DNA adsorption onto sepiolite. A: Mg^{2+}/Na^{+}, B: Mg^{2+}/K^{+} competition. Reaction conditions: 10 mM TrisHCl pH=7.5, Salmon Sperm DNA and sepiolite concentrations fixed at 615 ng.μl^{-1} and 1mg/ml, respectively. 50 μg of sepiolite were used in each experiment. Adsorption took place at 25°C for 24 hours under agitation at 700 rpm using a Thermomixer from Eppendorf.

4.4. Adsorption efficiency of different DNA conformations.

In further experiments we have compared the adsorption efficiency of different DNA conformations, i.e. sonicated linear double stranded DNA (mean of 300 bp), containing complex DNA sequences (from salmon sperm), circular plasmids (5.7 kbp long), double-strand linear oligo nucleotides, ds-oligo (15 bp) or linear single-strand oligonucleotides, ss-Oligo (15 nt) (Figure 4.5A and 4.5B). At initial DNA concentration lower than 300 $ng.\mu l^{-1}$ and using 50 μg of sepiolite, the behaviour of all kinds of the studied DNA was quite similar. At initial DNA concentration lower than 100 $ng.\mu l^{-1}$, the percentage of adsorbed DNA (from the initial sample) was greater than 50% (Figure 4.5A), reaching adsorption values higher than 70% at initial concentrations lower than 50 $ng.\mu l^{-1}$ for double stranded DNA. However, at higher concentration, the adsorption isotherms clearly pointed out marked differences between the adsorption of double-stranded and single–stranded DNA on the sepiolite (Figure 4.5B).

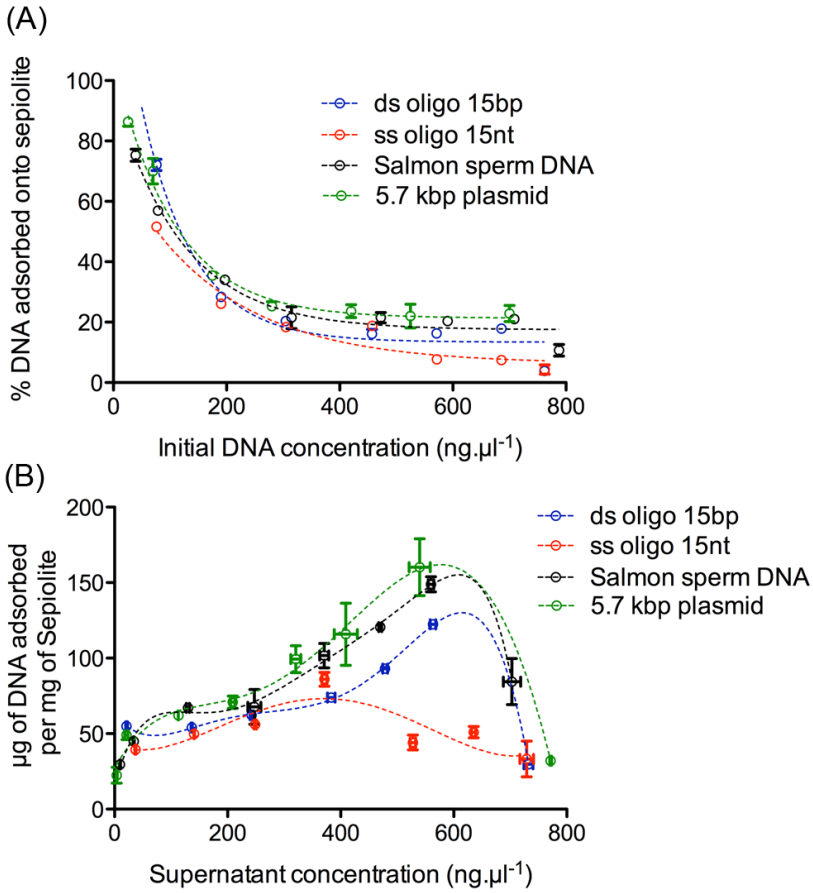

Figure 4.5 Comparison of adsorption of different DNA conformations onto sepiolite. (A) Same experimental data showed in (B) expressed in terms of initial DNA concentration vs. percentage of DNA adsorbed onto sepiolite. (B) Adsorption isotherm of different DNA conformations on sepiolite. Reaction conditions: 10 mM TrisHCl pH=7.5, 5 mM $MgCl_2$, sepiolite concentration fixed at 1 mg/ml. 50 µg of sepiolite were used in each experiment. Adsorption experiments were carried out at 25°C for 24 hours under agitation at 700 rpm using a Thermomixer from Eppendorf.

The double-stranded DNA presented maximum adsorption at an initial concentration of around 700 ng.µl^{-1}, which corresponds to a supernatant concentration of around 550 ng.µl^{-1}, after the adsorption. Beyond this initial concentration value, the amount of adsorbed DNA decreases. With ss-Oligo DNA the maximum of adsorption was two-fold lower than that of double-stranded DNA (Figure 4.5B), reached for an initial DNA concentration close to 460 ng.µl^{-1}, which corresponds to an equilibrium concentration of 370 ng.µl^{-1}.

4.5. DNA desorption from sepiolite.

Envisaging some possible biomedical applications of the Sep/DNA bionanocomposites, it is important to study the release and recover of the previously adsorbed DNA from the sepiolite.

With the aim to desorb the DNA from the sepiolite, first experiments were done by applying heat, here so-called "heating" method. A dispersion of the bionanocomposite was incubated for 5 minutes at 95 °C, following with an abrupt decrease of the temperature after those 5 min of incubation by immersing the sample in melting ice. Spectrophotometry analysis of the supernatant after centrifugation gave a mean value of 40% of DNA desorption, which confirms that certain amount of DNA could be desorbed from sepiolite just by heating.

Characterization of the recovered DNA using EMSA showed that a part of it was unable to maintain its double stranded conformation. Figure 4.6 shows in columns C and D the presence of single stranded DNA in samples recovered from bionanocomposites prepared in the presence of 5 mM $MgCl_2$ and 5 mM $CaCl_2$, respectively. TEM characterization of the desorbed DNA by heating also showed a lot of single stranded DNA together with double stranded DNA (Figure 4.7). These results point out that the "heating" method is inadequate for further biological use of desorbed DNA.

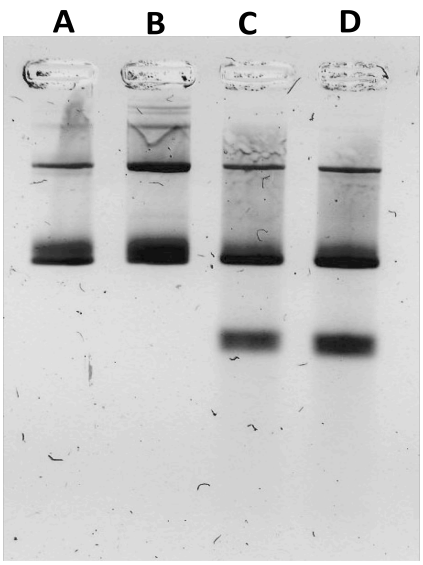

Figure 4.6 Characterization with EMSA of the DNA desorbed by the "heating" method. (A) Plasmid (5.7Kbp) control; (B) plasmid DNA in the supernatant after synthesis of the bionanocomposite and before heating the re-suspended pellet; (C) plasmid DNA desorbed from bionanocomposite obtained with 5 mM $MgCl_2$; (D) plasmid DNA desorbed from bionanocomposite obtained with 5 mM $CaCl_2$. Last line in C and D represents single stranded DNA.

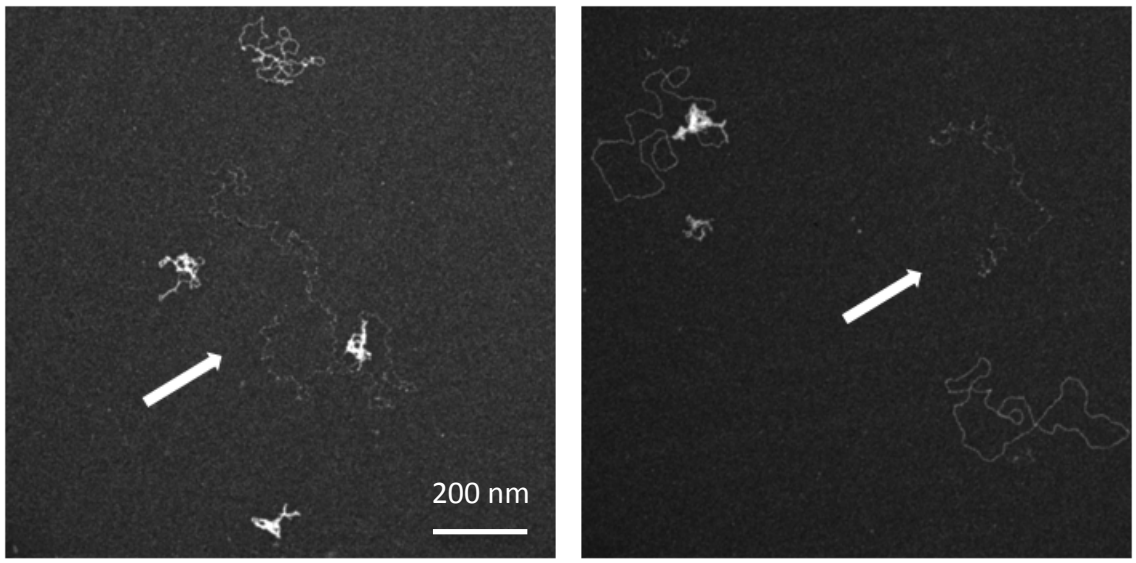

Figure 4.7 TEM images of the DNA desorbed by the "heating" method. White arrows pointed to single stranded DNA.

The second method used for DNA desorption was the so-called "chelation" method. In this case the bionanocomposite is re-suspended in Tris-EDTA. The simple resuspension of the bionanocomposite should not damage the DNA and could propitiate the quality and further biological efficiency of the desorbed DNA.

As it is already known, EDTA is a type of chelating agent, *i.e.* it has the ability to "sequester" metal ions such as Mg^{2+}, Ca^{2+}, Fe^{3+} as well as other metal ions. After being bound by EDTA, metal ions remain in solution but exhibit diminished reactivity. It is worth to mention that the EDTA is used for treating mercury and lead poisoning, to remove excess iron from the body, and to bind metal ions in general in the practice of chelation therapy[290,291].

In our case, DNA desorption could occur by chelation of the cation bridges that bind DNA molecules to the sepiolite surface. Thus, if DNA was bounded to sepiolite through multivalent cations, the use of this chelating agent might facilitate desorption of DNA from sepiolite. In this way, it has been tested the "chelation" method using various concentrations of EDTA (0, 5, 10 and 50 mM) (Figure 4.8).

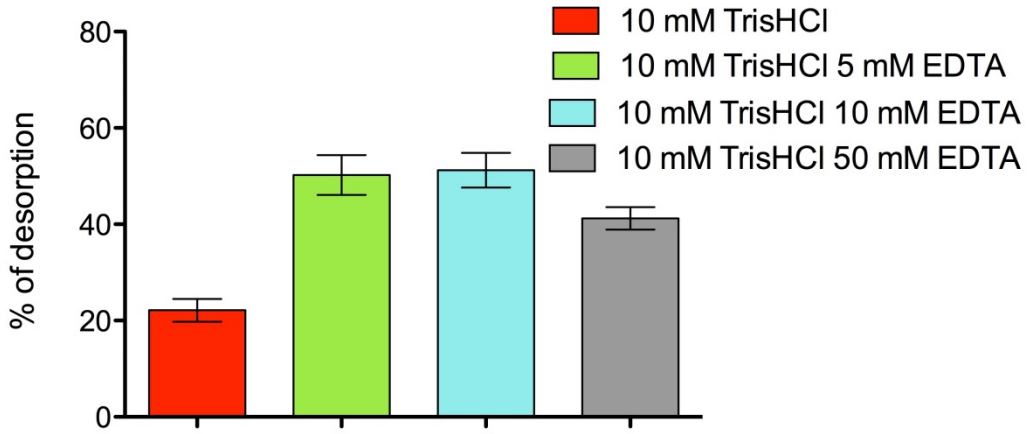

Figure 4.8 Comparison of DNA desorption efficiency of EDTA at different concentrations by applying "chelation" method. Reaction conditions: Initially, 0.5 ml of Sep/DNA samples were prepared using salmon sperm DNA at 640 ng.μl^{-1} in a sepiolite dispersion (1 mg/ml) in 10 mM TrisHCl and 5 mM $MgCl_2$. Resuspension in 0.1 ml solution of 10 mM TrisHCl, and EDTA at 5, 10 and 50 mM. After 15 min of incubation at room temperature, all samples were centrifugated at 5000 rpm for 5min, and the supernatant was measured using the UV-vis.

Maximum DNA desorption was obtained when bionanocomposites prepared using DNA from salmon sperm in the presence of 5 mM $MgCl_2$ were treated with 10 mM TrisHCl and 10 mM EDTA. Desorption decreases then for higher content of EDTA (Figure 4.8). This behaviour can be explained considering that chelation of magnesium ions by the EDTA occurs at 1:1 molar ratio, but an excess of EDTA could lead to further DNA re-adsorption. As it was already observed in Figure 4.3, EDTA slightly favour the DNA adsorption onto sepiolite by a suggested bridging between sepiolite and DNA through amino groups of EDTA. Another alternative effect of EDTA could be the extraction of Mg^{2+} ions located at the edges of the octahedral layers of sepiolite enhancing so the further re-adsorption of DNA. In fact, it can be admitted that a

spontaneous lixiviation of Mg^{2+} cations from sepiolite can take place when this mineral is dispersed in neutral or acidic solutions[2].

In order to compare the efficiency of the "chelation" method in the desorption of DNA from the bionanocomposites prepared in diverse media containing different cations, EDTA was used in desorption experiments carried out in bionanocomposites prepared in the presence of divalent, trivalent and tetravalent cations. Thus, Sep/DNA bionanocomposites prepared from salmon sperm DNA in the presence of 10 mM $MgCl_2$, 10 mM $CaCl_2$, 1 mM spermidine and 1 mM spermine were submitted to three subsequent steps of resuspension, one in the presence of 10 mM TrisHCl, and twice with 10 mM TrisHCl and 10 mM EDTA. Figure 4.9 shows both, the total amount of DNA initially adsorbed (represented in red bars) and the one desorbed after the desorption treatment (represented in green bars) in the four selected bionanocomposites correlated with the valence of the cation present during the adsorption process. However, the percentage of DNA that remain bounded to the sepiolite after the desorption process, clearly indicates that the efficiency in desorption was lower as the valence of the cation in the preparation medium was higher (e.g., 50.6% of desorption efficiency from the bionanocomposite prepared in the presence of spermine and 70 – 75% in bionanocomposites containing Mg^{2+} or Ca^{2+}).

[2] E. Ruiz-Hitzky, personal communication.

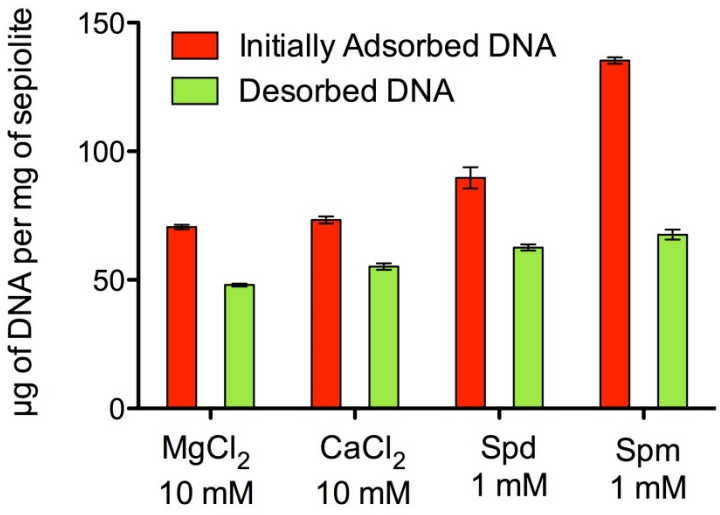

Figure 4.9 Comparison of the amount of desorbed salmon sperm DNA from bionanocomposites prepared in the presence of Mg^{2+}, Ca^{2+}, spermidine and spermine using the "chelation" method (re-suspension in TrisHCl EDTA).

A more detailed analysis for each re-suspension was also carried out to understand if there are different ways for DNA to become adsorbed in sepiolite under the studied experimental conditions. Thus, bionanocomposites prepared by adsorption of salmon sperm DNA in 0.5 ml of volume reaction containing 500 µg of sepiolite, were firstly re-suspended in 10 mM TrisHCl in order to remove and analyze the DNA which was weaker enough bonded to sepiolite for being spontaneusly desorbed just by re-suspension without any chelating agent. The suspension was centrifuged and the supernatant (*i.e.* the desorbed DNA) was analyzed using UV-vis spectrophotometry. The amount of DNA desorbed in this first re-suspension of the studied bionanocomposites is represented in blue colour in the graphics of Figure 4.10. The DNA recovered from bionanocomposites prepared in the presence of divalent cations (e.g., Mg^{2+} and Ca^{2+}) corresponds to around a fourth part of the total adsorbed DNA (Figure

4.10). In contrast, for the bionanocomposites prepared in the presence of spermidine and spermine only a 20% and 13% of DNA is desorbed just by resuspension of the system in TrisHCl (Figure 4.10), confirming a higher efficiency in DNA bonding for these polyvalent cationic species.

The DNA recovered from the bionancomposites re-suspended for a second time in this case using 10 mM TrisHCl and 10 mM EDTA, is represented in red colour in the graphics of Figure 4.10. This desorbed DNA is removed by "chelation" however, a third resuspension of the bionanocomposites was carried using 10 mM TrisHCl and 10 mM EDTA in order to assure a maximum removal of bonded DNA (percentage for this third treatment represented in green colour in the graphics of Figure 4.10). The total amount of desorbed DNA by "chelation" effect corresponds to the sum of the two last re-suspension treatments in the presence of EDTA and corresponds to 42% for bionanocomposites prepared in the presence of Mg^{2+}, 48% for bionanocomposites prepared in the presence of Ca^{2+} and spermidine, and 36% for bionanocomposites prepared in the presence of spermine (Figure 4.10).

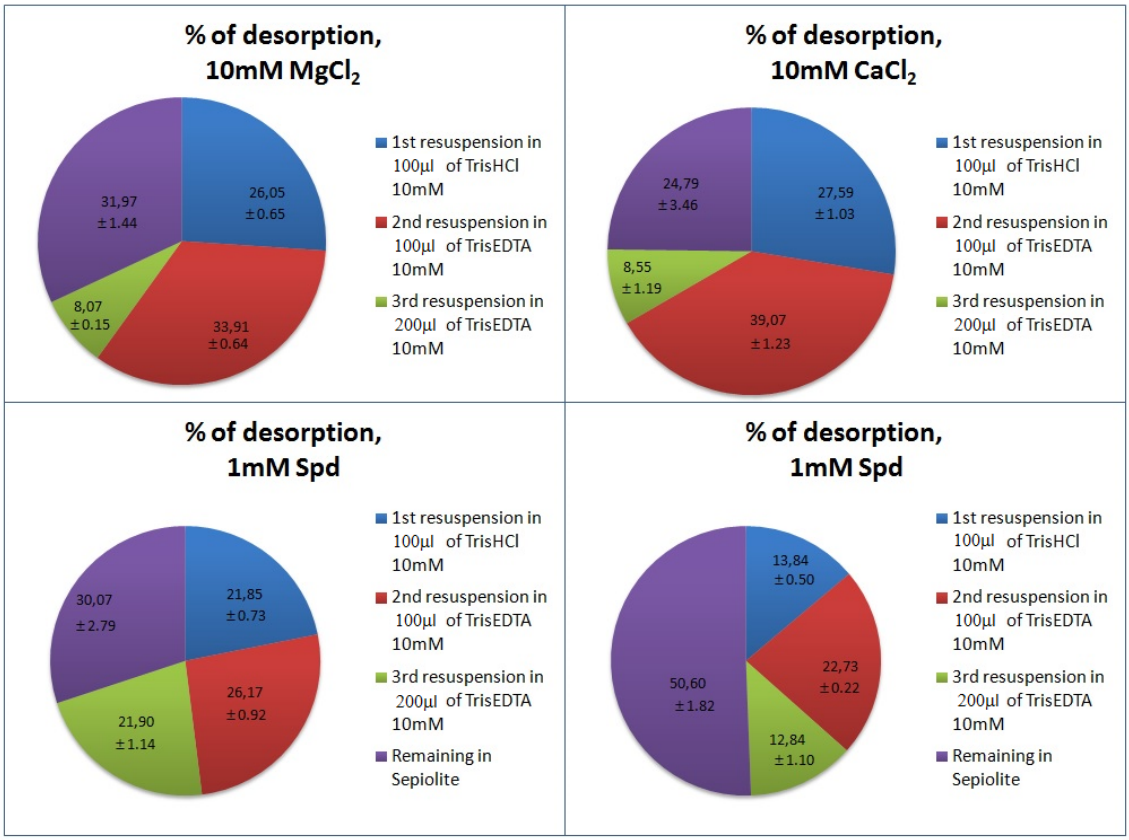

Figure 4.10 Percentage of DNA desorbed from sepiolite in each of the three subsequent re-suspension steps of the "chelation method" applied to Sep/DNA bionanocomposites prepared in the presence of $MgCl_2$, $CaCl_2$, spermidine and spermine at the concentration indicated in the graphics.

These last results indicate that it is remarkable the amount of DNA that still remains strongly adsorbed to the sepiolite, which represents around one-third of the initially adsorbed DNA, even a half in the case of the bionanocomposite prepared in the presence of spermine. This behaviour could be an evidence of a possible multilayer DNA formation on sepiolite surface, being evident a very strong interaction between the first layer of DNA directly adsorbed on the sepiolite surface.

Considering the difficulty for remove DNA from the bionanocomposite prepared in the presence of spermine (1 mM), a last experiment was carried out in order to compare the desorbed amount of DNA when the first re-suspension was made with TrisHCl and EDTA instead of only TrisHCl (Figure 4.11), and it was also added a fourth re-suspension step also using EDTA. From the data represented in Figure 4.11 it is deduced that the use of EDTA in the first re-suspension leads to a recover amount of about the double of the DNA compared to that obtained when the sample is re-suspended only in TrisHCl. In that case, with only two re-suspension treatments it is possible to recover a half of the DNA in the sample. This observation could be useful if there is interest in recovering higher amounts of DNA and thus the preparation of successive re-suspensions in TrisHCl and EDTA could be used to recover larger amounts of DNA from these bionanocomposites.

It was also analyzed the quality of the desorbed DNA using EMSA. In this case, a Sep/DNA bionanocomposite prepared from plasmid DNA *(5.7 Kbp)* and in the presence of 5 mM Mg^{2+} and 5 mM Ca^{2+} ions was treated using the "chelation" method (one re-suspension step) to desorb the DNA which was analyzed by electrophoresis (Figure 4.12).

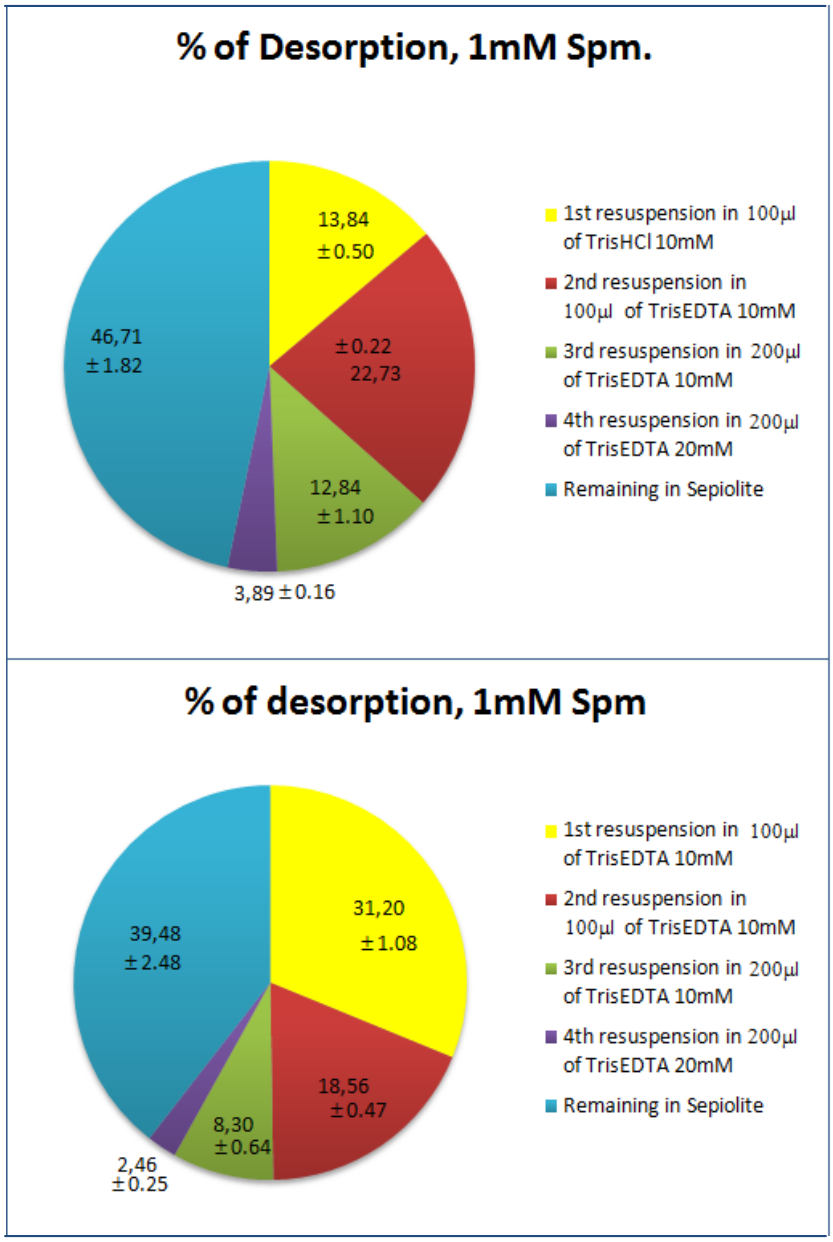

Figure 4.11 Percentage of DNA desorbed from sepiolite in four subsequent re-suspension steps applied the "chelation" method to Sep/DNA bionanocomposites prepared from salmon sperm DNA in presence of 1 mM spermine. First resuspension (represented in yellow) was in 100 µl of TrisHCl (up) and in 100 µl of TrisEDTA (down). Sep/DNA samples were prepared in presence of 1 mM spermine with the same protocol described in figure 4.9 and 4.10 captions.

Importantly, the different isoforms (super-coiled, linear, open circle) of the plasmid DNA, particularly the supercoiled form, were maintained also in the DNA recovered from the sepiolite (Figure 4.12). This result is of great relevance and it is a proof of the efficiency of the “chelation” method for recovering the adsorbed DNA. Moreover, the preservation of the DNA structure confirms that sepiolite is a good support for the DNA because their assembly does not provoke any alteration of its structure.

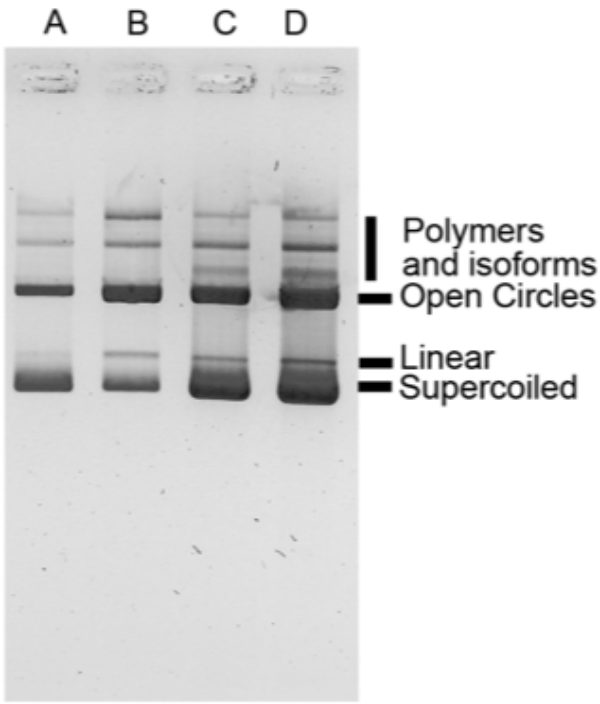

Figure 4.12 *Characterization with EMSA of desorbed DNA using the "chelation" method. A: Plasmid (5.7 Kbp) control; B: plasmid DNA in the supernatant after synthesis of the bionanocomposite prepared with 5 mM $MgCl_2$ and before re-suspending the pellet in TrisHCl and EDTA; C: plasmid DNA desorbed from the bionanocomposite obtained with 5 mM $MgCl_2$; D: plasmid DNA desorbed from bionanocomposite obtained with 5 mM $CaCl_2$.*

A study of the kinetics of the DNA desorption process from sepiolite was also carried out. Desorption also appeared to be very rapid. Indeed, a difference of less than 5% was observed in desorption efficiency, between immediate

desorption and that observed after 2 hours of incubation of Sep/DNA with the chelating agent (TrisEDTA) (Table 4.2). This result also supports the electrostatic nature of the interaction sepiolite–DNA.

Time (min)	Mass of initially adsorbed DNA (μg)	Mass of DNA desorbed (μg)	% of DNA desorption
0	5.919	4.255	71.89
15	5.459	4.01	73.46
30	5.899	4.025	68.23
60	5.629	3.72	66.09
120	5.699	3.945	69.22

Table 4.2 *Time of DNA desorption from sepiolite in Sep/DNA bionanocomposites prepared from salmon sperm DNA in presence of 5 mM $MgCl_2$ (one experiment). Reaction conditions for initial adsorption: 50 μl sample, 10 mM TrisHCl pH=7.5, 5 mM $MgCl_2$. Initial concentrations: sepiolite 1 mg/ml, DNA 670.68 ng.μl^{-1}. Reactions conditions for desorption: 50 μl sample, 10 mM TrisHCl pH=7.5, 5 mM EDTA.*

4.6. Physicochemical characterization of Sep/DNA bionanocomposites.

In order to confirm the modifications of sepiolite surface charges, in presence of multivalent cations and DNA molecules, the zeta potential was determined by an electrokinetic study in the presence of different salts with and without DNA (Table 4.3). The analysis of the zeta-potential of sepiolite with different salts in the medium confirmed that the presence of multivalent cations depressed the negative charge of the sepiolite, being the trivalent and tetravalent cations (spermidine and spermine, respectively) were the most efficient ions in this shielding effect, leading to a more complete surface charge inversion. Anyway, the presence of DNA able to interact with the external surface of sepiolite fibers leads to the formation of bionanocomposites provided of a net negative charge either in the presence or not of polyvalent cations. These results suggest that the interaction of DNA with the sepiolite surface implicates diverse mechanisms, being a complex assembling process. Importantly, this global negative charge of the Sep/DNA bionanocomposites is a favourable situation in view to have a system for DNA delivery into cell nuclei.

Sample composition	Zeta-Potential (mV)	Bionanocomposite	Zeta-Potential (mV)
Sepiolite 1 mg.ml^{-1} 10 mM TrisHCl pH=7.5	-11.7	Sepiolite 1 mg.ml^{-1} DNA 710 ng.µl^{-1} 10 mM TrisHCl pH=7.5.	-26.5
Sepiolite 1 mg.ml^{-1} 10 mM TrisHCl pH=7.5 10 mM $MgCl_2$	-4.33	Sepiolite 1 mg.ml^{-1} DNA 710 ng.µl^{-1} 10 mM TrisHCl pH=7.5 10 mM $MgCl_2$	-9.48
Sepiolite 1 mg.ml^{-1} 10 mM TrisHCl pH=7.5 10 mM $CaCl_2$	-5.08	Sepiolite 1 mg.ml^{-1} DNA 710 ng.µl^{-1} 10 mM TrisHCl pH=7.5 10mM $CaCl_2$	-10.0
Sepiolite 1 mg.ml^{-1} 10 mM TrisHCl pH=7.5 1 mM spermidine	+6.28	Sepiolite 1 mg.ml^{-1} DNA 710 ng.µl^{-1} 10 mM TrisHCl pH=7.5 1 mM spermidine	-12.5
Sepiolite 1 mg.ml^{-1} 10 mM TrisHCl pH=7.5 1 mM spermine	+12.8	Sepiolite 1 mg.ml^{-1} DNA 710 ng.µl^{-1} 10 mM TrisHCl pH=7.5 1 mM spermine	-8.09

Table 4.3 Zeta-potential values of 1 ml suspensions of different sepiolite – polycations – DNA (from salmon sperm) complexes. Measurements were performed on a Malvern Zetasizer Nano ZS. Z-average values in intensity at pH=7 were used as mean hydrodynamic size (Dh), and the zeta-potential was measured in a 0.01 M KNO_3 solution. HNO_3 or KOH was added to the solution to alter the pH.

The precise characterization of the interactions between DNA and the sepiolite surface, it was then carried out by Fourier transform infrared spectroscopy (FTIR). This technique has been previously employed to ascertain the interaction of diverse biomolecules such as polysaccharides[30], proteins[31] and phospholipids[15] with silanol groups at the external surface of sepiolite. Thus, in Sep/DNA bionanocomposites it has been also analyzed how the DNA adsorption specifically affected the intensity of the 3720 cm^{-1} band, assigned to the stretching OH vibrations of Si-OH located at the external surface of sepiolite[24,28]. Indeed, the interaction of adsorbed DNA with these groups perturbed such band, producing a shift toward lower frequency values, being then not observable in the spectrum of certain of the samples due to the overlapping with the broad band associated with the stretching OH modes of water molecules belonging to the sepiolite. Changes in the frequency of this band have been correlated with the interactions of diverse type of other species with the silanol group[16,17,29]. Moreover, the intensity of the perturbation of this specific band was also correlated with the presence of multivalent cations (Figure 4.13), consistently with the efficiency of DNA adsorption onto sepiolite (compare Figures 4.2, 4.3 and 4.13).

The decrease in the intensity of the IR band associated with the O-H stretching vibration mode of silanol groups may occurs in different extent which can be correlated with the degree in the surface coverage by the assembled species. In contrast, the band assigned to the stretching OH vibration mode of Mg-OH groups appearing at ca. 3680 cm^{-1} remains practically unaltered even at high amounts of adsorbed DNA. This null or very small alteration is expected as these type of hydroxyl groups are located inside the structural blocks of

sepiolite, far from its surface, and the adsorbed species cannot accede to them. In addition, as the dimensions of the cross-section of tunnels were about 1.1 × 0.4 nm^2, the DNA molecules showing a bigger size may mostly remain at the external surface of the fibers, the tunnels being practically inaccessible to them, as occurs in the case of many other polymeric species[15–17,29,292].

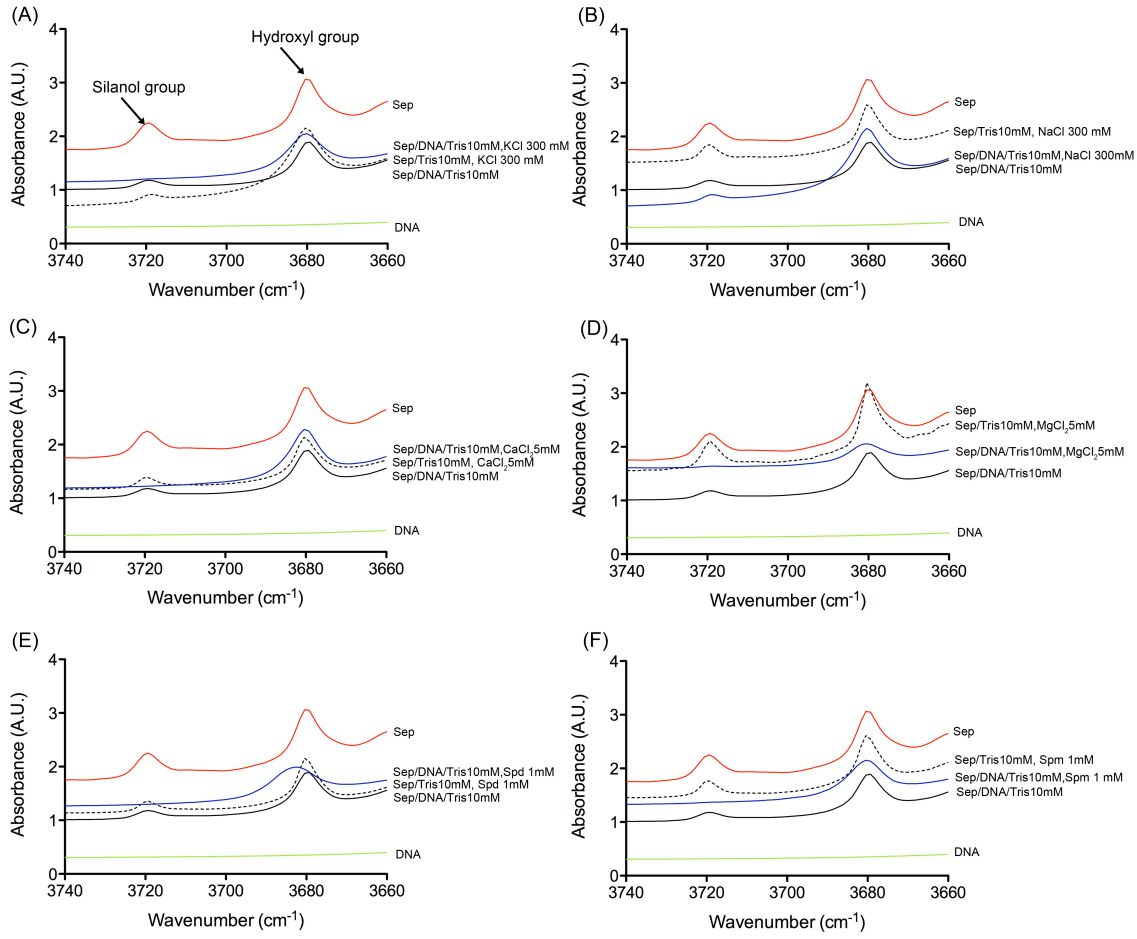

Figure 4.13 Comparison between Fourier transform infrared spectroscopy (FTIR) spectra of sepiolite, Sep/DNA bionanocomposites prepared without cations, and Sep/DNA prepared in the presence of monovalent (A: NaCl, B: KCl), divalent (C: $CaCl_2$, D: $MgCl_2$), trivalent (E: spermidine) and tetravalent (F: spermine) cations.

Sep/DNA bionanocomposites were also characterized by AFM and by TEM techniques. With AFM it was possible to observe some DNA plasmids (5.7 kbp) in a control sample (figure 4.14A) and also some DNA plasmids bonded to different sepiolite fibers (Figure 4.14B) forming a Sep/DNA bionanocomposite (sepiolite 1 mg/ml and PCMV plasmid with 5.7 Kbp at 10 ng.μl^{-1}). Difficulties of this technique rely in the high amount of time spent in finding single molecule of Sep/DNA complexes, due to the presence of aggregates. In phase-mode it is also possible to see the DNA on the sepiolite fiber (Figure 4.15).

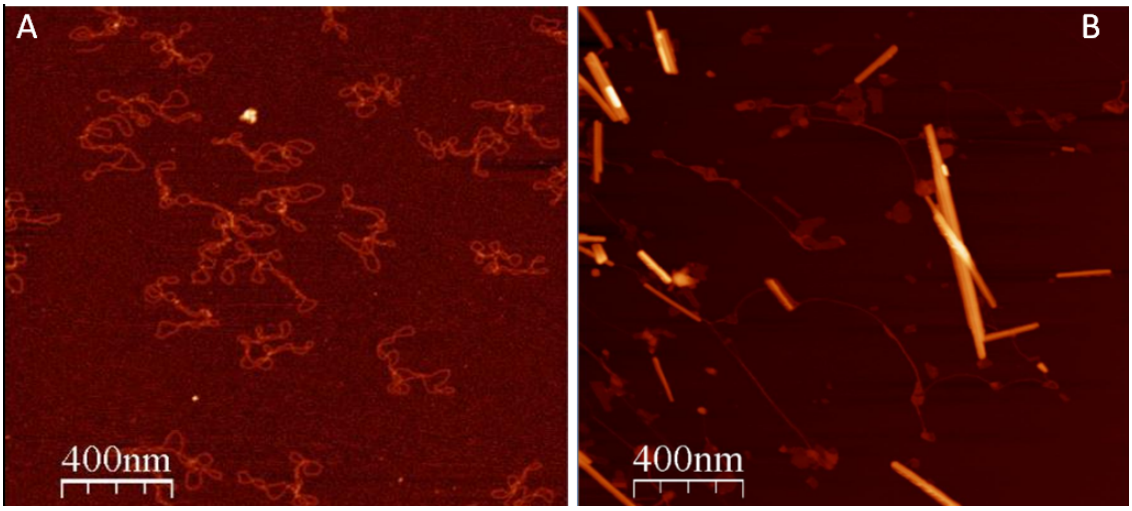

*Figure 4.14 Atomic force microscopy (AFM) images. (A) control images of PCMV plasmid 5.7 Kbp (*5 ng.μl^{-1}*). (B) Sep/DNA bionanocomposite (sepiolite at 1 mg/ml and* PCMV plasmid with 5.7 Kbp at 10 ng.μl^{-1}*).*

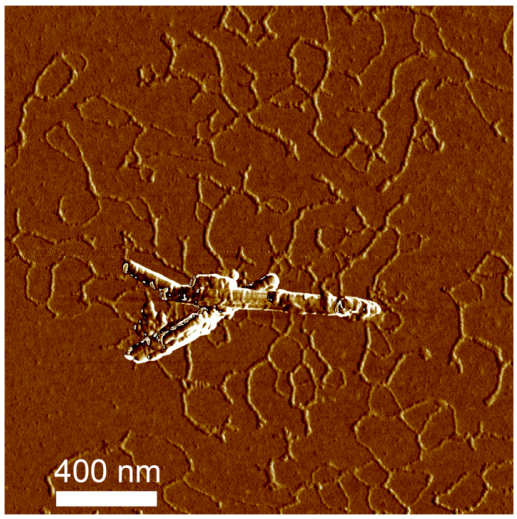

Figure 4.15 AFM images of Sep/DNA bionanocomposite (sepiolite at 1 mg/ml and PCMV plasmid with 5.7 Kbp at 20 ng.μl^{-1}) in phase-mode.

Figure 4.16 shows the control images of DNA using TEM. It is possible to observe the shape of condensed DNA in presence of spermidine (figure 4.8C) and spermine (figure 4.8D).

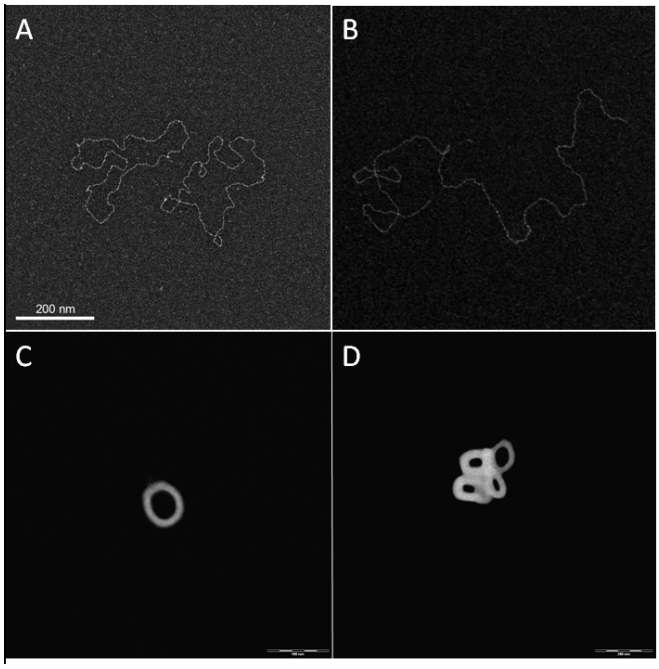

Figure 4.16 Transmission electron microscopy (TEM) control images of DNA. A: plasmid 5.7 Kbp, B: linearized plasmid 5.7 Kbp using EcoRI restriction enzime, C: Condensed plasmid 5.7 Kbp in presence of 1 mM spermidine, D: Condensed GFP plasmid in presence of 1 mM spermine.

By application of TEM it is possible to get more complementary information about the sepiolite - DNA interactions, as it is possible to get more images in less time. Figure 4.17 shows the interaction of DNA molecules with sepiolite fibers, and in Figure 4.18 it is possible to detail these interactions in single molecule images.

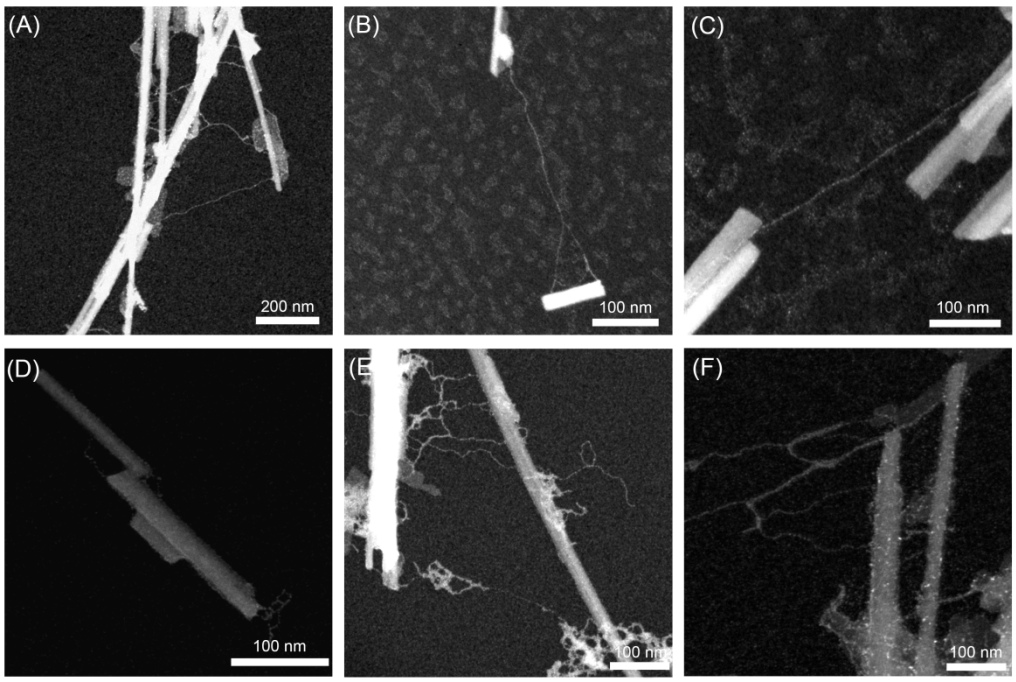

Figure 4.17 Dark field TEM images of plasmids 5.7 Kbp bounds on sepiolite fibers. (sepiolite at 1 mg/ml and PCMV plasmid with 5.7 Kbp at 10 ng.μl^{-1} and 20 ng.μl^{-1} in E and F).

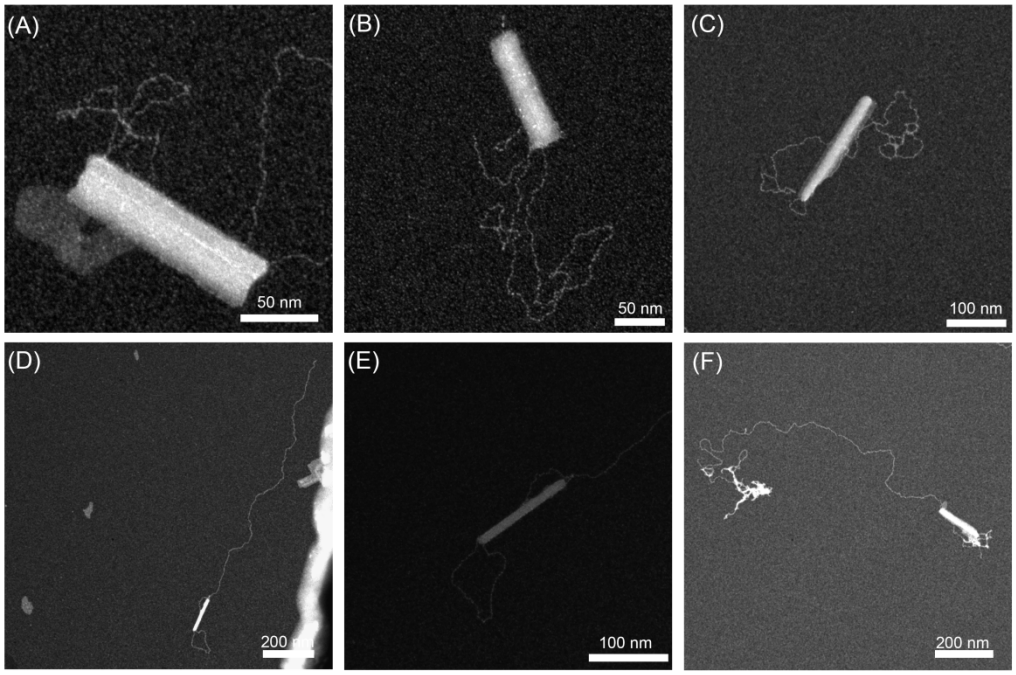

Figure 4.18 Dark field TEM images of single molecule sep/DNA bionanocomposites (plasmid 5.7 Kbp bounded to one sepiolite nanofiber).

Consistently with the FTIR spectrometry analysis, AFM and TEM analysis show that the DNA preferentially bound to sepiolite at the edge of the nanofiber and to its external surface. It appears that certain DNA molecules are bounded at one of their extremities, not to their entire length (Figure 4.18). It has been also observed that two different nanofibers could be linked throughout one DNA plasmid (figure 4.17b and 4.17c). When increases the DNA concentration, sepiolite nanofibers could be totally coated with DNA molecules (figure 4.17F). Finally, Figure 4.18D-F shows single molecule Sep/DNA complexes with linearized plasmids.

Structure of Chapter 5

5. Biological applications in mammalian cells: DNA transfection.

5.1. Sep/DNA - mammalian cells internalization

5.2. DNA transfection experiments.

5.3. Improvement of DNA transfection efficiency

5. Biological applications in mammalian cells: DNA transfection.

5.1. Sep/DNA - mammalian cells internalization.

For these experiments, the corresponding Sep/DNA bionanocomposite sample was prepared in the presence of 10 mM $MgCl_2$ or $CaCl_2$ solutions using the PUC19 plasmid for FACS, and the pCMV plasmid encoding for both, the resistance gene to G418 and the green fluorescent protein (GFP) for transfection experiments, respectively.

We first analyzed the interactions between the Sep/DNA bionanocomposites and the mammalian cells, in order to investigate if the presence of DNA at the external surface of the sepiolite could affect the internalization of nanofibers into cells. A time-kinetic of sepiolite and Sep/DNA uptake in V-79 hamster cells was carried out monitored by FACS. Both Sep and Sep/DNA tested concentration were 10 $ng.\mu l^{-1}$.

The Sep/DNA interaction with cells was efficient but delayed compared to sepiolite alone. Indeed, the time-kinetic analysis by FACS showed that only 5% of cells become fluorescent after 1 hour of contact with Sep/DNA bionanocomposite, while 20% of cells become fluorescent with sepiolite alone. After 4 hours of contact with Sep/DNA the intake appeared close to the frequency of fluorescent cells with sepiolite alone (26.6% and 36.6% respectively), then reached 35% of fluorescent cells after 6 hours (Figure 5.1).

These kinetics differences might result from the alteration of the zeta potential by the binding of the DNA onto sepiolite. Nevertheless, the uptake of Sep/DNA into cells becomes very efficiently after 6 hours of contact.

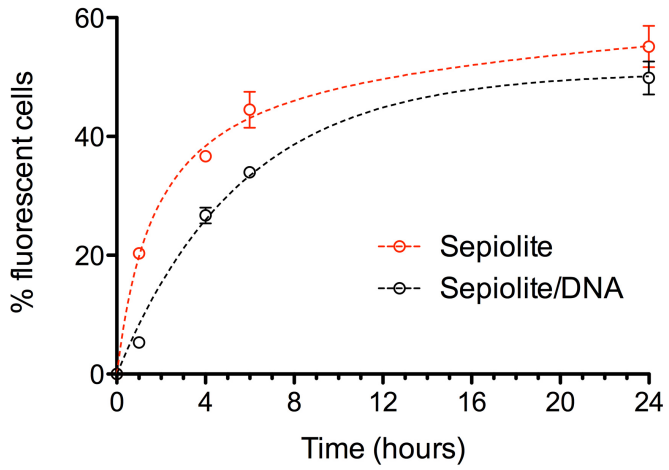

Figure 5.1 Results obtained with fluorescence activated cells sorting (FACS) for time kinetics for sepiolite and sep/DNA in V79 cells.

5.2. DNA transfection experiments.

Since the pCMV plasmid also encoding the resistance gene to G418 antibiotic, the "selection method" was chosen to identify the stable transfectants and to estimate the transfection efficiency of the bionanocomposite Sep/DNA in mammalian cells.

First, in order to know the appropriate dose of the antibiotic, i.e. the minimum dose of the antibiotic for eliminates all the non-resistant cells, but not transfected cells, a dose response to G418 in V79 cells was carried out. It is observed that 600 ng.μl^{-1} was the minimum dose of G418 able to eliminate all of

non resistant V79 cells. The image of the corresponding experiment is shown in Figure 5.2.

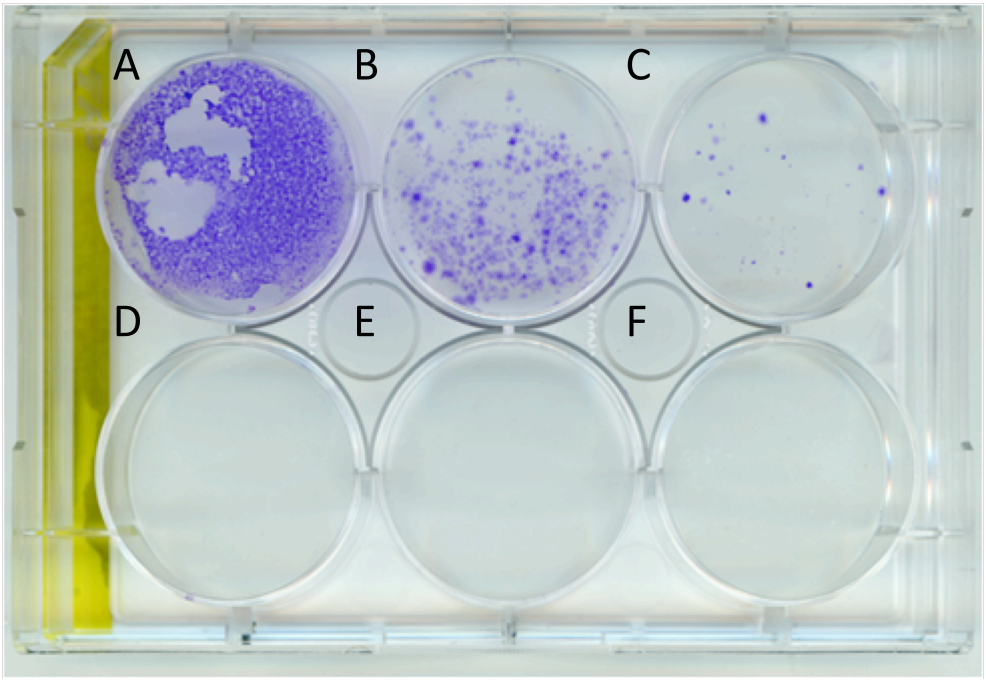

Figure 5.2 Dose response of V79 hamster cells after incubation for 10 days with G418 antibiotic. G418 concentrations: A: Control; B: 400 ng.μl^{-1}; C: 500 ng.μl^{-1}; D: 600 ng.μl^{-1}; E: 800 ng.μl^{-1}; F: 1000 ng.μl^{-1}.

We have then measured the efficiency of DNA transfer into mammalian cells by the action of the Sep/DNA bionanocomposites, which was prepared with in the presence of 10 mM $MgCl_2$ and 10 mM $CaCl_2$ solutions. The V79 cells were incubated with the bionanocomposite and 48 hours after, new cellular medium (MEM) was added in the presence of G418 antibiotic. Transfected cells were selected by the resistance to G418 conferred by the transferred plasmid bound to the sepiolite. After 10 days of selection with G418, stable resistant colonies were obtained (Figure 5.3). These data show that the Sep/DNA bionanocomposite is able to transfer the plasmid DNA bearing G418 resistance

genes into cells and to obtain stable transfectants after several days of selection.

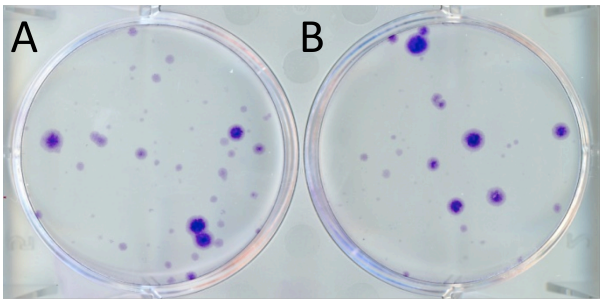

Figure 5.3 Picture of colonies of transfected V79 cells with Sep/DNA prepared with 10 mM $MgCl_2$ (A) and 10mM $CaCl_2$ (B). First day: 10^5 cells were plated in each well. Second day: 3 ml of new medium was added in presence of Sep/DNA bionanocomposite with 40 µg of sepiolite and 1 µg of bounded DNA presence of 10 mM $MgCl_2$ (A) and 10 mM $CaCl_2$ (B). After two days, cells were washed with PBS and new medium was added with antibiotic G418 at 600 $ng.µl^{-1}$ in order to start the selection. After 10 days cells colonies were stained with Giemsa (25% in ethanol).

We then compared the effect of the presence of different cations on the transfection efficiency. Thus, various bionanocomposites were prepared in the presence of 10 mM $CaCl_2$, 0.2 mM spermidine and 0.2 mM spermine. The use of $CaCl_2$ slightly stimulated the efficiency of transfection (Figure 5.4A-B compared to spermidine (Figure 5.4C-D) or spermine (Figure 5.4E-F), presumably due to the strong interaction of DNA on sepiolite in these conditions.

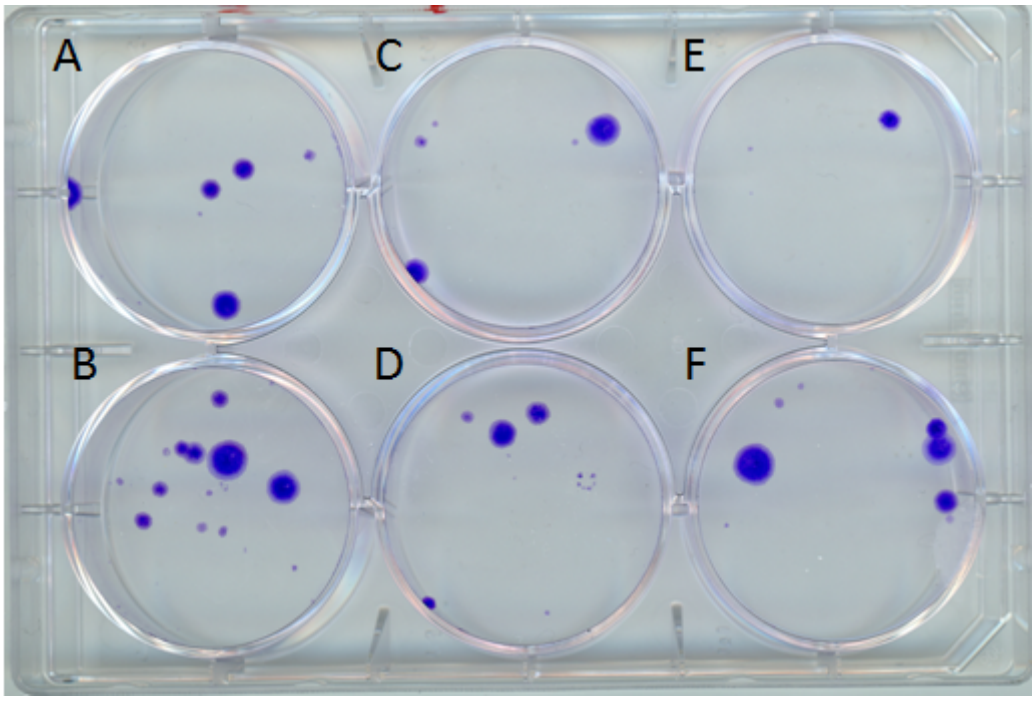

Figure 5.4 Picture of colonies of transfected V79 cells with Sep/DNA prepared with 10 mM $CaCl_2$ (A-B), 0.2 mM spermidine (C-D) and 0.2 mM spermine (E-F). First day: 10^5 cells were plated in each well. Second day: 3 ml of new medium was added in presence of Sep/DNA bionanocomposite with 40 µg of sepiolite and 1 µg of bounded DNA in presence of $CaCl_2$ (A-B), 0.2 mM spermidine (C-D) and 0.2 mM spermine (E-F). After two days, cells were washed with PBS and the new medium was added with antibiotic G418 at 600 ng.µl^{-1} in order to start the selection. After 10 days cells colonies were stained with Giemsa (25% in ethanol).

Interestingly, Sep/DNA can be used in different kind of cell lines. Indeed, human osteosarcoma cells (U2OS) were also transfected by the bio-nanocomposite. The dose response in this cell line for G418 is shown in Figure 5.5. It was observed that 800 ng.µl^{-1} was the minimum dose of G418 to eliminate all of the non-resistant U2OS cells (higher compared with the dose in V79). The stable transfectants obtained after selection with this dose of G418 are shown in Figure 5.6.

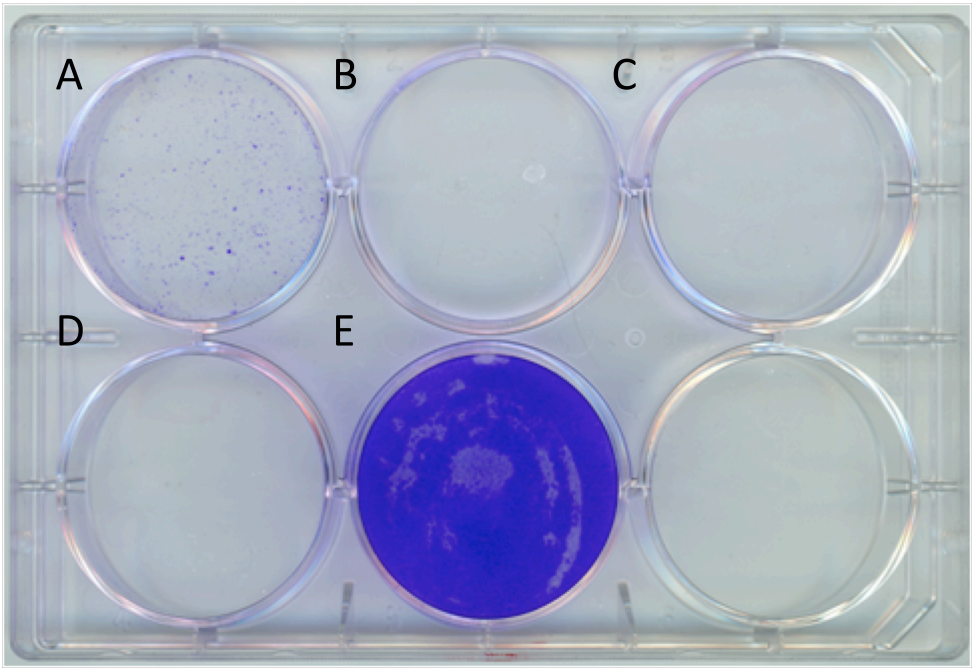

Figure 5.5 Dose response of U2OS human osteosarcoma cells after incubation for 10 days with G418 antibiotic. G418 concentrations: A: 600 ng.μl^{-1}*; B: 800* ng.μl^{-1}*; C: 1000* ng.μl^{-1}*; D: 1200* ng.μl^{-1}*; E: Control.*

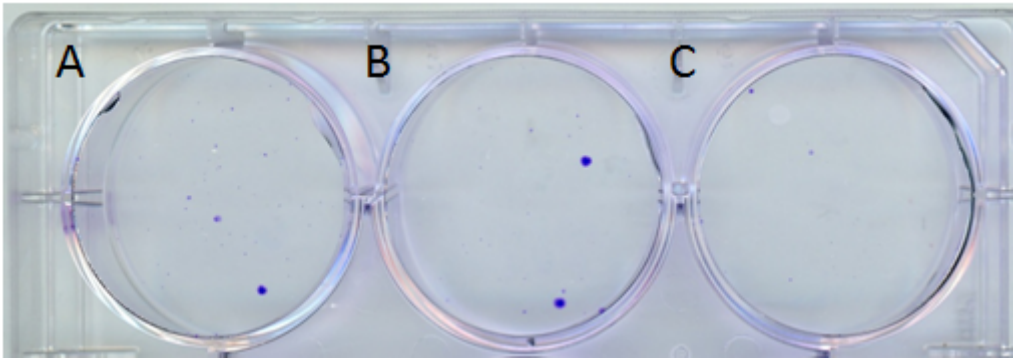

Figure 5.6 Stables colonies of GFP positives U2OS cells after transfection with Sep/DNA bionanocomposite in 48 hours, and then after 10 days of selection with G418 at 800 ng.μl^{-1}. Incubation with bionanocomposite obtained with: A -C: 10 mM $CaCl_2$.

Importantly, several negative controls were carried out: DNA alone, DNA in presence of tested cations (10 mM $CaCl_2$, 0.2 mM spermidine and 0.2 mM spermine), or sepiolite alone, and did not produced any colonies in any of the three times repeated experiments.

5.3. Improvement of DNA transfection efficiency.

As it was observed and discussed before and in Chapter 3, sepiolite spontaneously aggregates, leading to bright and non-homogenous fluorescent particles into cells, (Figures 3.5 - 3.7). This aggregation can constitute a limitation for efficient widespread transfection. We thus used sonicated sepiolite (sSep), in which aggregates should have been dispersed under the action of ultrasound irradiation. Then the bionanocomposite was synthetized with the plasmid and sonicated sepiolite (sSep/DNA).

We have then verified that cells efficiently internalize sSep (figure 5.9A,B) and sSep/DNA bio-nanocomposite. Interestingly, in contrast with non-sonicated sepiolite, the presence of sSep in cells is characterized by a diffuse signal (figure 5.7B) and by the lack of big aggregates (figure 5.7A, 5.8B).

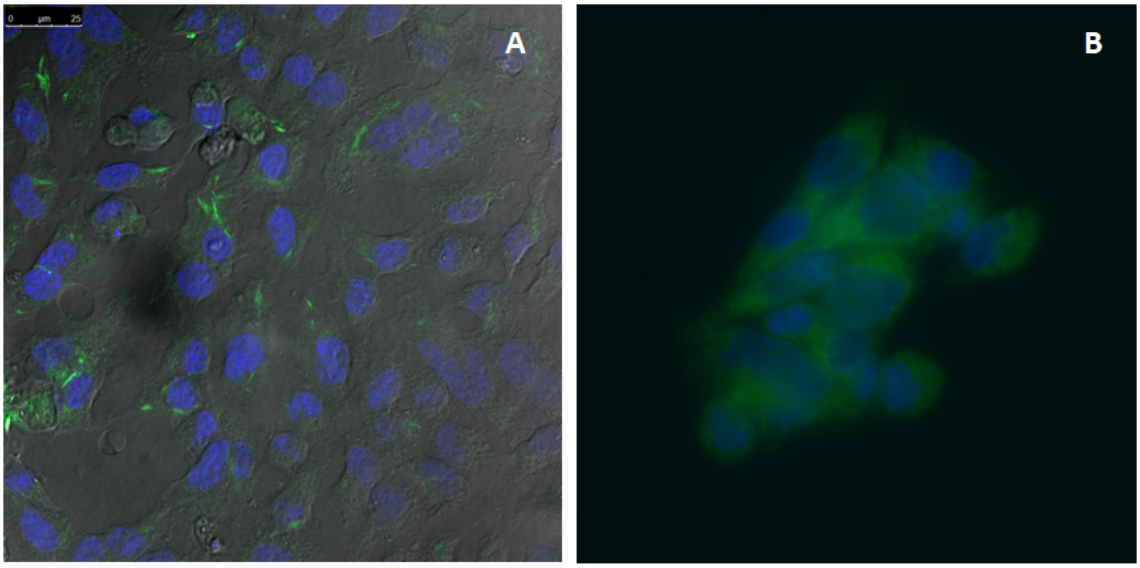

Figure 5.7 Fluorescence microscopy images of sonicated sepiolite (sSep) at 10 ng.μl^{-1} in V79 cells. A: Laser confocal microscopy image of in phase mode. B: fluorescence microscopy image.

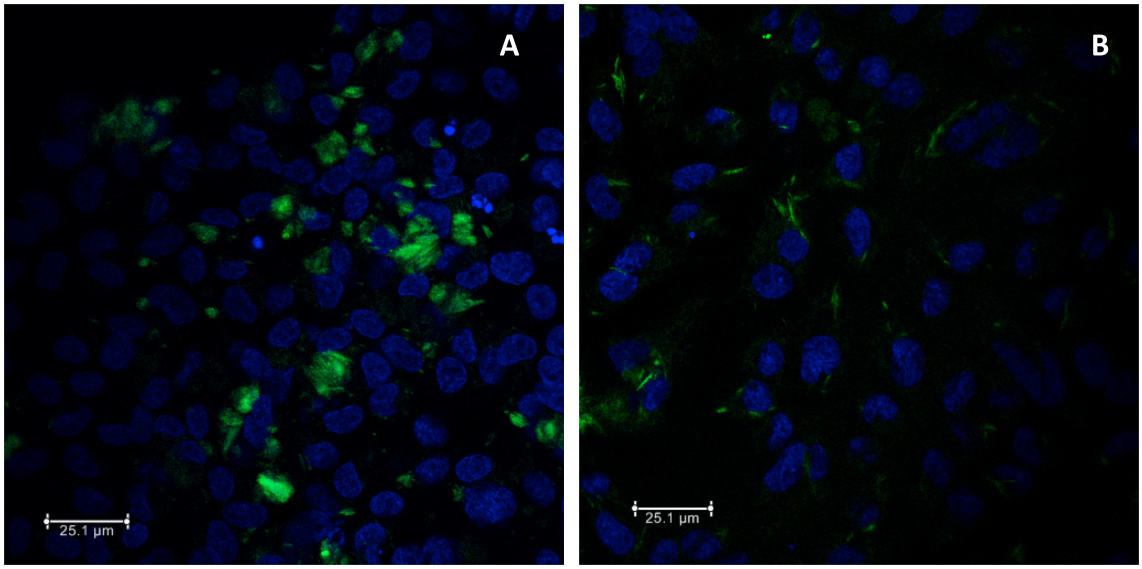

Figure 5.8 Laser confocal microscopy images. Comparison of sepiolite (A) and sSep (sonicated sepiolite) (B), both at 10 ng.μl^{-1} in V79 cells.

Strikingly, sonication of sepiolite prior assembled with DNA, strongly increases the efficiency of stable gene transfection in U2OS cells, by two orders

of magnitude (Figure 5.9). Indeed, the mean stable transfection efficiencies were 3 and 350 stable transfectant colonies per μg of DNA, with non-sonicated and sonicated sepiolite, respectively, i.e. more than 100-fold of stimulation.

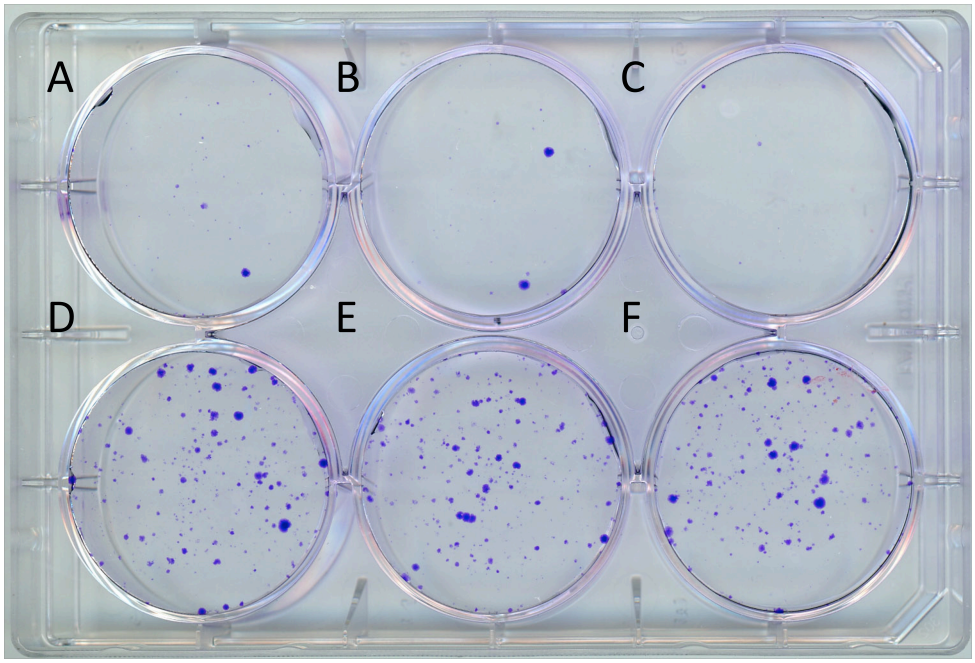

Figure 5.9 Comparison of number of colonies of transfected U2OS human cells with Sep/DNA (with vortexed sep in A, B and C), and sSep/DNA (with sonicated sep in D, E and F). First day: 10^5 cells were plated in each well. Second day: 9 ml of new medium was added (3 ml in each well) in presence of Sep/DNA bionanocomposite (A-C) and sSep/DNA (D-E) with 80 μg of sepiolite and 3 μg of bounded DNA in presence of $CaCl_2$. After two days, cells were washed with PBS and new medium was added with antibiotic G418 at 800 ng.μl-1 in order to start the selection. After 10 days cells colonies were stained with Giemsa.

Thus, because the low cost of sepiolite and the easy and convenient synthesis methods designed in the present work, the use of sSep becomes an advantageous efficient method for gene transfer delivery. In addition because sepiolite might bind different molecules many strategies aiming at the co-transfer of different kinds of bio-molecule can be designed.

Transfection is a complex process involving multiple steps, such as cellular binding, internalization and delivery into the cells. In our case, since endocytosis plays a pivotal role in sepiolite internalization, the endosomal escape could be a major factor that might affect the transfection efficiency.

Chloroquine is a weak base that can rapidly penetrate the plasma membrane, accumulate in acidic vesicles and increase the pH of the acidic compartment[293]. Preventing endosome acidification may subsequently inhibit hydrolytic enzymes such as proteases and nucleases[294]. In addition, chloroquine also causes the swelling and rupture of endosomal vesicle by increasing the osmotic pressure inside the acidic compartment[295]. Since it can neutralize acidic compartment and induce rupture of endocytic vesicles, adding chloroquine has been shown to improve nucleic acid transfer[294,296].

Unfortunately chloroquine can also inhibit the internalization of endogenous molecules by blocking the clathrin mediated endocytosis pathway. However, we have shown that in our case, chloroquine has a very moderate effect on the efficiency of sepiolite uptake (see the end of Chapter 3). Thus upon chloroquine exposure the transfection efficiency should results from the balance of two opposite process: the potential inhibition of cellular uptake versus the disruption of the endosomes and the protection against nuclease degradation.

Interestingly, treatment with chloroquine two-fold increased transfection efficiency, using sSep/DNA into human U2OS cells (Figure 5.10D-F). Amiloride only led to a slight increase (1.5-fold) in transfection efficiency in U2OS cells

(Figure 5.10G-I). Thus, in the current conditions, chloroquine promotes endosomal escape more efficiently than internalization inhibition.

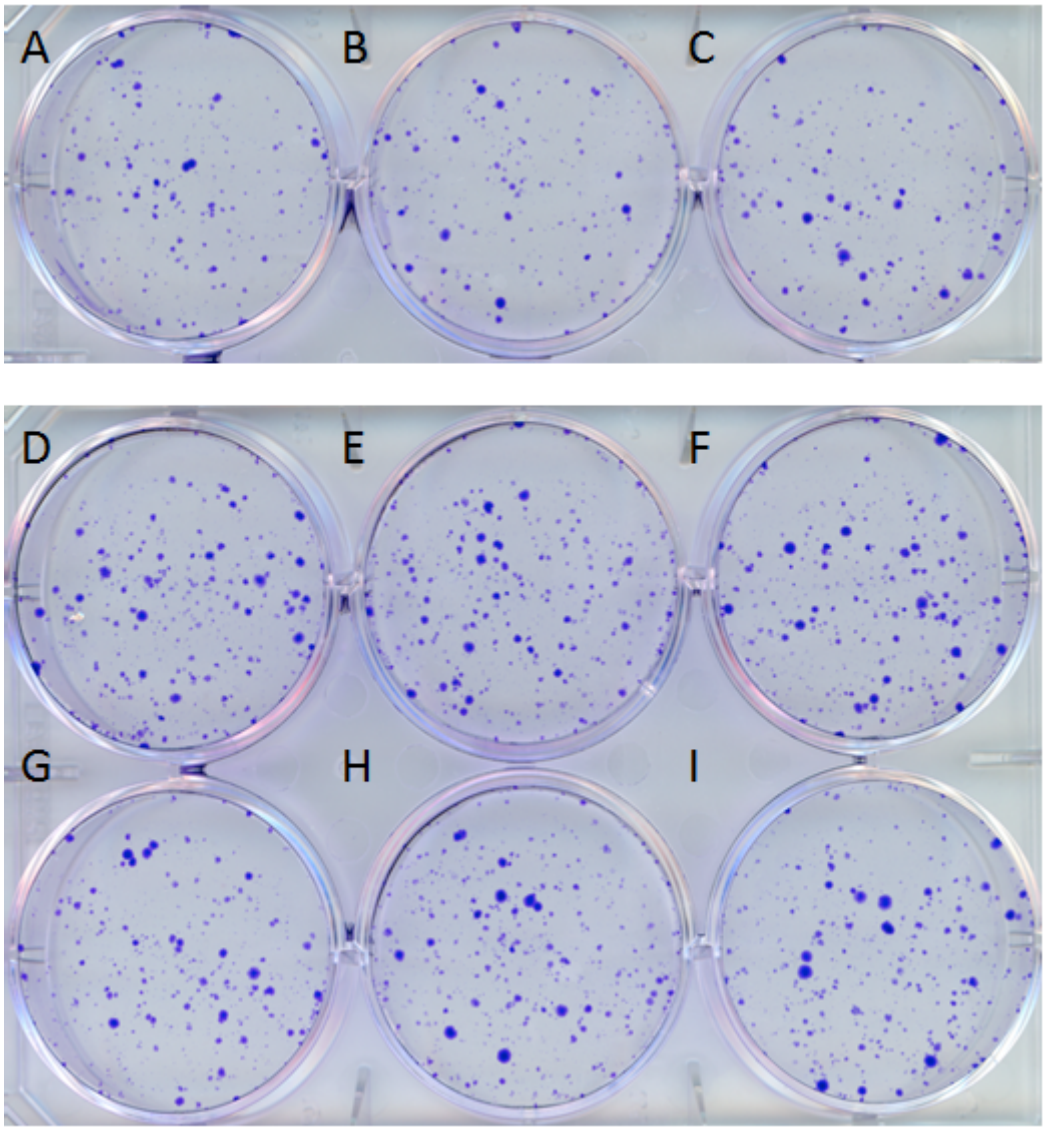

Figure 5.10 Comparison of number of colonies of transfected U2OS human cells with sSep/DNA (A-C), and sSep/DNA after incubation with 10 μM chloroquine (D-F) and 100 mM Amiloride (G-I).

Structure of Chapter 6

6. Biological applications in bacteria.

6.1. Sepiolite – bacteria interactions.

6.2. Bacterial transformation.

6.3. DNA purification and extraction from bacteria.

6. Biological applications in bacteria.

6.1. Sepiolite – bacteria interactions.

Experiments were also carried out in order to verify whether sepiolite can interact with prokaryotic cells, and then if it can be used as a nano - bio - platform to transform bacteria.

First, a set of experiments was performed in order to know the dose response and the kinetics response of sepiolite for binding to bacteria. Different amounts of sepiolite powder were added in 6 tubes to overnight saturated bacterial cultures and 6 tubes with LB as control. Pictures were taken every 10 min, and the optical density at 600 nm was determined by using spectrophotometric measurements in order to obtain qualitative information regarding the amount of bacteria in the culture. From those pictures it can be established that from 40 mg and higher amount of sepiolite (which corresponds to a concentration of 20 mg/ml) it is possible to clarify 2 ml of the saturated bacterial culture (Figure 6.1). Moreover, from results of optical density measurements it was observed that with less sepiolite concentration (10 mg/ml and higher, *i.e*. 20 mg of sepiolite in 2 ml of LB), it is possible to sediment almost all the bacteria after 20 min of addition of sepiolite just by gravity (Figure 6.2).

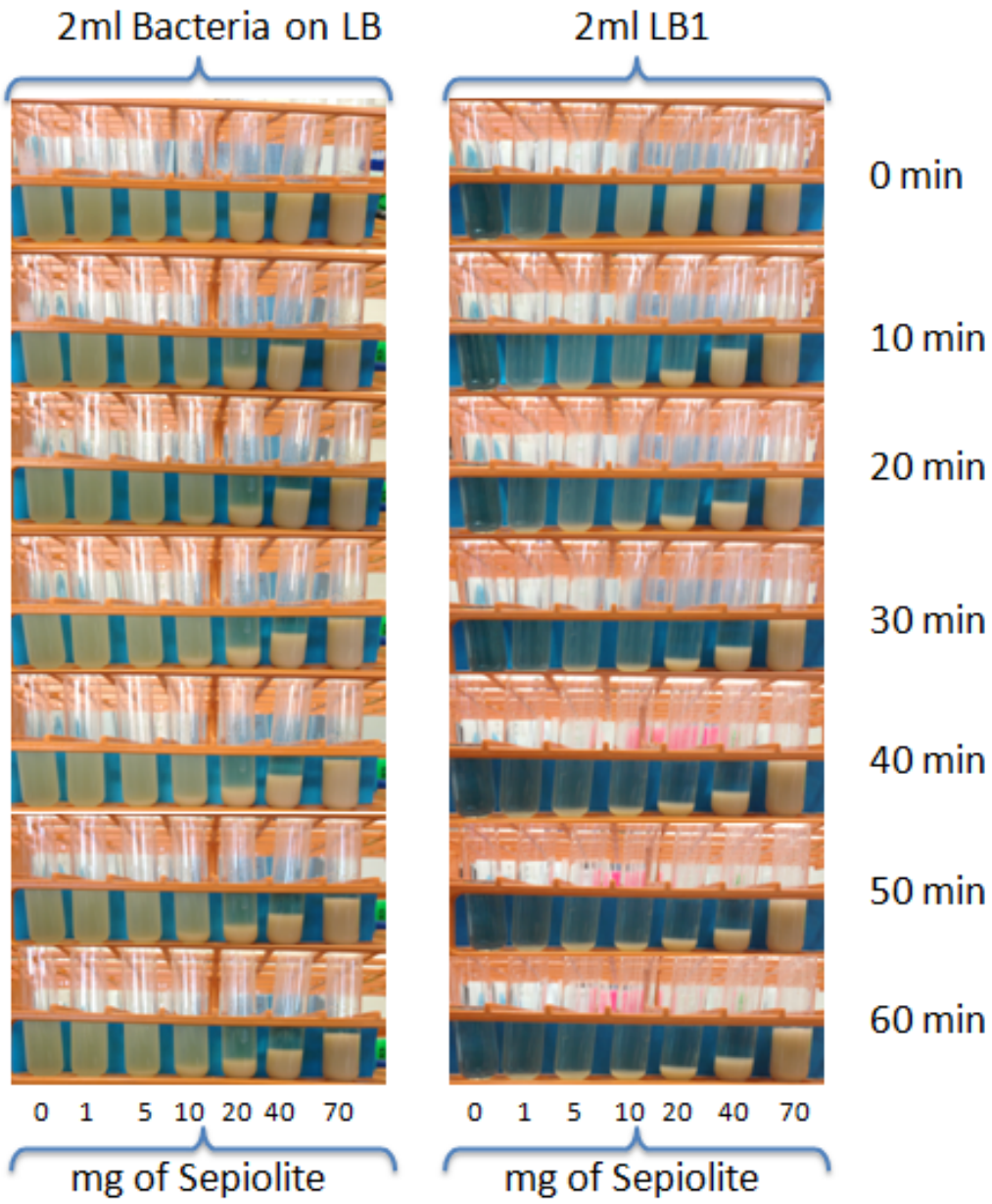

Figure 6.1 Pictures of the experiment of dose response and time kinetics of sepiolite in bacterial culture.

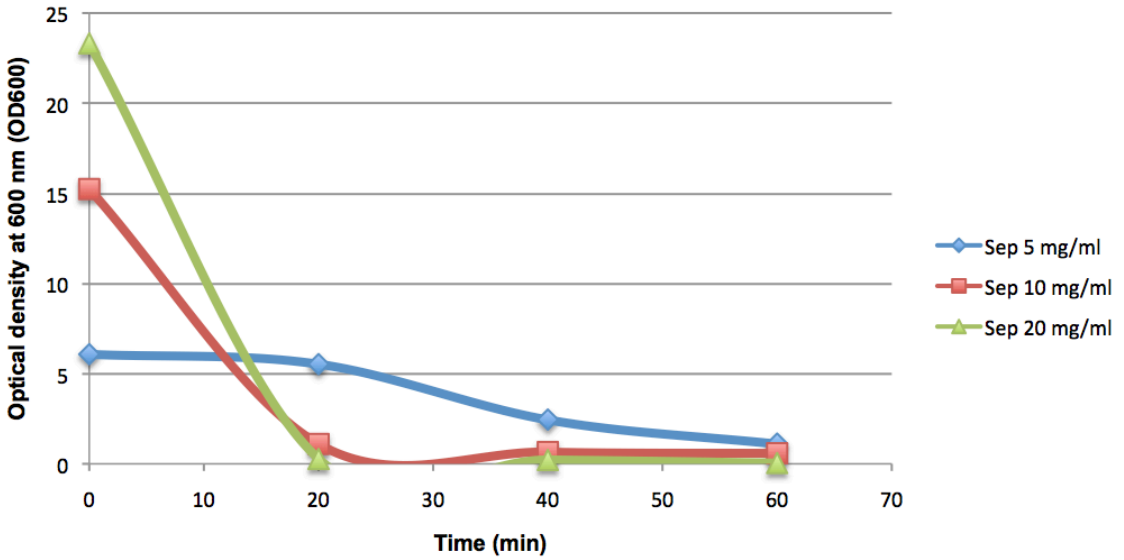

Figure 6.2 Time kinetics for bacterial sedimentation with sepiolite fibers. In Y axis it is shown the optical density at 600 nm from spectrophotometry measurements.

Figure 6.3 shows the response to the addition of sepiolite on bacterial culture in measurements after one hour of contact with the silicate. For sepiolite concentrations of 20 mg/ml and higher, there is almost no bacteria detected in the LB medium. This result evidences that sepiolite can interact with bacteria, and then as the bacteria becomes heavier, it can be sedimented faster in the bottom of the tube.

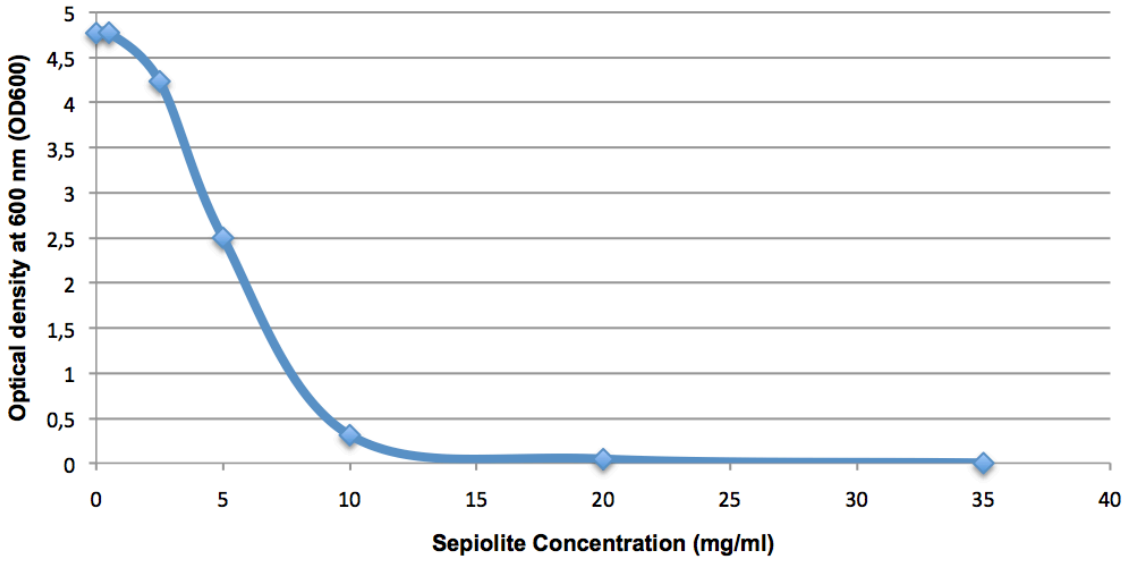

Figure 6.3 Optical density measured at 600 nm of the bacterial medium one hour after the addition of variable amounts of sepiolite.

In order to visualize, as well as to get more details regarding the interaction between sepiolite and bacteria, we performed an analysis by TEM. The sample for visualization is prepared from a logarithmic-phase culture of XL2 bacteria (OD600 0.5-1) in 10 ml of LB. In this experiment, 500 μl of the culture were centrifuged at 3000 rpm for 5 min, and then the pellet was re-suspended in 200 μl of a sepiolite suspension containing 1 mg of clay per ml. Finally, 5 μl of sample were placed in a carbon grid for TEM examination.

From the TEM characterization it was possible to confirm the interaction between sepiolite fibers and the bacterial membrane. Almost all bacteria were found with sepiolite nanofibers in contact with their cell membrane (Figure 6.4A-D).

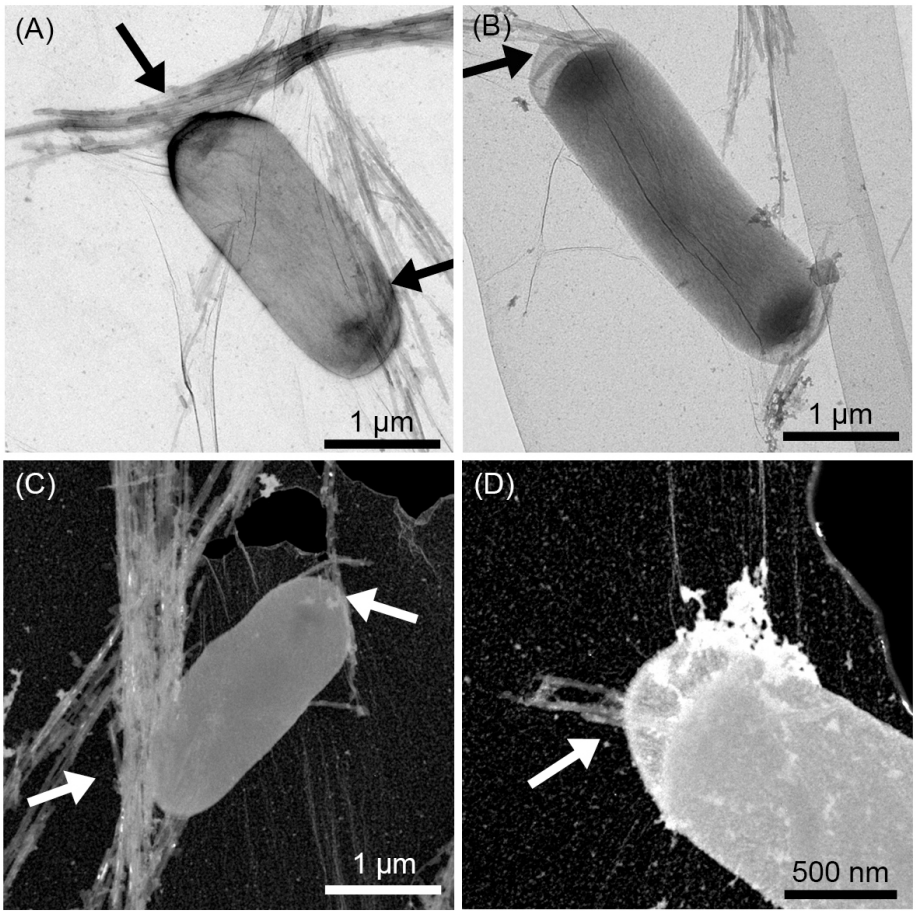

Figure 6.4 TEM images of sepiolite nanofibers in contact with XL2 bacteria (overnight culture of XL2 in 20 ml of LB, then 500 µl of bacteria in LB with 0D600 between 0.5 and 1 centrifuged at 3000 rpm for 5 min and resuspended in 200 µl of sepiolite at 1 mg/ml; 5 µl of this sample were placed in a carbon grid and measured with TEM).

Figures 6.5A and 6.6A shows the image of a complete bacteria with zooms in their respective contact regions (Figures 6.5B, 6.5C and 6.6B-E), where it is possible to detect that nanofibers interacts mostly with the edge of the bacteria and occasionally pierce its lateral surface.

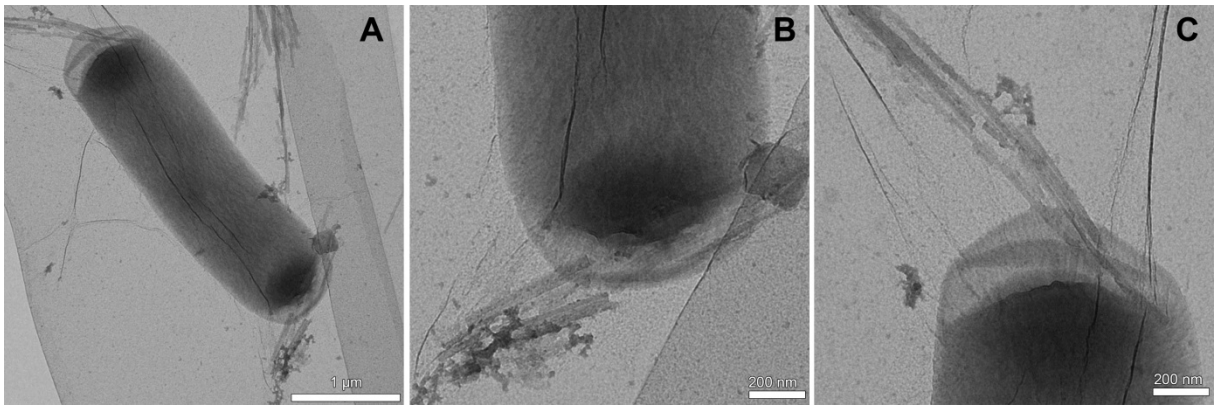

Figure 6.5 TEM image of a complete XL2 bacteria (A) with zoom in contact regions (B and C).

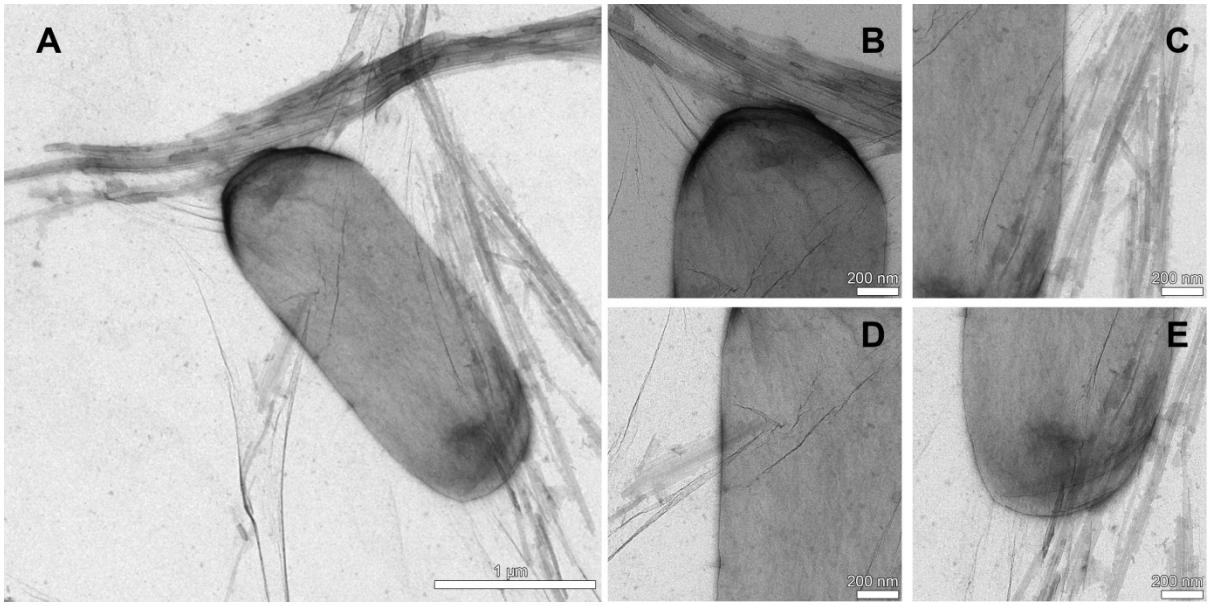

Figure 6.6 TEM image of a complete XL2 bacteria (A) with zoom in contact regions (B to E).

6.2. Bacterial transformation.

From these data, we hypothesized that it might be possible to improve bacterial transformation, which was previously based on the Yoshida Effect. As it was already described in section 1.5, current hypothesis is that the sliding

friction forces, arising between the surface of the agar and the stir stick when bacteria are spread, results in penetration of bacterial cells[265]. This leads to inoculation of the transforming DNA, which is adsorbed by the mineral nanofibers. The suggested mechanism was that inside the cell, the DNA is probably displaced by competition with small nucleic acids[275] so that it can be maintained and expressed. Using the corresponding protocol[265], we obtained from $3x10^4$ to $6x10^4$ transformants per μg of PUC19 plasmid.

After the physicochemical characterization of the Sep/DNA bionanocomposite, and according to the results obtained by TEM, we should be able to improve the transformation efficiency. First, the hypothesis we suggest that the bacterial transformation efficiency depends not only on the friction, but should also be proportionally correlated to the DNA previously adsorbed onto sepiolite nanofibers. Second, as discussed in Chapter 5, sepiolite spontaneously aggregates and this aggregation can constitute a limitation for efficient widespread transformation. The sonication of sepiolite leads to the dispersion of the aggregates, and then the active surface, which adsorbs DNA, increases and should increase the efficiency of contact with bacteria.

In the referred work[265], the bacterial pellet was resuspended in a solution of 100 μl of 5 mM HEPES pH 7.4 and 200 mM KCl, containing 10 μg of sepiolite, and then adding 50 ng of PUC19 plasmid encoding resistance to ampicillin, and immediately spread on agar plate containing ampicillin[265]. Therefore, in this method DNA is not previously assembled to sepiolite, prior spreading of the bacteria. In our case, we follow the same protocol but using the current buffer for Sep/DNA employed along in this work (*i.e.* 10 mM TrisHCl pH=7.5), and in the presence of a divalent cation at lower concentration (5 and 10 mM of $MgCl_2$

instead of 200 mM KCl as used in reference[265]). Thus, 50 ng of PUC19 plasmid was previously adsorbed in 10 µg of sepiolite dispersed in a solution of 100 µl of 10 mM TrisHCl pH 7.5 in the presence of 5 mM $MgCl_2$. The bacterial pellet was then re-suspended in the pre-assembled bionanocomposite suspension and immediately spread on agar plate. Following this protocol we obtained transfection efficiencies similar to that reported by Wilharm *et al.*[265] (Figure 6.7).

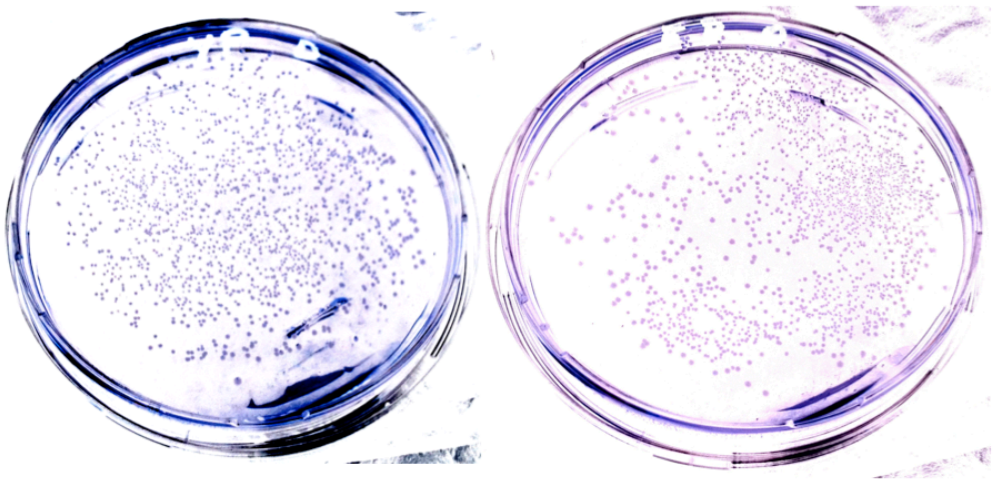

Figure 6.7 Left: Picture of the agar plate with transformants using the protocol reported by Wilharm et al.[265], with 5 mM HEPES and 200 mM KCl pH 7.4. Right: Picture of the agar plate with transformants using the same protocol but with 10 mM TrisHCl and 5 mM $MgCl_2$ pH 7.5. Around 1,500 colonies were obtained in both cases, with 50 ng of DNA, which mean $3x10^4$ transformants per µg of DNA.

We can propose that if the Sep/DNA complex is incubated with bacteria then given more time to the bionanocomposite for interacting in homogeneous way with more bacteria would result in an improvement of the transformation efficiency. To probe this hypothesis, the two experiments above mentioned were repeated, but in this case following by 1 hour of incubation with LB at 37°C after the re-suspension of bacterial pellet. The incubation

bacteria/bionanocomposite prior spreading resulted in an increase of the transformation efficiency in 5-fold for the protocol reported by Wilharm et al.[265], and 10-fold using our method (Figures 6.8 and 6.9).

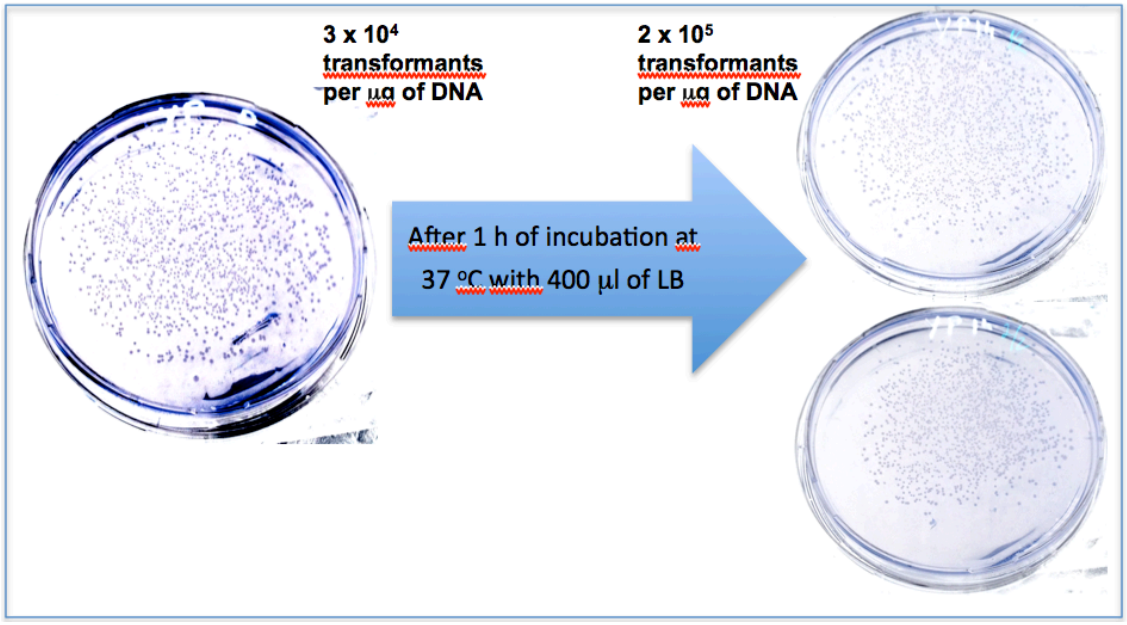

Figure 6.8 Improvement of bacterial transformation efficiency by incubation of 1 hour of sepiolite and DNA with bacteria at 37°C , following the protocol reported by Wilharm et al.[265] using 5 mM HEPES and 200 mM KCl pH 7.4 (image of the plate agar at left), an improvement of 5-fold was obtained, reaching 2x10^5 transformants per μg of DNA (with the same amount of bacteria, sepiolite and DNA used by Wilharm et al.[265] but incubating one hour in presence of LB, the obtained colonies are the sum of the two agar plates showed at right).

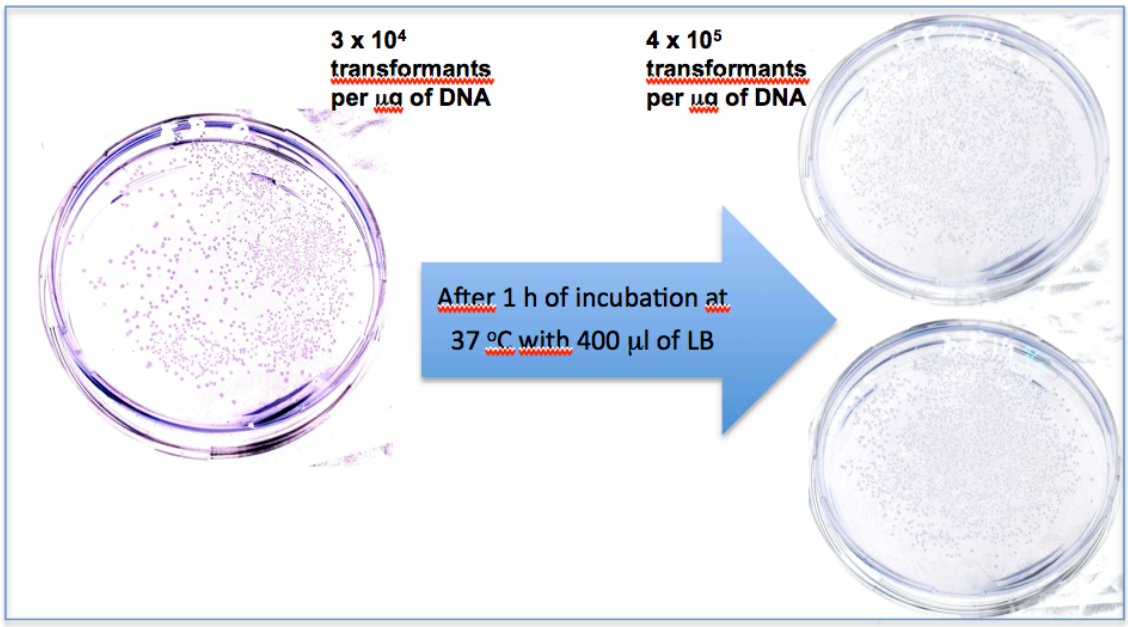

Figure 6.9 Improvement of bacterial transformation efficiency by incubation of 1 hour of Sep/ DNA with bacteria at 37 °C, following our method using 10 mM TrisHCl pH=7.5 and 5 mM $MgCl_2$, an improvement of 10-fold was obtained, reaching $4x10^5$ transformants (the sum of the colonies which grown in the two plates showed at right compared with the colonies which grown in the plate at left without incubation).

This improved protocol was followed to study the influence of the diverse polyvalent cations used in this work to the bacterial transformation efficiency. Thus, various bionanocomposites were prepared in the presence of 5 mM $MgCl_2$, 5 mM $CaCl_2$, 0.5 mM spermidine and 0.5 mM spermine. Results regarding the number of obtained colonies are shown in Table 6.1. The amount of adsorbed DNA varies depending on the nature of the cation present in the following sequence: $MgCl_2$ < $CaCl_2$ < spermidine < spermine. However, the bacterial transformation efficiency decreased with higher valencies ($MgCl_2$ > $CaCl_2$ > spermidine > spermine). Therefore, these results indicate that the efficiency can be correlated with the inverse of the cation valence, which may

be due to the stronger interaction between sepiolite and DNA when the adsorption is performed in the presence of cations of higher valence.

Sep/DNA prepared in presence of:	Transformants per μg of DNA.
5 mM $MgCl_2$	3.7×10^5
5 mM $CaCl_2$	2.5×10^5
0.5 mM spermidine	4.8×10^4
0.5 mM spermine	2.6×10^4

Table 6.1 Comparison of bacterial transformation efficiency of Sep/DNA bionanocomposites prepared in presence of different polyvalent cations. Efficiency is correlated with the inverse of the cation valence, which is possible ascribed to the stronger interaction between sepiolite and DNA with higher valence.

Finally, we also verified the influence of a previous treatment of sonication of the sepiolite suspension to corroborate if it can also increase the bacterial transformation efficiency. Using the same experimental conditions above mentioned, two bionanocomposites were prepared in the presence of 10 mM $MgCl_2$, but in one case using sepiolite and in the other one a sample of sonicated sepiolite. Remarkably, sonication of sepiolite prior assembly with DNA, more than 2-fold increases the bacterial transformation efficiency (Table 6.2). Indeed, we obtain $4x10^5$ and $9x10^5$ colonies with non-sonicated and sonicated sepiolite, respectively. In conclusion, compared to the previously reported protocol[265] we optimized transformation efficiencies by 30-fold.

Protocol	Transformants per μg of DNA.
Wilharm *et al.*[265].	3×10^4
Our method (without 1 h incubation)	3×10^4
Wilharm *et al.*[265]. (with 1 h incubation)	2×10^5
Our method (with 1 h incubation)	4×10^5
Our method using sSep	9×10^5

Table 6.2 Comparison of our method with and without the use of sonicated sepiolite, and the protocol reported by Wilharm *et al.*[265]*, with and without 1 h of incubation, in bacterial transformation efficiency.*

As it was already mentioned in the introduction, Rodriguez-Beltrán *et al*.[297] mixed sepiolite and DNA in presence of NaCl and reported around 10^5 transformants per μg of plasmid DNA[297]. In contrast, the low efficiency obtained in the protocol followed by Tan *et al*.[266] could be attributed to the fact that they made the sepiolite dispersion in LB instead of a buffer with the presence of cations. Additionally, according to our results we can obtain the following conclusions:

- For the bacterial transformation it is necessary to adsorb first the DNA onto sepiolite, *i.e.* to prepare the bionanocomposite Sep/DNA in the presence of a low concentration of a divalent cation, such as $MgCl_2$ or $CaCl_2$ in a concentration ranging from 5 to 10 mM. Following this method it is possible to adsorb the same or more amount of DNA compared to that adsorbed in the presence of monovalent cations at high concentrations (*e.g.* 200 mM KCl).
- Our results suggest that the Sep/DNA bionanocomposite is internalized into bacteria by means of the Yoshida effect (driven by friction forces), and not by spontaneous internalization of Sep/DNA bionanocomposite

neither by internalization by vortexing (which is not healthy for the bacteria).

- The bacterial transformation efficiency will be improved if sepiolite is previously sonicated, and with at least 30 min of incubation of Sep/DNA with bacteria in LB at 37 ^{o}C after re-suspending the bacterial pellet. The disaggregation of sepiolite fibers submitted to the sonication process, results in Sep/DNA bionanocomposite of smaller size which could facilitate the bacteria to internalize smaller complex following the Yoshida effect but without big damage of membrane and bacterial structure. The incubation could give more time to the bionanocomposite to interact in homogeneous way with more bacteria and then improve the transformation efficiency.

6.3. DNA purification and extraction from bacteria.

In all the measurements of the DNA concentration in the supernatant (Chapter 4), the Index of Purity was determined by the ratios A_{260}/A_{280} and A_{260}/A_{230}. In the case of plasmids and oligonucleotides, initial DNA samples were pure, with ratios $A_{260}/A_{280} \approx 1.8$ and $A_{260}/A_{230} \approx 2.0$. The commercial salmon sperm DNA was not pure since the initial ratios were $A_{260}/A_{280} \approx 1.4$ and the $A_{260}/A_{230} \approx 2.2$, revealing the presence of contaminants. Interestingly, in the DNA remained in the supernatant, the ratio $A_{260}/A_{280} = 1.81$ and $A_{260}/A_{230} = 2.07$ indicating the increase of the purity of the DNA. This suggests that the sepiolite could be also used for purifying DNA from contaminants. In addition, according to the results showed in Chapter 4, since we are able to modulate the efficiency

of DNA adsorption and desorption from sepiolite, we should be able to perform a plasmid DNA extraction from bacteria.

To test this hypothesis, in a first step a plasmid was amplified in bacteria. After cells lysis and denaturation step using classical methods, the extract was then incubated with sepiolite and DNA was recovered using EDTA (Figure 6.10 lane C). Interestingly, efficient DNA recovery from bacteria was observed with sepiolite. The efficiency of DNA extraction was 78.9 µg for 20 ml of cultured bacteria at saturation. In addition the index of purity A_{260}/A_{280} of 1.7 before precipitation indicates a good purity index. Consistently, the ratio of the different isoforms of the DNA (supercoiled *versus* open circle and linear) was not altered, compared to that of the commercial initial plasmid DNA.

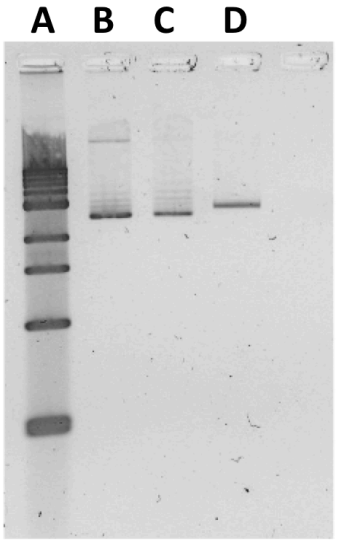

Figure 6.10 Gel electroforesis of extracted PUC19 plasmid from bacteria using sepiolite. A: step ladder. B: commercial PUC19 plasmid. C: extracted PUC 19 plasmid. D: extracted PUC19 plasmid digested with EcoRI.

Finally, the quality of the plasmid extracted from bacteria was confirmed by digestion with a restriction enzyme (Figure 6.10 lane D) and by TEM (Figure 6.11). The fact that the enzyme efficiently cleaved the DNA indicates that the

DNA extracted with sepiolite is suitable for further molecular biology experiments.

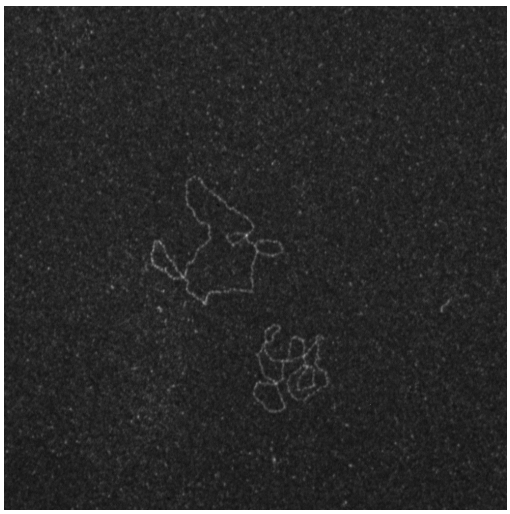

Figure 6.11 TEM image of extracted PUC19 using sepiolite.

Based on the above mentioned results we can propose the following protocol for DNA extraction using sepiolite:

- Overnight saturated culture of cells at 37 °C in 20 ml of LB (Luria-Bertani) medium, with 20μl of the adequate antibiotic and at constant shaking (200–250 rpm).
- Centrifugation at 4,500 g for 15 min at 4 °C.
- Carefully re-suspension of the pellet of bacterial cells in 4ml of Resuspension Buffer (S1).
- Addition of 4ml of Lysis Buffer to the suspension (S2).
- Gently mixing by inverting the tube 6–8 times.

- Incubation of the mixture at room temperature (18–25 °C) for 2– 3 min (max. 5 min).
- Addition of pre-cooled Neutralization Buffer (S3 at 4°C) to the suspension. Immediately gently mixing of the lysate by inverting the flask 6–8 times until a homogeneous suspension containing an off-white flocculate is formed. Incubation of the suspension on ice for 5 min.
- Filtration of the suspension using Waterman paper.
- Addition of concentrated $MgCl_2$ to the filtered suspension in order to obtain a final $MgCl_2$ concentration of 20 mM.
- Addition of Binding solution in order to have a final sepiolite concentration of 1 mg/ml. At this step the DNA is adsorbed onto sepiolite.
- Stirring of the suspension for at least 90 min.
- Centrifugation at 4,500 g for 5 min (discard supernatant).
- Re-suspension with 12 ml of washing solution and replacing the tube.
- Centrifugation at 4,500g for 5min (discard supernatant).
- Resuspension in 1ml of Elution Buffer.
- Ethanol precipitation into 1 ml of 10 mM TrisHCl pH=7.5.

After following this protocol, the DNA yield is around 80 μg. The used solutions were:

- Re-suspension Buffer (S1): 50 mM TrisHCl, 10 mM EDTA, 100 μg / ml RNase A, pH 8.0.
- Lysis Buffer (S2): 200 mM NaOH, 1% SDS.
- Neutralization Buffer (S3): 2.8 M KAc, pH 5.1.
- Binding solution: 10 mM TrisHCl, 20 mM $MgCl_2$, 4 mg/ml sepiolite suspension, pH=7.5.
- Washing solution: 10 mM TrisHCl, 20 mM $MgCl_2$, pH 7.5.
- Elution Buffer: 10 mM TrisHCl, 20 mM EDTA, pH 7.5.

All the above mentioned results constitute a novel application of fibrous clay minerals such as sepiolite, which appears as a useful tool for extracting DNA from bacteria, as well as a specific adsorbent for impurities accompanying DNA samples, such as proteins and other diverse type of biomolecules.

7. Conclusions and Perspectives.

In this Dissertation, bionanocomposites (Sep/DNA) based on the microfibrous silicate sepiolite and DNA were successfully prepared by direct assembly of both components, being characterized by using a combination of techniques including, AFM, TEM, UV-vis spectroscopy, Zeta-potential and FTIR. The DNA adsorption efficiency can be modulated by supplying multivalent cations in the reaction medium. It has been also showed that sepiolite can be spontaneously internalized into mammalian cells, mainly by endocytosis and macropinocytosis. Sepiolite is able to stably transfert DNA into bacteria and mammalian cells, and, moreover, it is possible to design strategies aiming an increase in the efficiency of DNA delivery. Therefore, because of its characteristics, sepiolite might represent a promising nano-carrier for DNA assembly and its further transfer into mammalian cells. In detail, the conclusions are:

- Sepiolite from Vallecas-Vicálvaro deposits could be spontaneously internalized into mammalian cells, mainly by endocytosis. Dose response experiments of sepiolite nanofibers in mammalian cells determined that the working concentration should be less than 50 $ng.\mu l^{-1}$. Higher concentrations could be toxic for the cells.
- DNA could spontaneously bind onto the external surface of the sepiolite. DNA adsorption efficiency could be modulated with polyvalent cations.

Our results suggest that the nature of the interactions of DNA assembled to sepiolite is mainly electrostatic.

- The DNA previously adsorbed onto sepiolite could be recovered, maintaining its biological activity. DNA desorption efficiency could be modulated using a chelation agent such as EDTA.
- It was proved that it is possible to use sepiolite for extracting DNA from bacteria, for DNA purification and for purification from bacterial contamination.
- Sepiolite constitutes a very promising nano-platform for vectorization of different molecules into bacteria and mammalian cells. With Sep/DNA bionanocomposites is possible to transform bacteria and obtain stable transfectants in mammalian cells.
- It is possible to design strategies for increasing the efficiency of DNA delivery.

Beside the properties revealed and analyzed in the present work, sepiolite possesses two additional properties that can potentially be helpful for genome engineering. Firstly, thanks to its natural fluorescence it should be possible to select cells containing Sep/DNA, by cell sorting. Secondly, targeted genome editing constitutes a promising approach for the *in situ* correction of a mutated gene, leading to the restoration of normal gene functions. Such strategies rely on homologous recombination (HR). Because HR can repair DNA double strand breaks (DSB), one promising strategy to increase the frequency of gene targeting is to generate a DSB in the target sequence. The development of engineered sequence-specific nucleases (zinc finger, TALE or sgRNA-Cas9 nuclease) now allows to generate the required DSBs in a given

locus of the mammalian genome[298]. Several studies have reported the feasibility of such approach *ex vivo* in human stem cells and primary cells, and in the liver of a mouse model of hemophilia B[299], thus providing a proof of concept for treatment of monogenic disease by genome editing with engineered nucleases. However, the delivery of a plasmid coding for the nuclease might result in chronic expression of the nuclease, upon integration of the plasmid DNA into the cell genome, jeopardizing genome integrity through off target cleavage by the nuclease. Such limitation should be avoid by transferring the nuclease under its protein forms, which should be sufficient to cleave the target sequence but cannot be integrated into the genome and which should be degraded according to its half time turn over, avoiding thus chronic expression. Therefore, a promising strategy would be to co-transfer into cells of the correcting sequence (DNA) and the nuclease (protein). Since sepiolite can binds both DNA and proteins, it might constitute an advantageous carrier for the co-delivery of these two different kinds of biological molecules.

Because the low cost of sepiolite, the easy and convenient synthesis methods designed in the present work, the possibilities to improve the transfection efficiency and the promising developments, sepiolite becomes an attractive tool for DNA delivery into mammalian cells. Therefore, after these preliminary results that show sepiolite DNA interaction leading to, increased DNA transfer efficiency, the selection cells containing sepiolite and co-delivery with biological molecules represent exciting challenges for future prospects.

Bibliography

(1) Choy, J.-H.; Kwak, S.-Y.; Jeong, Y.-J.; Park, J.-S. Inorganic Layered Double Hydroxides as Nonviral Vectors. *Angew. Chem. Int. Ed.* **2000**, *39*, 4041–4045.

(2) Lin, F.-H.; Chen, C.-H.; Cheng, W. T. K.; Kuo, T.-F. Modified Montmorillonite as Vector for Gene Delivery. *Biomaterials* **2006**, *27*, 3333–3338.

(3) Shi, Y.-F.; Tian, Z.; Zhang, Y.; Shen, H.-B.; Jia, N.-Q. Functionalized Halloysite Nanotube-Based Carrier for Intracellular Delivery of Antisense Oligonucleotides. *Nanoscale Res. Lett.* **2011**, *6*, 608.

(4) Choi, G.; Kwon, O.-J.; Oh, Y.; Yun, C.-O.; Choy, J.-H. Inorganic Nanovehicle Targets Tumor in an Orthotopic Breast Cancer Model. *Sci. Rep.* **2014**, *4*, 4430.

(5) Wu, H.; Shi, Y.; Huang, C.; Zhang, Y.; Wu, J.; Shen, H.; Jia, N. Multifunctional Nanocarrier Based on Clay Nanotubes for Efficient Intracellular siRNA Delivery and Gene Silencing. *J. Biomater. Appl.* **2014**, *28*, 1180–1189.

(6) Bergaya, F.; Lagaly, G. Chapter 1 General Introduction: Clays, Clay Minerals, and Clay Science. In *Developments in Clay Science*; Faïza Bergaya, B. K. G. T. and G. L., Ed.; Handbook of Clay Science; Elsevier, 2006; Vol. Volume 1, pp. 1–18.

(7) Clarkson, E. N. K. Genetic Takeover and the Mineral Origins of Life. By A. G. Cairns-Smith (first Published 1982, First Paperback Edition 1987). Cambridge University Press. ISBN 0 521 34682 7. *Genet. Res.* **1988**, *51*, 167–168.

(8) Darder, M.; Aranda, P.; Ruiz-Hitzky, E. Bionanocomposites: A New Concept of Ecological, Bioinspired, and Functional Hybrid Materials. *Adv. Mater.* **2007**, *19*, 1309–1319.

(9) Ruiz-Hitzky, E.; Aranda, P.; Darder, M. Bionanocomposites. In *Kirk-Othmer Encyclopedia of Chemical Technology*; John Wiley & Sons, Inc., 2000.

(10) Mittal, V. (Ed.) *Nanocomposites with Biodegradable Polymers: Synthesis, Properties, and Future Perspectives*; Oxford University Press, 2011.

11. Avérous, L.; Pollet, E.; (Eds.); *Environmental Silicate Nano-Biocomposites*; Green Energy and Technology; Springer London: London, 2012.

(12) Chivrac, F.; Pollet, E.; Schmutz, M.; Avérous, L. Starch Nano-Biocomposites Based on Needle-like Sepiolite Clays. *Carbohydr. Polym.* **2010**, *80*, 145–153.

(13) Ruiz-Hitzky, E.; Aranda, P.; Darder, M.; Rytwo, G. Hybrid Materials Based on Clays for Environmental and Biomedical Applications. *J. Mater. Chem.* **2010**, *20*, 9306–9321.

(14) Ruiz-Hitzky, E.; Darder, M.; Fernandes, F. M.; Wicklein, B.; Alcântara, A. C. S.; Aranda, P. Fibrous Clays Based Bionanocomposites. *Prog. Polym. Sci.* **2013**, *38*, 1392–1414.

(15) Wicklein, B.; Darder, M.; Aranda, P.; Ruiz-Hitzky, E. Bio-Organoclays Based on Phospholipids as Immobilization Hosts for Biological Species. *Langmuir* **2010**, *26*, 5217–5225.

(16) Wicklein, B.; Darder, M.; Aranda, P.; Ruiz-Hitzky, E. Phospholipid–Sepiolite Biomimetic Interfaces for the Immobilization of Enzymes. *ACS Appl. Mater. Interfaces* **2011**, *3*, 4339–4348.

(17) Wicklein, B.; Martín del Burgo, M. Á.; Yuste, M.; Darder, M.; Llavata, C. E.; Aranda, P.; Ortin, J.; del Real, G.; Ruiz-Hitzky, E. Lipid-Based Bio-Nanohybrids for Functional Stabilisation of Influenza Vaccines. *Eur. J. Inorg. Chem.* **2012,** 5186–5191.

(18) Kam, N. W. S.; Liu, Z.; Dai, H. Carbon Nanotubes as Intracellular Transporters for Proteins and DNA: An Investigation of the Uptake Mechanism and Pathway.

Angew. Chem. Int. Ed. **2006**, *45*, 577–581.
(19) Lacerda, L.; Russier, J.; Pastorin, G.; Herrero, M. A.; Venturelli, E.; Dumortier, H.; Al-Jamal, K. T.; Prato, M.; Kostarelos, K.; Bianco, A. Translocation Mechanisms of Chemically Functionalised Carbon Nanotubes across Plasma Membranes. *Biomaterials* **2012**, *33*, 3334–3343.
(20) Dutta, D.; Donaldson, J. G. Search for Inhibitors of Endocytosis: Intended Specificity and Unintended Consequences. *Cell. Logist.* **2012**, *2*, 203–208.
(21) Kim, M. H.; Park, D.-H.; Yang, J.-H.; Choy, Y. B.; Choy, J.-H. Drug-Inorganic-Polymer Nanohybrid for Transdermal Delivery. *Int. J. Pharm.* **2013**, *444*, 120–127.
(22) Park, D.-H.; Hwang, S.-J.; Oh, J.-M.; Yang, J.-H.; Choy, J.-H. Polymer–inorganic Supramolecular Nanohybrids for Red, White, Green, and Blue Applications. *Prog. Polym. Sci.* **2013**, *38*, 1442–1486.
(23) Yu, W. H.; Li, N.; Tong, D. S.; Zhou, C. H.; Lin, C. X. (Cynthia); Xu, C. Y. Adsorption of Proteins and Nucleic Acids on Clay Minerals and Their Interactions: A Review. *Appl. Clay Sci.* **2013**, *80–81*, 443–452.
(24) Ruiz-Hitzky, E. Molecular Access to Intracrystalline Tunnels of Sepiolite. *J. Mater. Chem.* **2001**, *11*, 86–91.
(25) *Developments in Palygorskite-Sepiolite Research: A New Outlook on These Nanomaterials*; Singer, A.; Galan, E., Eds.; Elsevier, 2011.
(26) Brauner, K.; Preisinger, A. Struktur und Entstehung des Sepioliths. *Tschermaks Mineral. Petrogr. Mitteilungen* **1956**, *6*, 120–140.
(27) Santaren, J.; Sanz, J.; Ruiz-Hitzky, E. Structural Fluorine in Sepiolite. *Clays Clay Miner.* **1990**, *38*, 63–68.
(28) Ahlrichs, J. L.; Serna, C.; Serratosa, J. M. Structural Hydroxyls in Sepiolites. *Clays Clay Miner.* **1975**, *23*, 119–124.
(29) Darder, M.; López-Blanco, M.; Aranda, P.; Aznar, A. J.; Bravo, J.; Ruiz-Hitzky, E. Microfibrous Chitosan−Sepiolite Nanocomposites. *Chem. Mater.* **2006**, *18*, 1602–1610.
(30) Alcântara, A. C. S.; Darder, M.; Aranda, P.; Ruiz-Hitzky, E. Polysaccharide–fibrous Clay Bionanocomposites. *Appl. Clay Sci.* **2014**, *96*, 2–8.
(31) Alcântara, A. C. S.; Darder, M.; Aranda, P.; Ruiz-Hitzky, E. Zein–Fibrous Clays Biohybrid Materials. *Eur. J. Inorg. Chem.* **2012**, *2012*, 5216–5224.
(32) Fernandes, F. M.; Ruiz, A. I.; Darder, M.; Aranda, P.; Ruiz-Hitzky, E. Gelatin-Clay Bio-Nanocomposites: Structural and Functional Properties as Advanced Materials. J. Nanosci. Nanotechnol. **2009**, *9*, 221–229.
(33) Fernandes, F. M.; Manjubala, I.; Ruiz-Hitzky, E. Gelatin Renaturation and the Interfacial Role of Fillers in Bionanocomposites. *Phys. Chem. Chem. Phys.* **2011**, *13*, 4901–4910.
(34) Ruiz-Hitzky, E.; Darder, M.; Aranda, P.; del Burgo, M. Á. M.; del Real, G. Bionanocomposites as New Carriers for Influenza Vaccines. *Adv. Mater.* **2009**, *21*, 4167–4171.
(35) Carretero León, M. I.; Pozo Rodríguez, M. *Mineralogía aplicada: salud y medio ambiente*; Thomson-Paraninfo: Madrid, 2007.
(36) Denizeau, F.; Marion, M.; Chevalier, G.; Cote, M. G. Absence of Genotoxic Effects of Nonasbestos Mineral Fibers. *Cell Biol. Toxicol.* **1985**, *1*, 23–32.
(37) Ruiz-Hitzky, E.; Ariga, K.; Lvov, Y. M. (Eds.) *Bio-Inorganic Hybrid Nanomaterials: Strategies, Synthesis, Characterization and Applications*; John Wiley & Sons, Weinheim, **2008**.
(38) Eduardo Ruiz-Hitzky, M. D. Editorial [Trends in Bio-Hybrid Nanostructured Materials Guest Editors: Eduardo Ruiz-Hitzky and Margarita Darder]. *Curr. Nanosci.*

2006, *2*, 153–153.
(39) Darder, M.; Colilla, M.; Ruiz-Hitzky, E. Chitosan–Clay Nanocomposites: Application as Electrochemical Sensors. *Appl. Clay Sci.* **2005**, *28*, 199–208.
(40) Ruiz-Hitzky, E.; Darder, M.; Aranda, P. Functional Biopolymer Nanocomposites Based on Layered Solids. *J. Mater. Chem.* **2005**, *15*, 3650–3662.
(41) Ruiz-Hitzky, E.; Darder, M.; Wicklein, B.; Fernandes, F. M.; Castro-Smirnov, F. A.; Martín del Burgo, M. A.; del Real, G.; Aranda, P. Advanced Biohybrid Materials Based on Nanoclays for Biomedical Applications. In Proc. SPIE on Nanosystems in Engineering and Medicine, S.H. Choi, J.H. Choy, U. Lee, V.K. Varadan Eds.; **2012**; Vol. 8548, p. 85480D–85480D–8.
(42) Darder, M.; Aranda, P.; Ferrer, M. L.; Gutiérrez, M. C.; del Monte, F.; Ruiz-Hitzky, E. Progress in Bionanocomposite and Bioinspired Foams. *Adv. Mater.* **2011**, *23*, 5262–5267.
(43) Dahm, R. Discovering DNA: Friedrich Miescher and the Early Years of Nucleic Acid Research. *Hum. Genet.* **2008**, *122*, 565–581.
(44) Mashaghi, A.; Katan, A. A Physicist's View of DNA. *ArXiv13112545 Phys. Q-Bio* **2013**.
(45) Watson, J. D.; Crick, F. H. C. Molecular Structure of Nucleic Acids: A Structure for Deoxyribose Nucleic Acid. *Nature* **1953**, *171*, 737–738.
(46) Wickham, S. F. J.; Bath, J.; Katsuda, Y.; Endo, M.; Hidaka, K.; Sugiyama, H.; Turberfield, A. J. A DNA-Based Molecular Motor That Can Navigate a Network of Tracks. *Nat. Nanotechnol.* **2012**, *7*, 169–173.
(47) Douglas, S. M.; Bachelet, I.; Church, G. M. A Logic-Gated Nanorobot for Targeted Transport of Molecular Payloads. *Science* **2012**, *335*, 831–834.
(48) Choy, J.-H.; Oh, J.-M.; Park, M.; Sohn, K.-M.; Kim, J.-W. Inorganic–Biomolecular Hybrid Nanomaterials as a Genetic Molecular Code System. *Adv. Mater.* **2004**, *16*, 1181–1184.
(49) Park, D.-H.; Han, C. J.; Shul, Y.-G.; Choy, J.-H. Avatar DNA Nanohybrid System in Chip-on-a-Phone. *Sci. Rep.* **2014**, *4*.
(50) Liang, W.; W. Lam, J. K. Endosomal Escape Pathways for Non-Viral Nucleic Acid Delivery Systems. In *Molecular Regulation of Endocytosis*; Ceresa, B., Ed.; InTech, 2012.
(51) El-Aneed, A. An Overview of Current Delivery Systems in Cancer Gene Therapy. *J. Control. Release Off. J. Control. Release Soc.* **2004**, *94*, 1–14.
(52) Yamamoto, M.; Curiel, D. T. Cancer Gene Therapy. *Technol. Cancer Res. Treat.* **2005**, *4*, 315–330.
(53) Johnson, L. A.; Morgan, R. A.; Dudley, M. E.; Cassard, L.; Yang, J. C.; Hughes, M. S.; Kammula, U. S.; Royal, R. E.; Sherry, R. M.; Wunderlich, J. R.; *et al.* Gene Therapy with Human and Mouse T-Cell Receptors Mediates Cancer Regression and Targets Normal Tissues Expressing Cognate Antigen. *Blood* **2009**, *114*, 535–546.
(54) Vigna, E.; Comoglio, P. M. Targeting the Oncogenic Met Receptor by Antibodies and Gene Therapy. *Oncogene* **2014**.
(55) Mavroudi, M.; Zarogoulidis, P.; Porpodis, K.; Kioumis, I.; Lampaki, S.; Yarmus, L.; Malecki, R.; Zarogoulidis, K.; Malecki, M. Stem Cells' Guided Gene Therapy of Cancer: New Frontier in Personalized and Targeted Therapy. *J. Cancer Res. Ther.* **2014**, *2*, 22–33.
(56) Malecki, M.; Dahlke, J.; Haig, M.; Wohlwend, L.; Malecki, R. Eradication of Human Ovarian Cancer Cells by Transgenic Expression of Recombinant DNASE1, DNASE1L3, DNASE2, and DFFB Controlled by EGFR Promoter: Novel Strategy for Targeted Therapy of Cancer. *J. Genet. Syndr. Gene Ther.* **2013**, *4*, 152.

(57) Zarogoulidis, P.; Darwiche, K.; Sakkas, A.; Yarmus, L.; Huang, H.; Li, Q.; Freitag, L.; Zarogoulidis, K.; Malecki, M. Suicide Gene Therapy for Cancer - Current Strategies. *J. Genet. Syndr. Gene Ther.* **2013**, *4*.
(58) Gaspar, H. B.; Parsley, K. L.; Howe, S.; King, D.; Gilmour, K. C.; Sinclair, J.; Brouns, G.; Schmidt, M.; Von Kalle, C.; Barington, T.; *et al.* Gene Therapy of X-Linked Severe Combined Immunodeficiency by Use of a Pseudotyped Gammaretroviral Vector. *Lancet* **2004**, *364*, 2181–2187.
(59) Aiuti, A.; Cattaneo, F.; Galimberti, S.; Benninghoff, U.; Cassani, B.; Callegaro, L.; Scaramuzza, S.; Andolfi, G.; Mirolo, M.; Brigida, I.; *et al.* Gene Therapy for Immunodeficiency due to Adenosine Deaminase Deficiency. *N. Engl. J. Med.* **2009**, *360*, 447–458.
(60) Griesenbach, U.; Alton, E. W. F. W.; UK Cystic Fibrosis Gene Therapy Consortium. Gene Transfer to the Lung: Lessons Learned from More than 2 Decades of CF Gene Therapy. *Adv. Drug Deliv. Rev.* **2009**, *61*, 128–139.
(61) Stewart, D. J.; Hilton, J. D.; Arnold, J. M. O.; Gregoire, J.; Rivard, A.; Archer, S. L.; Charbonneau, F.; Cohen, E.; Curtis, M.; Buller, C. E.; *et al.* Angiogenic Gene Therapy in Patients with Nonrevascularizable Ischemic Heart Disease: A Phase 2 Randomized, Controlled Trial of AdVEGF(121) (AdVEGF121) versus Maximum Medical Treatment. *Gene Ther.* **2006**, *13*, 1503–1511.
(62) Vincent, K. A.; Jiang, C.; Boltje, I.; Kelly, R. A. Gene Therapy Progress and Prospects: Therapeutic Angiogenesis for Ischemic Cardiovascular Disease. *Gene Ther.* **2007**, *14*, 781–789.
(63) Mariana Kiomy Osako; Hironori Nakagami; Ryuichi Morishita. Human Gene Therapy in Cardiovascular Diseases. In *Gene Therapy: Technologies & Applications*; Future Medicine Ltd, 2013; pp. 84–93.
(64) Demanèche, S.; Jocteur-Monrozier, L.; Quiquampoix, H.; Simonet, P. Evaluation of Biological and Physical Protection against Nuclease Degradation of Clay-Bound Plasmid DNA. *Appl. Environ. Microbiol.* **2001**, *67*, 293–299.
(65) Wolff, J. A.; Lederberg, J. An Early History of Gene Transfer and Therapy. *Hum. Gene Ther.* **1994**, *5*, 469–480.
(66) Bauer, G.; Anderson, J. S. *Gene Therapy for HIV*; SpringerBriefs in Biochemistry and Molecular Biology; Springer New York: New York, NY, 2014.
(67) Rodriguez, A.; del, A.; Angeles, M. Non-Viral Delivery Systems in Gene Therapy. In *Gene Therapy - Tools and Potential Applications*; Martin, F., Ed.; InTech, 2013.
(68) Jain, K. K. *The Handbook of Nanomedicine*; Springer, 2012.
(69) Xiang, S.; Zhang, X. Cellular Uptake Mechanism of Non-Viral Gene Delivery and Means for Improving Transfection Efficiency. In *Gene Therapy - Tools and Potential Applications*; Martin, F., Ed.; InTech, 2013.
(70) Graham, F. L.; van der Eb, A. J. A New Technique for the Assay of Infectivity of Human Adenovirus 5 DNA. *Virology* **1973**, *52*, 456–467.
(71) Neumann, E.; Schaefer-Ridder, M.; Wang, Y.; Hofschneider, P. H. Gene Transfer into Mouse Lyoma Cells by Electroporation in High Electric Fields. *EMBO J.* **1982**, *1*, 841–845.
(72) Zhang, G.; Gao, X.; Song, Y. K.; Vollmer, R.; Stolz, D. B.; Gasiorowski, J. Z.; Dean, D. A.; Liu, D. Hydroporation as the Mechanism of Hydrodynamic Delivery. *Gene Ther.* **2004**, *11*, 675–682.
(73) Kamimura, K.; Suda, T.; Zhang, G.; Liu, D. Advances in Gene Delivery Systems. *Pharm. Med.* **2011**, *25*, 293–306.
(74) Guo, X.; Huang, L. Recent Advances in Nonviral Vectors for Gene Delivery.

Acc. Chem. Res. **2012**, *45*, 971–979.
(75) Sanford, J. C. The Biolistic Process. *Trends Biotechnol.* **1988**, *6*, 299–302.
(76) Yager, E. J.; Dean, H. J.; Fuller, D. H. Prospects for Developing an Effective Particle-Mediated DNA Vaccine against Influenza. *Expert Rev. Vaccines* **2009**, *8*, 1205–1220.
(77) Kaur, T.; Slavcev, R. A.; Wettig, S. D. Addressing the Challenge: Current and Future Directions in Ovarian Cancer Therapy. *Curr. Gene Ther.* **2009**, *9*, 434–458.
(78) Prausnitz, M. R.; Mikszta, J. A.; Cormier, M.; Andrianov, A. K. Microneedle-Based Vaccines. *Curr. Top. Microbiol. Immunol.* **2009**, *333*, 369–393.
(79) Han, S.-W.; Nakamura, C.; Miyake, J.; Chang, S.-M.; Adachi, T. Single-Cell Manipulation and DNA Delivery Technology Using Atomic Force Microscopy and Nanoneedle. *J. Nanosci. Nanotechnol.* **2014**, *14*, 57–70.
(80) Han, S. W.; Nakamura, C.; Obataya, I.; Nakamura, N.; Miyake, J. A Molecular Delivery System by Using AFM and Nanoneedle. *Biosens. Bioelectron.* **2005**, *20*, 2120–2125.
(81) Han, S.-W.; Nakamura, C.; Kotobuki, N.; Obataya, I.; Ohgushi, H.; Nagamune, T.; Miyake, J. High-Efficiency DNA Injection into a Single Human Mesenchymal Stem Cell Using a Nanoneedle and Atomic Force Microscopy. *Nanomedicine Nanotechnol. Biol. Med.* **2008**, *4*, 215–225.
(82) Kate Rhodes, I. C. Cellular Laserfection. *Methods Cell Biol.* **2007**, *82*, 309–333.
(83) Clark, I. B.; Hanania, E. G.; Stevens, J.; Gallina, M.; Fieck, A.; Brandes, R.; Palsson, B. O.; Koller, M. R. Optoinjection for Efficient Targeted Delivery of a Broad Range of Compounds and Macromolecules into Diverse Cell Types. *J. Biomed. Opt.* **2006**, *11*, 014034.
(84) Jonathan L Compton, A. N. H. Hydrodynamic Determinants of Cell Necrosis and Molecular Delivery Produced by Pulsed Laser Microbeam Irradiation of Adherent Cells. *Biophys. J.* **2013**, *105*, 2221–2231.
(85) Junquera, E.; Aicart, E. Cationic Lipids as Transfecting Agents of DNA in Gene Therapy. *Curr. Top. Med. Chem.* **2014**, *14*, 649–663.
(86) Tschiche, A.; Malhotra, S.; Haag, R. Nonviral Gene Delivery with Dendritic Self-Assembling Architectures. *Nanomedicine,* **2014**, *9*, 667–693.
(87) Wu, J.; Huang, W.; He, Z. Dendrimers as Carriers for siRNA Delivery and Gene Silencing: A Review. *ScientificWorldJournal* **2013**, *2013*, 630654.
(88) Parker, B. A.; Stark, G. R. Regulation of Simian Virus 40 Transcription: Sensitive Analysis of the RNA Species Present Early in Infections by Virus or Viral DNA. *J. Virol.* **1979**, *31*, 360–369.
(89) Luthman, H.; Magnusson, G. High Efficiency Polyoma DNA Transfection of Chloroquine Treated Cells. *Nucleic Acids Res.* **1983**, *11*, 1295–1308.
(90) Xu, Z. P.; Zeng, Q. H.; Lu, G. Q.; Yu, A. B. Inorganic Nanoparticles as Carriers for Efficient Cellular Delivery. *Chem. Eng. Sci.* **2006**, *61*, 1027–1040.
(91) Ozkan, M. Quantum Dots and Other Nanoparticles: What Can They Offer to Drug Discovery? *Drug Discov. Today* **2004**, *9*, 1065–1071.
(92) Barbé, C.; Bartlett, J.; Kong, L.; Finnie, K.; Lin, H. Q.; Larkin, M.; Calleja, S.; Bush, A.; Calleja, G. Silica Particles: A Novel Drug-Delivery System. *Adv. Mater.* **2004**, *16*, 1959–1966.
(93) Bauer, L. A.; Birenbaum, N. S.; Meyer, G. J. Biological Applications of High Aspect Ratio Nanoparticles. *J. Mater. Chem.* **2004**, *14*, 517–526.
(94) Kolosnjaj, J.; Szwarc, H.; Moussa, F. Toxicity Studies of Carbon Nanotubes. *Adv. Exp. Med. Biol.* **2007**, *620*, 181–204.
(95) Lam, C.; James, J. T.; McCluskey, R.; Arepalli, S.; Hunter, R. L. A Review of

Carbon Nanotube Toxicity and Assessment of Potential Occupational and Environmental Health Risks. *Crit. Rev. Toxicol.* **2006**, *36*, 189–217.
(96) Corredor, C.; Hou, W.-C.; Klein, S. A.; Moghadam, B. Y.; Goryll, M.; Doudrick, K.; Westerhoff, P.; Posner, J. D. Disruption of Model Cell Membranes by Carbon Nanotubes. *Carbon* **2013**, *60*, 67–75.
(97) Poland, C. A.; Duffin, R.; Kinloch, I.; Maynard, A.; Wallace, W. A. H.; Seaton, A.; Stone, V.; Brown, S.; MacNee, W.; Donaldson, K. Carbon Nanotubes Introduced into the Abdominal Cavity of Mice Show Asbestos-like Pathogenicity in a Pilot Study. *Nat. Nanotechnol.* **2008**, *3*, 423–428.
(98) Balasubramanian, K.; Burghard, M. Chemically Functionalized Carbon Nanotubes. *Small* **2005**, *1*, 180–192.
(99) Pantarotte, D.; Partidos, C.; Graff, R.; Hoebeke, J.; Briand, J.; Prato, M.; Bianco, A. Synthesis, Structural Characterization, and Immunological Properties of Carbon Nanotubes Functionalized with Peptides. *J. Am. Chem. Soc.* **2003**, *125*, 6160–6164.
(100) Pantarotto, D.; Briand, J.-P.; Prato, M.; Bianco, A. Translocation of Bioactive Peptides across Cell Membranes by Carbon Nanotubes. *Chem. Commun.* **2004**, 16–17.
(101) Pérez-Martínez, F. C.; Carrión, B.; Ceña, V. The Use of Nanoparticles for Gene Therapy in the Nervous System. *J. Alzheimers Dis. JAD* **2012**, *31*, 697–710.
(102) Slowing, I. I.; Vivero-Escoto, J. L.; Wu, C.-W.; Lin, V. S.-Y. Mesoporous Silica Nanoparticles as Controlled Release Drug Delivery and Gene Transfection Carriers. *Adv. Drug Deliv. Rev.* **2008**, *60*, 1278–1288.
(103) Yamashita, S.; Fukushima, H.; Akiyama, Y.; Niidome, Y.; Mori, T.; Katayama, Y.; Niidome, T. Controlled-Release System of Single-Stranded DNA Triggered by the Photothermal Effect of Gold Nanorods and Its in Vivo Application. *Bioorg. Med. Chem.* **2011**, *19*, 2130–2135.
(104) Scherer, F.; Anton, M.; Schillinger, U.; Henke, J.; Bergemann, C.; Krüger, A.; Gänsbacher, B.; Plank, C. Magnetofection: Enhancing and Targeting Gene Delivery by Magnetic Force in Vitro and in Vivo. *Gene Ther.* **2002**, *9*, 102–109.
(105) Plank, C.; Schillinger, U.; Scherer, F.; Bergemann, C.; Rémy, J.-S.; Krötz, F.; Anton, M.; Lausier, J.; Rosenecker, J. The Magnetofection Method: Using Magnetic Force to Enhance Gene Delivery. *Biol. Chem.* **2003**, *384*, 737–747.
(106) Dawson, J. I.; Oreffo, R. O. C. Clay: New Opportunities for Tissue Regeneration and Biomaterial Design. *Adv. Mater.* **2013**, *25*, 4069–4086.
(107) Kawase, M.; Hayashi, Y.; Kinoshita, F.; Yamato, E.; Miyazaki, J.-I.; Yamakawa, J.; Ishida, T.; Tamura, M.; Yagi, K. Protective Effect of Montmorillonite on Plasmid DNA in Oral Gene Delivery into Small Intestine. *Biol. Pharm. Bull.* **2004**, *27*, 2049–2051.
(108) Wang, X.; Pei, X.; Du, Y.; Li, Y. Quaternized Chitosan/rectorite Intercalative Materials for a Gene Delivery System. *Nanotechnology* **2008**, *19*, 375102.
(109) Lavitrano, M.; Busnelli, M.; Cerrito, M. G.; Giovannoni, R.; Manzini, S.; Vargiolu, A. Sperm-Mediated Gene Transfer. *Reprod. Fertil. Dev.* **2006**, *18*, 19–23.
(110) Campos, V. F.; de Leon, P. M. M.; Komninou, E. R.; Dellagostin, O. A.; Deschamps, J. C.; Seixas, F. K.; Collares, T. NanoSMGT: Transgene Transmission into Bovine Embryos Using Halloysite Clay Nanotubes or Nanopolymer to Improve Transfection Efficiency. *Theriogenology* **2011**, *76*, 1552–1560.
(111) Oh, J.-M.; Choi, S.-J.; Lee, G.-E.; Kim, J.-E.; Choy, J.-H. Inorganic Metal Hydroxide Nanoparticles for Targeted Cellular Uptake through Clathrin-Mediated Endocytosis. *Chem. Asian J.* **2009**, *4*, 67–73.
(112) Desigaux, L.; Belkacem, M. B.; Richard, P.; Cellier, J.; Léone, P.; Cario, L.; Leroux, F.; Taviot-Guého, C.; Pitard, B. Self-Assembly and Characterization of

Layered Double hydroxide/DNA Hybrids. *Nano Lett.* **2006**, *6*, 199–204.
(113) Choy, J.-H.; Jung, J.-S.; Oh, J.-M.; Park, M.; Jeong, J.; Kang, Y.-K.; Han, O.-J. Layered Double Hydroxide as an Efficient Drug Reservoir for Folate Derivatives. *Biomaterials* **2004**, *25*, 3059–3064.
(114) Choy, J.-H.; Kwak, S.-Y.; Park, J.-S.; Jeong, Y.-J.; Portier, J. Intercalative Nanohybrids of Nucleoside Monophosphates and DNA in Layered Metal Hydroxide. *J. Am. Chem. Soc.* **1999**, *121*, 1399–1400.
(115) Kriven, W. M.; Kwak, S.-Y.; Wallig, M. A.; Choy, J.-H. Bio-Resorbable Nanoceramics for Gene and Drug Delivery. *MRS Bull.* **2004**, *29*, 33–37.
(116) Tyner, K. M.; Roberson, M. S.; Berghorn, K. A.; Li, L.; Gilmour, R. F., Jr; Batt, C. A.; Giannelis, E. P. Intercalation, Delivery, and Expression of the Gene Encoding Green Fluorescence Protein Utilizing Nanobiohybrids. *J. Control. Release Off. J. Control. Release Soc.* **2004**, *100*, 399–409.
(117) Choi, G.; Kwon, O.-J.; Oh, Y.; Yun, C.-O.; Choy, J.-H. Inorganic Nanovehicle Targets Tumor in an Orthotopic Breast Cancer Model. *Sci. Rep.* **2014**, *4*.
(118) Choy, J.-H.; Kwak, S.-Y.; Park, J.-S.; Jeong, Y.-J. Cellular Uptake Behavior of [γ-32P] Labeled ATP–LDH Nanohybrids. *J. Mater. Chem.* **2001**, *11*, 1671–1674.
(119) Zhang, K.; Xu, Z. P.; Lu, J.; Tang, Z. Y.; Zhao, H. J.; Good, D. A.; Wei, M. Q. Potential for Layered Double Hydroxides-Based, Innovative Drug Delivery Systems. *Int. J. Mol. Sci.* **2014**, *15*, 7409–7428.
(120) Li, A.; Qin, L.; Wang, W.; Zhu, R.; Yu, Y.; Liu, H.; Wang, S. The Use of Layered Double Hydroxides as DNA Vaccine Delivery Vector for Enhancement of Anti-Melanoma Immune Response. *Biomaterials* **2011**, *32*, 469–477.
(121) Cho, Y. W.; Kim, J.-D.; Park, K. Polycation Gene Delivery Systems: Escape from Endosomes to Cytosol. *J. Pharm. Pharmacol.* **2003**, *55*, 721–734.
(122) Hacein-Bey-Abina, S.; Garrigue, A.; Wang, G. P.; Soulier, J.; Lim, A.; Morillon, E.; Clappier, E.; Caccavelli, L.; Delabesse, E.; Beldjord, K.; *et al.* Insertional Oncogenesis in 4 Patients after Retrovirus-Mediated Gene Therapy of SCID-X1. *J. Clin. Invest.* **2008**, *118*, 3132–3142.
(123) Baum, C.; Düllmann, J.; Li, Z.; Fehse, B.; Meyer, J.; Williams, D. A.; von Kalle, C. Side Effects of Retroviral Gene Transfer into Hematopoietic Stem Cells. *Blood* **2003**, *101*, 2099–2114.
(124) Hacein-Bey-Abina, S.; von Kalle, C.; Schmidt, M.; Le Deist, F.; Wulffraat, N.; McIntyre, E.; Radford, I.; Villeval, J.-L.; Fraser, C. C.; Cavazzana-Calvo, M.; *et al.* A Serious Adverse Event after Successful Gene Therapy for X-Linked Severe Combined Immunodeficiency. *N. Engl. J. Med.* **2003**, *348*, 255–256.
(125) Raper, S. E.; Chirmule, N.; Lee, F. S.; Wivel, N. A.; Bagg, A.; Gao, G.; Wilson, J. M.; Batshaw, M. L. Fatal Systemic Inflammatory Response Syndrome in a Ornithine Transcarbamylase Deficient Patient Following Adenoviral Gene Transfer. *Mol. Genet. Metab.* **2003**, *80*, 148–158.
(126) Pérez-Martínez, F. C.; Guerra, J.; Posadas, I.; Ceña, V. Barriers to Non-Viral Vector-Mediated Gene Delivery in the Nervous System. *Pharm. Res.* **2011**, *28*, 1843–1858.
(127) Giacca, M. *Gene Therapy*; Springer, 2010.
(128) Alhaddad, A.; Durieu, C.; Dantelle, G.; Le Cam, E.; Malvy, C.; Treussart, F.; Bertrand, J.-R. Influence of the Internalization Pathway on the Efficacy of siRNA Delivery by Cationic Fluorescent Nanodiamonds in the Ewing Sarcoma Cell Model. *PLoS ONE* **2012**, *7*, e52207.
(129) Akinc, A.; Zumbuehl, A.; Goldberg, M.; Leshchiner, E. S.; Busini, V.; Hossain, N.; Bacallado, S. A.; Nguyen, D. N.; Fuller, J.; Alvarez, R.; *et al.* A Combinatorial

Library of Lipid-like Materials for Delivery of RNAi Therapeutics. *Nat. Biotechnol.* **2008**, *26*, 561–569.
(130) Von Gersdorff, K.; Sanders, N. N.; Vandenbroucke, R.; De Smedt, S. C.; Wagner, E.; Ogris, M. The Internalization Route Resulting in Successful Gene Expression Depends on Both Cell Line and Polyethylenimine Polyplex Type. *Mol. Ther.* **2006**, *14*, 745–753.
(131) Rejman, J.; Bragonzi, A.; Conese, M. Role of Clathrin- and Caveolae-Mediated Endocytosis in Gene Transfer Mediated by Lipo- and Polyplexes. *Mol. Ther.* **2005**, *12*, 468–474.
(132) Hufnagel, H.; Hakim, P.; Lima, A.; Hollfelder, F. Fluid Phase Endocytosis Contributes to Transfection of DNA by PEI-25. *Mol. Ther. J. Am. Soc. Gene Ther.* **2009**, *17*, 1411–1417.
(133) Hillaireau, H.; Couvreur, P. Nanocarriers' Entry into the Cell: Relevance to Drug Delivery. *Cell. Mol. Life Sci. CMLS* **2009**, *66*, 2873–2896.
(134) Whitehead, K. A.; Langer, R.; Anderson, D. G. Knocking down Barriers: Advances in siRNA Delivery. *Nat. Rev. Drug Discov.* **2009**, *8*, 129–138.
(135) Parton, R. G.; Simons, K. The Multiple Faces of Caveolae. *Nat. Rev. Mol. Cell Biol.* **2007**, *8*, 185–194.
(136) Pack, D. W.; Hoffman, A. S.; Pun, S.; Stayton, P. S. Design and Development of Polymers for Gene Delivery. *Nat. Rev. Drug Discov.* **2005**, *4*, 581–593.
(137) Khalil, I. A.; Kogure, K.; Akita, H.; Harashima, H. Uptake Pathways and Subsequent Intracellular Trafficking in Nonviral Gene Delivery. *Pharmacol. Rev.* **2006**, *58*, 32–45.
(138) El Ouahabi, A.; Thiry, M.; Pector, V.; Fuks, R.; Ruysschaert, J. M.; Vandenbranden, M. The Role of Endosome Destabilizing Activity in the Gene Transfer Process Mediated by Cationic Lipids. *FEBS Lett.* **1997**, *414*, 187–192.
(139) Medina-Kauwe, L. K.; Xie, J.; Hamm-Alvarez, S. Intracellular Trafficking of Nonviral Vectors. *Gene Ther.* **2005**, *12*, 1734–1751.
(140) Aderem, A.; Underhill, D. M. Mechanisms of Phagocytosis in Macrophages. *Annu. Rev. Immunol.* **1999**, *17*, 593–623.
(141) Kopatz, I.; Remy, J.-S.; Behr, J.-P. A Model for Non-Viral Gene Delivery: Through Syndecan Adhesion Molecules and Powered by Actin. *J. Gene Med.* **2004**, *6*, 769–776.
(142) Rabinovitch, M. Professional and Non-Professional Phagocytes: An Introduction. *Trends Cell Biol.* **1995**, *5*, 85–87.
(143) Rappoport, J. Z. Focusing on Clathrin-Mediated Endocytosis. *Biochem. J.* **2008**, *412*, 415.
(144) K Takei, V. H. Clathrin-Mediated Endocytosis: Membrane Factors Pull the Trigger. *Trends Cell Biol.* **2001**, *11*, 385–391.
(145) Mukherjee, S.; Ghosh, R. N.; Maxfield, F. R. Endocytosis. *Physiol. Rev.* **1997**, *77*, 759–803.
(146) Bareford, L. M.; Swaan, P. W. Endocytic Mechanisms for Targeted Drug Delivery. *Adv. Drug Deliv. Rev.* **2007**, *59*, 748–758.
(147) Conner, S. D.; Schmid, S. L. Regulated Portals of Entry into the Cell. *Nature* **2003**, *422*, 37–44.
(148) Mayor, S.; Pagano, R. E. Pathways of Clathrin-Independent Endocytosis. *Nat. Rev. Mol. Cell Biol.* **2007**, *8*, 603–612.
(149) Conner, S. D.; Schmid, S. L. Regulated Portals of Entry into the Cell. *Nature* **2003**, *422*, 37–44.
(150) Swanson, J. A.; Watts, C. Macropinocytosis. *Trends Cell Biol.* **1995**, *5*, 424–

428.
(151) Sarkar, K.; Kruhlak, M. J.; Erlandsen, S. L.; Shaw, S. Selective Inhibition by Rottlerin of Macropinocytosis in Monocyte-Derived Dendritic Cells. *Immunology* **2005**, *116*, 513–524.
(152) Hewlett, L. J.; Prescott, A. R.; Watts, C. The Coated Pit and Macropinocytic Pathways Serve Distinct Endosome Populations. *J. Cell Biol.* **1994**, *124*, 689–703.
(153) Dröse, S.; Altendorf, K. Bafilomycins and Concanamycins as Inhibitors of V-ATPases and P-ATPases. *J. Exp. Biol.* **1997**, *200*, 1–8.
(154) Maxfield, F. R. Weak Bases and Ionophores Rapidly and Reversibly Raise the pH of Endocytic Vesicles in Cultured Mouse Fibroblasts. *J. Cell Biol.* **1982**, *95*, 676–681.
(155) Mellman, I.; Fuchs, R.; Helenius, A. Acidification of the Endocytic and Exocytic Pathways. *Annu. Rev. Biochem.* **1986**, *55*, 663–700.
(156) Cotten, M.; Längle-Rouault, F.; Kirlappos, H.; Wagner, E.; Mechtler, K.; Zenke, M.; Beug, H.; Birnstiel, M. L. Transferrin-Polycation-Mediated Introduction of DNA into Human Leukemic Cells: Stimulation by Agents That Affect the Survival of Transfected DNA or Modulate Transferrin Receptor Levels. *Proc. Natl. Acad. Sci.* **1990**, *87*, 4033–4037.
(157) Erbacher, P.; Roche, A. C.; Monsigny, M.; Midoux, P. Putative Role of Chloroquine in Gene Transfer into a Human Hepatoma Cell Line by DNA/Lactosylated Polylysine Complexes. *Exp. Cell Res.* **1996**, *225*, 186–194.
(158) Hong, S.; Bielinska, A. U.; Mecke, A.; Keszler, B.; Beals, J. L.; Shi, X.; Balogh, L.; Orr, B. G.; Baker, J. R., Jr; Banaszak Holl, M. M. Interaction of Poly(amidoamine) Dendrimers with Supported Lipid Bilayers and Cells: Hole Formation and the Relation to Transport. *Bioconjug. Chem.* **2004**, *15*, 774–782.
(159) Lee, H.; Kim, I.-K.; Park, T. G. Intracellular Trafficking and Unpacking of siRNA/quantum Dot-PEI Complexes Modified with and without Cell Penetrating Peptide: Confocal and Flow Cytometric FRET Analysis. *Bioconjug. Chem.* **2010**, *21*, 289–295.
(160) Gupta, B.; Levchenko, T. S.; Torchilin, V. P. Intracellular Delivery of Large Molecules and Small Particles by Cell-Penetrating Proteins and Peptides. *Adv. Drug Deliv. Rev.* **2005**, *57*, 637–651.
(161) Lacerda, L.; Russier, J.; Pastorin, G.; Herrero, M. A.; Venturelli, E.; Dumortier, H.; Al-Jamal, K. T.; Prato, M.; Kostarelos, K.; Bianco, A. Translocation Mechanisms of Chemically Functionalised Carbon Nanotubes across Plasma Membranes. *Biomaterials* **2012**, *33*, 3334–3343.
(162) Kostarelos, K.; Lacerda, L.; Pastorin, G.; Wu, W.; Wieckowski, S.; Luangsivilay, J.; Godefroy, S.; Pantarotto, D.; Briand, J.-P.; Muller, S.; *et al.* Cellular Uptake of Functionalized Carbon Nanotubes Is Independent of Functional Group and Cell Type. *Nat. Nanotechnol.* **2007**, *2*, 108–113.
(163) Kam, N. W. S.; Liu, Z.; Dai, H. Carbon Nanotubes as Intracellular Transporters for Proteins and DNA: An Investigation of the Uptake Mechanism and Pathway. *Angew. Chem. Int. Ed Engl.* **2006**, *45*, 577–581.
(164) Pantarotto, D.; Singh, R.; McCarthy, D.; Erhardt, M.; Briand, J.-P.; Prato, M.; Kostarelos, K.; Bianco, A. Functionalized Carbon Nanotubes for Plasmid DNA Gene Delivery. *Angew. Chem. Int. Ed Engl.* **2004**, *43*, 5242–5246.
(165) Lopez, C. F.; Nielsen, S. O.; Moore, P. B.; Klein, M. L. Understanding Nature's Design for a Nanosyringe. *Proc. Natl. Acad. Sci. U. S. A.* **2004**, *101*, 4431–4434.
(166) Kang, B.; Chang, S.; Dai, Y.; Yu, D.; Chen, D. Cell Response to Carbon Nanotubes: Size-Dependent Intracellular Uptake Mechanism and Subcellular Fate.

Small **2010**, *6*, 2362–2366.
(167) Donkor, D. A.; Tang, X. S. Tube Length and Cell Type-Dependent Cellular Responses to Ultra-Short Single-Walled Carbon Nanotube. *Biomaterials* **2014**, *35*, 3121–3131.
(168) Zuhorn, I. S.; Kalicharan, R.; Hoekstra, D. Lipoplex-Mediated Transfection of Mammalian Cells Occurs through the Cholesterol-Dependent Clathrin-Mediated Pathway of Endocytosis. *J. Biol. Chem.* **2002**, *277*, 18021–18028.
(169) Chithrani, B. D.; Ghazani, A. A.; Chan, W. C. W. Determining the Size and Shape Dependence of Gold Nanoparticle Uptake into Mammalian Cells. *Nano Lett.* **2006**, *6*, 662–668.
(170) Muro, S.; Garnacho, C.; Champion, J. A.; Leferovich, J.; Gajewski, C.; Schuchman, E. H.; Mitragotri, S.; Muzykantov, V. R. Control of Endothelial Targeting and Intracellular Delivery of Therapeutic Enzymes by Modulating the Size and Shape of ICAM-1-Targeted Carriers. *Mol. Ther. J. Am. Soc. Gene Ther.* **2008**, *16*, 1450–1458.
(171) Gratton, S. E. A.; Ropp, P. A.; Pohlhaus, P. D.; Luft, J. C.; Madden, V. J.; Napier, M. E.; DeSimone, J. M. The Effect of Particle Design on Cellular Internalization Pathways. *Proc. Natl. Acad. Sci.* **2008**, *105*, 11613–11618.
(172) Gratton, S. E. A.; Napier, M. E.; Ropp, P. A.; Tian, S.; DeSimone, J. M. Microfabricated Particles for Engineered Drug Therapies: Elucidation into the Mechanisms of Cellular Internalization of PRINT Particles. *Pharm. Res.* **2008**, *25*, 2845–2852.
(173) Bergaya, F.; Theng, B. K. G.; Lagaly, G. (Eds.) *Handbook of Clay Science, Volume 1*; 1 edition.; Elsevier Science: Amsterdam; London, 2006.
(174) Sposito, G.; Skipper, N. T.; Sutton, R.; Park, S.; Soper, A. K.; Greathouse, J. A. Surface Geochemistry of the Clay Minerals. *Proc. Natl. Acad. Sci.* **1999**, *96*, 3358–3364.
(175) Lagaly, G. Chapter 5 Colloid Clay Science. In *Developments in Clay Science*; Faïza Bergaya, B. K. G. T. and G. L., Ed.; Handbook of Clay Science; Elsevier, 2006; Vol. Volume 1, pp. 141–245.
(176) Theng, B. K. G. Chapter 1 - The Clay Minerals. In *Developments in Clay Science*; B.K.G. Theng, Ed.; Formation and Properties of Clay-Polymer Complexes; Elsevier, 2012; Vol. Volume 4, pp. 3–45.
(177) Lvov, Y.; Abdullayev, E. Functional Polymer–Clay Nanotube Composites with Sustained Release of Chemical Agents. *Prog. Polym. Sci.* **2013**, *38*, 1690–1719.
(178) Brindley, G. W. Structural Mineralogy of Clays. *Clays Clay Miner.* **1952**, *1*, 33–43.
(179) Liu, M.; Jia, Z.; Jia, D.; Zhou, C. Recent Advance in Research on Halloysite Nanotubes-Polymer Nanocomposite. *Prog. Polym. Sci.* **2014**.
(180) E. Ruiz-Hitzky, P. Aranda, M. Serratosa, "Organic/Polymeric Interactions with Clays" Chapter 3 of Handbook of Layered Materials, S.M. Auerbach, K.A. Carrado & P.K. Dutta, Eds., Marcel Dekker, New York, **2004**; pp. 91-154.
(181) Governa, M.; Valentino, M.; Vison, I.; Monaco, F.; Amati, M.; Scancarello, G.; Scansetti, G. In Vitro Biological Effects of Clay Minerals Advised as Substitutes for Asbestos. *Cell Biol. Toxicol.* **1995**, *11*, 237–249.
(182) McConnochie, K.; Bevan, C.; Newcombe, R. G.; Lyons, J. P.; Skidmore, J. W.; Wagner, J. C. A Study of Spanish Sepiolite Workers. *Thorax* **1993**, *48*, 370–374.
(183) Baris, Y. I.; Sahin, A. A.; Erkan, M. L. Clinical and Radiological Study in Sepiolite Workers. *Arch. Environ. Health* **1980**, *35*, 343–346.
(184) López-Galindo, A.; Viseras, C.; Cerezo, P. Compositional, Technical and Safety Specifications of Clays to Be Used as Pharmaceutical and Cosmetic Products. *Appl.*

Clay Sci. **2007**, *36*, 51–63.
(185) Alcântara, A. C. S.; Darder, M.; Aranda, P.; Ruiz-Hitzky, E. Polysaccharide–fibrous Clay Bionanocomposites. *Appl. Clay Sci.* **2014**.
(186) Prévot, V.; Forano, C.; Besse, J. P. Hybrid Derivatives of Layered Double Hydroxides. *Appl. Clay Sci.* **2001**, *18*, 3–15.
(187) Arulraj, J. Intercalation of Organic Anions and Intracrystalline Reactions in Anionic Clays. *INFLIBNET* **2013**.
(188) Rives, V.; Angeles Ulibarri, M. Layered Double Hydroxides (LDH) Intercalated with Metal Coordination Compounds and Oxometalates. *Coord. Chem. Rev.* **1999**, *181*, 61–120.
(189) Leroux, F.; Besse, J.-P. Polymer Interleaved Layered Double Hydroxide: A New Emerging Class of Nanocomposites. *Chem. Mater.* **2001**, *13*, 3507–3515.
(190) Darder, M.; López-Blanco, M.; Aranda, P.; Leroux, F.; Ruiz-Hitzky, E. Bio-Nanocomposites Based on Layered Double Hydroxides. *Chem. Mater.* **2005**, *17*, 1969–1977.
(191) Nakayama, H.; Wada, N.; Tsuhako, M. Intercalation of Amino Acids and Peptides into Mg–Al Layered Double Hydroxide by Reconstruction Method. *Int. J. Pharm.* **2004**, *269*, 469–478.
(192) Braterman, P. S.; Xu, Z. P.; Yarberry, F. Layered Double Hydroxides (LDHs). **2004**, 373–474.
(193) Ladewig, K.; Xu, Z. P.; Lu, G. Q. (Max). Layered Double Hydroxide Nanoparticles in Gene and Drug Delivery. *Expert Opin. Drug Deliv.* **2009**, *6*, 907–922.
(194) Ruiz-Hitzky, E.; Aranda, P.; Darder, M.; Ogawa, M. Hybrid and Biohybrid Silicate Based Materials: Molecular vs. Block-Assembling Bottom-up Processes. *Chem. Soc. Rev.* **2011**, *40*, 801–828.
(195) Ruiz-Hitzky, E.; Darder, M.; Aranda, P.; Ariga, K. Advances in Biomimetic and Nanostructured Biohybrid Materials. *Adv. Mater.* **2010**, *22*, 323–336.
(196) Gómez-Romero, P.; Sanchez, C. Hybrid Materials, Functional Applications. An Introduction. In *Functional Hybrid Materials*; Gómez-Romero, P.; Sanchez, C., Eds.; Wiley-VCH Verlag GmbH & Co. KGaA, 2003; pp. 1–14.
(197) Gomez-Romero, P. Hybrid Organic–Inorganic Materials—In Search of Synergic Activity. *Adv. Mater.* **2001**, *13*, 163–174.
(198) Sanchez, C.; Julián, B.; Belleville, P.; Popall, M. Applications of Hybrid Organic–inorganic Nanocomposites. *J. Mater. Chem.* **2005**, *15*, 3559–3592.
(199) Sanchez, C.; Belleville, P.; Popall, M.; Nicole, L. Applications of Advanced Hybrid Organic-Inorganic Nanomaterials: From Laboratory to Market. *Chem. Soc. Rev.* **2011**, *40*, 696–753.
(200) Vallet-Regí, M.; Ruiz-Hernández, E. Bioceramics: From Bone Regeneration to Cancer Nanomedicine. *Adv. Mater.* **2011**, *23*, 5177–5218.
(201) T. J. Pinnavaia, G. W. Beall (Eds.) Polymer-Clay Nanocomposites, John Wiley & Sons, West Sussex, **2000**.
(202) Alexandre, M.; Dubois, P. Polymer-Layered Silicate Nanocomposites: Preparation, Properties and Uses of a New Class of Materials. *Mater. Sci. Eng. R Rep.* **2000**, *28*, 1–63.
(203) Giannelis, E. P. Polymer Layered Silicate Nanocomposites. *Adv. Mater.* **1996**, *8*, 29–35.
(204) Dujardin, E.; Mann, S. Bio-Inspired Materials Chemistry. *Adv. Mater.* **2002**, *14*, 775–788.
(205) Tang, Z.; Kotov, N. A.; Magonov, S.; Ozturk, B. Nanostructured Artificial Nacre. *Nat. Mater.* **2003**, *2*, 413–418.

(206) Belton, D. J.; Patwardhan, S. V.; Annenkov, V. V.; Danilovtseva, E. N.; Perry, C. C. From Biosilicification to Tailored Materials: Optimizing Hydrophobic Domains and Resistance to Protonation of Polyamines. *Proc. Natl. Acad. Sci.* **2008**, *105*, 5963–5968.
(207) Chen, R.; Wang, C.; Huang, Y.; Le, H. An Efficient Biomimetic Process for Fabrication of Artificial Nacre with Ordered-Nanostructure. *Mater. Sci. Eng. C* **2008**, *28*, 218–222.
(208) Ruiz-Hitzky, E.; Darder, M.; Aranda, P. An Introduction to Bio-Nanohybrid Materials. In *Bio-inorganic Hybrid Nanomaterials*; Ruiz-Hitzky, E.; Ariga, K.; Lvov, Y. M., Eds.; Wiley-VCH Verlag GmbH & Co. KGaA, 2007; pp. 1–40.
(209) Fratzl, P.; Weinkamer, R. Nature's Hierarchical Materials. *Prog. Mater. Sci.* **2007**, *52*, 1263–1334.
(210) Antonietti, M.; Fratzl, P. Biomimetic Principles in Polymer and Material Science. *Macromol. Chem. Phys.* **2010**, *211*, 166–170.
(211) Zhao, F.; Yin, Y.; Lu, W. W.; Leong, J. C.; Zhang, W.; Zhang, J.; Zhang, M.; Yao, K. Preparation and Histological Evaluation of Biomimetic Three-Dimensional Hydroxyapatite/Chitosan-Gelatin Network Composite Scaffolds. *Biomaterials* **2002**, *23*, 3227–3234.
(212) Dorozhkin, S. V. Calcium Orthophosphate-Based Biocomposites and Hybrid Biomaterials. *J. Mater. Sci.* **2009**, *44*, 2343–2387.
(213) Liu, X.; Smith, L. A.; Hu, J.; Ma, P. X. Biomimetic Nanofibrous Gelatin/apatite Composite Scaffolds for Bone Tissue Engineering. *Biomaterials* **2009**, *30*, 2252–2258.
(214) A, B.; P, T.; M, F.; B, B.; S, P.; L, S.; R, G. A Biomimetic Gelatin-Calcium Phosphate Bone Cement. *Int. J. Artif. Organs* **2004**, *27*, 664–673.
(215) Aranda, P.; Fernandes, F. M.; Wicklein, B.; Ruiz-Hitzky, E.; Hill, J. P.; Ariga, K. Bioinspired Materials Chemistry I: Organic–Inorganic Nanocomposites. In *Bioinspiration and Biomimicry in Chemistry*; Swiegers, G. F., Ed.; John Wiley & Sons, Inc., New York, **2012**; pp. 121–138.
(216) Livage, J.; Coradin, T.; Roux, C. Bioactive Sol-Gel Hybrids. In *Functional Hybrid Materials*; Gómez-Romero, P.; Sanchez, C., Eds.; Wiley-VCH Verlag GmbH & Co. KGaA, Weinheim, 2003; pp. 387–404.
(217) Avnir, D.; Coradin, T.; Lev, O.; Livage, J. Recent Bio-Applications of Sol–gel Materials. *J. Mater. Chem.* **2006**, *16*, 1013–1030.
(218) Sanchez, C.; Arribart, H.; Giraud Guille, M. M. Biomimetism and Bioinspiration as Tools for the Design of Innovative Materials and Systems. *Nat. Mater.* **2005**, *4*, 277–288.
(219) Zeng, Q. H.; Yu, A. B.; Lu, G. Q. (Max); Paul, D. R. Clay-Based Polymer Nanocomposites: Research and Commercial Development. *J. Nanosci. Nanotechnol.* **2005**, *5*, 1574–1592.
(220) Rhim, J.-W. Potential Use of Biopolymer-Based Nanocomposite Films in Food Packaging Applications. *Food Sci. Biotechnol.* **2007**, *16*, 691–709.
(221) Ruiz-Hitzky, E.; Darder, M.: Aranda, P. Progress in bionanocomposite materials. In *Annual Review of Nano Research Vol. 3,* Cao, G.Z., Zhang, Q.F., C.J. Brinker Eds. pp. 149-189; World Scientific Publishing Co., Singapore, **2010**.
(222) Sinharay, S.; Bousmina, M. Biodegradable Polymers and Their Layered Silicate Nanocomposites: In Greening the 21st Century Materials World. *Prog. Mater. Sci.* **2005**, *50*, 962–1079.
(223) Katti, K. S.; Katti, D. R.; Dash, R. Synthesis and Characterization of a Novel Chitosan/montmorillonite/hydroxyapatite Nanocomposite for Bone Tissue Engineering. *Biomed. Mater. Bristol Engl.* **2008**, *3*, 034122.

(224) Chung, J. H. Y.; Knetsch, M. L. W.; Koole, L. H.; Simmons, A.; Poole-Warren, L. A. Polyurethane Organosilicate Nanocomposites as Blood Compatible. *Coatings* **2012**, *2*, 45–63.
(225) Kokabi, M.; Sirousazar, M.; Hassan, Z. M. PVA–clay Nanocomposite Hydrogels for Wound Dressing. *Eur. Polym. J.* **2007**, *43*, 773–781.
(226) Darder, M.; Colilla, M.; Ruiz-Hitzky, E. Biopolymer−Clay Nanocomposites Based on Chitosan Intercalated in Montmorillonite. *Chem. Mater.* **2003**, *15*, 3774–3780.
(227) Wicklein, B.; Aranda, P.; Ruiz-Hitzky, E.; Darder, M. Hierarchically Structured Bioactive Foams Based on Polyvinyl Alcohol–sepiolite Nanocomposites. *J. Mater. Chem. B* **2013**, *1*, 2911–2920.
(228) Gallori, E.; Biondi, E.; Branciamore, S. Looking for the Primordial Genetic Honeycomb. *Orig. Life Evol. Biosphere J. Int. Soc. Study Orig. Life* **2006**, *36*, 493–499.
(229) Cleaves, H. J.; Crapster-Pregont, E.; Jonsson, C. M.; Jonsson, C. L.; Sverjensky, D. A.; Hazen, R. A. The Adsorption of Short Single-Stranded DNA Oligomers to Mineral Surfaces. *Chemosphere* **2011**, *83*, 1560–1567.
(230) Gesteland, R. F. *The RNA World, Third Edition*; 3 edition.; Cold Spring Harbor Laboratory Press: Cold Spring Harbor, New York, **2005**.
(231) Romanowski, G.; Lorenz, M. G.; Wackernagel, W. Adsorption of Plasmid DNA to Mineral Surfaces and Protection against DNase I. *Appl. Environ. Microbiol.* **1991**, *57*, 1057–1061.
(232) Lorenz, M. G.; Wackernagel, W. Adsorption of DNA to Sand and Variable Degradation Rates of Adsorbed DNA. *Appl. Environ. Microbiol.* **1987**, *53*, 2948–2952.
(233) Beall, G. W.; Sowersby, D. S.; Roberts, R. D.; Robson, M. H.; Lewis, L. K. Analysis of Oligonucleotide DNA Binding and Sedimentation Properties of Montmorillonite Clay Using Ultraviolet Light Spectroscopy. *Biomacromolecules* **2009**, *10*, 105–112.
(234) Saeki, K.; Kunito, T. Adsorptions of DNA Molecules by Soils and Variable-Charged Soil Constituents. *Curr. Res. Technol. Educ. Top. Appl. Microbiol. Microb. Biotechnol.* **2010**, *1*, 188–195.
(235) Cai, P.; Huang, Q.-Y.; Zhang, X.-W. Interactions of DNA with Clay Minerals and Soil Colloidal Particles and Protection against Degradation by DNase. *Environ. Sci. Technol.* **2006**, *40*, 2971–2976.
(236) Khanna, M.; Yoder, M.; Calamai, L.; Stotzky, G. X-Ray Diffractometry and Electron Microscopy of DNA from Bacillus Subtilis Bound on Clay Minerals. *Sci. Soils* **1998**, *3*, 1–10.
(237) Fiorito, T. M.; Icoz, I.; Stotzky, G. Adsorption and Binding of the Transgenic Plant Proteins, Human Serum Albumin, B-Glucuronidase, and Cry3Bb1, on Montmorillonite and Kaolinite: Microbial Utilization and Enzymatic Activity of Free and Clay-Bound Proteins. *Appl. Clay Sci.* **2008**, *39*, 142–150.
(238) Stotzky, G. Persistence and Biological Activity in Soil of the Insecticidal Proteins from Bacillus Thuringiensis, Especially from Transgenic Plants. *Plant Soil* **2005**, *266*, 77–89.
(239) Ivarson, K. C.; Schnitzer, M.; Cortez, J. The Biodegradability of Nucleic Acid Bases Adsorbed on Inorganic and Organic Soil Components. *Plant Soil* **1982**, *64*, 343–353.
(240) Paget, E.; Monrozier, L. J.; Simonet, P. Adsorption of DNA on Clay Minerals: Protection against DNaseI and Influence on Gene Transfer. *FEMS Microbiol. Lett.* **1992**, *97*, 31–39.
(241) Lorenz, M. G.; Wackernagel, W. Natural Genetic Transformation of Pseudomonas Stutzeri by Sand-Adsorbed DNA. *Arch. Microbiol.* **1990**, *154*, 380–385.

(242) Jeffrey, W. H.; Paul, J. H.; Stewart, G. J. Natural Transformation of a marineVibrio Species by Plasmid DNA. *Microb. Ecol.* **1990**, *19*, 259–268.
(243) Vandeventer, P. E.; Lin, J. S.; Zwang, T. J.; Nadim, A.; Johal, M. S.; Niemz, A. Multiphasic DNA Adsorption to Silica Surfaces under Varying Buffer, pH, and Ionic Strength Conditions. *J. Phys. Chem. B* **2012**, *116*, 5661–5670.
(244) Dauphin, L. A.; Moser, B. D.; Bowen, M. D. Evaluation of Five Commercial Nucleic Acid Extraction Kits for Their Ability to Inactivate Bacillus Anthracis Spores and Comparison of DNA Yields from Spores and Spiked Environmental Samples. *J. Microbiol. Methods* **2009**, *76*, 30–37.
(245) Rittich, B.; Spanová, A. SPE and Purification of DNA Using Magnetic Particles. *J. Sep. Sci.* **2013**, *36*, 2472–2485.
(246) Melzak, K. A.; Sherwood, C. S.; Turner, R. F. B.; Haynes, C. A. Driving Forces for DNA Adsorption to Silica in Perchlorate Solutions. *J. Colloid Interface Sci.* **1996**, *181*, 635–644.
(247) *Nucleic Acids and Proteins in Soil*; Nannipieri, P.; Smalla, K., Eds.; Soil Biology; Springer Berlin Heidelberg, 2006; Vol. 8.
(248) Cai, P.; Huang, Q.; Zhu, J.; Jiang, D.; Zhou, X.; Rong, X.; Liang, W. Effects of Low-Molecular-Weight Organic Ligands and Phosphate on DNA Adsorption by Soil Colloids and Minerals. *Colloids Surf. B Biointerfaces* **2007**, *54*, 53–59.
(249) Yamamoto, K.; Otsuka, H.; Takahara, A. Preparation of Novel Polymer Hybrids from Imogolite Nanofiber. *Polym. J.* **2006**, *39*, 1–15.
(250) Jiravanichanun, N.; Yamamoto, K.; Kato, K.; Kim, J.; Horiuchi, S.; Yah, W.-O.; Otsuka, H.; Takahara, A. Preparation and Characterization of imogolite/DNA Hybrid Hydrogels. *Biomacromolecules* **2012**, *13*, 276–281.
(251) Hou, Y.; Wu, P.; Zhu, N. The Protective Effect of Clay Minerals against Damage to Adsorbed DNA Induced by Cadmium and Mercury. *Chemosphere* **2014**, *95*, 206–212.
(252) Mignon, P.; Sodupe, M. Theoretical Study of the Adsorption of DNA Bases on the Acidic External Surface of Montmorillonite. *Phys. Chem. Chem. Phys.* **2011**, *14*, 945–954.
(253) Paget, E.; Lebrun, M.; Freyssinet, G.; Simonet, P. The Fate of Recombinant Plant DNA in Soil. *Eur. J. Soil Biol.* **1998**, *34*, 81–88.
(254) Gallori, E.; Bazzicalupo, M.; Dal Canto, L.; Fani, R.; Nannipieri, P.; Vettori, C.; Stotzky, G. Transformation of Bacillus Subtilis by DNA Bound on Clay in Non-Sterile Soil. *FEMS Microbiol. Ecol.* **1994**, *15*, 119–126.
(255) Ciaravella, A.; Scappini, F.; Franchi, M.; Cecchi-Pestellini, C.; Barbera, M.; Candia, R.; Gallori, E.; Micela, G. Role of Clays in Protecting Adsorbed DNA against X-Ray Radiation. *Int. J. Astrobiol.* **2004**, *3*, 31–35.
(256) Biondi, E.; Branciamore, S.; Maurel, M.-C.; Gallori, E. Montmorillonite Protection of an UV-Irradiated Hairpin Ribozyme: Evolution of the RNA World in a Mineral Environment. *BMC Evol. Biol.* **2007**, *7 Suppl 2*, S2.
(257) Scappini, F.; Casadei, F.; Zamboni, R.; Franchi, M.; Gallori, E.; Monti, S. Protective Effect of Clay Minerals on Adsorbed Nucleic Acid against UV Radiation: Possible Role in the Origin of Life. *Int. J. Astrobiol.* **2004**, *3*, 17–19.
(258) Hoyo, C. D.; Vicente, M. A.; Rives, V. Application of Phenyl Salicylate-Sepiolite Systems as Ultraviolet Radiation Filters. *Clay Miner.* **1998**, *33*, 467–474.
(259) Hoyo, C. del; Vicente, M. A.; Rives, V. Preparation of Drug-Montmorillonite UV-Radiation Protection Compounds by Gas-Solid Adsorption. *Clay Miner.* **2001**, *36*, 541–546.
(260) Branciamore, S.; Gallori, E.; Szathmáry, E.; Czárán, T. The Origin of Life:

Chemical Evolution of a Metabolic System in a Mineral Honeycomb? *J. Mol. Evol.* **2009**, *69*, 458–469.
(261) Franchi, M.; Gallori, E. A Surface-Mediated Origin of the RNA World: Biogenic Activities of Clay-Adsorbed RNA Molecules. *Gene* **2005**, *346*, 205–214.
(262) Erdem, A.; Kuralay, F.; Çubukçu, H. E.; Congur, G.; Karadeniz, H.; Canavar, E. Sensitive Sepiolite-Carbon Nanotubes Based Disposable Electrodes for Direct Detection of DNA and Anticancer Drug-DNA Interactions. *The Analyst* **2012**, *137*, 4001–4004.
(263) Yoshida, N. Discovery and Application of the Yoshida Effect: Nano-Sized Acicular Materials Enable Penetration of Bacterial Cells by Sliding Friction Force. *Recent Pat. Biotechnol.* **2007**, *1*, 194–201.
(264) Yoshida, N.; Sato, M. Plasmid Uptake by Bacteria: A Comparison of Methods and Efficiencies. *Appl. Microbiol. Biotechnol.* **2009**, *83*, 791–798.
(265) Wilharm, G.; Lepka, D.; Faber, F.; Hofmann, J.; Kerrinnes, T.; Skiebe, E. A Simple and Rapid Method of Bacterial Transformation. *J. Microbiol. Methods* **2010**, *80*, 215–216.
(266) Tan, H.; Fu, L.; Seno, M. Optimization of Bacterial Plasmid Transformation Using Nanomaterials Based on the Yoshida Effect. *Int. J. Mol. Sci.* **2010**, *11*, 4961–4972.
(267) Rodríguez-Beltrán, J.; Elabed, H.; Gaddour, K.; Blázquez, J.; Rodríguez-Rojas, A. Simple DNA Transformation in Pseudomonas Based on the Yoshida Effect. *J. Microbiol. Methods* **2012**, *89*, 95–98.
(268) Rodriguez-Beltran, J.; Rodriguez-Rojas, A.; Yubero, E.; Blazquez, J. The Animal Food Supplement Sepiolite Promotes a Direct Horizontal Transfer of Antibiotic Resistance Plasmids between Bacterial Species. *Antimicrob. Agents Chemother.* **2013**, *57*, 2651–2653.
(269) Yoshida, N.; Ikeda, T.; Yoshida, T.; Sengoku, T.; Ogawa, K. Chrysotile Asbestos Fibers Mediate Transformation of Escherichia Coli by Exogenous Plasmid DNA. *FEMS Microbiol. Lett.* **2001**, *195*, 133–137.
(270) Yoshida, N.; Kodama, K.; Nakata, K.; Yamashita, M.; Miwa, T. Escherichia Coli Cells Penetrated by Chrysotile Fibers Are Transformed to Antibiotic Resistance by Incorporation of Exogenous Plasmid DNA. *Appl. Microbiol. Biotechnol.* **2002**, *60*, 461–468.
(271) Yoshida, N.; Nakajima-Kambe, T.; Matsuki, K.; Shigeno, T. Novel Plasmid Transformation Method Mediated by Chrysotile, Sliding Friction, and Elastic Body Exposure. *Anal. Chem. Insights* **2007**, *2*, 9–15.
(272) Yoshida, N.; Saeki, Y. Chestnut Bur-Shaped Aggregates of Chrysotile Particles Enable Inoculation of Escherichia Coli Cells with Plasmid DNA. *Appl. Microbiol. Biotechnol.* **2004**, *65*, 566–575.
(273) Yoshida, N.; Takebe, K. Quantitative Detection of Asbestos Fiber in Gravelly Sand Using Elastic Body-Exposure Method. *J. Ind. Microbiol. Biotechnol.* **2006**, *33*, 827–833.
(274) Landrigan, P. J.; Nicholson, W. J.; Suzuki, Y.; Ladou, J. The Hazards of Chrysotile Asbestos: A Critical Review. *Ind. Health* **1999**, *37*, 271–280.
(275) Yoshida, N.; Ide, K. Plasmid DNA Is Released from Nanosized Acicular Material Surface by Low Molecular Weight Oligonucleotides: Exogenous Plasmid Acquisition Mechanism for Penetration Intermediates Based on the Yoshida Effect. *Appl. Microbiol. Biotechnol.* **2008**, *80*, 813–821.
(276) Choi, H.-A.; Lee, Y.-C.; Lee, J.-Y.; Shin, H.-J.; Han, H.-K.; Kim, G.-J. A Simple Bacterial Transformation Method Using Magnesium- and Calcium-Aminoclays.

J. Microbiol. Methods **2013**, *95*, 97–101.
(277) De Cian, A.; Praly, E.; Ding, F.; Singh, V.; Lavelle, C.; Le Cam, E.; Croquette, V.; Piétrement, O.; Bensimon, D. ATP-Independent Cooperative Binding of Yeast Isw1a to Bare and Nucleosomal DNA. *PLoS One* **2012**, *7*, e31845.
(278) Binnig, G.; Quate, C. F.; Gerber, C. Atomic Force Microscope. *Phys. Rev. Lett.* **1986**, *56*, 930–933.
(279) Pastré, D.; Hamon, L.; Landousy, F.; Sorel, I.; David, M.-O.; Zozime, A.; Le Cam, E.; Piétrement, O. Anionic Polyelectrolyte Adsorption on Mica Mediated by Multivalent Cations: A Solution to DNA Imaging by Atomic Force Microscopy under High Ionic Strengths. *Langmuir ACS J. Surf. Colloids* **2006**, *22*, 6651–6660.
(280) Hamon, L.; Pastré, D.; Dupaigne, P.; Le Breton, C.; Le Cam, E.; Piétrement, O. High-Resolution AFM Imaging of Single-Stranded DNA-Binding (SSB) protein–DNA Complexes. *Nucl Acids Res* **2007**, *35*, e58.
(281) Alhaddad, A.; Durieu, C.; Dantelle, G.; Le Cam, E.; Malvy, C.; Treussart, F.; Bertrand, J.-R. Influence of the Internalization Pathway on the Efficacy of siRNA Delivery by Cationic Fluorescent Nanodiamonds in the Ewing Sarcoma Cell Model. *PLoS ONE* **2012**, *7*, e52207.
(282) Can, M. F.; Çınar, M.; Benli, B.; Özdemir, O.; Çelik, M. S. Determining the Fiber Size of Nano Structured Sepiolite Using Atomic Force Microscopy (AFM). *Appl. Clay Sci.* **2010**, *47*, 217–222.
(283) Wicklein, B.; Darder, M.; Aranda, P.; Ruiz-Hitzky, E. Bio-Organoclays Based on Phospholipids as Immobilization Hosts for Biological Species. *Langmuir* **2010**, *26*, 5217–5225.
(284) Beall, G. W.; Sowersby, D. S.; Roberts, R. D.; Robson, M. H.; Lewis, L. K. Analysis of Oligonucleotide DNA Binding and Sedimentation Properties of Montmorillonite Clay Using Ultraviolet Light Spectroscopy. *Biomacromolecules* **2009**, *10*, 105–112.
(285) Saeki, K.; Kunito, T. Adsorptions of DNA Molecules by Soils and Variable-Charged Soil Constituents. *Curr. Res. Technol. Educ. Top. Appl. Microbiol. Microb. Biotechnol.* **2010**, *1*, 188–195.
(286) Nguyen, T. H.; Elimelech, M. Plasmid DNA Adsorption on Silica: Kinetics and Conformational Changes in Monovalent and Divalent Salts. *Biomacromolecules* **2007**, *8*, 24–32.
(287) Pastré, D.; Hamon, L.; Landousy, F.; Sorel, I.; David, M. O.; Zozime, A.; Le Cam, E.; Piétrement, O. Anionic Polyelectrolyte Adsorption on Mica Mediated by Multivalent Cations: A Solution to DNA Imaging by Atomic Force Microscopy under High Ionic Strengths. *Langmuir* **2006**, *22*, 6651–6660.
(288) Pastré, D.; Piétrement, O.; Fusil, S.; Landousy, F.; Jeusset, J.; David, M.-O.; Hamon, L.; Le Cam, E.; Zozime, A. Adsorption of DNA to Mica Mediated by Divalent Counterions: A Theoretical and Experimental Study. *Biophys. J.* **2003**, *85*, 2507–2518.
(289) Saeki, K.; Kunito, T.; Sakai, M. Effects of pH, Ionic Strength, and Solutes on DNA Adsorption by Andosols. *Biol. Fertil. Soils* **2010**, *46*, 531–535.
(290) Olivieri, N. F.; Brittenham, G. M.; McLaren, C. E.; Templeton, D. M.; Cameron, R. G.; McClelland, R. A.; Burt, A. D.; Fleming, K. A. Long-Term Safety and Effectiveness of Iron-Chelation Therapy with Deferiprone for Thalassemia Major. *N. Engl. J. Med.* **1998**, *339*, 417–423.
(291) Rogan, W. J.; Dietrich, K. N.; Ware, J. H.; Dockery, D. W.; Salganik, M.; Radcliffe, J.; Jones, R. L.; Ragan, N. B.; Chisolm, J. J.; Rhoads, G. G. The Effect of Chelation Therapy with Succimer on Neuropsychological Development in Children Exposed to Lead. *N. Engl. J. Med.* **2001**, *344*, 1421–1426.

(292) Alcântara, A. C. S.; Darder, M.; Aranda, P.; Ruiz-Hitzky, E. Polysaccharide–fibrous Clay Bionanocomposites. *Appl. Clay Sci.*
(293) Maxfield, F. R. Weak Bases and Ionophores Rapidly and Reversibly Raise the pH of Endocytic Vesicles in Cultured Mouse Fibroblasts. *J. Cell Biol.* **1982**, *95*, 676–681.
(294) Cotten, M.; Langle-Rouault, F.; Kirlappos, H.; Wagner, E.; Mechtler, K.; Zenke, M.; Beug, H.; Birnstiel, M. L. Transferrin-Polycation-Mediated Introduction of DNA into Human Leukemic Cells: Stimulation by Agents That Affect the Survival of Transfected DNA or Modulate Transferrin Receptor Levels. *Proc. Natl. Acad. Sci. U. S. A.* **1990**, *87*, 4033–4037.
(295) Khalil, I. A.; Kogure, K.; Akita, H.; Harashima, H. Uptake Pathways and Subsequent Intracellular Trafficking in Nonviral Gene Delivery. *Pharmacol. Rev.* **2006**, *58*, 32–45.
(296) Erbacher, P.; Roche, A. C.; Monsigny, M.; Midoux, P. Putative Role of Chloroquine in Gene Transfer into a Human Hepatoma Cell Line by DNA/lactosylated Polylysine Complexes. *Exp. Cell Res.* **1996**, *225*, 186–194.
(297) Rodríguez-Beltrán, J.; Elabed, H.; Gaddour, K.; Blázquez, J.; Rodríguez-Rojas, A. Simple DNA Transformation in Pseudomonas Based on the Yoshida Effect. *J. Microbiol. Methods* **2012**, *89*, 95–98.
(298) Gaj, T.; Gersbach, C. A.; Barbas, C. F. ZFN, TALEN, and CRISPR/Cas-Based Methods for Genome Engineering. *Trends Biotechnol.* **2013**, *31*, 397–405.
(299) Anguela, X. M.; Sharma, R.; Doyon, Y.; Miller, J. C.; Li, H.; Haurigot, V.; Rohde, M. E.; Wong, S. Y.; Davidson, R. J.; Zhou, S.; *et al.* Robust ZFN-Mediated Genome Editing in Adult Hemophilic Mice. *Blood* **2013**, *122*, 3283–3287.

List of figures

experiments. The working concentration for sepiolite was fixed to 10 ng.μl^{-1} for experiments with mammalian cells.

Figure 3.4 Dots-plots from FACS experiment, for data corresponding to 3 and 6 hours after the addition of sepiolite into V79 cells at different concentrations (0 ng.μl^{-1}, 10 ng.μl^{-1}, and 50 ng.μl^{-1} and 100 ng.μl^{-1}). The zone P1 corresponds to living cells, and P3 corresponds to green fluorescent cells (channel FL1A, 530 nm) due to the presence of sepiolite, from P1 region. 10,000 cells were counted in all experiments. Without sepiolite, only 1% of cells are naturally fluorescent. At 6 hours of addition of sepiolite, only 32% and 7% were living cells at 50 ng.μl^{-1} and 100 ng.μl^{-1} of sepiolite, respectively. The working concentration for sepiolite was fixed to 10 ng.μl^{-1} for experiments with mammalian cells.

Figure 3.5 Laser confocal microscopy images of sepiolite fibers inside V79 cells. Concentration of sepiolite dispersion in MEM: 0, 5 and 50 ng.μl^{-1}. Channels: IR (infrared), red, green and blue, at given excitation and emission wavelengths. Sepiolite has a natural fluorescence in green and red, and is not fluorescent in blue and infrared. The blue fluorescence represents the Daco-Dapi staining of the cells nucleus. In merged images, we confirm that sepiolite fibers were uptaken by the cells. Wavelengths of excitation and fluorescence emission are indicated. The scale bar represents 25 μm.

Figure 3.6. Laser confocal microscopy image of of sepiolite fibers inside V79 cells. Concentration of sepiolite dispersion in MEM: 10 ng.μl^{-1}(Left) and 5 0ng.μl^{-1} (Right).

Figure 3.7. Fluorescence microscopy images of sepiolite fibers inside V79 cells. Concentration of sepiolite dispersion in MEM: A-B: 5 ng.μl^{-1}, C:10 ng.μl^{-1} and D: 50 ng.μl^{-1}.

Figure 3.8. TEM images of a set of three different V79 cells (A, D and G) with zooming in respective internal sepiolite fiber localizations (10 ng.μl^{-1} sepiolite in 5.10^6 cells).

Figure 3.9 TEM images of V79 cells showing different cellular uptake mechanisms of sepiolite fibers.

Figure 4.1 Results from a previous study carried out at the ICMM-CSIC[41] on DNA adsorbed onto sepiolite. A) Adsorption isotherm of salmon sperm DNA (50mM HAc/NaAc pH=4.8) on sepiolite at 30^{o}C (equilibrium at 24 hours under agitation. B), C) FE-SEM images of the Sep/DNA bionanocomposite prepared in this acidic medium condition.

Figure 4.2 (A) Adsorption isotherm of DNA on sepiolite carried out in presence of various multivalent cations. Reaction conditions: 10 mM TrisHCl pH=7.5; sepiolite concentration fixed at 1mg/ml and the mass to 50 μg. Adsorption experiments at 25^{o}C for 24 hours under agitation at 700 rpm in a Thermomixer from Eppendorf. (B) Same experimental data expressed in terms of initial DNA concentration vs. percentage of DNA adsorbed onto sepiolite.

Figure 4.3 Effect of the presence of cations with different valence on DNA adsorption. Reaction conditions: 10 mM TrisHCl pH=7.5, salmon sperm DNA and sepiolite concentrations fixed at 615 ng.μl^{-1} and 1 mg/ml, respectively. 50 μg of sepiolite were used in each experiment. Adsorption took place at 25^{o}C for 24 hours under agitation at 700 rpm using a Thermomixer from Eppendorf.

Figure 4.4 Competition between monovalent and divalent cations in DNA adsorption onto sepiolite. A: Mg^{2+}/Na^{+}, B: Mg^{2+}/K^{+} competition. Reaction conditions: 10 mM TrisHCl pH=7.5, Salmon Sperm DNA and sepiolite concentrations fixed at 615 ng.μl^{-1} and 1 mg/ml, respectively. 50 μg of sepiolite were used in each experiment. Adsorption took place at 25^{o}C for 24 hours under agitation at 700 rpm using a Thermomixer from Eppendorf.

Figure 4.5 Comparison of adsorption of different DNA conformations onto sepiolite. (A) Same experimental data showed in (B) expressed in terms of initial DNA concentration vs. percentage of DNA adsorbed onto sepiolite. (B) Adsorption isotherm of different DNA conformations on sepiolite. Reaction conditions: 10 mM TrisHCl pH=7.5, 5 mM $MgCl_2$, sepiolite concentration fixed at 1mg/ml. 50 μg of sepiolite were used in each experiment. Adsorption experiments were carried out at 25^{o}C for 24 hours under agitation at 700 rpm using a Thermomixer from Eppendorf.

Figure 4.6 Characterization with EMSA of the DNA desorbed by the "heating" method. (A) Plasmid (5.7Kbp) control; (B) plasmid DNA in the supernatant after synthesis of the bionanocomposite and before heating the re-suspended pellet; (C) plasmid DNA desorbed from bionanocomposite obtained with 5 mM $MgCl_2$; (D) plasmid DNA desorbed from bionanocomposite obtained with 5 mM $CaCl_2$. Last line in C and D represents single stranded DNA.

Figure 4.7 TEM images of the DNA desorbed by the "heating" method. White arrows pointed to single stranded DNA.

Figure 4.8 Comparison of DNA desorption efficiency of EDTA at different concentrations by applying "chelation" method. Reaction conditions: Initially, 0.5 ml of Sep/DNA samples were prepared using salmon sperm DNA at 640 ng.μl^{-1} in a sepiolite dispersion (1 mg/ml) in 10 mM TrisHCl and 5 mM $MgCl_2$. Resuspension in 0.1 ml solution of 10 mM TrisHCl, and EDTA at 5, 10 and 50 mM. After 15 min of incubation at room temperature, all samples were centrifugated at 5000 rpm for 5min, and the supernatant was measured using the UV-vis.

Figure 4.9 Comparison of the amount of desorbed salmon sperm DNA from bionanocomposites prepared in the presence of Mg^{2+}, Ca^{2+}, spermidine and spermine using the “chelation” method (re-suspension in TrisHCl EDTA).

Figure 4.10 Percentage of DNA desorbed from sepiolite in each of the three subsequent re-suspension steps of the “chelation method” applied to Sep/DNA bionanocomposites prepared in the presence of $MgCl_2$, $CaCl_2$, spermidine and spermine at the concentration indicated in the graphics.

Figure 4.11 Percentage of DNA desorbed from sepiolite in four subsequent re-suspension steps applied the "chelation" method to Sep/DNA bionanocomposites prepared from salmon sperm DNA in presence of 1 mM spermine. First resuspension (represented in yellow) was in 100 μl of TrisHCl (up) and in 100 μl of TrisEDTA (down). Sep/DNA samples were prepared in presence of 1 mM spermine with the same protocol described in figure 4.9 and 4.10 captions.

Figure 4.12 *Characterization with EMSA of desorbed DNA using the "chelation" method. A: Plasmid (5.7 Kbp) control; B: plasmid DNA in the supernatant after synthesis of the bionanocomposite prepared with 5 mM $MgCl_2$ and before re-suspending the pellet in TrisHCl and EDTA; C: plasmid DNA desorbed from the bionanocomposite obtained with 5 mM $MgCl_2$; D: plasmid DNA desorbed from bionanocomposite obtained with 5 mM $CaCl_2$.*

Figure 4.13 Comparison between Fourier transform infrared spectroscopy (FTIR) spectra of sepiolite, Sep/DNA bionanocomposites prepared without cations, and Sep/DNA prepared in the presence of monovalent (A: NaCl, B: KCl), divalent (C: $CaCl_2$, D: $MgCl_2$), trivalent (E: spermidine) and tetravalent (F: spermine) cations.

*Figure 4.14 Atomic force microscopy (AFM) images. (A) control images of PCMV plasmid 5.7 Kbp (*5 ng.μl^{-1}*). (B) Sep/DNA bionanocomposite (sepiolite at 1 mg/ml and* PCMV plasmid with 5.7 Kbp at 10 ng.μl^{-1}*).*

Figure 4.15 AFM images of Sep/DNA bionanocomposite (sepiolite at 1 mg/ml and PCMV plasmid with 5.7 Kbp at 20 ng.μl^{-1}) in phase-mode.

Figure 4.16 Transmission electron microscopy (TEM) control images of DNA. A: plasmid 5.7 Kbp, B: linearized plasmid 5.7 Kbp using EcoRI restriction enzime, C: Condensed plasmid 5.7 Kbp in presence of 1 mM spermidine, D: Condensed GFP plasmid in presence of 1 mM spermine.

Figure 4.17 Dark field TEM images of plasmids 5.7 Kbp bounds on sepiolite fibers. (sepiolite at 1 mg/ml and PCMV plasmid with 5.7 Kbp at 10 ng.μl^{-1} and 20 ng.μl^{-1} in E and F).

Figure 4.18 Dark field TEM images of single molecule sep/DNA bionanocomposites (plasmid 5.7 Kbp bounded to one sepiolite nanofiber).

Figure 5.1 Results obtained with fluorescence activated cells sorting (FACS) for time kinetics for sepiolite and sep/DNA in V79 cells.

Figure 5.2 Dose response of V79 hamster cells after incubation for 10 days with G418 antibiotic. G418 concentrations: A: Control; B: 400 ng.μl^{-1}; C: 500 ng.μl^{-1}; D: 600 ng.μl^{-1}; E: 800 ng.μl^{-1}; F: 1000 ng.μl^{-1}.

Figure 5.3 Picture of colonies of transfected V79 cells with Sep/DNA prepared with 10 mM $MgCl_2$ (A) and 10mM $CaCl_2$ (B). First day: 10^5 cells were plated in each well. Second day: 3 ml of new medium was added in presence of Sep/DNA bionanocomposite with 40 μg of sepiolite and 1 μg of bounded DNA

Figure 6.4 TEM images of sepiolite nanofibers in contact with XL2 bacteria (overnight culture of XL2 in 20 ml of LB, then 500 μl of bacteria in LB with 0D600 between 0.5 and 1 centrifuged at 3000 rpm for 5 min and resuspended in 200 μl of sepiolite at 1 mg/ml; 5 μl of this sample were placed in a carbon grid and measured with TEM).

Figure 6.5 TEM image of a complete XL2 bacteria (A) with zoom in contact regions (B and C).

Figure 6.6 TEM image of a complete XL2 bacteria (A) with zoom in contact regions (B to E).

Figure 6.7 Left: Picture of the agar plate with transformants using the protocol reported by Wilharm et al.[265], with 5 mM HEPES and 200 mM KCl pH 7.4. Right: Picture of the agar plate with transformants using the same protocol but with 10 mM TrisHCl and 5 mM $MgCl_2$ pH 7.5. Around 1,500 colonies were obtained in both cases, with 50 ng of DNA, which mean $3x10^4$ transformants per μg of DNA.

Figure 6.8 Improvement of bacterial transformation efficiency by incubation of 1 hour of sepiolite and DNA with bacteria at 37°C , following the Protocol reported by Wilharm et al.[265] using 5 mM HEPES and 200 mM KCl pH 7.4 (image of the plate agar at left), an improvement of 5-fold was obtained, reaching $2x10^5$ transformants per μg of DNA (with the same amount of bacteria, sepiolite and DNA used by Wilharm et al.[265] but incubating one hour in presence of LB, the obtained colonies are the sum of the two agar plates showed at right).

Figure 6.9 Improvement of bacterial transformation efficiency by incubation of 1 hour of Sep/ DNA with bacteria at 37 °C, following our method using 10 mM TrisHCl pH=7.5 and 5 mM $MgCl_2$, an improvement of 10-fold was obtained, reaching $4x10^5$ transformants (the sum of the colonies which grown in the two plates showed at right compared with the colonies which grown in the plate at left without incubation).

Figure 6.10 Gel electroforesis of extracted PUC19 plasmid from bacteria using sepiolite. A: step ladder. B: commercial PUC19 plasmid. C: extracted PUC 19 plasmid. D: extracted PUC19 plasmid digested with EcoRI.

Figure 6.11 TEM image of extracted PUC19 using sepiolite.

List of tables

Annexed publication:

- Advanced biohybrid materials based on nanoclays for biomedical applications.

Other publications:

- Nonextensivity and Tsallis Entropy in DNA Fragmentation Patterns by Ionizing Radiation.
- Present status of radiation interaction with DNA-strand-break cross-section and fragment-size distributions.

Advanced biohybrid materials based on nanoclays for biomedical applications

Eduardo Ruiz-Hitzky[*a], Margarita Darder[a], Bernd Wicklein[a], Francisco M. Fernandes[a], Fidel A. Castro-Smirnov[a], M. Angeles Martín del Burgo[b], Gustavo del Real[b], Pilar Aranda[a]
[a]Instituto de Ciencia de Materiales de Madrid, CSIC, C/ Sor Juana Inés de la Cruz 3, 28049 Madrid, Spain; [b]Instituto Nacional de Investigación y Tecnología Agraria y Alimentaria, Ctra. de la Coruña Km 7,5 28040 Madrid, Spain.

ABSTRACT

Bio-nanohybrids prepared by assembling natural polymers (polysaccharides, proteins, nucleic acids, etc) to nanosized silicates (nanoclays) and related solids (layered double hydroxides, LDHs) give rise to the so-called bionanocomposites constituting a group of biomaterials with potential applications in medicine. In this way, biopolymers, including chitosan, pectin, alginate, xanthan gum, ι-carrageenan, gelatin, zein, and DNA, as well as phospholipids such as phosphatidylcholine, have been incorporated in layered host matrices by means of ion-exchange mechanisms producing intercalation composites. Also bio-nanohybrids have been prepared by the assembly of diverse bio-polymers with sepiolite, a natural microfibrous magnesium silicate, in this case through interactions affecting the external surface of this silicate. The properties and applications of these resulting biomaterials as active phases of ion-sensors and biosensors, for potential uses as scaffolds for tissue engineering, drug delivery, and gene transfection systems, are introduced and discussed in this work. It is also considered the use of synthetic bionanocomposites as new substrates to immobilize microorganisms, as for instance to bind Influenza virus particles, allowing their application as effective low-cost vaccine adjuvants and carriers.

Keywords: biohybrids, bionanocomposites, clay minerals, sepiolite, biopolymers, medical applications, Influenza vaccines.

1. INTRODUCTION

The development of functional hybrid materials, based on the bottom-up assembly at the nanometric scale of polymeric moieties with nano- and micro-metric sized inorganic solids, is widely known especially for clay-based materials.[1] The growing relevance of the resulting nanoarchitectures is due to the possibility to obtain advanced nanostructured materials whose properties cover a wide range of applications, including electrical, electrochemical, optical, optoelectronic, magnetic, catalytic, selective molecular adsorption, ionic-molecular recognition or controlled release of bioactive species.[2-7] Not only is the hybrid materials class receiving increasing attention due to its functional properties, but also for its capacity to substantially improve the mechanical, rheological, thermal, and barrier properties as compared to conventional materials. An outstanding example of these improvements is achieved by polymer-clay nanocomposites[8-10] and more recently by the so-called bio-nanocomposites in which the polymer is of biological origin.[11-14] These materials also present an important role in the development of biomimetic and bioinspired materials.[15-18] Actually, Nature creates such fine structures based on building block combinations and self-assembly processes. Therefore, those observed structures in biological systems have been recognized as practical tools and inspiration for fabrication of advanced materials.[19] Many important advances using biomimetic approaches involve carbonates and phosphates, for instance to prepare artificial nacre, bone, and other bionanocomposites[20-27] but silica, silicates and polysiloxanes also offer a viable alternative for preparation of biohybrids since their chemistry is extremely versatile, allowing the formation of hierarchical superstructures, supramolecular materials and other multifunctional bioinspired systems.[1,11,19,27-31] The present contribution focuses on the diverse approaches to prepare biohybrid materials specifically based on clay minerals, by assembling of smectites and sepiolite to molecular and polymeric species of biological origin, with the aim of developing suitable nanostructured materials for potential biomedical applications.

*eduardo@icmm.csic.es; phone 34 91 3349000; fax 34 91 3720623; http://www.icmm.csic.es/mmi/new/erh_index.html

Nanosystems in Engineering and Medicine, edited by Sang H. Choi, Jin-Ho Choy, Uhn Lee, Vijay K. Varadan,
Proc. of SPIE Vol. 8548, 85480D · © 2012 SPIE · CCC code: 1605-742/12/$18 · doi: 10.1117/12.999995

2. ASSEMBLING BIOPOLYMERS TO CLAY MINERALS: BIONANOCOMPOSITES

It is widely known that synthetic polymers derived from petroleum are commonly used for nanocomposites preparation. The use of biopolymers, instead of synthetic polymers, represents a major advantage as these materials combine diverse biopolymers (proteins, lipids, polysaccharide, etc.) with inorganic solids (silica, silicates, phosphates, carbonates, etc.) giving rise to more ecological materials. These bionanocomposites often mimic the composition, structure, and behavior of natural hybrid materials present in different living organisms.[15-18,21] Scientific research in the field of biohybrid materials, and particularly in bionanocomposites, is experiencing a remarkable growth, which is pointed out by the exponential evolution of scientific publications in the last years, as typically shown for emerging lines (Figure 1).

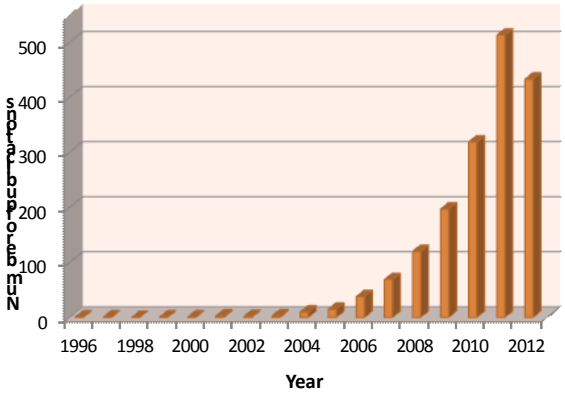

Figure 1. Evolution of the publications number of bio-hybrids/bio-nanocomposites. Data from SciVerse Scopus (September, 2012).

The bio-hybrid nanocomposites lie on the borderline between the inorganic and the living world, being of extreme importance due to their non-toxic, biocompatible, and biodegradable behavior, properties that place this class of materials as good candidates for potential biomedical applications (tissue engineering, artificial bone, genetic therapy, etc.) among other advanced applications.[5,6,11,12,32-34] Another important point refers to the benefit associated with the use of biological sources of polymers to generate the so-called *green plastics* or *green nanocomposites*, avoiding therefore the indiscriminate consumption of petroleum derivates and enhancing the biodegradability as opposed to the non-ecological conventional plastics.[35] In this context, our group has pioneered the innovative development of biohybrid materials based on layered or fibrous clay minerals combined with biopolymers such as polysaccharides (chitosan, alginate, pectin, carrageenans…), proteins (gelatin, zein), nucleic acids (DNA) and lipids (phosphatidylcholine).[11,21,36-46]

Typical clay minerals used in the preparation of these bionanocomposites are smectites (montmorillonite, hectorite, saponite, beidellite, etc.) which are 2:1 layer silicates whose structure is formed by the repetition of octahedral alumina sheets sandwiched between two tetrahedral silica sheets (Figure 2a). Isomorphic substitutions of silicon, aluminium and other metal atoms in those sheets by ions with lower charge result in a net negative charge that is compensated by cations in the interlayer region. Smectites show swelling capability and the interlayer cations can be easily exchanged with other cations, including organic cations and positively charged biomolecules. Other clay minerals that deserve more and more interest for bionanocomposite preparations show microfibrous morphologies, such as palygorskite and sepiolite (Figure 2b). Sepiolite is a hydrated magnesium silicate[47,48] whose structure is composed of ribbons of a 2:1 phyllosilicate structure with a discontinuous sheet of octahedral magnesium oxide hydroxide sandwiched by tetrahedra silica sheets. These building blocks form channels and tunnels that are accessible to water and other small molecules.[49] Sepiolite also exhibits free silanol groups (Si-OH) along the external surface of these channels, which are susceptible to interact with diverse functional groups via hydrogen bonding. This silicate shows a low cation exchange capacity related to the existence of isomorphic substitutions as occurs in smectites, being also able to interact with charged species.

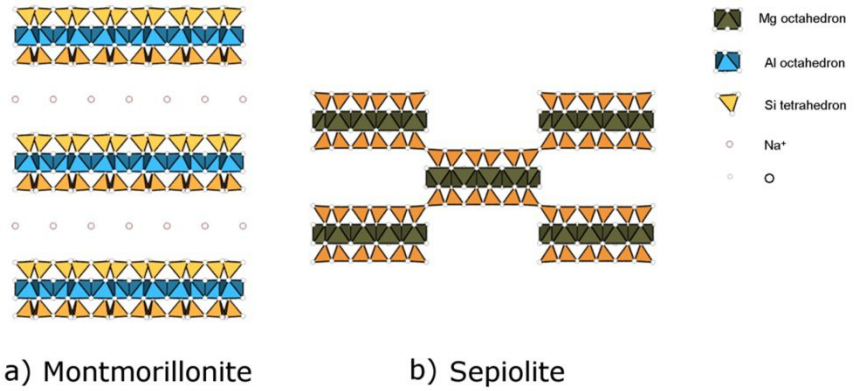

Figure 2. Structural representation of smectite layered silicate (a) and microfibrous clay sepiolite (b).

The firstly reported clay-based bionanocomposites refer to the intercalation of chitosan in layered silicates.[38] At low concentrations of chitosan in slightly acid aqueous solutions the intercalation of the polymer progresses by a cation-exchange reaction until incorporation of a monolayer of the biopolymer in the interlayer region of montmorillonite. The use of high amounts of polysaccharide exceeding the cation-exchange capacity (CEC) may lead to the uptake of chitosan in a bilayer configuration, being the excess of intercalated biopolymer accompanied of counter-ions in order to compensate the excess of positively charged groups of chitosan chains. In this situation the initial CEC of the clay is reversed to an anion-exchange capacity (AEC) in the resulting bio-nanocomposite. These AEC properties are of special interest for the development of active phases in electrochemical sensors for anions detection.[50] In the same way, it is possible to prepare bionanocomposites based on the assembly of chitosan to sepiolite.[39] The resulting materials show improved mechanical properties and also functional properties related to their anionic exchange capacity, which could be of interest for electroanalytical applications.

Another group of bionanocomposites refers to the assembling of collagen and gelatin to different types of inorganic substrates.[40] In the case of clay-based bionanocomposites it has been observed that sepiolite can control the cristallinity of the gelatin matrix, having an important impact on the mechanical properties of the resulting bionanocomposites. At 20% mass fraction of sepiolite the elastic modulus of the bionanocomposite increased by a factor of 2.2 as a result of both the mechanical reinforcement of the silicate inside the polymer matrix, but also as a result of the crystallinity variation induced by the clay particles.[51,52] This last group of bionanocomposites can be of interest for biomedical applications especially in tissue engineering related to the development of scaffolds for bone regeneration.[40] For these types of applications it is required that the bionanocomposites are provided of adequate macroporosity and good mechanical properties. The development of such types of bionanocomposite materials exhibiting a hierarchical porosity, with micro and mesoporosity, together with macropores of tens and hundreds of micrometers requires their conformation as foams. Amongst the diverse foaming techniques the most common procedure in the case of bionanocomposites consists in the application of freeze-drying or supercritical drying processes to biopolymer-clay hydrogels.[46] In this context, we have applied this methodology to the development of diverse ultra-light foams based on bionanocomposites that combine polysaccharides and proteins with clay minerals, mainly sepiolite. Several patents[53-55] based on these results indicate the different fields of application of this class of materials, including acoustic and thermal insulation, and packaging materials. In biomedical applications these biohybrids can be of interest as carrier of pharmaceutical and biological species. In this way, biohybrid foams can serve as support of biological entities or even living organisms to cellular solids as for instance microalgal cells.[23,46] Functional proteins and enzymes may also be introduced in the bionanocomposite foam by mixing them with the starting components prior to freeze-drying. In this last case, the biocompatibility of the foams helps to preserve the catalytic activity of entrapped enzymes allowing the development of bioreactors. A recent example of this application is a macroporous PVA foam in which the reinforcing agent is a phospholipid-modified sepiolite used as support of urease enzyme, which introduces the catalytic functionality in the system.[56]

3. BIOMIMETIC & SUPPORTED MEMBRANES

Inspiration from naturally occurring structures is an interesting source of active and multifunctional smart materials systems. In this context, the biological cell membrane is of special interest because it hosts a great variety of molecules acting as receptors in the interaction with the external environment and therefore, can inspire diverse functional architectures for the development of novel biotechnological tools. Thus, bioinspired materials based on solid supported bilayer lipid membranes are applied in technological fields such as biosensors, artificial photosynthesis, or drug delivery. The key to their success lies in the close resemblance to cell membranes and the accompanied capacity to accommodate biological entities with diminished loss of biological activity. Our group has developed a new class of biohybrid materials based on the interaction of phospholipids with clay minerals that results in biomimetic interfaces which allow for the association of different types of biological species such as enzymes, proteins, virus particles, or toxins and their exploitation in technological relevant areas such as biosensing, influenza vaccination, or as toxin sequestrants. Lipid adsorption on montmorillonite can be performed either from liposome suspensions or from organic solutions (Figure 3). The acidic character of interlayer water bonded to exchangeable cations may interact with the phosphate group of the PC molecule and turn the entire lipid molecule cationic which would enable the cation exchange mechanism.[44] In the case of sepiolite the assembling with the PC molecules occurs via hydrogen bonding with the silanol groups on the external surface of this fibrous clay, making possible the incorporation of PC as mono- or bilayer that cover the external silicate surface.[44] The resulting materials can be used as biomimetic interfaces (biointerfaces) for adsorption of enzymes, such as the cytoplasmic enzyme urease and the membrane-associated enzyme cholesterol oxidase. The excellent enzyme stabilization properties of the sepiolite supported lipid matrices were explored for the construction of urea sensors and cholesterol bioreactors.[45] In the case of the cholesterol bioreactor, the presence of superparamagnetic magnetite nanoparticles previously assembled to sepiolite,[57] allows the easier recovery of the bioreactor from the reaction media with the help of a magnet.[58]

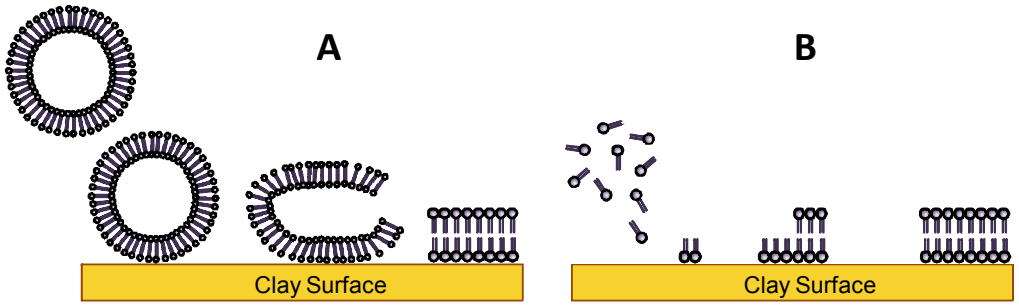

Figure 3. Scheme of PC adsorption on a clay surface from aqueous solution by liposome deposition (A) and from ethanol phase by molecular self-assembly (B). Adapted from Ref. 59.

4. DNA AND VIRUSES SUPPORTED ON CLAYS

A further step in the development of clay-based materials at the frontier of biological and mineral worlds refers to the interaction of DNA and virus particles with clay minerals. Thus, nucleic acids (low molecular weight DNA from salmon sperm) can be spontaneously adsorbed on the external surface of microfibrous sepiolite through hydrogen-bonding interactions with external silanol groups present on this silicate following a L-type adsorption isotherm (Figure 4A).[60] These interactions provoke the agglomeration of the fibrous clays and the DNA biopolymer as shown in figure 4B. We have observed a protection of the adsorbed DNA towards the degradation by the action of DNase enzyme. This type of supported DNA-clay systems is potentially of interest in view to carry out non-viral gene transfection.

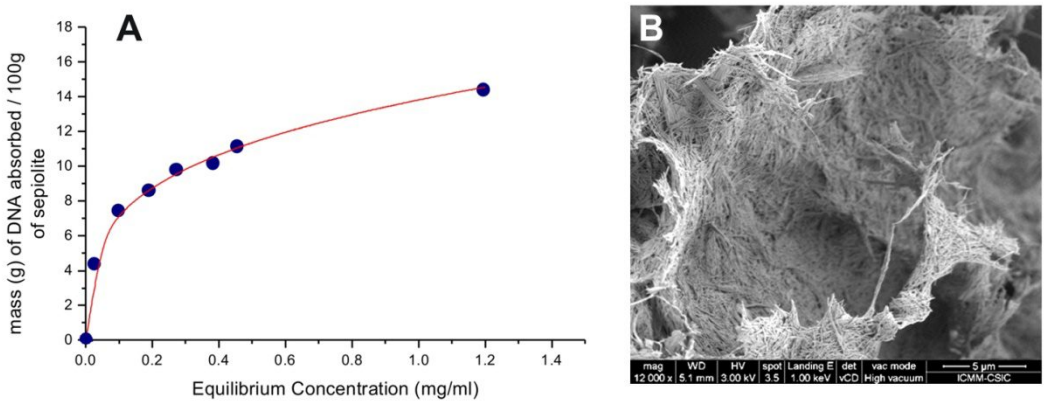

Figure 4. Adsorption isotherm (298 K) of DNA on sepiolite from aqueous solution (A) and FE-SEM image of the DNA-sepiolite nanocomposite (B).

Unmodified sepiolite is not able to retain viral particles, as the virus agglomerated in large clusters on the mineral surface. However, bionanocomposite consisting in the assembling of negatively charged natural polysaccharides (e.g., xanthan) or phospholipids (e.g., PC) with sepiolite allows for the incorporation of Influenza virus particles resulting in novel bio-hybrid systems. For instance, xanthan-sepiolite bionanocomposites are able to assemble Influenza viral particles with a homogeneous distribution on the modified fibres.[43] The presence of negatively charged sites from the xanthan biopolymer assembled to the silicate sepiolite facilitates its binding to virus particles. The integrity and bioactivity of these supported viral particles are preserved and water dispersions can be directly used as intranasal or intramuscular flu vaccines and experiments carried out in mice demonstrate that the virus/bio-nanocomposites induce the formation of specific antibodies and protect against Influenza virus infection acting as a new and efficient co-adjuvant of vaccines.[43] In an alternative approach, sepiolite-PC biohybrids can be also used as biomimetic interfaces for the immobilization not only of the entire viral particle but also of specific surface antigens as the haemagglutinin (HA) or neuraminidase (NA) from influenza virus.[61] It could be shown that the sepiolite supported lipid membrane afforded an environment where those surface proteins showed comparable activity to its native environment and therewith, one can speak about biomimetic association of HA and NA on the sepiolite-lipid hybrid.[59] A more practical issue in vaccine manufacturing is the thermal stability of the associated antigenic compound, which may become especially critical in countries of the Third World, where the cold-chain for vaccine preservation is not always assured. It could be shown, that influenza virus adsorbed on the sepiolite biohybrid preserved its neuraminidase activity as well as its immunogenic potential until 50 ºC in a higher extent than the free virus and the viruses stabilized on the conventional carriers based on aluminum hydroxide gels.[61] Moreover, these results may be of interest for other novel biomedical applications of these biohybrids such as uses in the development of biosensors, bioreactors, or drug-delivery systems.

5. CONCLUDING REMARKS

Biohybrids resulting from the assembly of biopolymers and particulate inorganic solids such as clay minerals, are versatile materials that show biocompatibility, which is of great interest in view of diverse potential biomedical applications. For instance, bionanocomposites can be conformed as highly porous and bio-compatible hybrid materials showing good mechanical properties, which may be of potential interest as scaffolds in tissue engineering for bone repair. In other cases, they can be used as support of different biological entities including cells and viruses. Clay-lipid biohybrids are versatile, safe, non-toxic, and biocompatible materials that behave as biomimetic lipid interfaces resembling cellular membranes, having a possible contribution in the development of biosensors, enzymatic bioreactors, or as adjuvant of vaccines. Sepiolite spontaneously adsorbs DNA protecting it against degradation by the action of DNase enzyme, which can be of potential interest in applications as non-viral agents for gene-therapy. However, this

type of biohybrid materials is still far from actual uses in biomedicine. The interaction mechanisms between the biological entities and the substrates are still largely unknown and both fundamental and applied (eg. *in vivo* assays) research are required to prove their activity, effect and efficiency.

ACKNOWLEDGEMENTS

This work was supported by the Spanish CICYT (MAT2009-09960 and MAT2012-31759 projects).

REFERENCES

[1] Ruiz-Hitzky, E., Aranda, P., Darder, M. and Ogawa, M., "Hybrid and biohybrid silicate based materials: molecular vs. block-assembling bottom-up processes," Chem. Soc. Rev., 40(2), 801-828 (2011).
[2] Sanchez, C., Lebeau, B., Chaput, F. and Boilot, J. P., "Optical properties of functional hybrid organic-inorganic nanocomposites," Adv. Mater., 15(23), 1969-1994 (2003).
[3] Gomez-Romero, P., "Hybrid organic-inorganic materials - In search of synergic activity," Adv. Mater., 13(3), 163-174 (2001).
[4] Gómez-Romero, P. and Sanchez, C., [Functional Hybrid Materials] Wiley-VCH, Weinheim (2004).
[5] Sanchez, C., Julian, B., Belleville, P. and Popall, M., "Applications of hybrid organic-inorganic nanocomposites," J. Mater. Chem., 15(35-36), 3559-3592 (2005).
[6] Vallet-Regí, M. and Ruiz-Hernández, E., "Bioceramics: From Bone Regeneration to Cancer Nanomedicine," Adv. Mater., 23(44), 5177-5218 (2011).
[7] Sanchez, C., Belleville, P., Popall, M. and Nicole, L., "Applications of advanced hybrid organic-inorganic nanomaterials: from laboratory to market," Chem. Soc. Rev., 40(2), 696-753 (2011).
[8] Pinnavaia, T. J. and Beall, G., [Polymer-Clay Nanocomposites] John Wiley & Sons, New York (2000).
[9] Alexandre, M. and Dubois, P., "Polymer-layered silicate nanocomposites: preparation, properties and uses of a new class of materials," Mater. Sci. Eng. R-Rep., 28(1-2), 1-63 (2000).
[10] Giannelis, E. P., "Polymer layered silicate nanocomposites," Adv. Mater., 8(1), 29-35 (1996).
[11] Darder, M., Aranda, P. and Ruiz-Hitzky, E., "Bionanocomposites: A new concept of ecological, bioinspired, and functional hybrid materials," Adv. Mater., 19(10), 1309-1319 (2007).
[12] Ruiz-Hitzky, E., Aranda, P. and Darder, M. "Bionanocomposites," [Kirk-Othmer Enciclopedia of Chemical Technology]. John Wiley & Sons, Hoboken, NJ, pp. 1-28 (2008).
[13] Mittal, V., [Nanocomposites with Biodegradable Polymers. Synthesis, Properties, and Future Perspectives] Oxford University Press, New York (2011).
[14] Avérous, L. and Pollet, E., [Environmental Silicate Nano-biocomposites] Springer-Verlag, London (2012).
[15] Dujardin, E. and Mann, S., "Bio-inspired materials chemistry," Adv. Mater., 14(11), 775-788 (2002).
[16] Tang, Z. Y., Kotov, N. A., Magonov, S. and Ozturk, B., "Nanostructured artificial nacre," Nature Mater., 2(6), 413-418 (2003).
[17] Belton, D. J., Patwardhan, S. V., Annenkov, V. V., Danilovtseva, E. N. and Perry, C. C., "From biosilicification to tailored materials: Optimizing hydrophobic domains and resistance to protonation of polyamines," Proc. Natl. Acad. Sci. U.S.A., 105(16), 5963-5968 (2008).
[18] Chen, R., Wang, C.-a., Huang, Y. and Le, H., "An efficient biomimetic process for fabrication of artificial nacre with ordered-nano structure," Mater. Sci. Eng. C-Biomimetic Supramol. Syst., 28(2), 218-222 (2008).
[19] Ruiz-Hitzky, E., Darder, M., Aranda, P. and Ariga, K., "Advances in Biomimetic and Nanostructured Biohybrid Materials," Adv. Mater., 22(3), 323-336 (2010).
[20] Fratzl, P. and Weinkamer, R., "Nature's hierarchical materials," Prog. Mater. Sci., 52(8), 1263-1334 (2007).
[21] Ruiz-Hitzky, E., Darder, M. and Aranda, P. "An introduction to Bio-nanohybrid materials," in: Ruiz-Hitzky, E., Ariga, K. and Lvov, Y. M., editors. [Bio-inorganic Hybrid Nanomaterials, Strategies, Syntheses, Characterization and Applications]. Wiley-VCH, Weinheim, pp. 1-32 (2008).
[22] Antonietti, M. and Fratzl, P., "Biomimetic Principles in Polymer and Material Science," Macromol. Chem. Phys., 211(2), 166-170 (2010).

[23] Zhao, F., Yin, Y. J., Lu, W. W., Leong, J. C., Zhang, W. J., Zhang, J. Y., Zhang, M. F. and Yao, K. D., "Preparation and histological evaluation of biomimetic three-dimensional hydroxyapatite/chitosan-gelatin network composite scaffolds," Biomaterials, 23(15), 3227-3234 (2002).
[24] Dorozhkin, S., "Calcium orthophosphate-based biocomposites and hybrid biomaterials," Journal of Materials Science, 44(9), 2343-2387 (2009).
[25] Liu, X., Smith, L. A., Hu, J. and Ma, P. X., "Biomimetic nanofibrous gelatin/apatite composite scaffolds for bone tissue engineering," Biomaterials, 30(12), 2252-2258 (2009).
[26] Bigi, A., Torricelli, P., Fini, M., Bracci, B., Panzavolta, S., Sturba, L. and Giardino, R., "A biomimetic gelatin-calcium phosphate bone cement," Int. J. Artif. Organs, 27(8), 664-673 (2004).
[27] Aranda, P., Fernandes, F. M., Wicklein, B., Ruiz-Hitzky, E., Hill, J. P. and Ariga, K. "Bioinspired Materials Chemistry: Organic-Inorganic Nanocomposites," in: Swiegers, G. F., editor. [Bioinspiration and Biomimicry in Chemistry]. John Wiley & Sons, New York (in press).
[28] Livage, J., Coradin, T. and Roux, C. "Bioactive Sol-Gel Hybrids," in: Gómez-Romero, P. and Sanchez, C., editors. [Functional Hybrid Materials]. Wiley-VCH, Weinheim, pp. 387-404 (2004).
[29] Avnir, D., Coradin, T., Lev, O. and Livage, J., "Recent bio-applications of sol-gel materials," J. Mater. Chem., 16(11), 1013-1030 (2006).
[30] Sanchez, C., Arribart, H. and Guille, M., "Biomimetism and bioinspiration as tools for the design of innovative materials and systems," Nature Mater., 4(4), 277-288 (2005).
[31] Ruiz-Hitzky, E., Ariga, K. and Lvov, Y. M., [Bio-inorganic Hybrid Nanomaterials, Strategies, Syntheses, Characterization and Applications] Wiley-VCH, Weinheim (2008).
[32] Zeng, Q. H., Yu, A. B., Lu, G. Q. and Paul, D. R., "Clay-based polymer nanocomposites: Research and commercial development," J. Nanosci. Nanotechnol., 5(10), 1574-1592 (2005).
[33] Rhim, J. W., "Potential use of biopolymer-based nanocomposite films in food packaging applications," Food Sci. Biotechnol., 16(5), 691-709 (2007).
[34] Ruiz-Hitzky, E., Darder, M. and Aranda, P. "Progress in bionanocomposite materials," in: Cao, G., Zhang, Q. and Brinker, C. J., editors. [Annual Review of Nanoresearch]. World Scientific Publishing, Singapore, pp. 149-189 (2010).
[35] Ray, S. S. and Bousmina, M., "Biodegradable polymers and their layered silicate nano composites: In greening the 21st century materials world," Prog. Mater. Sci., 50(8), 962-1079 (2005).
[36] Ruiz-Hitzky, E. and Darder, M., "Trends in bio-hybrid nanostructured materials," Curr. Nanosci., 2(3), 153-153 (2006).
[37] Alcantara, A. C. S., Aranda, P., Darder, M. and Ruiz-Hitzky, E., "Zein-clay biohybrids as nanofillers of alginate based bionanocomposites," Abstr. Pap. Am. Chem. Soc., 241, 114-115 (2011).
[38] Darder, M., Colilla, M. and Ruiz-Hitzky, E., "Biopolymer-clay nanocomposites based on chitosan intercalated in montmorillonite," Chem. Mater., 15(20), 3774-3780 (2003).
[39] Darder, M., Lopez-Blanco, M., Aranda, P., Aznar, A. J., Bravo, J. and Ruiz-Hitzky, E., "Microfibrous chitosan-sepiolite nanocomposites," Chem. Mater., 18(6), 1602-1610 (2006).
[40] Fernandes, F. M., Darder, M., Ruiz, A. I., Aranda, P. and Ruiz-Hitzky, E. "Gelatine-based bio-nanocomposites," in: Mittal, V., editor. [Nanocomposites with Biodegradable Polymers. Synthesis, Properties, and Future Perspectives]. Oxford University Press, New York, pp. 209-233 (2011).
[41] Fernandes, F. M., Ruiz, A. I., Darder, M., Aranda, P. and Ruiz-Hitzky, E., "Gelatin-clay bio-nanocomposites: structural and functional properties as advanced materials," J. Nanosci. Nanotechnol., 9(1), 221-229 (2009).
[42] Ruiz-Hitzky, E., Darder, M. and Aranda, P., "Functional biopolymer nanocomposites based on layered solids," J. Mater. Chem., 15(35-36), 3650-3662 (2005).
[43] Ruiz-Hitzky, E., Darder, M., Aranda, P., Martin del Burgo, M. Á. and del Real, G., "Bionanocomposites as New Carriers for Influenza Vaccines," Adv. Mater., 21, 4167-4171 (2009).
[44] Wicklein, B., Darder, M., Aranda, P. and Ruiz-Hitzky, E., "Bio-organoclays Based on Phospholipids as Immobilization Hosts for Biological Species," Langmuir, 26(7), 5217-5225 (2010).
[45] Wicklein, B., Darder, M., Aranda, P. and Ruiz-Hitzky, E., "Phospholipid–Sepiolite Biomimetic Interfaces for the Immobilization of Enzymes," ACS Appl. Mater. Interfaces, 3(11), 4339-4348 (2011).
[46] Darder, M., Aranda, P., Ferrer, M. L., Gutiérrez, M. C., del Monte, F. and Ruiz-Hitzky, E., "Progress in Bionanocomposite and Bioinspired Foams," Adv. Mater., 23(44), 5262-5267 (2011).
[47] Brunauer, K. and Preisinger, A., "Struktur und Entstehung des Sepioliths," Miner. Petrol., 6(1-2), 120-140 (1956).

[48] Santaren, J., Sanz, J. and Ruiz-Hitzky, E., "Structural fluorine in sepiolite," Clays Clay Miner., 38(1), 63-68 (1990).
[49] Ruiz-Hitzky, E., "Molecular access to intracrystalline tunnels of sepiolite," J. Mater. Chem., 11(1), 86-91 (2001).
[50] Darder, M., Colilla, M. and Ruiz-Hitzky, E., "Chitosan-clay nanocomposites: application as electrochemical sensors," Appl. Clay Sci., 28(1-4), 199-208 (2005).
[51] Fernandes, F. M., "On the structural and functional properties of sepiolite in polymer-clay nanocomposites and materials derived thereof," Autonomous University of Madrid, Madrid (2011).
[52] Fernandes, F. M., Manjubala, I. and Ruiz-Hitzky, E., "Gelatin renaturation and the interfacial role of fillers in bionanocomposites," Phys. Chem. Chem. Phys., 13(11), 4901-4910 (2011).
[53] Ruiz Hitzky, E., Aranda, P., Darder, M. and Alcantara, A. C. S., "Materiales composites basados en biohíbridos zeína-arcilla, su procedimiento de obtención y usos de estos materiales," Spanish patent, PCT/ES2010/070404 (2010).
[54] Ruiz-Hitzky, E., Aranda, P., Darder, M., Fernandes, F. M. and Matos, C. R. S., "Espumas rígidas de tipo composite basadas en biopolímeros combinados con arcillas fibrosas y su método de preparación," Spanish patent, 2342871 (2010).
[55] Ruiz-Hitzky, E. and Fernandes, F. M., "Composición de material carbonoso obtenible por carbonización de un biopolímero soportado sobre arcilla," Spanish patent, P201130835 (2011).
[56] Wicklein , B., Darder , M., Aranda , P. and Ruiz-Hitzky, E., "Enzyme supporting phospholipid-sepiolite hybrids incorporated in polymer matrices for biosensor and bioreactor applications," 2010 SEA-CSSJ-CMS Trilateral Meeting on Clays General Meeting (2010).
[57] Ruiz-Hitzky , E., Aranda , P. and González-Alfaro, Y., Spanish patent, PCT ES2011/070145 (2011).
[58] González-Alfaro, Y., Aranda, P., Fernandes, F. M., Wicklein, B., Darder, M. and Ruiz-Hitzky, E., "Multifunctional Porous Materials Through Ferrofluids," Adv. Mater., 23(44), 5224-5228 (2011).
[59] Wicklein, B., "Bio-Nanohybrid Materials Based on Clays and Phospholipids," Autonomous University of Madrid, Madrid (2011).
[60] Darder, M., Castro, F. A., Aranda, P., Martín del Burgo, M. A., del Real, G. and Ruiz-Hitzky, E., "Bionanocomposites based on the assembly of DNA and viruses with sepiolite," 3rd International Seminar on Nanosciences and Nanotechnologies (2010).
[61] Wicklein, B., Parra Yuste, M., Martín del Burgo, M. Á., Darder, M., Escrig Llavata, C., Aranda, P., Ortín, J., del Real, G. and Ruiz-Hitzky, E., "Lipid-based bio-nanohybrids for functional stabilization of influenza vaccines," Eur. J. Inorg. Chem., (doi:10.1002/ejic.201200579).

Journal of Modern Physics, 2012, 3, 431-437
doi:10.4236/jmp.2012.36059 Published Online June 2012 (http://www.SciRP.org/journal/jmp)

Nonextensivity and Tsallis Entropy in DNA Fragmentation Patterns by Ionizing Radiation

Carlos Antonio Marante Valdés[1], Fidel Antonio Castro Smirnov[2], Oscar Rodríguez Hoyos[3], João Dias de Toledo Arruda-Neto[4,5]

[1]Centro de Estudios Avanzados de Cuba (CEAC), Havana, Cuba
[2]Universidad de las Ciencias Informáticas (UCI), Havana, Cuba
[3]Instituto Superior de Tecnologías y Ciencias Aplicadas (InSTEC), Havana, Cuba
[4]Physics Institute, University of São Paulo, São Paulo, Brasil
[5]CEPESq/UniÍtalo—Italy-Brazilian University Center, São Paulo, Brazil
Email: carlos.mv@cea.cu

Received March 17, 2012; revised April 10, 2012; accepted April 20, 2012

ABSTRACT

Nonextensive statistical mechanics as in Tsallis formalism was used in this study, along with the dynamical Hamiltonian rod-like DNA model and the maximum entropy criteria for Tsallis' entropy, so as to obtain length distribution of plasmid fragments, after irradiation with very high doses, assuming that the system reaches metaequilibrium. By intensively working out the Grand Canonical Ensemble (used to take into account the variation of the number of base pairs) a simplified expression for Fragment Size Distribution Function (FSDF) was obtained. This expression is dependent on two parameters only, the Tsallis q value and the minimal length of the fragments. Results obtained from fittings to available experimental data were adequate and the characteristic behavior of the shortest fragments was clearly documented and reproduced by the model, a circumstance never verified from theoretical distributions. The results point to the existence of an entropy which characterizes fragmentation processes and depending only on the q entropic index.

Keywords: Nonextensive Statistics; Tsallis Entropy; DNA Fragment Distribution; Theoretical Distribution; Fragment Minimum Length; DNA Data Analysis

1. Introduction

A wide range of studies related to the biological action of ionizing radiation at the cellular level identified the DNA molecule at the top in the hierarchy of possible biological targets. Molecular damages in DNA define the subsequent fate of the cell and could lead to reproductive cell death, apoptosis, mutations and cancer transformations. After treatment of cells by ionizing radiation there is a broad spectrum of radiation-induced damages which can finally lead to the different endpoints. DNA radiation induced effects are mostly: breaking of one strand, called Single Strand Break (SSB), breaking of the two strands, Double Strand Breaks (DSB), nitrogen base damage, and clustered DNA damages (in case of heavy charged particles).

DSB, including the clustered DNA damages, is the most harmful effect since it has a non-negligible probability in inducing cell death, mutation or carcinogenesis. Studying how DSBs occur and the mechanisms by which the cell repairs them, has caught the attention of many investigators, mainly because of many possible applications as *e.g.* in the improvement of cancer treatment protocols. There are many studies attempting an understanding of DSBs by using several techniques to measure the number and size of fragments after irradiation. The two most successful techniques are pulsed field gel electrophoresis and atomic force microscopy (AFM). The latter being more recent, enabling better resolution, and as such, has been intensively and extensively used.

From a theoretical point of view there are several approaches in obtaining distribution of fragments. One of the most used models is the Random Breaking Model (RBM) [1]. It describes the distribution of fragments at high doses, but fails for shorter fragments, and does not account for the correlation between fragments. Since correlations are present in the formation of DSBs [2], said correlations between the fragments would also be expected. It has already been shown in [3] that long-range correlations between fragments imbedded in a random walk kinematics strongly suggest that DNA constitutes a system driven by nonextensive statistics, with FSDs described by power laws with fractionary exponents (but not by exponential functions as in extensive statistics), where the exponents are functions of both the long-range

potential and the system degree of freedom. There is a pioneering work applying nonextensivity when the distribution function is obtained by maximizing Tsallis' entropy, providing new interesting results at high doses [4]. Monte Carlo based methods yield good data reproducibility for a wide range of doses, but usually needing 5 or more parameters. However, these methods fail in correctly reproducing smaller fragments at high doses [5]. It is noted, for instance, that besides the shortcomings in coping with the region of smaller fragments, the distribution obtained in [4] has a parameter which does not have a precise physical meaning.

Following here this last approach [4], fragment distribution length based on the maximization of Tsallis' entropy was obtained, by taking into account not only length of the fragments but also their energy values as well.

Firstly, the theoretical background is exposed in the **Method** section, beginning with the Tsallis's entropy as a start point for all the subsequent developments. Nonextensive Statistical Mechanics is briefly revisited in order to lay the foundation for its using, and at the end of the section it is proposed a physical model for the DNA fragmentation at very high doses, which allowed us to obtain the FSDFs. In the **Results** section, the FSDFs are tested with available experimental data from literature, which comprises several types of ionizing particles and at several doses, leading to an empirical simplification of the formula obtained. A parametrization of one of the model's parameter as function of dose is proposed, by considering plasmids in a HEPES buffer. In **Conclusions** the significance and the novelty are highlighted.

2. Method

Tsallis' entropy (S_q) is a generalization of Boltzmann-Gibbs entropy (S_{BG}), which has succeeded in the description of many systems previously seeming to elude conventional statistical mechanics. Its form is [6]:

$$S_q = -k\frac{1-\sum_{i=1}^{W} p_i^{\,q}}{1-q}, \tag{1}$$

where q is a real number greater than zero. For $q \to 1$ holds $S_q \to S_{BG}$. The probability that the system is in the i^{th} microstate is p_i and k is the Boltzmann's constant. The value of q can be derived from the dynamics of the system provided exactly known. Alternatively, q could be extracted from experiments by fitting procedures. This entropic form in Equation (1) implies that if A and B are two independent systems, in the sense that $p_{ij}^{A+B} = p_i^A p_j^B$, one is led to

$$\frac{S_q(A+B)}{k} = \frac{S_q(A)}{k} + \frac{S_q(B)}{k} + (1-q)\frac{S_q(A)}{k}\frac{S_q(B)}{k}. \tag{2}$$

This formulation implies that the Tsallis' entropy is generally non-extensive, while that of Boltzmann-Gibbs' is extensive. Not only the entropy formulation changed, but also the ways by which mean values are calculated. For the sake of simplicity and for our purposes we used the so-called "q-mean value" for the energy,

$$\sum_{i=1}^{W} p_i^{\,q} E_i = U_q, \tag{3}$$

although this choice in Equation (3) is not unique (in reference [7] a detailed discussion of all possible choices can be found). For the grand canonical ensemble the obtained distribution function is [8]:

$$p_i^{(N)} = \frac{\left[1-(1-q)\beta'(E_i-\mu_N N)\right]^{\frac{1}{1-q}}}{\Xi_q}, \text{ with} \tag{4}$$

$$\Xi_q = \sum_{N=0}^{\infty}\sum_{i=1}^{W}\left[1-(1-q)\beta'(E_i-\mu_N N)\right]^{\frac{1}{1-q}}, \tag{5}$$

where β' was used instead of β to remark that β' is not the reciprocal of kT [7].

Nonextensive statistical mechanics works in the metaequilibrium, *i.e.* when the system is in a metastable state (including equilibrium as a special case), which is often achieved in stationary regimes or in non-equilibrium organized states. Before the irradiation of the samples all fragments have approximately the same lengths. As doses increase fragments with all possible lengths are produced. At very high doses the most likely fragments are the smaller, while the remaining show a very low or nearly null probability. In this paper it is assumed that the system reaches metaequilibrium during irradiation, when it organizes itself by gathering energy with radiation.

Our system is considered as an ensemble of plasmids, each one having N base pairs closely related to its length through $L = Na$, where a is the distance between base pairs; under normal conditions a = 0.34 nm. In the fragmentation process at high doses, energy is distributed among the system's constituents faster than when low doses are involved. This fact allows considering solutions as if plasmids were imbedded in a thermal reservoir at an effective temperature. Furthermore, recalling that one is dealing with a highly excited system, energy necessary to remove a base pair from the plasmid is considered, a kind of base pair chemical potential, constant and independent of the base pairs specificities. This circumstance shows why the grand canonical ensemble is most appropriate. Thus, the distribution should be the same as in Equation (4). To find $p^{(N)}$ (the probability to find a fragment with N base pairs) it is necessary to compute energy values of the plasmids, which can be obtained from the DNA coupled road model [9] without considering folding motion (mostly valid for supercoiled

plasmids). The basic ingredient of this road like model consists in approaching the DNA as a set of coupled disks (which are the base pairs) with longitudinal (u_n) and rotational (φ_n) degrees of freedom. In this way, one is able to take into account the size of the fragments as well as their energies.

The Hamiltonians are specified by the following expressions, where the sum runs through all values of the base pairs; M denotes the mass of each base pair and I refers to their moment of inertia. Thus,

$$H = H_s + H_r \,, \tag{6}$$

$$H_s = \sum_n \frac{M\dot{u}_n^{\,2}}{2} + \frac{K_s}{2}\left(u_{n+1} - u_n\right)^2 \,, \tag{7}$$

$$H_r = \sum_n \frac{I\dot{\varphi}_n^{\,2}}{2} + \frac{K_r}{2}\left(\varphi_{n+1} - \varphi_n\right)^2 \,, \tag{8}$$

where K_s is the longitudinal stiffness constant and K_r is the stiffness associated with rotations. Solutions obtained by solving the dynamical equations are plane waves. Plasmids in metaequilibrium are constantly excited by radiation from the environment, generating wave trains traveling in both directions. They are expected to overlap, forming standing waves. For the longitudinal case

$$u_n = 2u_0 \cos\left(Kna + \delta_s\right)\cos\left(\omega_s t + \eta_s\right) . \tag{9}$$

For rotational coordinates a similar expression is obtained; K is the wave number ($K = 2\pi/ma$) and m ranges in principle from 2 to $2N$. Substituting the stationary solutions in the Hamiltonian and transforming summations into integrals, plus assuming that the plasmid is a closed structure and also that for $n > 12$ (the resolution of the AFM, approximately) holds $\sin(\pi/n) \approx \pi/n$, we obtain

$$H = 2\left(K_s u_0^{\,2} + K_r \varphi_0^{\,2}\right) N \frac{\pi}{m} . \tag{10}$$

However, the system cannot absorb an arbitrarily large amount of energy. There should be a specific $m_{\min}$, as well as given values for the amplitudes and stiffness constants, so that the plasmid is broken into a number of fragments approximately equal to the number of nodes $2N/m_{\min}$, and this would occur when $\delta_s - \delta_r = \pi$. The longitudinal and rotational waves must be in phase or in counter phase, since nodes must match in order to fulfill the equilibrium condition: $u \to 0$ and $\varphi \to 0$, simultaneously. Therefore, the energy in Equation (10) have to be equal to the number of nodes mentioned above multiplied by the dissociation energy of two consecutive base pairs μ_N. Substituting in Equation (5), and integrating in L instead of summing in N it is obtained

$$\Xi_q = \int_{\frac{L_{\min}}{2}}^{\infty} \frac{\mathrm{d}L}{a} \sum_{m=m_{\min}}^{2N} \left[1 - \beta'\mu_N N\left(q-1\right)\left(1 - \frac{2}{m}\right)\right]^{\frac{1}{1-q}} , \tag{11}$$

where $L_{\min}/2$ is the length of the shortest fragment. As $2/m$ decreases swiftly to zero, it can be neglected when compared to unity, thus allowing obtaining the probability distribution

$$p(L)\mathrm{d}L = \frac{\left(2L - L_{\min}\right)\left[1 - \frac{\beta'\mu_N}{a}\left(q-1\right)L\right]^{\frac{1}{1-q}}}{\int_{\frac{L_{\min}}{2}}^{\infty}\left(2L - L_{\min}\right)\left[1 - \frac{\beta'\mu_N}{a}\left(q-1\right)L\right]^{\frac{1}{1-q}}\mathrm{d}L}\mathrm{d}L \,, \tag{12}$$

where q must be in the range (1 - 3/2).

3. Results

The most accurate experimental results for length distributions of fragments are reported in the form of histograms with 50 nm width bars. Fittings performed to the experimental data showed that $\beta'\mu_N/a \to -\infty$, although there is a wide range of values for which the fitting results change slightly. Calculating this limit in Equation (12) leads to the final simplified equation for the Fragment Size Distribution Function (FSDF), which only depends on the Tsallis q value and on the minimal length of the fragments ($L_{\min}/2$):

$$p(L)\mathrm{d}L = \frac{2\left(2-q\right)\left(3-2q\right)}{\left(q-1\right)^2 L_{\min}}\left(2\frac{L}{L_{\min}} - 1\right)\left(\frac{2L}{L_{\min}}\right)^{\frac{1}{1-q}}\mathrm{d}L \,, \tag{13}$$

Substituting $L_{\min} = P1$, and $q = P2$, the fitting was performed for a total of 20 experimental results reported in the literature. It should be noted that the fragment size pattern obtained for a given dose also depends on the solution where the plasmids were diluted. The experiments analyzed here were carried out by using two different solutions: water and HEPES buffer. They differ significantly as to the diffusion length of the free radicals created in the ionization of the medium, being much higher in water. Therefore, one needs a much lower dose in water to achieve effects similar to those with the HEPES buffer.

Figure 1, panel **a**, shows the experimental distribution of fragments and the theoretical fitting for irradiation of plasmids (80% in supercoiled conformation) with ^{12}C ions at 8 Gy in water [10]. There is, in panel **b**, another experiment with Ni ions at 3000 Gy, with supercoiled plasmids in HEPES buffer [5]. R^2 is the squared correlation coefficient. It can be seen that the model is capable of reproducing the initial peak of the experimental distribution.

Figures 2 and **3** show results for irradiations with electrons and neutrons, respectively, at several doses.

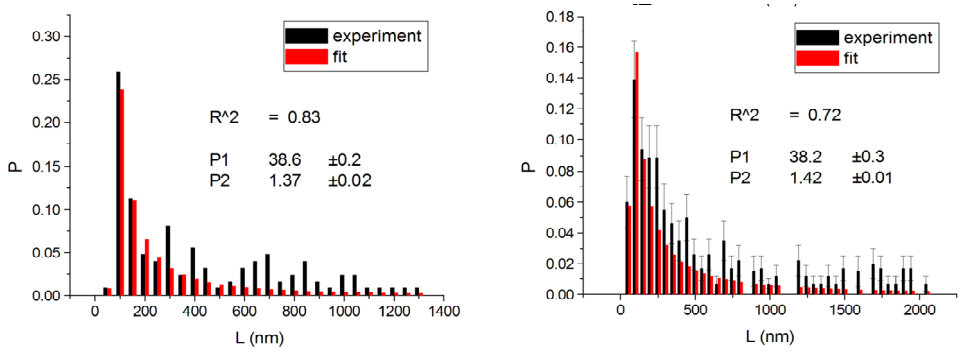

Figure 1. Irradiation with ^{12}C ions at 8 Gy in water [10] (a), with Ni ions at 3000 Gy in HEPES buffer [5] (b).

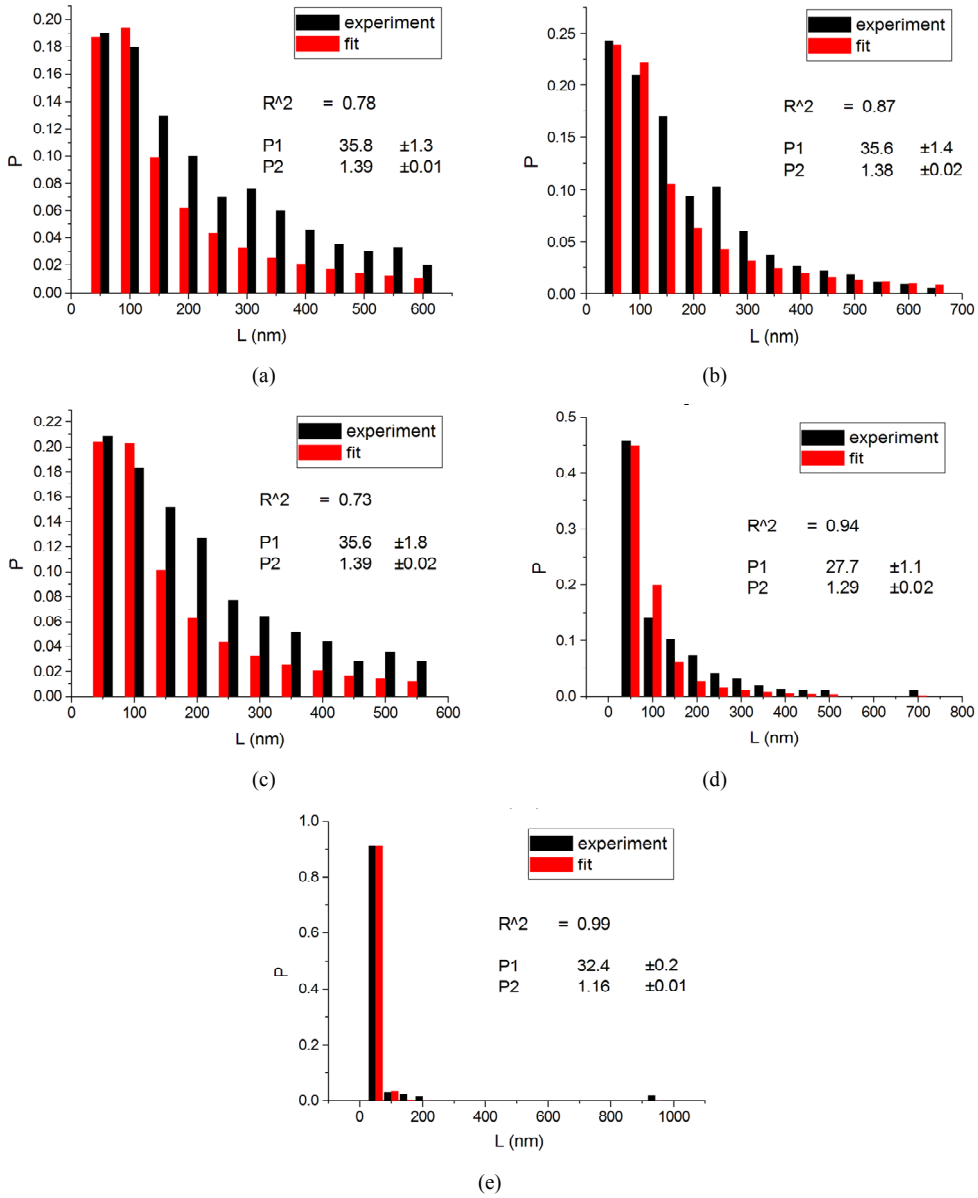

Figure 2. Irradiations with electrons at 5000 Gy [4] (a); 6000 Gy [11] (b); 7000 Gy [4] (c); 8000 Gy [12] (d) and 10,000 Gy [12] (e).

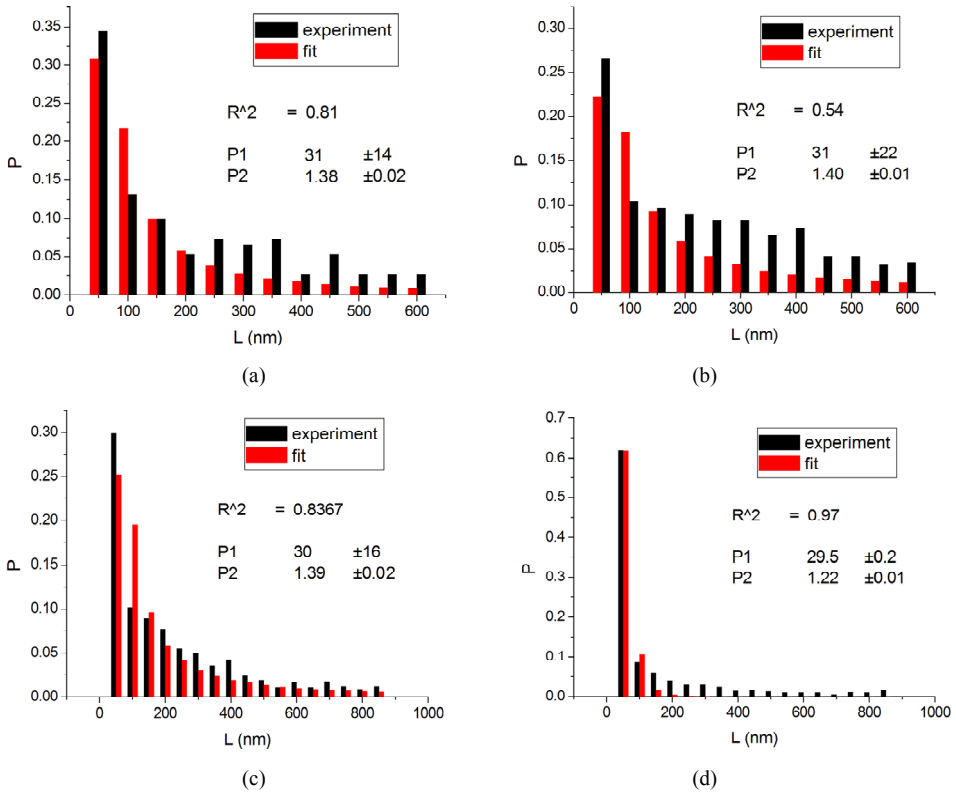

Figure 3. Irradiations with neutrons at 5000 Gy [4] (a); 7000 Gy [4] (b); 7500 Gy [13] (c) and 10,000 Gy [13] (d).

Figure 4 shows the results at 10,000 Gy for gammas and Ar ions. In order to appraise to which extent fitting quality varies with dose, the dose range was divided into five equal intervals and within each of these the average value of R^2 was calculated. **Figure 5** shows how the fitting is linearly improved with the increasing doses, indicating that the model functions better when doses are higher.

The behavior of $L_{\min}$ with dose in a total of 13 experiments with better resolution (bar width equal to 50 nm) was studied, and those performed with buffer were chosen. For dose values pertaining to more than one experiment, an average of $L_{\min}$ was computed. This allowed obtaining a parametrization in the form of a linear function with $R^2 = 0.65$ (**Figure 6**):

$$L_{\min} = 39.7(\pm 2.0) - 0.00089(\pm 0.00029)D, \qquad (14)$$

where D is the dose.

If one substitutes the parametrization in Equation (14) into Equation (13), aiming at achieving new fittings, the obtained values of q are very close to the original, except in one case. This can be seen in **Figures 7** and **8** where the experiments were listed on the horizontal axis; significantly, only the 11th experiment differs from the original. The error bars correspond to the uncertainty provided by the fitting.

Another result obtained by fitting reveals that in 70% of the cases q is in the interval $q = 1.40 \pm 0.03$, independently of the type of ionizing particles. The remaining 30% is distributed almost uniformly from 1.16 to 1.37, as shown by the histogram in **Figure 9**. Therefore, the parameter q is predominant in a narrow interval. Related to the q values, an interesting feature emerge; that of the entropy S_q, associated with the distribution of the fragments by length and energy, when considering the distribution function in Equation (4) and the limit $\beta'\mu_N \to -\infty$ (a must be positive and must not vanish). One can observe in **Figures 10** and **11** that for q values around those predominantly obtained by fitting, the entropy is almost independent of the remaining two parameters ($L_{\min}$ and a). The results point to the existence of entropy characterizing the fragmentation process and depending strongly on the q entropic index and weakly on the others parameters.

4. Conclusions

A novel approach has been established in order to compute fragment length distribution at very high doses. A new Fragment Size Distribution Function was obtained using a nonextensive grand canonical ensemble, with good fitting results of experimental data at different doses. This is the first time a FSDF for DNA under radiation is obtained departing from a physical model and with a potential-like decay for long fragments without the *a priori* conjecture of having this kind of behavior.

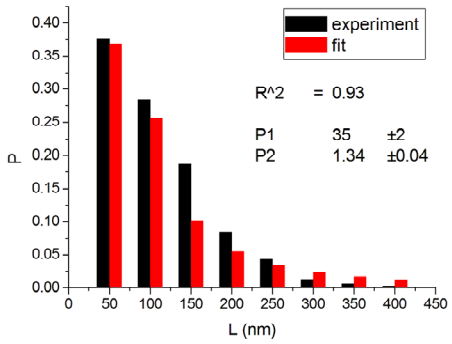

(a)

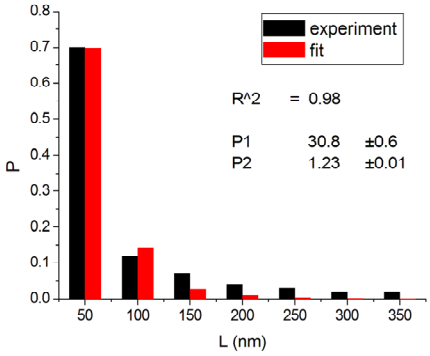

(b)

Figure 4. Irradiation at 10,000 Gy with gamma (a) [14] and Ar ions (b) [14].

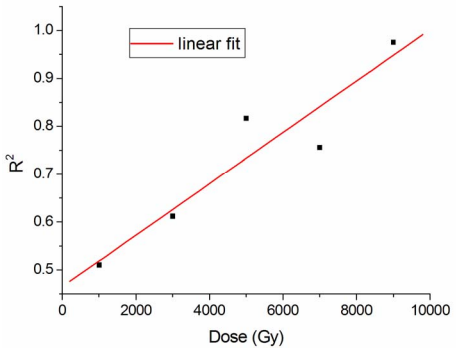

Figure 5. Linear fit with R^2_{fit} = 0.88.

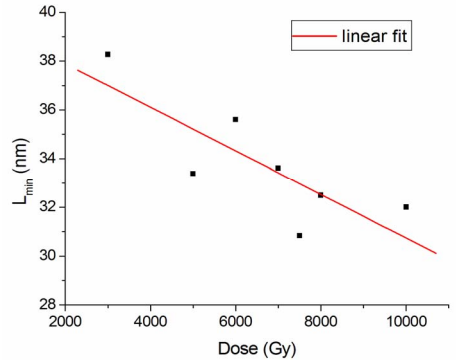

Figure 6. L_{min} parametrization in Equation (16).

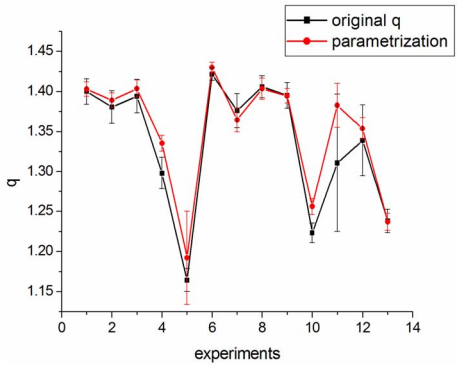

Figure 7. q variation with parametrization in Equation (16).

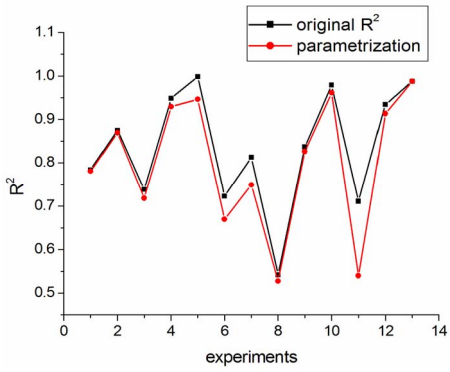

Figure 8. R^2 variation with parametrization in Equation (16).

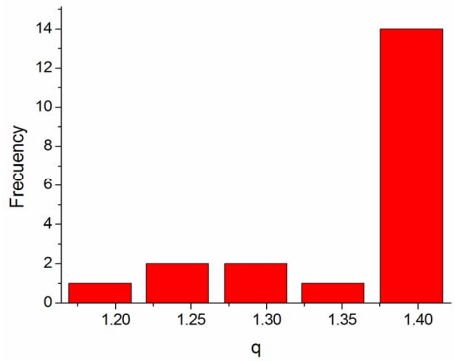

Figure 9. Histogram of the q values obtained by fitting.

Interestingly, the theoretical distribution was able to reproduce the initial peak, sometimes present in irradiation with heavy ions (**Figure 1**); hence, it does not merely reproduce the potential-like decays, constituting thus an improvement of the former models. The present study also found that information on the fragmentation process, via S_q, depends heavily on q, while dependence on the remaining parameters, as L_{min} and a, is considerably weaker, irrespective of what kind of particle is involved in the irradiation, provided q is approximately higher than 1.37 (occurrence of 70 % in all the examined cases). Although the model improves the data description as doses increase, it is clear that the necessity to analyze

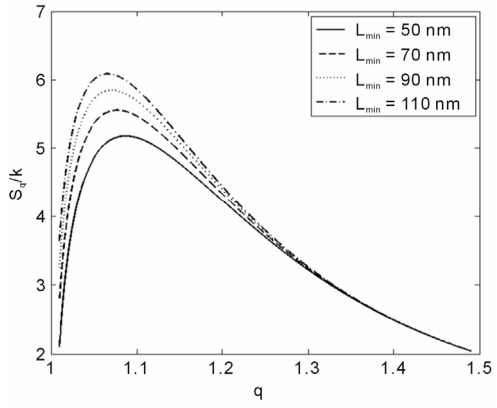

Figure 10. S_q/k vs. q for the distance between base pairs a = 0.34 nm and several L_{min}.

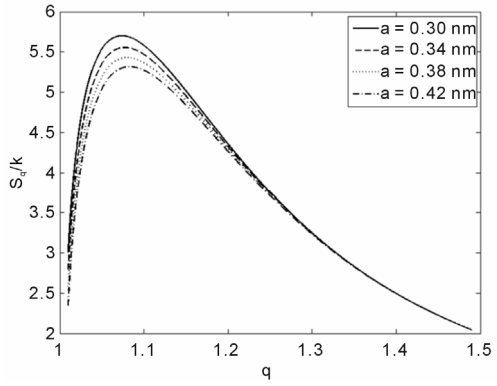

Figure 11. S_q/k vs. q for L_{min} = 70 nm and several values of the base pairs separation a.

more experiments remains. It should be noted, notwithstanding, that the parametrization in Equation (14) for HEPES buffer works quite well with the data so far available, where only one fitting parameter (q) was necessary.

REFERENCES

[1] K. Fuquan, *et al*., "Analysis of Length Distribution of Short DNA Fragments Induced by ^{7}Li Ions Using the Random-Breakage Model," *Chinese Science Bulletin*, Vol. 50, No. 9, 2005, pp. 841-844. doi:10.1360/982004-827

[2] M. Löbrich, P. K. Cooper and B. Rydberg, "Non-Random Distribution of DNA Double-Strand Breaks Induced by Particle Irradiation," *International Journal of Radiation Biology*, Vol. 70, No. 5, 1996, pp. 493-503. doi:10.1080/095530096144680

[3] F. A. Castro, O. Rodriguez and J. D. T. Arruda-Neto. "Present Status of Radiation Interaction with DNA-Strand-Break Cross-Section and Fragment-Size Distributions," *Radiation Effects and Defects in Solids*, Vol. 162, No. 3-4, 2007, pp. 237-245. doi:10.1080/10420150601134616

[4] O. Sotolongo-Costa, *et al*., "A Non Extensive Approach for DNA Breaking by Ionizing Radiation," 2002.

[5] T. Elsässer, *et al*., "Biophysical Modeling of Fragment Length Distributions of DNA Plasmids after X and Heavy-Ion Irradiation Analyzed by Atomic Force Microscopy," *Radiation Research*, Vol. 169, No. 6, 2008, pp. 649-59. doi:10.1667/RR1028.1

[6] C. Tsallis, F. Baldovin, R. Cerbino and P. Pierobon. "Introduction to Nonextensive Statistical Mechanics and Thermodynamics," 2003.

[7] C. Tsallis, R. Mendes and A. Plastino, "The Role of Constraints within Generalized Nonextensive Statistics," *Physica A*, Vol. 261, No. 3-4, 1998, pp. 534-554. doi:10.1016/S0378-4371(98)00437-3

[8] S. Curilef, "Generalized Statistical Mechanics for the N Body Quantum Problem—Ideal Gases," *Zeitschrift Für Physik B Condensed Matter*, Vol. 100, No. 3, 1995, pp. 433-440.

[9] L. V. Yakushevich, "Nonlinear Physics of DNA," 2nd Edition, Wiley-VCH Verlag-GmbH & Co. KGaA, Weinheim, 2004.

[10] S. Li, *et al*., "Atomic Force Microscopy Measurement of DNA Fragment Induced by Heavy Ions," *Chinese Physics Letters*, Vol. 22, No. 4, 2005, pp. 1010-1013. doi:10.1088/0256-307X/22/4/064

[11] D. Pang, J. E. Rodgers, B. L. Berman, S. Chasovskikh and A. Dritschilo, "Spatial Distribution of Radiation-Induced Double-Strand Breaks in Plasmid DNA as Resolved by Atomic Force Microscopy," *Radiation Research*, Vol. 164, No. 6, 2005, pp. 755-765. doi:10.1667/RR3425.1

[12] J. D. T. Arruda-Neto, *et al*., "Personal Communication," *Journal of Biological Physics*, in Press.

[13] D. Pang, B. L. Berman, S. Chasovskikh, J. E. Rodgers and A. Dritschilo, "Investigation of Neutron-Induced Damage in DNA by Aromic Force Microscopy: Experimental Evidence of Clustered DNA Lesions," *Radiation Research*, Vol. 150, No. 6, 1998, pp. 612-618. doi:10.2307/3579883

[14] D. Pang, *et al*., "Radiation-Generated Short DNA Fragments May Perturb Non-homologous End-joining and Induce Genomic Instability," *Journal of Radiation Research*, Vol. 52, No. 3, 2011, pp. 309-319. doi:10.1269/jrr.10147

Radiation Effects & Defects in Solids
Vol. 162, Nos. 3–4, March–April 2007, 237–245

Present status of radiation interaction with DNA–strand-break cross-section and fragment-size distributions

F. A. CASTRO SMIRNOV*†, O. RODRIGUEZ‡ and J. D. T. ARRUDA NETO§

†Universidad de las Ciencias Informáticas, Carretera a San Antonio, Km 2,
Reparto Torrens, Boyeros, Habana, Cuba
‡Instituto Superior de Tecnologias y Ciencias Aplicadas,Quinta de Los Molinos,
Ave. Salvador Allende y Luaces, 6163 Habana, Cuba
§Physics Institute, University of São Paulo, 05315-970 São Paulo, Brasil

(Received 25 July 2006; in final form 25 October 2006)

A cross-section formula for single strand brakes via radiation in the DNA molecule is reviewed and discussed, showing that it describes well-existing data for a wide range of linear energy transfer (LET). Recently published DNA fragment-size distributions (FSDs) data, obtained by irradiation of plasmids with electrons and neutrons, are presented. These results are analyzed and interpreted on the basis of a model developed by the Sao Paulo group, in which by introducing a long-range correlation among the jumps in a random walk, a power-law function is obtained for the probability distribution. The power-law exponent is a function of both the correlation potential and the degree of freedom of the system. It is shown that plasmidial DNA behaves as a nonextensive system, with FSDs described by power laws but not by exponential functions (as in extensive statistics). A pronounced crossover for electron-irradiation data and a change from 1 to 3 in the degree of freedom for neutron irradiation at a high dose were observed. A likely interpretation for these two features is presented and discussed. Perspectives for further developments in this area are presented and addressed.

Keywords: DNA-radiation interaction; Strand-break cross section; Strands fragment-sizes; Power law distributions

1. Introduction

This work is part of a project developed in collaboration with Universities from Havana and Sao Paulo. The project is intended, first, to develop a model aimed at the calculation of cross-sections for radiation-induced single strand breaks (SSB) and double strand breaks (DSB) formation in DNA molecules; secondly, to improve the description of the DNA double-strand mechanical properties by incorporating long-range correlations among the DNA constituents; finally, to set up novel fundamentals in order to advance the study of dosimetry at the nanoscale (nanodosimetry).

*Corresponding author. Email: fsmirnov@yahoo.com

Radiation Effects & Defects in Solids
ISSN 1042-0150 print/ISSN 1029-4953 online © 2007 Taylor & Francis
http://www.tandf.co.uk/journals
DOI: 10.1080/10420150601134616

In this sense, we will discuss selected issues on the present status of calculations for indirect interactions cross-sections in irradiated DNA, aimed at a further development of a model which intertwines statistical behavior and long-range correlation on the cross-section approach. It will also be shown that the distributions of fragments size of irradiated DNA molecules follow power laws, which would provide important information on fine mechanical DNA properties.

2. An existing model approach for SSB cross-sections

We show in figure 1 a small portion of DNA irradiated in the cell interior. The water in the cytosol and the DNA molecules are the most important targets for the radiation energy deposition. Damage in biomolecules, including the DNA, occur when they receive any type of ionizing radiation. These damages can be produced by direct ionization of the biomolecule (direct interactions) or by the formation of damaging reactive radicals (indirect interactions).

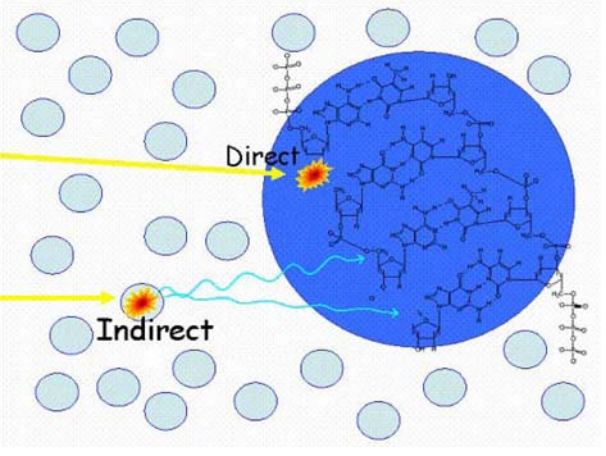

Figure 1. Radiation interaction with DNA.

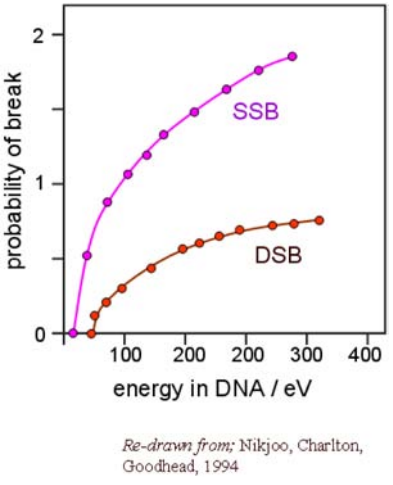

Figure 2. SSB and DSB probability rates.

We note, initially, that the two main types of radiation damage in the DNA molecule are SSB and DSB. Figure 2 shows the experimental results from the literature [1] for the probabilities at which these two kinds of damage can occur. It is also noticeable how the SSB is more probable than DSB at different energies.

We note that when DNA damages are not (or deficiently) repaired, particularly those arising from DSB, cell death or mutation could be induced, where the latter could lead to cancer formation. The high LET radiations are the main cause of this kind of damages. In view of this, the complete understanding of radiobiological effects depends crucially on the cross-sections for the production of these kinds of damages, discriminating between direct and indirect interactions of radiation with the DNA. On the basis of this circumstance, we argue that cross-sections for the induction of SSB and DSB should be considered as important ingredients for the planning of any radiotherapy treatment. However, finer calculations of these cross-sections rely on precise information about the DNA mechanical properties leading to DSB, an issue discussed below.

However, existing calculation results are restricted to cross-sections for DNA SSB because they can be easily observed and quantified by using the electrophoresis technique [2]. In this sense, use is made of some important aspects of the Bethe theory for the ionizing process, for example, the ionizing rate and distribution along the radiation track [3], plus the assumption that the direct interaction between the incident particle and the DNA molecule is negligible in comparison to the indirect effect, when radiation energies are not much higher than some tenths of MeV.

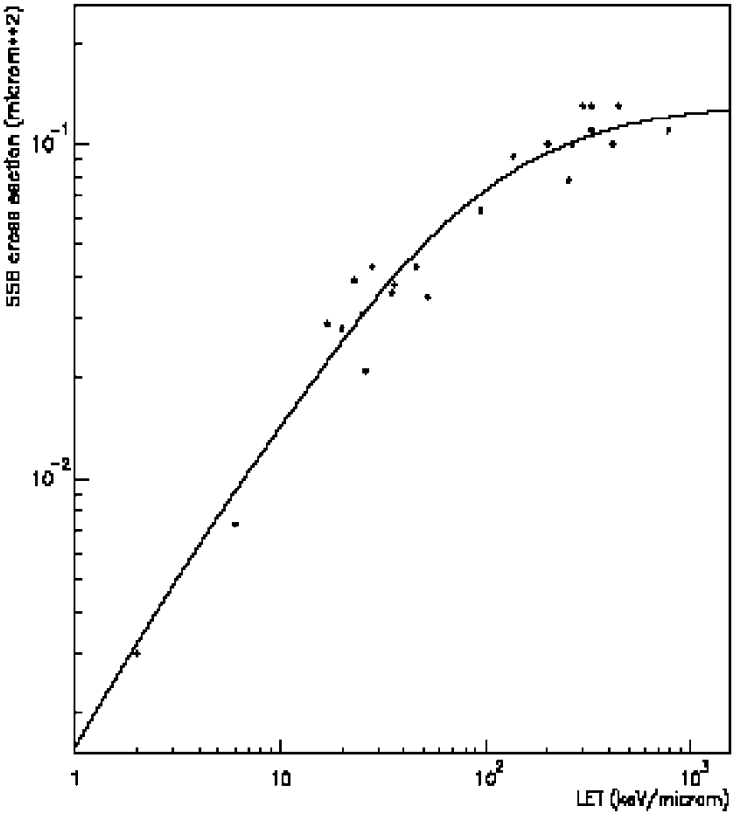

Figure 3. The cross-section for the SSB as a function of the LET [2, 3].

Thus, the SSB cross-section for an incident radiation with LET equal to ε is given by the following expression [4]:

$$\sigma_{\mathrm{SSB}} = \frac{\alpha\varepsilon}{1+\beta\varepsilon}, \tag{1}$$

where

$$\beta = \xi k, \quad k = \frac{1}{\varepsilon_{\mathrm{a}}}, \quad \alpha = k\sigma_{\mathrm{d}} r_{\mathrm{i}}. \tag{2}$$

Here, ξ (expressed in length dimension) is a proportionality factor depending on range properties of the ions and on the solution's physical characteristics; ε_{a} is the average energy transferred to an atom of the medium during its ionization process; σ_{d} is the cross-section for the damage induced by the incident radical. This quantity is related to the structure of the DNA molecule and to its chemical interactions with the radical produced in the medium. It also depends on the properties of the target molecule. r_i is the radical average range; it depends on the distance the produced radical will reach away from the ionizing track and depends on the medium properties too. k is related to the minimum energy necessary for the radical production.

The radiation-induced damage has, therefore, a cross section which is approximately linear at low LET and deviates from linearity as the LET increases.

The result (equation (1)) is compared in figure 3 with data from the literature [5] obtained for incident particles with different LET values. We fitted the curve defined by equation (1) to these data, obtaining for the parameters α and β the following results: $\alpha = (1.6 \pm 0.2) \cdot 10^{-3}\,\mu\mathrm{m}^3/\mathrm{KeV}$, $\beta = (1.2 \pm 0.2) \cdot 10^{-2}\,\mu\mathrm{m/KeV}$. The nice fitting obtained is an indication of the reliability of the model developed elsewhere [4].

3. Results for DNA fragments size distributions

The knowledge of mechanical properties of DNA [6] is required to understand the structural dynamics of cellular processes, such as replication and transcription, as well as in providing a conceptual framework for mechanical assays of enzymes that act on DNA [7]. However, a complete description of DNA mechanics must also consider particular characteristics arising from scaling and possible nonlinearity aspects of the DNA complex structures. In fact, biological molecules are highly deformable, hence highly nonlinear objects, and DNA should not be an exception to this rule. Hence, a stringent but destructive test of the correlations (short or long range) among the parts of an object simply is the random breaking of the whole object and measuring the size of its pieces, as proposed and elaborated by Brouers and Sotolongo-Costa [8]. The corresponding fragment-size power law contains the information we are looking for.

Now we show, in this regard, experimental results for DNA fragment-size distributions (FSDs), where DNA fragmentation is a consequence of the DSB production. Irradiation of DNA with high doses of ionizing radiations, as neutrons and electrons, is quite effective to induce this kind of damage, as recently performed by Pang *et al.* [9, 10].

Figures 4–7 show the results obtained from irradiation of plasmidial DNA with electrons and neutrons. In these plots, we show FSDs for different incident energy doses. On the X-axis, we have the size of the fragments (ℓ), which was measured by atomic force microscopy and expressed in units of base-pairs [9, 10]. On the Y-axis appear a number of fragments with a given length. Each figure presents three different plots for the same data set: log–linear, log–log and linear–linear. We show, by means of a model approach, that their analysis through fitting procedures is best described by assuming a power-law distribution function (see below).

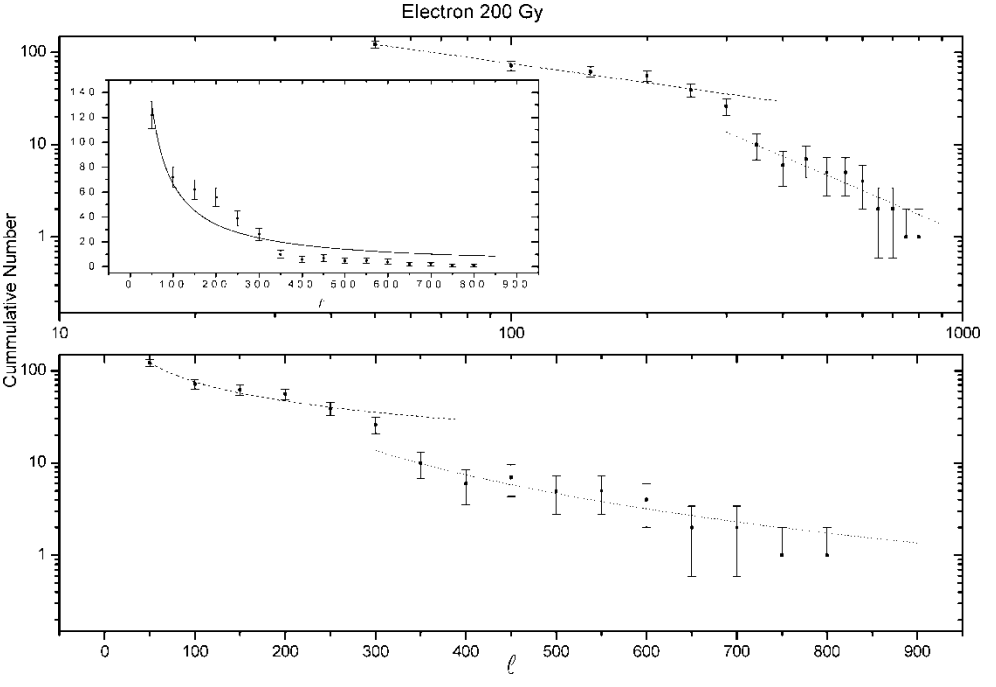

Figure 4. Distribution of DNA fragments size (ℓ), irradiated with an electron dose of 200 Gy (data points).

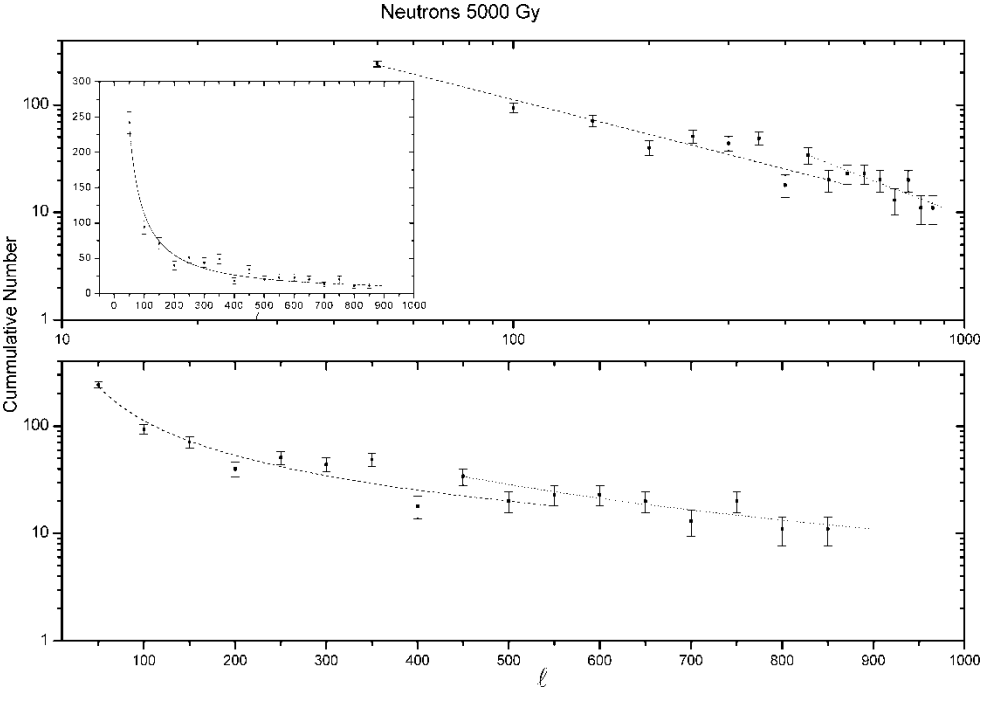

Figure 5. Same as in figure 4 for a neutron dose of 5000 Gy. All fittings were performed with single functions.

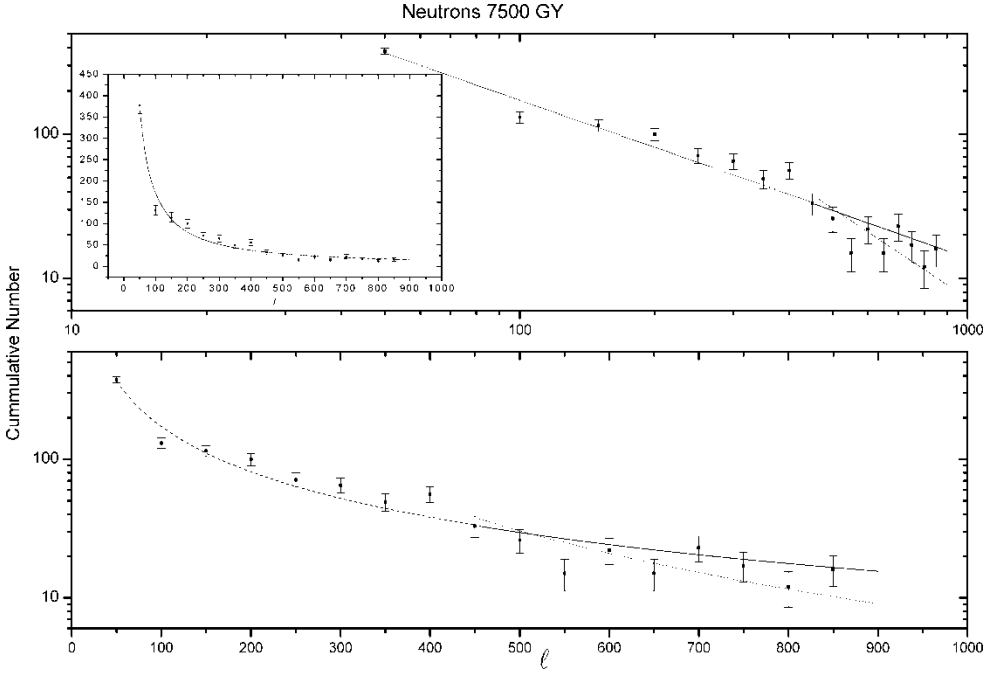

Figure 6. Same as in figure 5 for a neutron dose of 7500 Gy.

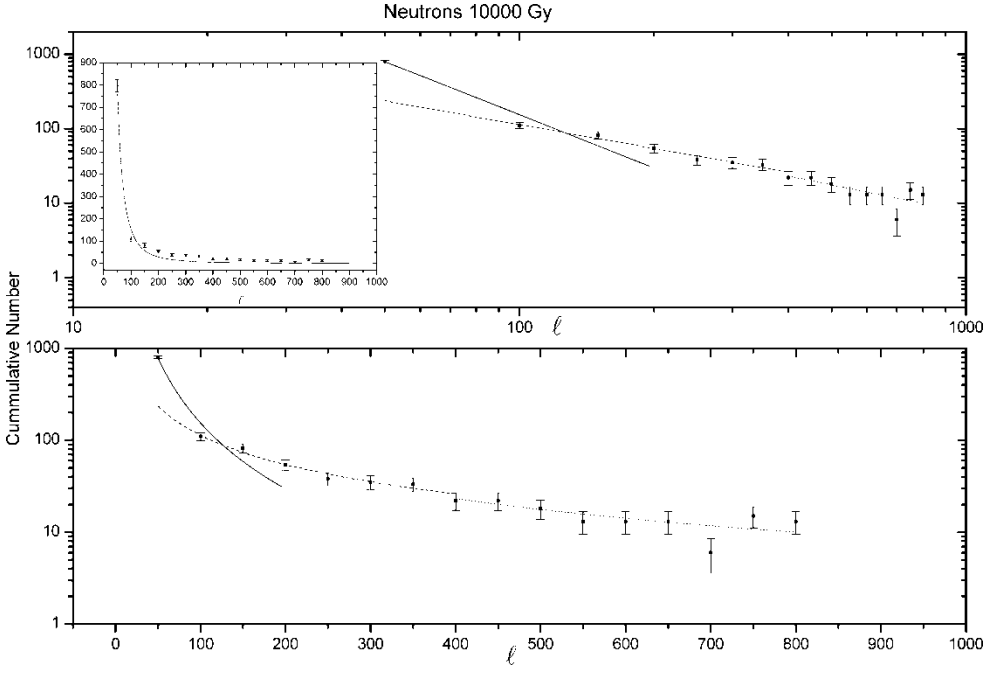

Figure 7. Same as in figure 5 for a neutron dose of 10 KGy.

4. Model approach for DNA FSDs

By introducing a long-range interaction potential among DNA constituents, it is possible to obtain a power-law function for the probability distribution of fragment sizes, where the power-law exponent is determined by both the correlation potential and the degree of freedom of the macromolecule [11].

Actually, in a system constituted of elements interacting by means of short-range forces, each of these elements interacts only with the elements of the system in its close vicinity. This is known as a simple random walk, and the most notorious example in this category is the Brownian motion. Because of the short-range character of the interaction, each particle undergoes random jumps to one of its nearest neighbor sites, and the jumping lengths are small. Let us assume, on the other hand, that the elements of a distribution (*e.g.* DNA fragments with sizes represented by l) exhibit long-range interaction, described by a correlation potential behaving proportionally to $1/r^{\gamma}$. In our analogy with the Brownian motion, r is the modulus of a vector connecting two successive jumps of the walk, and $l = n \cdot a$ (n is an integer) is the net displacement with a distribution given by [12]

$$p(l) \sim l^{-\beta} \tag{3}$$

with

$$\beta = \frac{f+1}{2} \cdot (2-\gamma), \tag{4}$$

where f is the degree of freedom associated with the system (see more on this below).

This last result shows explicitly that the power-law exponent is determined by both the correlation potential (represented by γ; it is an intrinsic property of the DNA double strand, associated with its nonextensive/nonlinear character) and the geometrical structure of the system (revealed by its degree of freedom f), which is a property related to the size of the fragments. To some extent, f depends on the type and intensity of the radiation, that is, the ability of the radiation process to produce short or long fragments.

The data obtained with electrons (figure 4) are particularly revealing, where two components show up distinctly, indicating that the DNA FSD obtained with electrons presents two different fragmentation regimes. The system 'cross' from one regime 'over' to another regime. This is a well-known crossover (see, *e.g.* [13, figure 2]). For neutrons, a single power law is sufficient.

In table 1, we show the fitting results for the power-law exponents. We also analyzed these same sets of data by means of expressions for fragment size distribution function (FSDF) obtained by Sotolongo *et al.* [8], using the thermostatistics approach proposed by Tsallis [14] – the two approaches provided very similar fitting results (differences $<0.5\%$).

We can see again the two obtained exponents for irradiation at low LET radiation with electrons and the jump of the power-law exponent by a factor of 2 when the neutron-irradiation dose reached 10 KGy. These results are compelling evidence of both nonextensivity and crossover at the nanoscale.

Table 1. Power-law exponents obtained by fittings to the data [11].

Dose (Gy)	β (eq. 3)
200(e)	0.97/0.69
5000(n)	1.05
7500(n)	1.10
10,000(n)	2.36

The results presented above constitute a stringent but destructive test of correlations among the DNA fragments. The statistical behavior we could see strongly suggests, although does not prove, the existence of long-range correlations in the DNA.

5. Conclusions

From the material presented, analyzed, and discussed in this review, it becomes clear that

- the cross-section for the SSB formation in DNA, developed by the Sao Paulo group [2], works very well in a wide LET range;
- power laws emerge whenever a long-range correlation is imposed among the elements of a system and when its evolution is treated by a conventional random walk kinematics;
- the FSDs are described by power laws with fractionary exponents;
- a crossover is observed in data sets obtained with low LET radiation with electrons, since this type of radiation probes the DNA without destroying most of its mechanical properties;
- when applied to DNA FSDs, the random walk plus long-range correlations formalism strongly suggests that this macromolecule constitutes a system governed by nonextensive statistics.

6. Final remarks and perspectives

The FSD is determined, qualitatively speaking, by the combination of two quantities:

(1) the number of DSB, since each of these events locally disrupt the double-stranded chain, and
(2) the probability distribution of the DSB's all along the chain extension.

The second quantity is predominantly of statistical nature (*e.g.* extensive or non-extensive), whereas the first is proportional to the cross-section for the DSB formation, σ_{DSB}. Also, this cross-section is responsible for introducing the dependence with dose. However, since a DSB is formed by two closely located SSBs, we have that

$$\sigma_{\mathrm{DSB}} \alpha (\sigma_{\mathrm{SSB}})^2.$$

Therefore, the σ_{SSB} cross-section is one of the ingredients for the build-up of the size distribution. In this sense, we envisage the following perspectives for future studies.

- To develop a model calculation for SSB and DSB cross-sections by taking into account the size correlations among the several parts of the double strand when hit by radiation of different LETs. To obtain more DNA cross-section data for SSB and DSB, combined with FSDs, for radiations with quite distinct LETs, ranging from alpha particles to X-ray. For the cross-section calculations, which takes into account the long-range correlation, one should propose to describe the direct interaction cross-section by an expression of the Markov chain type. This is a chain of probabilities conditioned to the energetic residuum of the former reaction.
- This work, by contributing to the unraveling of DNA properties, could propitiate new insights into the key aspects of radiotherapy, particularly those associated with the interplay damage/repair in the DNA of tumor cells.

References

[1] H. Nikjoo, P. O'Neil, M. Terrissol *et al.*, Int. J. Radiat. Biol. **66**(5) 453–457 (1994).
[2] A. Chaterjee, Nucl. Instrum. Meth. A **280** 439–448 (1989).
[3] H.A. Bethe, Ann. Physik **5** 325 (1930).
[4] A. Deppman, A.N. Gouveia, J.D.T. Arruda-Neto *et al.*, Braz. J. Phys. **34**(3A) 21–25 (2004).
[5] M. Scholz and G. Kraft, Rad. Prot. Dos. **52** 29 (1994).
[6] J. Howard, *Mechanics of Motor Proteins and the Cytoskeleton* (Sinauer Associates, Massachusetts, 2001).
[7] C. Bustamante, Z. Bryant and S.B. Smith, Nature **421** 423 (2003).
[8] F. Brouers and O. Sotolongo-Costa, Europhys. Lett. **62** 808 (2003).
[9] D. Pang, PhD thesis, The George Washington University, Washington D.C. (1997).
[10] D. Pang, B.L. Berman, S. Chasovskikh *et al.*, Rad. Res. **150** 612 (1998).
[11] J.D.T. Arruda-Neto, J. Mesa, C. Garcia *et al.*, Biophys. Rev. Lett. (submitted).
[12] M. Caria, *Measurement Analysis* (Imp. Coll. Press, London, 2000).
[13] R. Ramaswamy and R.K. Azad, Phys. Scripta **T106** 21 (2003).
[14] C. Tsallis, J. Stat. Phys. **52** 479 (1998).